THE UNIVERSITY
of EDINBURGH

Application of Synthetic Polymer Matrices to Develop an *In Vitro* Thymus

Paul Rouse

Thesis submitted for the degree of Doctor of Philosophy

The University of Edinburgh

2019

Declaration

I declare that this thesis has been composed solely by myself and that it has not been submitted, in whole or in part, in any previous application for a degree. Except where states otherwise by reference or acknowledgment, the work presented is entirely my own

Paul Rouse

Acknowledgments

A big shout out to the Blackburn lab. I like to think of it as a family effort that got me through the PhD. Clare, thank you for all the fantastic supervision these past years. You have taught me what it means to be a scientist and, in my own small steps, a supervisor myself. Tim, thank you for all the long, rambling monologues; Frank, for those snappy one liners; Jo, for soaking up all my bad luck and Dominique, for showing me that even the most organised of us all can have a desktop completely saturated with junk. When I first started, it was the burden of Dianna and Frances to put me on the straight and narrow and I look back fondly at the (quite public) times you told me off for not following a protocol correctly or vaping in the office space. I am also looking forward to the future and working with Viktoria and Celine, I think you two are great additions to the team.

I was able to get through the PhD without learning too much chemistry, which I am incredibly grateful for. I am indebted to Mark, Cairnan and Sesha for all your generosity and support. Sylke and Nath, despite the long, three-month work placement, I couldn't have asked for better hosts or industry supervisors.

Now that I am finished, I realise that the main reason I was able to get this PhD finished was the support given to me by the House of Rouse. You four are truly the most special of people. And finally, my home-away-from-home Koko, Francesco and Jen, it really is the end of an era. Esme, thank you for your support, snuggles and cuddles along the way.

"And all the science I don't understand

It's just my job five days a week"

- Bernie Taupin and Elton John, Rocket Man

Abstract

The thymus is the primary lymphoid organ responsible to generating a self-restricted and self-tolerant repertoire of peripheral T-cell receptors. This process is collectively called thymopoiesis and depends on dynamic interactions between the developing T-cells (thymocytes) and the thymic stroma. The main functional element of the thymic stroma is the thymic epithelial cell (TEC), which mediate T-cell lineage development and T cell repertoire selection.

Modelling thymopoiesis *in vitro* is currently limited to two techniques. The original technique is termed reaggregate thymic organ culture (RTOC) and is the only method of culturing *ex vivo* TEC. Unfortunately, the scarcity of TEC makes RTOC very low throughput. To overcome this limitation OP9 cells were engineered to ectopically express the Notch ligand DLL1. OP9-DLL1 cells recapitulate the initial phase of thymopoiesis, T-cell lineage commitment, but not central tolerance induction.

In 2014, our lab published a direct lineage reprogramming strategy that was able to generate cells that could mediate all stages of thymopoiesis from an abundant cell type. The strategy reprograms murine embryonic fibroblasts into induced thymic epithelial cells (iTEC). This thesis outlines experiments through which I optimised the iTEC protocol into a standardised process suitable for scale-up and uses novel synthetic polymer matrices to culture iTEC in both two- and three-dimensions.

Synthetic polymers emulate native extra cellular matrices (ECMs) but have key advantages such as tuneable physical and chemical properties and controllable degradation. This thesis identifies polyacrylates that are capable of supporting both *ex vivo* TEC and iTEC in culture *in vitro*. Investigation into the behaviour of iTEC on the selected polymers demonstrate more consistent behaviours than had previously been achieved and therefore this is the first step in creating a defined protocol for iTEC manufacture that reduces the inherent variablity of reprogramming strategies.

This thesis also proposed and tested a new method for the culture of thymic stroma, which aims to occupy an underdeveloped technical niche. Miniaturisation of the reaggregate thymic

organ culture process starting from both native TEC and iTEC allowed production of hundreds micro-physiological thymi able to support T cell development. This provides proof-of-principle for a new *in vitro* thymic organ culture technology compatible with high-throughput screening technologies, whilst requiring a small fraction for the total tissue requirement of RTOC. Evidence is presented that this reductionist system will be able to query specific hypotheses by producing precise observations, in higher throughput, than currently used techniques.

Lay Summary

T-cells are an important part of the immune system. This type of white blood cell is established very early in life to protect the body against disease. T-cells develop in a special organ called the thymus, through interactions with a type of cell called thymic epithelial cells (TEC). In early life, when the T-cell population is being established, the thymus is very active, but once the immune system does not require new T-cells, the thymus begins to reduce in size and degenerate. This process is called age-related involution and represents healthy shrinking of the thymus.

However, people live longer and travel more frequently than in the past. This means people have greater chance of developing age-related diseases like cancers and encountering new, exotic pathogens when traveling as adults. Age-related involution prevents the thymus from developing new T-cells to counter these problems, which makes the elderly more susceptible to diseases they have not already encountered.

To overcome this, our laboratory proposes to create a large source of transplantable TEC. Currently, we have established a mouse model for this system, called induced thymic epithelial cells (iTEC). The ultimate goal is to transplant iTEC into adults, or children born without a thymus, so they can establish new T-cells to protect against disease.

In this thesis, I address two challenges that limit the potential of iTEC. I outline a method that increased the number of iTEC that could be produced at any given time, which is required to make transplantable tissues and to reduce the variation shown between batches. I then identify new tools to culture iTEC in the laboratory and show these new tools can improve how iTEC are currently developed. Finally, I propose a novel method of testing cells in the laboratory by creating many miniature thymi in the dish, with the aspiration this technique will one day aid thymus-related drug discovery.

Table of Contents

Abbreviations

2-deoxyguanosine (2-dGuo)
3-[(3-Cholamidopropyl)dimethylammonio]-2-Hydroxy-1-Propanesulfonate (CHAPSO)
4′,6-diamidino-2-phenylindole (DAPI)
(Z)-4-Hydroxytamoxifen (4OHT)
7-Aminoactinomycin D (7AAD)
Bone Morphogenetic Protein 4 (BMP4)
C-C motif receptor (CCR)
Claudin-3 and Claudin-4 (CLDN3/4)
Cluster of Differentiation (CD)
Coefficient of Variation (CoV)
Colony Stimulating Factor 1 (CSF1)
Corticomedullary Junction (CMJ)
C-X-C motif (CXC)
Delta-like ligand (DLL)
Dendritic Epidermal T-Cell (DETC)
Deoxyribonucleic Acid (DNA)
Deoxyribonucleotide Triphosphate (dNTPs)
Double Negative (DN)
Double Positive (DP)
Early Growth Response (EGR)
Early Thymic Progenitor (ETP)
Embryonic day (E)
Extracellular Matrix (ECM)
Extracellular Signal-Related Kinase (ERK)
Fetal Thymic Organ Culture (FTOC)
Fez Family Zinc-Finger 2 (FEZF2)
Fibroblast Growth Factor (FGF)
Fibronectin (FN)
Fluorescence Activated Cell Sorting (FACS)
Fluorescence Minus One (FMO)
FMS-like tyrosine kinase receptor-3 (FLT3)
Forkhead Box G1 (FOXNG1)
Forkhead Box N1 (FOXN1)
Forkhead box protein O1 (FOXO1)
Glial cell missing 2 (GCM2)
grafted-RTOC (gRTOC)
Green Fluorescent Protein (GFP)
Haematopoietic Stem Cells (HSCs)
human Embryonic Stem Cells (hESC)
Human Leukocyte Antigen (HLA)
Human Pluripotent Stem Cells (hPSC)
Induced Thymic Epithelial cells (iTEC)

Inhibitor of DNA binding 3 (ID3)
Intercellular Adhesion Molecule (ICAM)
Interleukin-7 (IL-7)
Invariant chain (Ii)
Invariant pre-αTCR (pTα)
ISL LIM Homeobox 1 (ISL1)
iTEC-based RTOC (iRTOC)
Jagged (JAG)
Keratin 5 (K5)
Keratin 8 (K8)
Keratin 14 (K14)
Krüpple-like Factor 2 (KLF2)
Lineage (Lin)
Lineage^{-}SCA-1^{+}c-KIT^{+} (LSKs)
Lymphoid Tissue Inducer (LTi)
Magnesium Chloride (MgCl2)
Major Histocompatibility Complexes (MHC)
Mean Fluorescence Intensity (MFI)
Medullary Dendritic Cells (DCs)
Medullary TEC (mTEC)
Membrane Bound-KIT Ligand (m-KITL)
Methoxyethyl methacrylate (MEMA)
MHC Class I (MHC1)
MHC Class II (MHC2)
Miniaturised-Reaggregate Thymic Organ Culture (MTOC)
MCR Centre for Regenerative Medicine (SCRM)
Murine Embryonic Fibroblasts (MEFs)
Murine Embryonic Stem Cells (mESC)
Natural Killer Cells (NK)
Neural Crest Cell (NCC)
NF-κB–inducing kinase (NIK)
NOD/SCID/gamma (NSG^{TM})
Non-Obese Diabetic (NOD)
Nuclear Factor Kappa-B (NFκ-B)
Paraformaldehyde (PFA)
Phosphate-Buffered Saline (PBS)
Platelet-Derived Growth Factor Receptor (PDGFR)
Polyethylene Glycol (PEG)
Potassium Chloride (KCl)
Power (β)
RANK-ligand (RANKL)
Reaggregate Thymic Organ Culture (RTOC)
Reverse Transcription-quantitative Polymerase Chain Reaction (RT-qPCR)
Receptor Activator of Nuclear Factor kappa-B (RANK)

Recombinase Activating (RAG)
Relative Centrifugal Force (rcf)
Retinoblastoma Tumour Suppressor (RB)
Runt-related Transcription Factor (RUNX)
Second Order Polynomial (Quadratic)
Severe Combined Immunodeficiency *(SCID)*
Single Positive (SP)
Smoothened (Smo)
Sonic hedgehog (SHH)
Sphingosine-1-Phosphate Receptor 1 (S1PR1)
Spinocerebellar Ataxia type 1 (SCA-1)
Suppressor of Cytokine Signalling One (SOCS-1)
T helper–inducing POZ/Krüppel-like factor (THPOK)
T-cell receptor (TCR)
Time zero (t_0)
Third Pharyngeal Pouches (3PP)
Three-Dimensional (3D)
Thymic Epithelial Cells (TEC)
Thymic Epithelial Progenitor Cell (TEPC)
Thymic Mesenchyme (TM)
Thymus Seeding Precursors (TSPs)
Thymus-Specific Serine Protease (TSSP)
Tissue-Restricted Antigens (TRA)
Transporter Associated with Antigen Processing (TAP)
Tumour Necrosis Factor (TNF)
Two-Dimensional (2D)
Ulex Europaeus Agglutinin I (UEA1)
Variable (Diversity) Joining (V(D)J)
Vascular Cell Adhesion Protein (VCAM)
Wild Type (WT)
Wingless/Integrated (WNT)
Yellow Fluorescent Protein (YFP)
Yes-associated protein (YAP)

List of Figures

List of Tables

List of Equations

1. Chapter One: Introduction

1.1. Thymopoiesis

1.1.A. Definition of Thymocyte Sub-Populations and Thymic Structure

The thymus is the obligate site of T-cell development. Its stromal compartment provides a series of unique microenvironments required to mediate the complex sequential processes that produce a mature, functional T-cell repertoire (Figure C1.1). T cell development can be broken down into a series of events based on the expression of key surface markers on the developing T-cells, or thymocytes. The two coreceptors for the T-cell receptor (TCR), cluster of differentiation (CD) 4 and CD8, are usually used for this purpose (Petrie and Zúñiga-Pflücker, 2007). Thymocytes progress from $CD4^{-}CD8^{-}$ double negative (DN) phases, into the $CD4^{+}CD8^{+}$ double positive (DP) phase, wherein they undergo a lineage fate decision to generate the $CD4^{+}CD8^{-}$ or $CD4^{-}CD8^{-}$ single positive (SP) thymocytes that eventually egress from the thymus (Taniuchi, 2018). During each of these phases, thymocytes undergo maturational changes that ensures the thymus contributes a pool of T cells that each express a unique TCR, but collectively express a diverse repertoire of self-restricted, self-tolerant TCR, to the peripheral immune system (Takahama, 2006). Overall, the development of this T cell repertoire is termed thymopoiesis (Figure C1.1).

Cells begin thymopoiesis as DN thymocytes (Figure C1.1). In 1993, this was characterised into four stages based upon expression of CD25 and CD44 (Godfrey *et al*., 1993). The initial stage was termed DN1 and is characterised by as $CD25^{-}CD44^{+}$, thymocytes then progress into DN2 and upregulate CD25. In DN3 thymocytes downregulate CD44 and finally DN4 thymocytes downregulate CD25 to become $CD25^{-}CD44^{-}$ (Figure C1.1). In the years since the original publication, the heterogeneity within each of these subpopulations has been further characterised (Bhandoola *et al*., 2007; Falk and Eichmann, 2002). However, understanding the role of these sub-populations is not central to this thesis and, therefore, these subpopulations are not discussed further herein except for an important sub-population within DN1 thymocytes. Within DN1, the most immature thymocyte population is called the Early Thymic Progenitor (ETP) and is believed to represent the canonical T cell progenitor. It is defined as $CD117(cKit)^{+}CD25^{-}$ $CD4^{-}CD8^{-}TCR\beta^{-}TCR\gamma^{-}Nk1.1^{-}CD11b^{-}Gr\text{-}1^{-}CD19^{-}CD11c\text{-}Ter119^{-}$ (Bhandoola *et al*., 2007). Whilst the ETP is not a homogeneous population in itself,

this thesis will largely assume it to be the initiation point of thymopoiesis (De Obaldia *et al*., 2013).

The tightly controlled and sequentially ordered process of thymopoiesis is established by the thymic stroma, the main effectors of which are Thymic Epithelial Cells (TEC) (Abramson and Anderson, 2017).Within the thymus, two broad sub-populations of TEC are found, and are segregated into cortical and medullary regions. Haematopoietic precursors enter the thymus through blood vessels situated at the junction between these regions, the corticomedullary junction (CMJ) (Figure C1.1) (Buono *et al*., 2016; Itoi *et al*., 2001). Interaction with NOTCH ligands enforces T-cell lineage commitment as thymocytes move through the cortex towards its edge at the subcapsular region (Benz *et al*., 2004). Once a thymocyte has developed a unique TCR, it begins to migrate back towards the CMJ. Interactions with cTEC ensure only those thymocytes with a TCR that interacts with peptide in the context of self-major histocompatibility complexes (MHC) within a particular affinity range are conferred survival signals. This is termed positive selection (Takada *et al*., 2017) (Figure C1.1). Thymocytes that survive are licensed to migrate into the medulla of the thymus, which is populated with medullary TEC (mTEC). Interactions with mTEC, and medullary dendritic cells (DCs), remove thymocytes with TCRs that bind peptide:self MHC complexes at high affinity, or select such cells to become T regulatory cells (T_{regs}). Deletion of self-reactive T cell clones is termed negative selection (Cosway *et al*., 2017), whilst the wider process is termed central tolerance induction (Figure C1.1). Once this process is complete thymocytes emigrate from the thymus via blood vessels at the CMJ (Figure C1.1) (James *et al*., 2018).

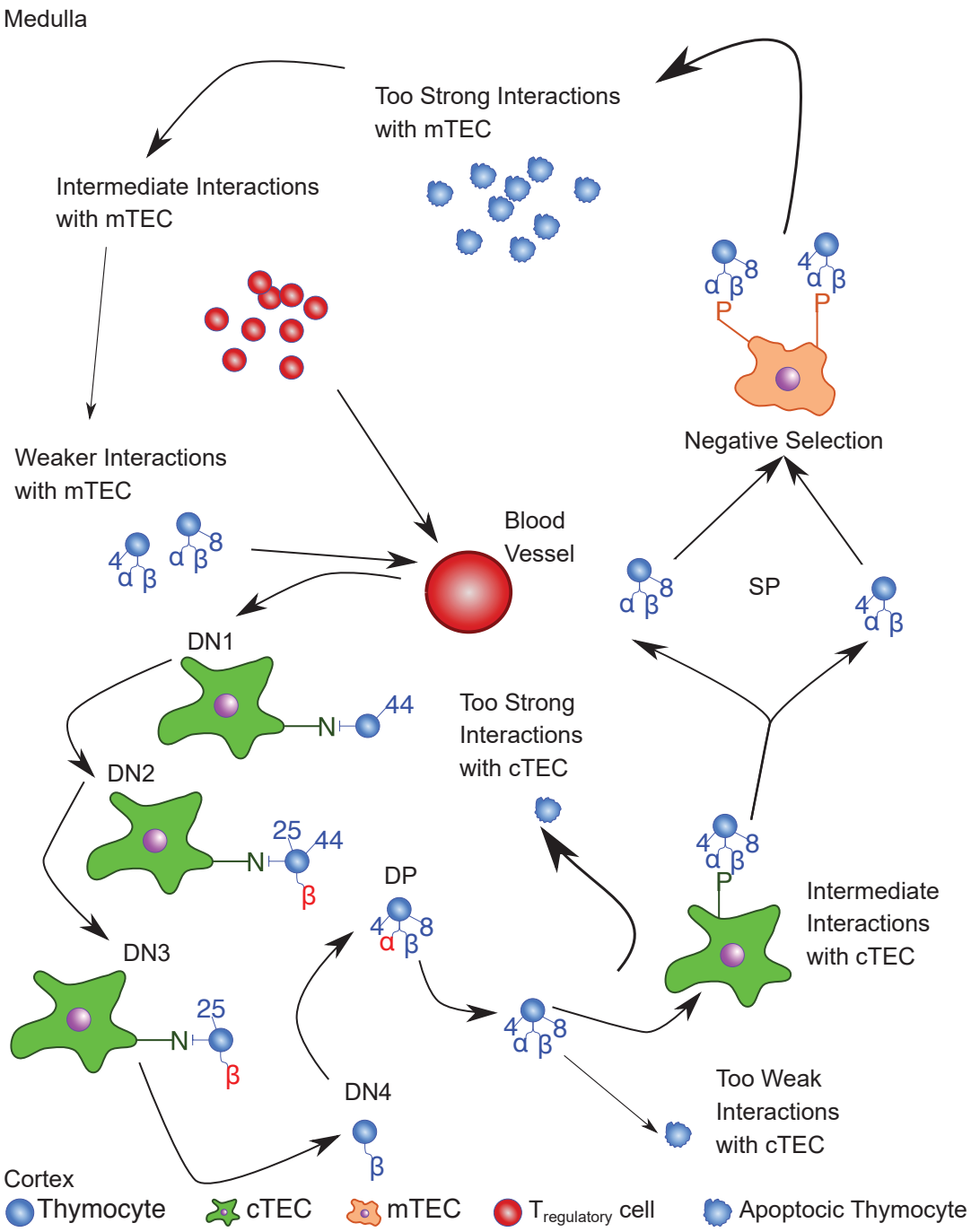

Figure C1.1: A Map of αβ T-cell Thymopoiesis

Representation of thymopoiesis with respect to only the key markers used to track thymocytes progressing through thymopoiesis at each phase. Cells enter the thymus at the corticomedullary junction. Upon receiving Notch signaling, thymocytes progress through the DN phases, which is tractable with CD25 and CD44. DN thymocytes must produce a unique TCRβ chain to progress into the DP phase. In the DP phase thymocytes must complete the TCR by producing a TCRα chain. Interactions with cTEC ensure only thymocytes with a self-restricted TCR survive and enter the SP phase. SP thymocytes are licensed to migrate into medulla, in which interactions with mTEC ensure only thymocytes with a self-tolerant TCR are allowed to emigrate into the periphery. N = Notch ligand, P = peptide:MHC, β =TCRβ chain, α= TCRα chain.

1.1.B. Colonisation of the Thymus by Haematopoietic Progenitor Cells

The first event in thymopoiesis is recruitment of bone marrow-resident precursors into the thymus from the blood system (Martins *et al*., 2012). Various candidates have been proposed for the identity of this precursor, all of which are downstream progeny of bone marrow-derived haematopoietic stem cells (HSCs) (Sultana *et al*., 2012). While it is still not possible to isolate a pure population of HSCs by flow cytometry or any other method, a population enriched for HSC may be obtained by a sorting protocol which excludes mature cells from most haematopoietic lineages (using an antibody 'cocktail' commonly referred to as 'lineage (lin)'), and positively selecting cells from the remaining population of $CD45^+$ cells using the surface makers c-KIT and Spinocerebellar ataxia type 1 (SCA-1) (Spangrude *et al*., 1988). Within $CD45^+Lin^-c\text{-}KIT^+SCA\text{-}1^+$ cells, expression of FMS-like tyrosine kinase receptor-3 (Flt3) further defines three distinct populations: self-renewing HSC ($FLT3^-$), multipotent progenitors ($FLT3^{low}$) and lymphoid-primed multipotent progenitors ($FLT3^{high}$) (Sultana *et al*., 2012). Also downstream of HSCs are common lymphoid progenitors ($FLT3^{high}$, IL-$7R\alpha^+$). Both populations express two key chemokine receptors: C-C motif receptor (CCR) 7 and CCR9 (Zlotoff *et al*., 2010). Knockout models heavily implicate CCR7, CCR9 and C-X-C motif (CXC) Receptor 4, and associated ligands CCL21, CCL25 and CXCL12, in thymic homing, making these precursors candidates for thymic seeding (Calderón and Boehm, 2011; Liu *et al*., 2006; Schwarz *et al*., 2007; Sultana *et al*., 2012; Zlotoff *et al*., 2010). Transcriptomic analyses comparing the ETP, to the lymphoid-primed multipotent progenitors (LMPP) and common lymphoid progenitors (CLP) found the ETP was more similar to the LMPP, making this population the likely thymus-seeding cell (Allman *et al*., 2003; Bell and Bhandoola, 2008; Lu *et al*., 2005; Luc *et al*., 2012; Wada *et al*., 2008).

In the late fetal and adult thymus, haematopoietic cells are thought to enter the thymus at the CMJ by extravasation from post capillary venules (Takahama, 2006). While the mechanism of action is undescribed, Petrie and Zúñiga-Pflücker (2007) propose a similar mechanism to the common lymphocyte extravasation mechanism: the leukocyte adhesion cascade. In this model, colonisation would take place via a three-stage process in which lymphocyte

progenitors first migrate to the thymus through the blood system and, upon arrival, tether to the endothelium and enter the thymus as the CMJ (Vestweber, 2015).

1.1.C. Early Thymocyte Development

1.1.C.I. ETPs

ETPs have been shown via clonal level studies to have the potential to differentiate into T-cell, B-cell and granulocyte-macrophage but not megakaryocyte-erythroid lineages (Luc *et al*., 2012). Commitment of ETPs to the T-cell lineage is imposed by NOTCH signalling, and is as an essential function of cTEC (Hozumi *et al*., 2008; Koch *et al*., 2008). Buono and colleagues (2016) present compelling data that ETPs occupy a unique niche provided by c-KIT^{+} endothelial cells at the CMJ. Like cTEC, these endothelial cells provide localised membrane bound-KIT Ligand (m-KITL) to support ETPs. The availability of KITL is reduced as thymocytes move into the cortex, which has a microenvironment established increasing by cTEC that express less c-KIT than the thymic endothelial cells. This gradient controls the release of ETPs from the CMJ as they progress further through thymopoiesis and downregulate c-KIT by DN3. Evidence for this proposition was gathered when the authors deleted exon seven of the *Kitl* gene, which codes the transmembrane domain. The result was a functional and stable variant of the protein that was unable to be anchored at the cellular membrane and was secreted, perturbing the KITL gradient that established the CMJ niche.

Mammals have four Notch receptors, all of which are expressed during thymopoiesis (Dzhagalov and Phee, 2012; Petrie and Zúñiga-Pflücker, 2007). ETPs predominately express NOTCH 1, and conditional knock out studies established that signalling through NOTCH 1 is required for T cell commitment (Radtke *et al*., 1999). There are five ligands that associate with the NOTCH receptors: Delta-like ligand (DLL) -1, -3 and -4 and Jagged (JAG) 1 and 2 (Fiorini *et al*., 2009). Two studies from Koch (2008) and Hozumi (2008) *et al.* demonstrated that DLL4 is indispensable for T cell lineage commitment, by characterising TEC-specific DLL4 knockout mice (*Foxn1*^{Cre}:*Dll4*$^{flox/flox}$). Without DLL4 expression in cTEC, B-cells rather than T cells developed in the thymus. It is surprising that redundancy with other

Notch ligands was not observed, as *in vitro* data indicate that DLL4, DLL1 and to a lesser extent JAG2, are able to mediate T cell lineage commitment (Mohtashami *et al*., 2010; Van De Walle *et al*., 2011).

ETPs have huge proliferative capacity and respond to proliferative signalling environment of the thymus to undergo a 1000-fold expansion over a period of approximately 10 days (Martins *et al*., 2012; Shortman *et al*., 1990). Rodewald and colleagues (1995) showed that c-KIT (*ckit*$^{-/-}$) deficient models have 50% fewer total thymocytes with the DN1 and DN2 thymocyte sub-populations exhibiting a 40-fold reduction compared to wild-type littermates. Notably, thymocyte subset distribution was not affected. This highlights that the perturbation was most focused on the early proliferative processes. Kenins and colleagues (2010) showed that FLT3 is non-reductant for maintenance of ETPs. Fetal thymic organ cultures produced from mice with dysfunctional FLT3 (*Flt3*$^{-/-}$) had reduced ETP populations compared to those from wild type (WT) mice. This perturbation was only observed in immature populations as more mature subsets had recovered, implying other regulatory mechanisms compensated for FLT3 deficiency. TEC secrete interleukin-7 (IL-7), a non-redundant cytokine that contributes to almost all stages of thymopoiesis and is also implicated at this early stage (Petrie and Zúñiga-Pflücker, 2007). ETPs express relatively low levels of the IL-7 receptor CD127, which then increases, peaking at DN2 (Yu *et al*., 2004), after which it is transcriptionally downregulated in DP cells through suppressor of cytokine signalling one (SOCS-1), a process vital for thymocyte death by neglect during positive selection (Yu *et al*., 2006, 2004).

1.1.D. Double Negative Two

Upon receipt of NOTCH signal, DN1 thymocytes upregulate CD25 to transition to the DN2 of thymocyte development, characterised by initiation of Variable (Diversity) Joining (V(D)J) region recombination at the TCR γ, δ and β loci (Figure C1.1). Development of the TCR is dependent upon expression and rearrangement of the four TCR chains: α and β, γ and δ. These characterise the two distinct T-cell populations: αβ T-cells express a heterodimer of αTCR and βTCR, while γδ T-cells express γTCR and δTCR chains (Wilson *et al*., 1994).

Lineage dictates the peripheral function of T-cells. αβ T-cells are a key component of the adaptive immune system, while γδ T-cells are hypothesised to bridge the innate and adaptive immune systems with the γδ-TCR not being restricted to recognising peptides within the context of MHC (Gogoi and Chiplunkar, 2013).

The immune system requires a diverse αβ TCR repertoire and this is generated through combinatorial recombination of the segmented TCR loci. This V(D)J exon recombination is regulated by expression of the recombinase activating (RAG) proteins RAG-1 and RAG-2 (Livák *et al*., 1999). At DN2, recombination of γTCR, δTCR and βTCR genes begins (Notarangelo *et al*., 2001). IL-7 is implicated in γδ T-cell maturation and has been linked to chromatin accessibility for RAG-mediated cleavage in the V(D)J recombination of γTCR chain (Huang *et al*., 2001; Ye *et al*., 2001). Note that not all DN2 thymocytes acquire T-cell lineage, some retain potential for, and mature into, natural killer cells (NK) and DCs (Lu *et al*., 2005).

DN2 thymocytes migrate toward the subcapsular region of the cortex where, upon arrival, they will develop into DN3 thymocytes (Takahama, 2006) (Figure C1.1). This sequential movement is maintained by chemokine gradients and has been linked to CCR7/CCL21, CCR9/CCL25 and CXCR4/CXCL12 that increase toward the outer edge of the cortex (Benz *et al*., 2004; Misslitz *et al*., 2004; Plotkin *et al*., 2003). How DN2 thymocytes achieve this migration was investigated by Prockop and colleagues (2002) who assessed the affinity of DN1, DN2 and DN3 thymocytes for fibronectin (FN) and laminin-1 binding using static adhesion experiments. DN1 and DN3 thymocytes showed high affinity for FN while DN2s showed a similar or lower affinity for FN as for polystyrene beads coated in bovine serum albumin. As the DN2 stage can be considered a transition between DN1, located at the CMJ, and DN3, located in the subcapsular region, this supports the notion DN2 thymocytes use cellular adhesion rather than matrix adhesion to facilitate migration (Petrie and Zúñiga-Pflücker, 2007; Shukla *et al*., 2017). Immunohistochemistry and competitive inhibition assays confirmed this interaction utilises Vascular Cell Adhesion protein 1 (VCAM-1) expressed on cTEC and its receptor on thymocytes (Prockop *et al*., 2002; Shukla *et al*., 2017). Furthermore, E-cadherin is a homotypic adhesion molecule that mediates thymocyte

adhesion to TEC (Petrie and Zúñiga-Pflücker, 2007). Antibodies that blocked this interaction prevented transition of DN thymocytes into DP thymocytes, while blocking thymocyte to Extracellular Matrix (ECM) interactions, through integrin αEβ7, did not perturb thymopoiesis in Fetal Thymic Organ Culture (FTOC) (Müller *et al*., 1997). This highlights the importance of thymocyte to TEC interactions, over thymocyte to ECM.

1.1.E. Double Negative Three Thymocytes

The migration of DN2 thymocytes toward the subcapsular region ends with downregulation of CD44 to transition into DN3 (Koch and Radtke, 2011). TCRβ recombination is initiated in most thymocytes during the DN2 phase and in all by DN3 (Koch and Radtke, 2011). Schmitt and colleagues (2004) showed that Notch signalling was required until the DN3 stage, at which point NK and DC potential is lost. Whether DN3 thymocytes continue down γδ or αβ T-cell lineage depends on which TCR chains have successfully recombined. This is likely to be a competitive event as there is evidence of βTCR recombination in γδ T-cells and of αβ TCR chains in γδ T-cells (Livák *et al*., 1999). Successful recombination of γδ TCR concurrent with activation of the extracellular signal-related kinase (ERK)-early growth response (EGR)-inhibitor of DNA binding 3 (ID3) pathway facilitates γδ lineage commitment and NOTCH-independent maturation (Lauritsen *et al*., 2009). Most thymocytes enter the αβ lineage, via a process called β-selection (Dzhagalov and Phee, 2012). β-selection occurs when a productively rearranged TCRβ chain pairs with the invariant pre-αTCR (pTα) and CD3 complex proteins to form the pre-TCR, and initiation of this process is characterised by upregulation of CD27 concomitant with expression of TCRβ (Taghon *et al*., 2006). Signalling through the pre-TCR is ligand-independent, although affected by receipt of Notch and CXCR4 signals, and initiates a cascade of downstream processes including down-regulation of *Cd25*, *pre-Tα, Rag1* and *Rag2* inhibition of further βTCR V(D)J recombination, proliferation, differentiation and rescue from apoptosis (Janas and Turner, 2010; Koch and Radtke, 2011; Michie and Zúñiga-Pflücker, 2002). Note that β-selection is a key check point, thymocytes that do not successfully produce a βTCR are not conferred survival signals via the pre-TCR and apoptose (Petrie *et al*., 1995).Thymocytes that undergo β-selection transition to the DN4 stage of development, while thymocytes that do not successfully

produce the pre-TCR and are also not selected to become αβT-cells are selected against and undergo programmed cell death (Koch and Radtke, 2011; von Boehmer, 2005).

Onset of β-selection predominantly occurs in DN3 thymocytes at the subcapsular region (Petrie and Zúñiga-Pflücker, 2007). In addition to providing migratory signals, CXCR4/CXCL12 act as co-stimulators for β-selection (Plotkin *et al*., 2003). Trampont and colleagues (2010) engineered a conditional *Cxcr4* knockout model in which *Cxcr4* is deleted once thymocytes reach the DN2 stage using Lck^{Cre} (Lck^{Cre}:$Cxcr4^{flox/flox}$). This resulted in disruption of the migratory path of DN2 thymocytes but also reduced the relative population sizes of DN4 against DN3 compared to controls. This implied that removal of CXCR4 inhibited β-selection, with more DN3 thymocytes failing the β-selection check point. γδ T-cell development remained intact, conforming to this hypothesis. Furthermore, when looking at whether CXCR4 conferred survival signals to DN3 thymocytes, Trampont and colleagues (2010) found that DN3 thymocytes without CXCR4 in OP9-DL1 co-cultures lost viability faster than those with CXCR4 signalling intact. The authors concluded that this was due to loss of expression of the pre-TCR-induced pro-survival molecule: BCL-2A1.

Notch signalling also plays a non-redundant role in β-selection by regulating cellular metabolism through activation of the Akt pathway phosphatidylinositol 3-kinase (Ciofani and Zúñiga-Pflücker, 2005; Maillard *et al*., 2006). RBP-J deficiency in DN3 thymocytes dramatically reduced absolute cell numbers at all subsequent stages of thymopoiesis (Tanigaki *et al*., 2004).

1.1.F. Double Negative Four Thymocytes

Cells that pass the β-selection gate transition to the DN4 stages of development, which is characterised by a rapid proliferative burst. There is conflicting evidence regarding whether the proliferation during the DN4 phase is directly affected by pre-TCR signalling, or is instigated by an independent mechanism (Michie and Zúñiga-Pflücker, 2002; Petrie *et al*., 2000; Petrie and Zúñiga-Pflücker, 2007). Counterintuitively to the nomenclature, from the DN3 stage, thymocytes begin upregulation of CD4 and CD8, which marks the beginning of the transition into DP thymocytes (Petrie *et al*., 1990).

The subcapsular region provides extrinsic factors stimulating proliferation. The GTPase, RHO has been associated with all stages of thymopoiesis as it implicated for β1 and β2 integrin activation required for thymocyte adhesion (Vielkind *et al*., 2005). Galandrini and colleagues (1997) produced a model with conditional expression of the RHO inhibitor *C. botulinum* C3 once thymocytes reach DN2 stage ($Lck^{C.\ botulinum\ C3}$). These mice showed delayed production of SP thymocytes until one week post-natal, as compared to E15.5 in WT mice, which was attributed to increased apoptosis at the DN3 stage (Vielkind *et al*., 2005). Furthermore, inhibition of RHO caused defects in cell cycle progression in DN4 thymocytes (Galandrini *et al*., 1997). Therefore, integrin expression and activation, mediated through RHO, are implicated in pro-survival signals of DN3 and proliferation of DN4.

The integrin heterodimer α6β4 is upregulated during the DN3 phase and shows affinity for laminin-5, which is abundant in subcapsular region (Kim *et al*., 2000). MAP kinases are specifically activated via α6β4, directly linking α6β4 with proliferation and survival of DN3s and DN4s. In FTOC experiments, Kim and colleagues (2000) showed that blocking laminin-5 produced a 40% reduction in total intrathymic thymocyte population with a 75-90% reduction in DN2 and DN3 populations compared with untreated controls.

1.1.G. Double Positive Thymocytes

Once they reach the DP phase, thymocytes begin migrating back towards the thymic medulla (Koch and Radtke, 2011) (Figure C1.1). The initial event during this phase is V(D)J recombination of the *Tcrα* locus, with thymocytes instigating a second wave of RAG expression (Petrie *et al*., 1995). Once a productive TCRα rearrangement has been made, TCRα complexes with the TCRβ (replacing pTα) to form the αβTCR (Klein *et al*., 2009). DP thymocytes that express an αβTCR heterodimer then undergo a process termed positive selection, which occurs as during the migration back to the CMJ (Penit, 1988).

Positive selection occurs when a DP thymocyte expressing a αβTCR interacts with a peptide:self-MHC expressed by a cTEC (Figure C1.1). At this stage of development, the strength of the interaction determines whether, or not, the thymocyte is conferred survival signals. 95% of DP thymocytes express αβTCRs with too great or too weak affinity for self-

MHC, and these cells undergo apoptosis (Hogquist *et al*., 2005). Those thymocytes with a αβTCR that binds self-MHC presented on cTEC in the right affinity window undergo positive selection and are signalled to survive. Positive selection is closely associated with the SP4 and SP8 fate choice, which is also made at the DP stage of development (Littman, 2016). Classical instructive explanations of thymopoiesis suggest that when a αβTCR interacts with MHC Class I (MHC1) the thymocyte downregulates CD4, while if it interacts with MHC Class II (MHC2) the thymocyte downregulates CD8 (Germain, 2002). Two seminal publications in 1995 made it evident that the above model was a simplification of a multifaceted process (Littman, 2016). Suzuki and colleagues (1995) presented observations that, while commitment to SP4 was dependent on MHC signalling, SP8 commitment was MHC independent. Furthermore, Lundberg and colleagues (1995) used transplantation studies to show that $CD4^{+}CD8^{mid}TCR^{mid}$ thymocytes give rise to both SP8 and SP4 thymocytes but $CD4^{low}CD8^{+}$ exclusively only give rise to further CD8 SP thymocytes. This led to Singer and colleagues (Brugnera *et al* 2000) proposing the kinetic signalling model, which is now accepted by the field (Littman, 2016). First, successful TCR engagement results in downregulation of CD8 at the transcriptional level generating an intermediate thymocyte population: $CD4^{+}CD8^{low}$. Those thymocytes with a αβTCR that recognises MHC2 will continue to receive active TCR signalling, which leads to further upregulation of CD4 and progression into SP4 thymocytes. The remaining thymocytes that do not have a TCR capable of recognising MHC2 and have downregulated CD8, cannot recognise MHC1 and do not receive continued TCR signalling. This initiates a process called coreceptor reversal, an IL-7-dependent and TCR-independent mechanism, to generate SP8 thymocytes (Taniuchi, 2018). The nomenclature refers to the different *kinetics* in TCR activation. Loss of the CD8 coreceptor prevents TCR that recognise peptide:MHC1 from having sustained activation, while TCRs that recognise peptide:MHC2 maintain TCR activation despite absence of CD8. Therefore, it is the regulation of CD4 and CD8 expression that dictates lineage decision.

Many regulatory elements have been identified to affect expression of the *cd4*, *cd8α* and *cd8β* genes. Most notable is the *Cd4* transcription silencer *S4* and two of the transcription

factors that bind to its sequence. Members of the Runt-related transcription factor (RUNX) family activate *S4* while the T helper–inducing POZ/Krüppel-like factor (THPOK) prevents its activity (Taniuchi, 2018). Thymocytes with a TCR specific to MHC2 maintain TCR signalling and upregulate THPOK, preventing *S4* activation, to become SP4 thymocytes. Thymocytes with a TCR specific to MHC1 cannot maintain TCR signalling and so upregulate the RUNX factors and activate *S4*, which represses *cd4* and the thymocytes progress to SP8. In addition to IL-7 mediating coreceptor reversal, there is evidence IL-7 encourages thymocyte proliferation in SP thymocytes (Tani-ichi *et al*., 2013).

Notably, the nature of thymocyte adhesion interactions changes, transitioning away from integrins with affinity for VCAM-1 toward those affinity for Intercellular Adhesion Molecule (ICAM)-1 (Witt *et al*., 2005). These interactions yield different functionalisation. DP thymocytes arrest the cell cycle and do not require proliferative signalling (Penit, 1988). Also, for the first time, thymocytes do not require Notch signalling from the thymic stroma (Tanigaki *et al*., 2004). Instead, DP thymocytes migrate toward the medulla via random walking (Witt *et al*., 2005). This is hypothesised to encourage the multiple interactions with cTEC necessary to perform positive selection (Petrie and Zúñiga-Pflücker, 2007).

1.1.H. Single Positive Thymocytes

Thymocytes that have successfully undergone positive selection are licenced to migrate into the outer region of the thymic medulla, an area rich in DC cells and mTEC (Shortman and Naik, 2007). Interactions with both mTEC and DC provide cognate TCR-peptide:MHC interactions essential for imposing central tolerance on the developing repertoire. The main objective of negative selection is to remove any thymocytes with a self-MHC restricted TCR that recognises self-peptide. Thus any thymocytes that display affinity to such peptides are induced into apoptosis, a process termed clonal deletion, or are committed to the regulatory T-cell lineage (Klein *et al*., 2014; Kyewski and Peterson, 2010). In order to perform clonal deletion effectively, mTEC express a very wide repertoire of genes that are normally tissue or developmentally restricted, through a process termed promiscuous gene expression, which controls expression of so-called tissue restricted antigens (TRAs). Two transcription

factors mediate this process: a major regulator of TRA expression in the thymus is the autoimmune regulator AIRE, which is expressed in mTEC. More recently, the Fez family zinc-finger 2 (FEZF2) has been purported to play a role in AIRE-independent TRA expression (Takaba *et al*., 2015). However, there is some controversy regarding the original publication (Cosway *et al*., 2017). DCs can also present these mTEC-expressed antigens via the process of cross-presentation (Klein *et al*., 2009).

Migration through the medulla is regulated by chemokines. SP thymocytes upregulate CCR4 and CCR7. This encourages directed migration towards CCL19 and CCL21, which are secreted by mTEC (Cowan *et al*., 2014; Witt *et al*., 2005). ICAM-1 is essential to mediate thymocyte to stromal adhesion, which is necessary for negative selection (Kishimoto *et al*., 1996). Furthermore, there is evidence that DCs secrete CCL17, which binds CCR4, to actively attract thymocytes (Lieberam and Förster, 1999). Throughout negative selection, thymocytes migrate deeper into the medulla, away from the DC rich outer edge (Kurobe *et al*., 2006). During this migration, thymocytes are presented with peripheral peptides by mTEC and DC. Cognate TCR-peptide:MHC instigate a pro-apoptotic event that eliminates any autoreactive thymocytes (Petrie and Zúñiga-Pflücker, 2007). There is substantial evidence that thymocytes require more than MHC interactions to reach maturation (Dyall and Nikolic-Zugić, 1999). Tang and colleagues (2016) showed that a specific subset of DCs called plasmacytoid DCs express IL-27 within the thymic medulla and when this is knocked out, thymocytes are unable to complete thymopoiesis. Moreover, the addition of endogenous IL-27 rescued the phenotype during *in vitro* assays.

SP thymocytes transition through several intermediate stages before completing negative selection (Li *et al*., 2007). Xing and colleagues (2016), show that there are three subpopulations of both CD4 and CD8 SP thymocytes, identified via flow cytometric analysis of CD69 and MHC1. Importantly, the authors demonstrate district functional differences between these subpopulations with respect to the effect of TCR stimulation, ability to secrete cytokines and capacity for thymic egression: Semi-mature thymocytes ($CD69^{+}MHC1^{-}$) represent thymocytes most recently positively selected; Mature 1 ($CD69^{+}MHC1^{+}$)

thymocytes acquire the ability to proliferate after TCR stimulation; Mature 2 ($CD69^{-}MHC1^{+}$) thymocytes demonstrated both TCR-stimulated proliferation and a competency to secrete cytokines. Strikingly, Mature 2 thymocytes upregulate key genes for thymic egress such as sphingosine-1-phosphate receptor 1 (S1PR1). Conditional knockout of S1PR1 in thymocytes (Lck^{Cre}:$S1PR1^{flox/flox}$) significantly reduced the number of T-cells in the periphery and accumulated within the thymus (Allende *et al*., 2004; Matloubian *et al*., 2004). In keeping with these data, James and colleagues (2018) postulated a mechanism of egression in which, upon reaching the Mature 2 phase, thymocytes upregulate Forkhead Box Protein O1 (FOXO1) and Krüpple-Like Factor 2 (KLF2), which in turn upregulates S1PR1 and CD62L and downregulates CD69 (Alfonso *et al*., 2006; Bai *et al*., 2007; Bankovich *et al*., 2010; Fabre *et al*., 2008). This process then directs thymocytes to follow a S1P gradient towards the CMJ to exit the thymus and begin peripheral maturation (Figure C1.1).

1.2. Thymic Organogenesis

1.2.A. Overview of Thymic Organogenesis

Thymopoiesis is mediated through thymocyte interaction with the microenvironment. Thymic stromal cells establish and maintain this environment, which allows a transient thymocyte population to follow a defined maturation pathway (Figure C1.1). The chief effectors of this are TEC. Therefore, understanding how thymopoiesis is established and maintained is closely associated with the developmental processes that establish TEC. This thesis breaks down TEC development into two phases, based upon expression of a single transcription factor. Forkhead Box N1 (FOXN1), a member of the Forkhead or winged helix superfamily, can be considered the master transcription factor of the TEC developmental program (Figure C1.2). Null mutations in *Foxn1* cause hairlessness and athymia in the classical *nude* ($Foxn1^{null}$) phenotype. Experimentation suggested that the *nude* thymic phenotype resulted from a block in the TEC developmental program at Embryonic day (E) 11.5, ultimately leading to retention of a cystic thymic rudiment without haematopoietic colonisation or normal TEC structures (Blackburn *et al*., 1996). Bleul and colleagues (2006) confirmed this hypothesis using a revertible null allele of *Foxn1*, showing that reversion of the *Foxn1* null

allele in a single cell was sufficient to instigate TEC development resulting in generation of a small thymic lobe capable of supporting thymopoiesis and containing both cortical and medullary TEC populations. This supports a two-phase model of organogenesis: a FOXN1 independent phase, in which third pharyngeal pouches (3PP) are specified to the TEC lineage and in which the thymic rudiment forms and migrates, and a FOXN1 dependant phase in which TEC differentiation and maintenance confers thymic functionality (Vaidya *et al*., 2016). Therefore, thymic organogenesis can be parsed into the establishment of the thymic rudiment as the FOXN1 independent phase and development of the TEC program as the FOXN1 dependant phase.

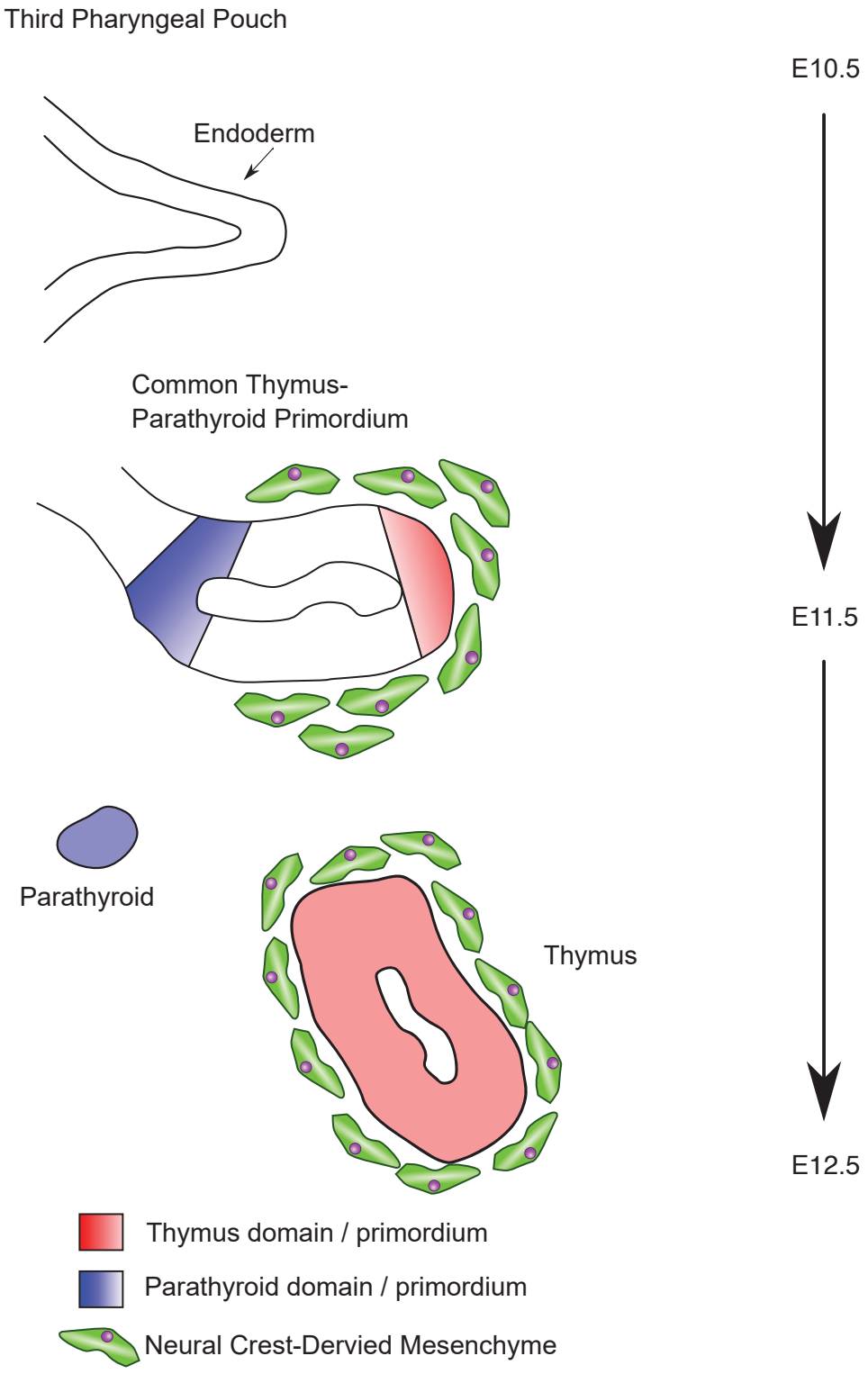

Figure C1.2: Early Events of Thymic Organogenesis
Representation of the third pharyngeal pouch between E10.5 and E12.5. At E11.5 *Foxn1* expression is initiated in the ventral domain of the common thymus-parathyroid primordium. Over time, *Foxn1* expression spreads into the central domain. At E12.5 the rudiments have separated and the thymus begins migration. Images adapted from Vaidya, Briones Leon and Blackburn, 2016.

1.2.B. FOXN1 Independent Establishment of the Thymic Rudiment

The thymus derives from the endoderm of the 3PP, which can be observed from ~E9.0 as bilateral buddings of the foregut (Vaidya *et al*., 2016). The 3PP generates both the parathyroid gland and the epithelial compartment of the thymic rudiment (Figure C1.2). This is observable using expression of the transcription factors: Glial cell missing 2 (Gcm2) in the dorsal anterior, parathyroid-fated region and Forkhead Box G1 (Foxg1) and ISL LIM Homeobox 1 (Isl1) in the ventral posterior, thymic-fated region (Bain *et al*., 2016; Gordon *et al*., 2001; Wei and Condie, 2011). This process is governed by a network of transcription factors including HOXA3, PAX1/9, EYA1, SIX1 and SIX4 network and dysfunction in any gene results in impaired organogenesis (Manley and Condie, 2010; Xu *et al*., 2002).

Gordon and colleagues (2004) were first to show that mammalian TEC are generated exclusively the endoderm of the 3PP by isolating the endoderm component from E8.5 to E9.0 3PP and engrafting it under the kidney capsule of *nude* mice. This fragment was sufficient to establish a fully functional thymus with complete thymocyte populations and cortical and medullary architecture. This functional evidence, along with lineage tracing in whole embryo culture, established that the thymus originates from the endoderm of the 3PP, independently from the surrounding ectoderm, and that the rudiment is already specified to the thymic development program at the early timepoint of E8.5-9.0 (Le Douarin and Jotereau, 1975).

1.2.C. FOXN1 Dependent Development of the TEC Program

At E11.25, the thymus-specified 3PP endoderm strongly upregulates expression of *Foxn1* (Gordon *et al*., 2001; Nehls *et al*., 1994). As previously discussed, whilst not essential for specification of the TEC lineage or establishment of the thymic rudiment, FOXN1 is essential for differentiation of TEC and thus for development of a functional thymus able to support thymopoiesis (Blackburn *et al*., 1996; Bleul *et al*., 2006; Gordon *et al*., 2004; Nowell *et al*., 2011; Ripen *et al*., 2011).

The mechanisms regulated by FOXN1 are sufficient to recapitulate TEC functionality in unrelated cell-types. Bredenkamp and colleagues (2014) enforced *Foxn1* expression in

murine embryonic fibroblasts (MEFs), largely recapitulating the FOXN1-dependant phase of thymic development. Importantly, upon transplantation under the kidney capsule of *nude* (*Foxn1*^{null}) or syngeneic mice, these cells, termed Induced Thymic Epithelial Cells (iTEC), differentiated into both cortical and medullary TEC and emulated thymopoiesis by populating the recipient with T-cells.

FOXN1 is also able to restore functionality to TEC that have undergone healthy, age-related degeneration called thymic involution (Bredenkamp *et al*., 2014). Downregulation of *Foxn1* was hypothesised to be a main driver of involution and it is an early hallmark of the process (Ortman *et al*., 2002). In itself this implicates FOXN1 in thymic homeostasis, without which TEC fail to maintain functionality (Chen *et al*., 2009). Bredenkamp and colleagues (2014) upregulated high levels of functional FOXN1 expression in post-involution TEC, demonstrating that this intervention was sufficient to reverse age-related thymic involution and restore T-cell output and TEC phenotype and architecture to close to juvenile levels. This effect was observed in both the cortical and medullary compartments, with key genes being progressively downregulated during involution and then, upon FOXN1 upregulation, being restored close to pre-involution levels. Therefore, FOXN1 is essential for TEC functionality, development and maintenance and *Foxn1* downregulation is a hallmark of thymic involution and loss of function. However some notable effectors of thymopoiesis are maintained interpedently of FOXN1, such as IL-7 (Zamisch *et al*., 2005).

Despite the significant contribution of FOXN1 to the functionality of the thymus, the upstream elements governing and establishing *Foxn1* expression are poorly characterised. *Foxn1* has been shown to positively autoregulate, although whether this is direct or indirect is yet to be elucidated (Bredenkamp *et al*., 2014; Vaidya *et al*., 2016; Zook *et al*., 2011). Members of the E2F family of transcription factors have demonstrated the capacity to bind to the presumptive *Foxn1* promoter region. Retinoblastoma tumour suppressor (RB) proteins negatively regulate EF2: knocking out 5/6 members of the RB family increased *Foxn1* expression and thymus size in a murine model. Furthermore, E2F, which is negatively regulated by RB, was shown to bind the *Foxn1* promoter in chromatin immunoprecipitation assays.

1.2.D. Mesenchymal Influences on the Developing Thymus

By E12.5 the thymic rudiment has begun to separate from the pharynx and the parathyroid domain to begin migrating to its final position above the heart (Abramson and Anderson, 2017). During this process the TEC population proliferates and expands, with the proportion of Ki67^{+} TEC peaking around E14.5 (Jenkinson *et al*., 2007). The thymic stroma contains many cell types, in addition to TEC. Neural Crest Cell (NCC) – derived mesenchyme develops in close association to the epithelial compartment. Two studies have lineage traced the contribution of NCC-derived mesenchyme in thymus organogenesis. These both used conditional expression of Yellow Fluorescent Protein to indelibly mark cells, and their progeny, that expressed *Sox10* (*Sox10*^{Cre}:*eYFP*$^{flox/flox}$) or *Wnt1* (*Wnt1*^{Cre}:*eYFP*$^{flox/flox}$) (*Wnt1*^{Cre} - Foster *et al.*, 2008; *Sox10*^{Cre} - Müller *et al.*, 2008). At E11.5 Yellow Fluorescent Protein (YFP)$^{+}$ cells (using the SOX10 system) had encapsulated, but not infiltrated, the epithelium of the thymic rudiment (Müller *et al*., 2008). By E13.5, although most YFP^{+} cells were present in the capsule of the thymus, there was evidence of YFP^{+} cells within the epithelium. This proportion grew through E15.5 to E17.5 at which point there was evidence that the YFP^{+} cells were organising within the thymus into Three-Dimensional (3D) structures. Comparing thymi taken from new-born and three-months postnatal mice, over time there were fewer YFP^{+} cells in the capsule with most cells being within the organ itself, organising into a network associating with vasculature (Foster *et al*., 2008). This was also reported in thymi from eight-months postnatal mice (Müller *et al*., 2008).

It is interesting to note that YFP^{+} cells infiltrated the epithelium after E11.5, but before E13.5. In a study investigating the effect of FOXN1 on haematopoietic colonisation of the rudiment, Itoi and colleagues (2001), showed that fibronectin expressing cells did not infiltrate the nude *(Foxn1*^{null}) thymus between E11.5 and E13.5. Furthermore, in a hypomorphic *Foxn1* variant (*Foxn1*$^{R/R}$), this process was delayed (Nowell *et al*., 2011). Therefore, FOXN1 upregulation at E11.5 appears to instigate NCC-derived mesenchymal infiltration of the thymic anlage.

Collectively, it was concluded that NCC-derived cells contributed to the pericyte population that support the endothelia of the thymus (Foster *et al*., 2008; Müller *et al*., 2008). Both

studies observed a switch from Platelet-Derived Growth Factor Receptor (PDGFR)α^{+}PDGFRβ^{+} to PDGFRα^{-}PDGFRβ^{+} expression pattern, spatially between YFP^{+} cells in the capsule and within the thymus and over time. Foster and colleagues (2008) postulated that this process marked the switch between supporting the proliferation of the epithelium to the vasculature. This is support by knockout models, PDGFRα deficiencies produces hypocellular but functional thymi while PDGFRβ dysfunction predisposes toward microvascular haemorrhaging, affirming the importance of these proteins in these roles (Itoi *et al*., 2007; Jenkinson *et al*., 2007; Levéen *et al*., 1994; Soriano, 1994).

Griffith and colleagues (2009) presented evidence that NCC deficiency, in a *Pax3* null (*Pax3*^{Splotch}) mouse model, affected the patterning of the E10.5 3PP into thymus and parathyroid domains. By E11.5 the *Pax3*^{null} model had a larger proportion of cells specified to a thymic-fate and a smaller parathyroid domain than WT controls. The loss of NCC did not affect cell death or proliferation, demonstrated by maintaining a consistent overall 3PP volume between the mutant and controls, it shifted the border between the parathyroid and thymic domains. The authors noted similarities between this model and a model deficient in Sonic Hedgehog (SHH) and proposed that NCC-derived cells could be contributing to SHH signalling, which is implicated in establishing the parathyroid domain. Furthermore, it was observed that thymic rudiment fails to detach and thus becomes ectopic in the *Pax3* null mutants. While the exact mechanism that mediate this process is known it appears likely to result from perturbation of the NCC-derived mesenchyme (Griffith *et al*., 2009).

The most accepted role played by perithymic mesenchyme is the secretion of factors that promote TEC proliferation and growth such as Fibroblast Growth Factor (FGF) 7 and FGF10, which have a common receptor, FGFR2IIIb (Abramson and Anderson, 2017). FGFR2IIIb deficient (*Fgfr2IIIb* $^{-/-}$) models show extreme hypocellularity within the thymus: comparatively, the WT thymus greatly increased in size until E17.5 while the mutant remained the same (Revest *et al*., 2001). Jenkinson and colleagues (2007), performed kidney grafting experiments of both whole E12.5 thymic lobes and lobes with the encapsulating layer of mesenchyme removed. Grafted Lobes without mesenchyme retained the capacity to support TEC differentiation but the graft did not expand, highlighting both the importance of thymic

mesenchyme (TM) in controlling TEC proliferation but also the ability of the rudiment to develop independently (Auerbach, 1960). The authors noted that all grafted lobes became colonised with kidney capsule-derived mesenchyme. To probe why this was not able to fully compensate for the discarded thymic-derived mesenchyme, the authors examined differences in gene expression, and showed that TM uniquely express IGF1, IGF2, FGF7 and FGF10.

1.2.E. Haematopoietic Colonisation of the Thymus

Expression of *Foxn1* is essential for colonisation of the thymic rudiment by haematopoietic progenitors (Itoi *et al*., 2001). The progenitors first arrive in the mesenchymal layer at E11.5 and begin to migrate into the epithelium at ~E12.0, with this migration being strictly dependent on FOXN1(Luis *et al*., 2016). Haematopoietic colonisation is linked to expression of CCL25, CCL21 and CXCL12 in the rudimental TEC and absence of these chemokines leads to loss of haematopoietic colonisation of the thymic rudiment (Calderón and Boehm, 2011). These represent FOXN1 targets and there is evidence that loss of haematopoietic colonisation in *nude* models (*Foxn1*^{null}) is effect via loss of these chemokines (Žuklys *et al*., 2016).

Ineffective colonisation of the thymus not only prevents the formation of a T-cell repertoire, but also perturbs TEC development, post-E15.5. This dynamic communication between the epithelial and haematopoietic compartments is termed cross-talk (Shores *et al*., 1991). In studies on severe combined immunodeficiency *(SCID)* mice, Singer and colleagues (1991) first observed that the presence of TCR expressing lymphocytes was essential for development of medullary regions in postnatal thymi. This phenotype was reversed upon transplantation of wild-type bone marrow, with the presence of thymocytes stimulating development of a medullary compartment. In a later study, Klug and colleagues (2002) showed that early embryonic TEC patterning occurs correctly in *Rag2* and common cytokine receptor γ-chain-deficient (*Rag*$^{-/-}$*Tcrγ*$^{-/-}$) mice. It was not until E17.5 that the mutants' keratin profiles became distinguishable from WT mice and showed hypoplastic thymi with perturbed TEC patterning. Therefore, crosstalk is dispensable for the initiation of TEC patterning to

generate the cTEC and mTEC sub-lineages and for generation of the cortical compartment, but is essential for further development of an expanded, functional medullary (Klug *et al*., 2002).

As discussed above, mTEC express a range of TRAs and present peptides derived from these proteins to SP thymocytes during negative selection. The ability of mTEC to provide TRAs is called promiscuous gene expression. The transcription factor AIRE has been identified as a key regulator of this process (Anderson *et al*., 2002) and is detectable by E16 (Lopes *et al*., 2015). To date, two lymphoid contributors have been implicated in the cross-talk process required to establish *Aire* expression in mTEC: the lymphoid tissue inducer (LTi) ($CD3^{-}CD4^{+}IL\text{-}7R\alpha^{+}$) and the invariant $V\gamma5^{+}TCR^{+}$ dendritic epidermal T-cell (DETC) progenitor (Roberts *et al*., 2012). Knocking out LTi using RAR-related orphan receptor gamma deficient *(Rorc*$^{-/-}$) mice or DETC using TCRδ knockout (*Tcrδ*$^{-/-}$*)* mice resulted in a significant reduction of *Aire*$^{+}$ mTEC by E17. Double knockout mice had a further reduction, confirming the importance of both lymphocytes in establishing a functioning medulla. It is interesting to highlight that the double knockout did not abolish *Aire* expression and that therefore additional uncharacterised mechanisms may also regulate *Aire* expression.

The current model for mTEC development suggests a stepwise differentiation process, with cells progressively differentiating through phenotypically defined mTEC progenitor stages. Activation of the Nuclear Factor Kappa-B (NFκ-B) signalling pathway by Receptor Activator of Nuclear Factor kappa-B (RANK), a member of the Tumour Necrosis Factor (TNF) superfamily, and Lymphotoxin β is crucial for generation of $AIRE^{+}$ mTEC; ablation of RANK on mTEC or RANK-ligand (RANKL) on lymphoid cells resulted in a suppression of AIRE expression in the embryonic thymus (Akiyama *et al*., 2016, 2008; Cosway *et al*., 2017). Note, that this section only covers the haematopoietic influences on medullary formation. The specification of mTEC will be discussed in greater detail, which aims to discuss the developmental pathways of TEC.

1.2.F. Molecular Mechanisms Dictating Thymic Organogenesis

1.2.F.I. Thymic Morphogenesis

Other than FOXN1, Bone Morphogenetic Protein 4 (BMP4), Wingless/Integrated (WNT) and SHH are heavily implicated in thymic development. *Bmp4* is expressed in the ventral thymic-fated 3PP endoderm and surrounding mesenchyme between E10.5 and E12.5, whilst its antagonist *Noggin* is expressed in the dorsal, parathyroid region of the 3PP (Patel *et al*., 2006). Gordon and colleagues (2010), used three conditional models to knock out *Bmp4* in the 3PP epithelium and mesenchyme from E9.5 using *Foxg1*^{Cre}, in TEC from E11.5 using *Foxn1*^{Cre} and in the NCC-derived mesenchyme using *Wnt1*^{Cre}. The *Foxg1*^{Cre} model led to perturbations in morphogenic events such as: separation of the thymic from the parathyroid primordium; migration of the E12.5 thymus; colonisation by haematopoietic cells and formation of the mesenchymal thymic capsule, while cell differentiation, specification and *Foxn1* expression remained intact but delayed. This phenotype was not present when *Bmp4* was deleted solely in TEC from E11.5. Furthermore, deletion of *Bmp4* solely in the mesenchyme using Wnt1^{Cre} did not result in a phenotype. Collectively, these data suggest that *Bmp4* is necessary for only a short window of time, during the FOXN1-independent phase of thymic development, and that expression in the 3PP endoderm rather than in the surrounding mesenchyme is essential for normal thymus development.

Note, that removing *Bmp4* expression using the *Foxg1*^{Cre} did not ablate BMP signalling within the rudiment. There was no difference when the mutant and WT littermates were stained for phosphorylated SMAD 1/5/8, which was used as a readout of active BMP signalling. Therefore, the described effects should be attributed to loss of BMP4 originating in the 3PP epithelium and mesenchyme rather than complete abolition of BMP signalling. Furthermore, the expression pattern of *Foxg1*^{Cre} in the mesenchyme was inconsistent, with differences being noted between embryos and between the left and right rudiments within the same embryo.

1.2.F.II. Regulation of *Foxn1* expression

Prior to the above publication, there was evidence linking BMP4 to positive regulation of *Foxn1* (Bleul and Boehm, 2005; Soza-Ried *et al*., 2008; Tsai *et al*., 2003). The *Foxg1*^{Cre} model was associated with a delay in organ separation, lumen closure and haematopoietic

colonisation. Therefore, the model might reduce but not ablate BMP signalling to diminish positive regulation of *Foxn1* and slow, rather than prevent the mechanics, of these FOXN1-dependent processes (Gordon *et al*., 2010).

A more recent publication further probed the cooperative interaction between BMP4 and *Foxn1* (Swann *et al*., 2017a). Noggin is an antagonist of BMP4 and if the above mechanism is true, therefore a negative regulator of *Foxn1*. By placing Noggin under control of the *Foxn1* promotor (*Foxn1*^{Noggin}), the authors created a system in which *Foxn1* activation is representative of WT but once activated its becomes repressed by production of Noggin and inhibition of BMP2, 4 and 7 signalling (Bleul and Boehm, 2005). In this model, the E15.5 thymus was a mosaic of *Foxn1*$^{+}$ and *Foxn1*$^{-}$ TEC. This expression pattern is notable when compared to reducing the amount of FOXN1 within the system by introducing a null allele (*Foxn1*$^{-}$). Mice heterozygous with the *Foxn1* null allele (*Foxn1*$^{-/+}$) have smaller thymi without the population of *Foxn1*$^{-}$ TEC. Therefore, a comparison between these two systems highlights the differences between TEC expressing less *Foxn1* from the point of initiation and TEC that expressed WT levels of *Foxn1* at the point of initiation but, as the levels of Noggin steady increased, were unable to positively regulate its expression via BMP signalling. The mosaic pattern of *Foxn1*$^{+}$ and *Foxn1*$^{-}$ TEC of the (*Foxn1*^{Noggin}) mouse shows that some TEC fail to maintain *Foxn1* expression in the absence of BMP signalling.

The role played by WNT signalling in regulating *Foxn1* expression is not completely understood. In 2002, Balciunaite and colleagues demonstrated *Wnt4* and *Wnt5b* mRNA expression in 3PP cells obtained by laser-capture microdissection. The same authors demonstrated by over expression assays in cell lines that stimulation of WNT signalling resulted in increased *Foxn1* expression. However, a more recent study, did not support these findings (Swann *et al*., 2017b). These investigators knocked out β-catenin, the obligate intracellular regulator of canonical WNT signalling, in all TEC from ~E12.0 using *Foxn1*^{Cre} (*Foxn1*^{Cre}:*Ctnnb*$^{flox/flox}$) and also studied constitutive Nlk deficient (*Nlk*$^{-/-}$) mice in which noncanonical WNT signalling is abrogated. At E15.5 both models had correctly positioned thymi, with cortical and medullary architecture and robust *Foxn1* expression, but with reduced total cellularity and a proportional reduction in cTEC.

In addition, these investigators tested the hypothesis that *Wnt* overexpression upregulates *Foxn1*. The authors produced models with TEC- specific over-expression of WNT4 (*Foxn1*^{Wnt4}) and stabilised β-catenin (*Foxn1*^{Ctnnb}). No thymic tissue was detectable in the thoracic cavity of new-born mice with TEC- specific over-expression of β-catenin (*Foxn1*^{Ctnnb}). Using a LacZ reporter (*Foxn1*^{lacZ}) an ectopic rudiment was traced to the cervical region, approximately level with the thyroid cartilage. In E15.5 embryos of the TEC-conditional expression of β-catenin (*Foxn1*^{Ctnnb}), the characteristic TEC networks were replaced with cystic structures of squamous epithelium and migration of the rudiment was found to be arrested laterally to the carotid artery. Early E12.5 tissues were also heavily perturbed with the thymus and parathyroid domains failing to separate from each other. At both embryonic ages, levels of FOXN1 was reduced compared to those found in WT tissues as shown on both the mRNA and protein level (using a *Foxn1*^{EGFP} reporter). In turn this prevented haematopoietic colonisation of the rudiment, which persisted to adulthood. Note that this model (*Foxn1*^{Ctnnb}) perturbed the migration but not function of the parathyroid.

The TEC-specific WNT4 over-expression model (*Foxn1*^{Wnt4}) had a less pronounced phenotype, which is in keeping with model producing a weaker activation of WNT target genes than the β-catenin over-expression model (*Foxn1*^{Ctnnb}). Migration of the rudiment was still perturbed, in E15.5 embryos it was situated adjacent to the trachea and level with the thyroid cartilage. However, there was evidence of reticulated TEC architecture and haematopoietic colonisation. Focusing on new-born tissues, there was a reduced total cellularity within the transgenic thymi including TEC, compared to the WT. Notably, the cortical (Ly51^{+}) and medulla (UEA1^{+}) TEC patterning was perturbed with a relative increase in the number of unassigned TEC (Ly51^{-}UEA1^{-}) and aberrant populations with intermediate staining profiles. The authors concluded that WNT overexpression dysregulated TEC differentiation or selective survival of atypical TEC subsets.

Given the proposition that the TEC-specific overexpression of β-catenin (*Foxn1*^{Ctnnb}) produces a greater over expression of WNT targets than the TEC-specific WNT4 over-expression model (*Foxn1*^{Wnt4}), it can be stated that as WNT signalling was more excessively expressed, the perturbation of thymic organogenesis was increased. This can be linked to

FOXN1, both directly as demonstrated in the overexpression of β-catenin (*Foxn1*^{Ctnnb}) model on the mRNA and protein level, compared to WT, and the inhibition of key FOXN1-associated features of thymic organogenesis such as haematopoietic colonisation and organisation of the TEC structure in the β-catenin over-expression (*Foxn1*^{Ctnnb}) compared to the WNT4 over-expression model (*Foxn1*^{Wnt4}). Therefore, the above is evidence that WNT signalling negative regulates FOXN1.

It was also demonstrated that the TEC-specific WNT4 over-expression model (*Foxn1*^{Wnt4}) prevented TEC from differentiating from a presumptive non-patterned state (Ly51^{-}UEA1^{-}) and/or heavily selected for the survival/proliferation of this population at the expense of the other subsets found in new-born thymus. Furthermore, TEC-specific loss of β-catenin (*Foxn1*^{Cre}:*Ctnnb*$^{flox/flox}$) and therefore activation of WNT associated target genes, reduced total cellularity of the thymus and increased the proportion of cTEC over mTEC. Collectively, increasing WNT prevented TEC from correctly differentiating while decreasing WNT increased the number of mTEC compared to cTEC from initiation of *Foxn1* to E15.5.

The role of canonical WNT signalling in the activation of FOXN1 was not investigated in the above study. However early work from Mulroy and colleagues (2002) provide evidence that *Wnt1* and *Wnt4* double knockout (*Wnt1*$^{-/-}$*Wnt4*$^{-/-}$) mice have thymi capable of supporting thymopoiesis, with significantly less total cellularity, until the phenotype results in death at birth, suggesting it is not required for thymic function or *Foxn1* expression but expansion of either the whole thymus or haematopoietic compartment.

All three members of the Hedgehog family are expressed in the thymus (Saldaña *et al*., 2016). Focusing on SHH, there is evidence that it is instrumental in deciding the parathyroid – thymus fate boundaries. Model with a constitutive SHH knockout (*Shh*$^{-/-}$), do not develop a parathyroid domain as shown by *Foxn1* expression extending to the pharynx of the shared rudiment (Moore-Scott and Manley, 2005). Gain of function studies were used to assess whether overexpression of SHH would alter the boundaries between the rudiment. Most notably, SHH was conditionally activated in the endoderm (*Foxa2*^{CreERt2}*Rosa26*$^{floxSTOPflox:SmoM2}$) by enforcing expression of an active form of Smoothened (SmoM2). This

induced expression of GCM2 (glial cells missing transcription factor 2) in the central domain, partially extending into the ventral domain of the shared rudiment. Expression of *Tbx1* was negatively associated with *Foxn1*, which suggests that SHH acts to negatively regulate *Foxn1* via TBX1. As noted above BMP4 is an essential positive regulator of FOXN1, enforced activation of the SHH signalling pathway in the endoderm (*Foxa2*^{CreERt2}:*Rosa26*^{floxSTOPflox}:SmoM2) did not affect BMP4, leading the authors to postulate that BMP4 inhibits TBX1, which ensured the ventral domain of the rudiment retained *Foxn1* and thymus specification (Bain *et al*., 2016).

Saldaña and colleagues (2016) found that SHH deficient (*Shh*$^{-/-}$) E15.5 embryos had a smaller thymus with a significantly lower proportion of cTEC to mTEC than WT littermates, but retained *Foxn1* expression. Due to embryonic lethality, the E15.5 thymi were cultured using a FTOC system, the mutant cultures developed fewer total TEC and a reduced proportion were mTEC. Interestingly, MHC2 was higher in mutant FTOC. To isolate the effect of SHH to the FOXN1-dependant phase, the authors used a TEC-specific conditional knockout (*Foxn1*^{Cre}*Shh*$^{flox/flox}$) model. The TEC phenotype paralleled that of the constituent knockout FTOC. When examining the effect on thymopoiesis, the mutated thymi contained a higher proportion of SP4 and SP8 against DP thymocytes with higher expression of CD3 and CD5. This conclusion was confirmed by a recent study on Gli3 knockout (*Gli3*$^{-/-}$) mutants highlighting the Shh repression promotes thymocyte differentiation and positive selection (Solanki *et al*., 2018). That both constituent and TEC-conditional SHH deficiency models report a similar phenotype highlights that the correct Shh - Gli3 interplay is essential throughout organogenesis.

1.2.F.III. Bipotent Progenitor TEC

Patterning of the thymus into functionally distinct cortical and medullary regions occurs early in thymic development (Klug *et al*., 2002; Nowell *et al*., 2011; Rodewald, 2008). Klug and colleagues used Keratin expression to track the emergence of cTEC and mTEC throughout organogenesis, using Keratin 8 (K8) to identify cTEC and Keratin 5 (K5), mTEC (Klug *et al*., 2002, 1998). These authors showed that at E11.5 3PP endoderm was exclusively K8^{+}K5^{-}.

However as early as E12.5, the central region of the rudiment contained a population of $K8^{+}K5^{+}$ TEC. This double positive population was maintained until E15.5 when $K8^{-}K5^{+}$ TEC emerge to form the earliest TEC population with an mTEC-like Keratin profile. However, later papers show evidence that emergence of the medulla lineage occurs earlier (Baik *et al*., 2016; Nowell *et al*., 2011; Rodewald *et al*., 2001). It is now clear that, during thymus organogenesis, a common thymic epithelial progenitor cell (TEPC) can exist. As discussed above, Boehm colleagues (2006), using a mouse model homozygous for a revertible null Foxn1 allele, showed that a single TEPC could produce small thymi containing both cTEC and mTEC progeny. Concurrently, Rossi and colleagues (2006) showed that when a single E12.5 TEC was injected into a host E12.5 thymus and grafted on to the kidney capsule, it was able to contribute to both the medulla and the cortex of the graft.

The putative existence and identity of the bipotent TEPC was presented four years previously. Bennett and colleagues (2002) showed that dissociated E12.5 $PLET1^{+}$ TEC were able to form functional thymi with normal cortical and medullary architecture, when grafted under the kidney capsule in nude mice (Bennett *et al*., 2002; Depreter *et al*., 2008). A later study determined that E12.5 TEC almost uniformly (95%) expressed PLET1, aligning the data presented by Rossi, and Bennett, *et al*. (Rossi *et al*., 2006). The same functionality was extended to E15.5 $PLET1^{+}MHC2^{+}$ TEC, which were able to constitute a patterned thymus capable of mediating thymopoiesis when grafted onto the kidney capsule of syngeneic mice (Gill *et al*., 2002).

Controversy arose around whether $PLET1^{+}$ TEPC were a sub-population of progenitor TEC or whether early TEC contain transient bipotency that was lost throughout development. Rossi and colleagues (2007), performed kidney graft experiments using $PLET1^{+}$ and $PLET1^{-}$ TEC from E14.5, E16.5 and E18.5. Strikingly in the E14.5 and E16.5 timepoints, both $PLET1^{+}$ and $PLET1^{-}$ TEC produced patterned grafts. Furthermore, using E18.5 tissue, $PLET1^{+}$ TEC were unable to form grafts while PLET1- were.

Whilst it is clear that PLET1 marks bipotent founder TEC in the early thymic primordium, whether or not it marks TEPC (either bipotent or sub-lineage restricted) at later stages

should be re-evaluated with contemporary understanding of self-organisation (Gjorevski *et al*., 2014). Given the evidence that the medulla emerges early in the TEC developmental program, both Gill (2002) and Rossi (2007) contributed both progenitor and pre-patterned TEC into the grafts. This makes it difficult to distinguish between whether the successful formation of the grafts can be attributed to the progenitors, which differentiated into functioning cortical and medulla compartments, or the pre-patterned TEC self-organising into functioning cortical and medulla compartments. The more mature the input thymic tissue, the more vulnerable the experiment is to this error (Baik *et al*., 2016; Nowell *et al*., 2011; Rodewald *et al*., 2001). Self-organisation also explains the contrasting result that Gill and colleagues were unable to successfully recover grafted E15.5 PLET1^{-} TEC while Rossi and colleagues were able to recover 83.3% of E14.5 and 100% of E16.5 PLET1^{-} grafts. Rossi and colleagues used 100,000 TEC in each graft while Gill and colleagues used 2,500. The large disparity in input number highlights that Rossi and colleagues' experimental design was more vulnerable to incorrectly attributing graft survival as a consequence of progenitor action, rather than self-organisation of a large body of pre-patterned TEC. Collectively, these studies conclusively show that at E12.5, PLET1 marks progenitor TEC, while at E18.5, most PLET1^{+} TEC do not appear to function as TEPC. The role of TEPC and of PLET1 throughout thymic organogenesis requires further elucidation. However, a more recent study demonstrated that the only bipotent progenitor TEC population that could be identified in the adult thymus using a clonal-resolution, transplantation assay, was PLET1^{+} (Ulyanchenko *et al*., 2016).

1.2.G. mTEC Divergence from the Common Progenitor

How mature lineage-restricted TEC are generated from bipotent TEPC is not clear. Some evidence suggests that cortical / medullary divergence is FOXN1-independent and does not require haematopoietic-derived cross-talk, with further evidence suggesting that for the mTEC lineage, emergence is independent of RELB (Baik *et al*., 2016; Klug *et al*., 2002; Nowell *et al*., 2011). There is evidence that mTEC lineage is the progeny of cells that expressed markers associated with cortical function. The hypothesis that all TEC pass through a β5t^{+} stage was strongly supported by two *in vivo* lineage tracing studies. Here,

β5t$^+$ TEC were heritably labelled using a doxycycline-regulatable Cre in conjunction with *β5t-rtTA* (Mayer *et al*., 2016) or by knocking Cre into β5t (Ohigashi *et al*., 2013). Both studies found that a substantial proportion of mTEC had arisen from progenitors that once expressed β5t.

Evidence exists for mTEC-restricted progenitors. The lineage-restricted hypothesis was initiated from early evidence that each medullary islet was the progeny of an individual cell (Rodewald *et al*., 2001). In 2014, Sekai and colleagues (2014), proposed and phenotypically characterised lineage-restricted progenitors using expression of the tight junction components Claudin-3 and Claudin-4 (CLDN3/4) and functionally validated them using the *aly/aly* mouse model, which has defective NF-κB–inducing kinase (NIK) and thus impaired mTEC development. This phenotype was rescued in RTOC experiments in which E14.5 *aly*/*aly* TEC were mixed with sorted CLDN3$^+$CLDN4$^+$ WT TEC. The graft contained functional AIRE$^+$ mTEC that prevented development of multiorgan autoimmunity and did not contribute to the cortex. Given that *Cldn3* and *Cldn4* are expressed in mature mTEC, to better characterise the progenitor population the authors proposed the marker SSEA1. When reaggregated with age-matched dissociated thymic cells and grafted under the kidney capsule, E14.5 SSEA1$^+$CLDN3$^+$CLDN4$^+$ cells had significantly greater reconstitution potential then SSEA1$^-$CLDN3$^+$CLDN4$^+$ cells. While these cells were proposed as mTEC stem cells, convincing evidence for self-renewal of this population has not been shown (Sekai *et al*., 2014).

In 2016, two papers investigated the role of NF-κB in the differentiation of the proposed mTEC stem cell (Akiyama *et al*., 2016; Baik *et al*., 2016). In an effort to characterise the effect of RANK on these, Baik and colleagues (2016) engineered a *Rank*^{VENUS} reporter model and found that SSEA1$^+$CLDN3$^+$CLDN4$^+$ mTEC did not express RANK. Throughout organogenesis, within the CLDN3$^+$CLDN4$^+$ TEC population, RANK expression emerged as a nonoverlapping population with SSEA1$^+$ mTEC. When spiked into an age-matched RTOC, RANK$^+$SSEA1$^-$CLDN3$^+$CLDN4$^+$ preferentially contributed mTEC progeny. Therefore, the authors hypothesised that RANK expression is essential for downstream differentiation in a RELB dependant mechanism (Baik *et al*., 2016).

Akiyama and colleagues (2016) presented evidence of a similar progenitor population that exhibited RANK expression. However, this population also bound Ulex Europaeus Agglutinin I (UEA1), which is regarded as a pan-mTEC marker. Akiyama and colleagues showed that grafted-RTOC (gRTOC) generated from *aly/aly* thymi and spiked with $UEA1^{+}RANK^{high}MHC2^{mid}CD80^{-}$ TEC (termed pMECs) were also able to generate $AIRE^{+}$ medullary regions and rescue the autoimmune phenotype. It was shown that canonical NF-κβ (*Traf6*$^{-/-}$) and noncanonical NF-κβ (*Relb*$^{-/-}$) deficient models blocked pMEC differentiation at different stages. In *Traf6*$^{-/-}$ thymi, mTEC differentiation was blocked at the pMEC stage ($UEA1^{+}RANK^{high}MHC2^{mid}CD80^{-}$), while in *Relb*$^{-/-}$ thymi mTEC differentiation was blocked at a $UEA1^{+}RANK^{lo}MHC2^{lo}CD24^{hi}$ stage (termed pro-pMECs), which was proposed to represent an earlier stage of mTEC development. Pro-pMECs were able to differentiate into functional $AIRE^{+}$ mTEC when spiked into *aly/aly* gRTOC. Collectively, these data suggested a model in which RANK and LTβR activation of RELB induce pro-pMECs to differentiate to generate pMEC and then RANK activation of TRAF6 is required for pMECs to differentiate into mature $AIRE^{+}$ mTEC. However, the picture of mTEC differentiation is far from complete.

1.2.H. cTEC Lineage Specialisations

Despite evidence that the all TEC, are progeny from cells expressing markers that persist through the cTEC lineage and are essential for its function, the cTEC are not a persistent bipotent progenitor population (Mayer *et al*., 2016; Ohigashi *et al*., 2013). As discussed previously, cTEC are specialist cells responsible for enforcing T-cell lineage upon recent haematopoietic immigrants and for mediating positive selection, in which cTEC employ unique peptide processing and presentation machinery (Figure C1.3) (Hozumi *et al*., 2008; Kincaid *et al*., 2016; Koch *et al*., 2008). This can be separated into processes that generate the peptide repertoire for presentation to SP8 thymocytes on MHC1 and to SP4 thymocytes on MHC2.

Newly formed MHC2 proteins contain an invariant chain (Ii) in the prospective peptide binding domain (Takada *et al*., 2017). Once transferred to a late endosome, Ii is proteolytically degraded leaving a peptide formed of amino acids 81 to 104 bound to the

MHC2 peptide binding groove (Nakagawa *et al*., 1998). This short peptide is termed CLIP. In a process catalysed by H-2M in mouse and HLA-DM in humans, CLIP is replaced with peptides present in the endosome for presentation on MHC2 (Honey *et al*., 2002; Takada *et al*., 2017) (Figure C1.3).

In cTEC there are two unique proteins that shape the MHC Class II peptide repertoire. Thymus-specific serine protease (TSSP) plays a critical yet undefined role in peptide processing as shown by TSSP deficient (*Prss16*$^{-/-}$) mouse models (Gommeaux *et al* 2009) (Figure C1.3). The TSSP deficient thymus had reduced MHC2^{high} cTEC, but similar thymic and peripheral T-cell cellularity at 10-11 weeks postnatal mice. The proportions of SP4 / SP8 thymocytes were also reported to be similar although these data were not shown. However, when crossed onto the Class II-restricted TCR transgenic lines Marilyn and OT-II, there was a loss of SP4 T-cells compared to both *Prss16*$^{+/+}$ and *Prss16*$^{-/+}$ controls. This indicates that TSSP deficient cTEC either present a smaller variety of peptides or do not effectively modify peptides to have the desired avidity for TCR, which is compensated for by TCR diversity in WT mice but is observable in TCR transgenic strains. Notably, there was no phenotype when crossed onto the OT-I TCR transgenic line, confirming that TSSPs role is exclusive to MHC2 and SP4 T-cell generation (Gommeaux *et al*., 2009). Later studies show that TSSP deficiency affects the peripheral function of SP4 T-cells, which express an altered TCR repertoire that lead to poorer antigen responses and resistance of NOD models to colitis-associated colorectal tumour formation and diabetes compared to controls (Brisson *et al*., 2015; Serre *et al*., 2015; Viret *et al*., 2015).

Another key protein is cathepsin L in the mouse (the human homolog is cathepsin V or cathepsin L2), which plays a vital role in proteolytic degradation of Ii into CLIP to process self-peptides for presentation (Figure C1.3). Its expression is unique to cTEC (Honey *et al*., 2002; Nakagawa *et al*., 1998), with other APCs, including mTEC, expressing alternative proteins such as cathepsin S (Shi *et al*., 1999; Takada *et al*., 2017). Nakagawa and colleagues (1998) characterised the cathepsin L deficient mouse model (*Ctsl*$^{-/-}$), highlighting that the thymic and peripheral SP4 T-cell counts were 60-80% reduced and demonstrated

weaker responses to antigen stimulation compared to heterozygous (*Ctsl*$^{+/-}$) littermates. T-cells remained self-tolerant, providing evidence that Cathepsin L affects SP4 T-cell generation and positive selection but not negative selection. Subsequently, the Rudensky group published a report showing Cathepsin L mediated this effect both via the degradation of Ii into CLIP and also by regulating the processing of peptides for MHC2 presentation (Honey *et al*., 2002). Furthermore, the group engineered a CIITA-expressing fibroblast cell line to compare the peptides generated by cathepsin L and cathepsin S, and concluded that each produced an overlapping but non-redundant peptide repertoire (Hsieh *et al*., 2002).

cTEC also express unique peptide processing mechanisms to generate self-peptides for expression in the context of MHC1, for positive selection (Figure C1.3). The leading model of positive selection is the affinity model, which suggests that the affinity of the TCR-peptide:MHC interaction determines whether a thymocyte successfully undergoes positive selection (Takada *et al*., 2017). In 1994, Hogquist and colleagues reported observations from the OT-I TCR transgenic model, in which thymocytes express a TCR that recognises the chicken ovalbumin peptide 257-264 (SIINFEKL) in the context of MHC Class I. Amino acid substitutions were used to increase or decrease the affinity of the peptide to the transgenic TCR. The authors showed higher affinity peptides biased toward negative selection while lower affinity induced positive selection (Hogquist *et al*., 1994; Takada *et al*., 2017).

Most nucleated cells present self-peptides upon MHC1 as part of immunosurveillance. Many of these are derived from cytoplasmic self-proteins, which are degraded by proteasomes before being tagged to the endoplasmic reticulum via Transporter Associated with Antigen Processing (TAP) (Figure C1.3). The peptides are loaded upon MHC1 and relocated to the cellular membrane for presentation (Takada *et al*., 2017). cTEC employ a specialised proteasome which generates a unique peptide repertoire for presentation upon MHC1 (Figure C1.3). There are three types of proteasome. All three types contain four heptameric rings aligned into a barrel shape with two outer α-rings and two inner β-rings (Groll *et al*., 1997; Unno *et al*., 2002). It is the composition of the β-ring that differentiates the proteasomes. The constituent proteasome has β1 to β7 subunits, the immunoproteasome has IFN-γ–inducible subunits β1i, β2i, β5i in place of the numerical counterparts. In the

thymus, the thymoproteasome substitutes in β5t (*Psmb11*) in place of β5i, and is unique to cTEC (Murata *et al*., 2007; Ripen *et al*., 2011). Kincaid and colleagues (2016) engineered knockout mice that lacked β1i *(Psmb9$^{-/-}$)*, β2i *(Psmb10$^{-/-}$)*, β5i *(Psmb8$^{-/-}$)* and β5t *(Psmb11$^{-/-}$)*, and in which the thymoproteasome was thus replaced with the constituent proteasome in cTEC. The peptide repertoire generated by the constituent proteasome was unable to mediate positive selection, as demonstrated by a >90% loss of TCRβ^{+} SP8 T-cells in this model.

To compare the effect of the immunoproteasome to the thymoproteasome, Murata and colleagues (2007) replaced the single exon of *Psmb11* with the *Venus* Fluorescent protein, to engineer the β5t deficient mouse *(Psmb11$^{-/-}$)*. In this mouse, cTEC expressed β5i rather than β5t; effectively substituting the thymoproteasome for the immunoproteasome. β5t deficient cTEC were shown to have a functioning, MHC1-loading, peptide processing pathway. However, the peptide repertoire presented to thymocytes was altered (Takada *et al*., 2017). The loss of β5t and its associated peptide repertoire substantially diminished the size of the SP8 T-cell population in both the thymus and periphery demonstrating a clear role for β5t in SP8 thymocyte generation. Within the thymus, the β5t deficient model produced, on average 24% less SP8 thymocytes which were associated with less TCRβ^{high} cells (50.2%) compared to WT (80.7%). Follow up studies found T-cells positively selected on immunoproteasome-derived peptides also displayed weaker immune responsiveness and TCR diversity (Nitta *et al*., 2010; Takada *et al*., 2015). Collectively, these data have established that, while the thymoproteasome is not essential for SP8 T-cell generation, it is required for normal positive selection and production of a functional SP8 T cell repertoire.

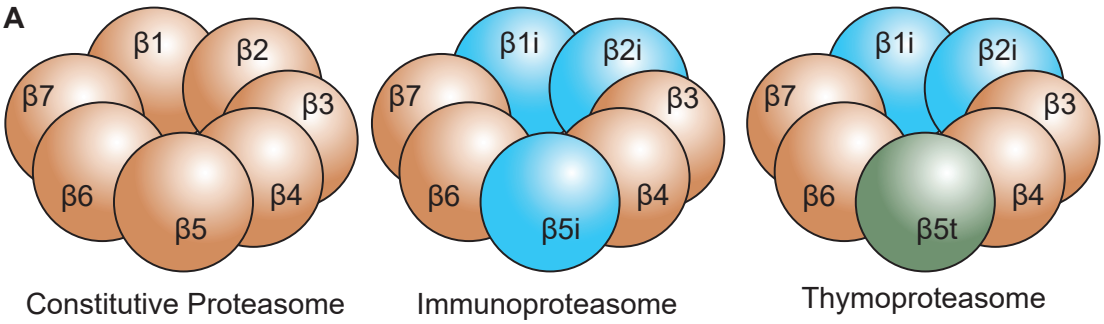

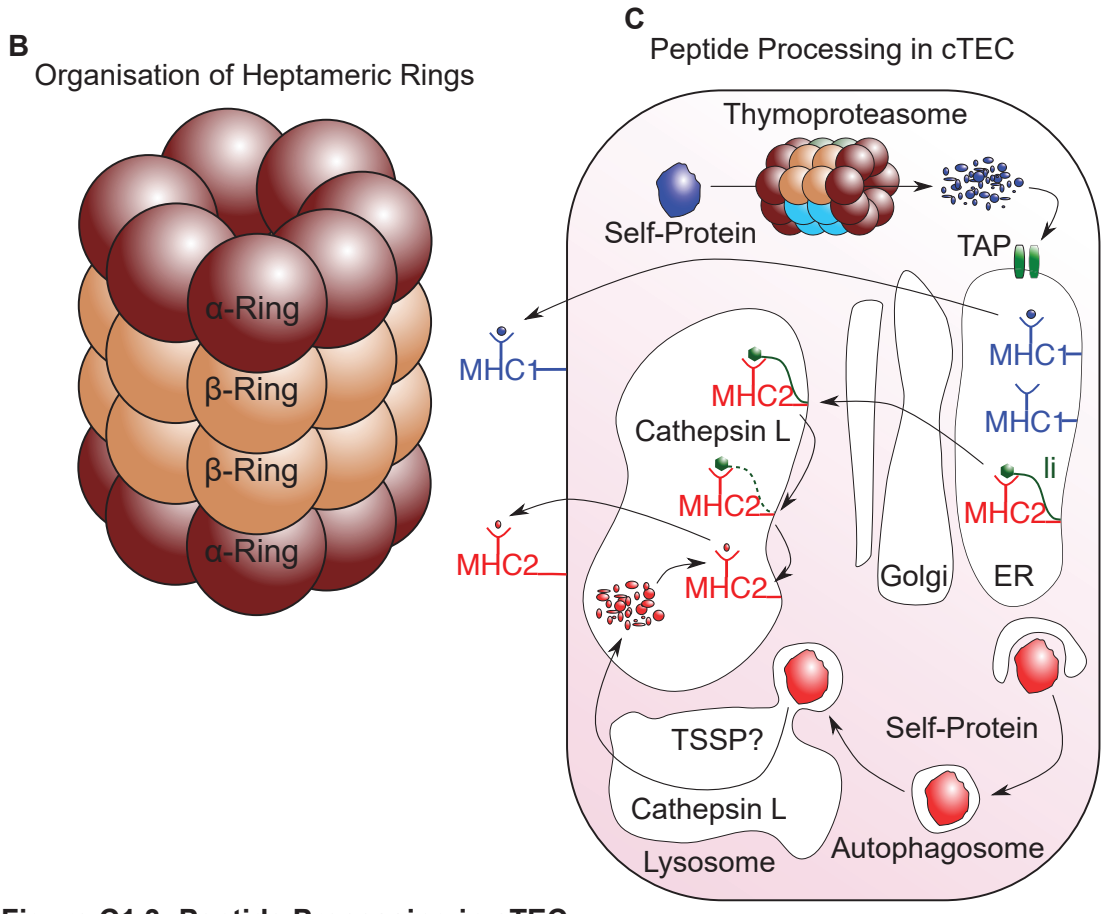

Figure C1.3: Peptide Processing in cTEC

A. Representative diagram of the composition of the β-rings of the constitutive proteasome, immunoproteasome and thymoproteasome. The β5t sub-unit is unique to the thymoproteasome, which is exclusively expressed in cTEC. **B**. The organisation of the α-rings and β-rings in the 20s proteasome. **C**. The peptide processing in cTEC. Invariant chain (Ii), endoplasmic reticulum (ER), major histocompatibility complex (MHC), transporter associated with antigen processing (TAP), thymus-specific serine protease (TSSP). Images adapted from Takada, Kondo and Takahama, 2017.

1.3. Strategies for Supporting T cell Development *in vitro*

Development of an *in vitro* culture system that fully recapitulates the thymus functions required to support T cell differentiation and repertoire selection has not yet been achieved. Currently used methods are unable to preserve key *in vivo* characteristics of primary thymic stromal cells and established cell lines fail to recapitulate the original tissue (Anderson *et al*., 1998; Anderson and Jenkinson, 2007; Auerbach, 1960; Jenkinson and Anderson, 1994). Auerbach described a system for culturing whole thymic lobes *in vitro*, that was able to sustain thymopoiesis (Auerbach, 1960; Jenkinson and Owen, 1990). Subsequent investigators refined this technique by including a dissociation, selection and reaggregation process, hence developing a system that could be used to determine individual contributions to thymopoiesis (Anderson *et al*., 1993). Attempts to simplify this approach have largely hinged around establishing thymic stromal cell lines, able to support some or all elements of thymopoiesis in monolayer culture conditions, but to date these have essentially been unsuccessful.

To circumvent this problem, and Schmitt and colleagues (2002) showed that transgenic expression of the Notch ligand DLL1 in the OP9 bone marrow stromal cell line enabled this line to mediate T-cell lineage commitment of haematopoietic precursors, and to support subsequent thymopoiesis to the double positive stage of development. This *in vitro* model has facilitated investigation of T-cell lineage development and has prompted the creation of other cell-line based systems (Montel-Hagen *et al*., 2019; Seet *et al*., 2017; Shukla *et al*., 2017; Simons *et al*., 2018). Additionally, some progress has been made towards producing thymic stromal cells *in vitro* using directed differentiation and direct lineage reprogramming strategies (Bredenkamp *et al*., 2014; Lai and Jin, 2009; Su *et al*., 2015). The above strategies are each discussed in detail below, in relation to their ability to support native thymopoiesis and their current technical limitations.

1.3.A. Culture systems recapitulating the Native Thymic Environment

1.3.A.I. FTOC and RTOC

Early attempts to recapitulate T cell development *in vitro* utilised explant culture of fetal thymic lobes, and this model is still used today (Anderson *et al*., 1993; Auerbach, 1960; Jenkinson *et al*., 1982). In brief, dissected whole embryonic thymic rudiments are cultured at the liquid-air interface, supported by a porous membrane that mediates nutrient exchange between the lobe and tissue culture medium. The position of the lobe, exposed to air, was found to be beneficial to αβ T-cell development, a metabolically active process hypothesized to have a high oxygen demand (Germeraad *et al*., 2003). This culture system is called FTOC. Strikingly, FTOC allows not only the lymphoid cells initially contained within the explanted thymus, but also exogenously supplied lymphoid progenitors, to undergo thymopoiesis, even when the two components are harvested from different species (Fisher *et al*., 1990). This was first demonstrated in experiments in which the explanted lobe was initially depleted for lymphoid cells, by culture in 1.35 mM 2-deoxyguanosine (2-dGuo) for five-days, and subsequently supplied with T-cell precursors from a different genetic background (Jenkinson *et al*., 1982). This accessible system for supporting thymopoiesis from a defined starting haematopoietic population proved an essential tool for understanding thymic biology. For example, Godfrey and colleagues (1993) used this methodology to characterise the progression of thymocytes through T-cell lineage specification based upon CD25 and CD44 expression, which remains standard nomenclature (Petrie and Zúñiga-Pflücker, 2007).

Jenkinson and colleagues (1992) developed an important extension to the FTOC approach, by including a step that allowed examination of the role of individual stromal and haematopoietic components in the regulation of thymopoiesis. This was achieved by dissociating fetal thymic lobes into a single cell suspension, then reaggregating selected thymic elements and culturing the reaggregated fetal thymic tissue as required (Anderson *et al*., 1993). This technique is termed Reaggregate Thymic Organ Culture (RTOC). RTOC may also be grafted into an ectopic location in a recipient mouse (grafted RTOC; gRTOC). The site most often used is the kidney capsule, which allows the RTOC to develop, with host-derived vasculature supporting haematopoietic immigration and emigration (Bennett *et al*., 2002; Rodewald *et al*., 2001). This process is widely used to investigate aspects of thymus

biology including TEC differentiation, and engrafting into immunodeficient mice allows observation of how thymopoiesis affects peripheral TCR repertoire composition and function (Bennett *et al*., 2002; Rodewald *et al*., 2001). Notably, unlike their *in vitro* counterparts, gRTOC undergo self-organisation such that clear cortical and medullary compartments are present in the recovered grafts (Bennett *et al*., 2002; Rodewald *et al*., 2001).

TEC are highly sensitive to their microenvironment, and have been shown to dramatically alter their gene expression profiles when removed from the thymic niche (Anderson *et al*., 1998). It was demonstrated that upon culture in skin stem cell conditions, some TECs were reprogrammed into a multipotent skin stem cell-like state, that could contribute to the skin and hair follicle in the skin morphogenetic assay, whilst losing the ability to mediate thymopoiesis (Bonfanti *et al*., 2010). This suggests that one of the principals underlying the success of FTOC is that preservation of the thymic niche preserves TEC function.

It should be noted that the degree to which RTOC recapitulate native thymus functionality has not been fully quantified. Given the precise molecular cascades governing TEC differentiation, the sensitivity of TEC to the surrounding microenvironment and the highly disruptive nature of RTOC generation, it is pertinent to assume that TEC differentiation is at least partially perturbed when creating RTOC. This is a potentially confounding variable when generalising from the behaviour of TEC in gRTOC to that of the native thymus, including around TEC progenitor regulation. Thus, *in vitro* assays cannot be considered conclusive evidence of native TEC behaviours *in vivo*.

RTOC remains the only system in which T-cell differentiation, central tolerance and TEC differentiation can all be modelled (Anderson and Jenkinson, 2007; Jenkinson and Anderson, 1994). Why RTOC recapitulate behaviours of the native thymus, while other culture techniques such as monolayer culture are not able to, remains poorly understood (Mohtashami and Zuniga-Pflucker, 2006). Notably, successful RTOC is widely considered to rely on the use of thymic tissue from the early stages of organogenesis: by E19.5 or P0: organ cultures rapidly lose total viable cell numbers within four to five days (Ueno *et al*., 2005). This suggests that the capacity for generating a functional organoid operates during a

defined window of development, with either the cellular compartment losing the intrinsic ability, or later microenvironments failing to nurture, TEC functionality. Experimental observation of this was reported by Rossi and colleagues (2007) who observed reduced differentiation potential of TEC taken from E12.5 compared to E18.5 gRTOC.

McCune and colleagues demonstrated that the murine kidney capsule could support a xenografts of human thymic material (McCune *et al*., 1988). Tissue was donated from the ninth gestational week and transplanted under the kidney capsule for 13 weeks. SCID mice were used as the recipients of the grafts, as these mice cannot establish a lymphoid system. As shown in gRTOC created from murine tissue, the graft was infiltrated by the host's vasculature system. The functionality of this was demonstrated by providing human fetal liver cells to the blood system of the SCID mouse recipient. The human cells were able to colonise the graft, undergo thymopoiesis and emigrate from the thymus. Remarkably, this did not produce graft vs host disease, which was taken as evidence that the emigrating T-cells had been exposed to both donor and recipient peptides during central tolerance.

Farley and colleagues (2013) first demonstrated that human fetal tissue was compatible with gRTOC. Tissue was collected from the eighth week of gestation, dissociated, reaggregated with MEFs and cultured as RTOC for 24 hours before grafting under the kidney capsule of a Non-Obese Diabetic (NOD)/SCID mouse. The human-gRTOC was regionalised into $UEA1^{+}$ and human leukocyte antigen (HLA) $class2^{high}$ regions.

Chung and colleagues (2014) argue that gRTOC is suitable to culture post-natal human tissues from ages ranging between 10 days and five months. However, the conclusions of the study are confounded by a poorly characterised 2D expansion protocol. The authors expanded tissue fragments in two different medium, one selecting for TM and the other for TEC. Strikingly, after three to four weeks both cultures retained expression of key genes of the native tissue, including the TEC-selective culture showing maintained expression of both FOXN1 and AIRE. However, no time zero controls were included and therefore no comparisons can be made regarding the relative expression levels of these genes as a consequence of the culture method.

After this expansion, the authors placed cells from TEC-selective medium, cells from TM-selective medium and 95% pure $CD34^+$ cord blood cells into RTOC and observed the emergence of $CD3^+$ DP, SP4 and SP8 thymocytes after four weeks. Again, no purified passage zero controls were used and so the experiment is confounded by the poorly defined nature of the input cell populations particularly from the TEC-selective medium, which comprised of only 39.1% $EpCAM^+$ cells. Grafted under the kidney capsules in an NOD/SCID/gamma (NSG^{TM}) mouse model with a humanised blood system, the gRTOC-recruited bone marrow precursors and contributed T-cells into the periphery with evidence of TCRβ diversity. However, no T-cell functionality or central tolerance assays were performed.

1.3.A.II. Decellularised Thymic ECM

ECM is an essential component of the extracellular microenvironment and has been shown to direct cellular behaviours in other organ and tissue systems (Gjorevski *et al*., 2014). The hypothesis that presenting a complete, native thymic ECM to TEC is beneficial for maintaining *ex vivo* function has been explored by two papers using decellularized tissue as a scaffold for cell culture.

The first publication claiming to have completed this was confounded by poor experimental design and absence of controls. Fan and colleagues (2015) used a detergent-perfusion system to decellularise three to four-week postnatal thymi. They then seeded the resulting decellularized ECM with a $CD45^+$ cell-depleted thymic stroma cell preparation plus HSC and grafted this reaggregate into a nude recipient (H-2^b). The enriched thymic stroma preparation contained ~18% SP thymocytes (H-$2^{b/g7}$). Therefore, since these cells could proliferate within the periphery of the haplotype-matched nude (H-2^b) and reject mismatched (H-2^k) but not matched (H-2^b and H-$2^{g/7}$) skin grafts, it cannot be concluded that the engrafted decellularised scaffold contributed anything more than releasing the already present mature thymocytes into the periphery once the graft was vascularised.

Hun and colleagues (2017), used a different detergent-perfusion based decellularisation process termed 3-[(3-Cholamidopropyl)dimethylammonio]-2-Hydroxy-1-Propanesulfonate (CHAPSO) to produce scaffolds from seven week old postnatal thymi. No *in vitro* data were

reported as the authors focused on kidney grafting experiments. The CHAPSO-scaffolds were seeded with E14.5 TEC ($CD45^{-}EpCAM^{+}$) and TM ($CD45^{-}EpCAM^{-}$) and were able to mediate thymopoiesis from recruited haematopoietic precursors after five weeks. Compared to standard control gRTOC, the CHAPSO-scaffold-based grafts showed significantly improved TEC and TM proliferation. This led to a three-fold increase in the number of total CDSP4 T-cell and SP8 T-cells in the blood, taken as a proportion of total $CD45^{+}$ cells, five weeks after engraftment with either gRTOC or the CHAPSO-scaffold. However, there was no direct investigation of whether this affected T-cell function or central tolerance. The authors also sectioned grafts recovered after five weeks of transplantation, to investigate the TEC structure. Staining for keratin 5, keratin 8 and LY51 found that the CHAPSO-scaffolds was predominantly populated by mTEC, with the structures containing very few cTEC. The authors employed a clonogenic 3D culture system first described by Wong and colleagues (2014) to test whether exposing embryonic TEC to ECM derived from postnatal thymi affected TEC behaviour. When supplemented to the clonogenic assay, the addition of postnatal thymic ECM decreased *Foxn1* expression and promoted medullary differentiation, reinforcing the earlier observation that CHAPSO-scaffolds were predominantly populated with mTEC.

1.3.A.III. Artificial Scaffold Materials

Using decellularised ECM-scaffolds invites cells to adapt a pre-existing pattern, which might constrain cellular behaviours if the appropriate cells are not seeded into the appropriate pre-created niche (Gjorevski *et al*., 2014). Furthermore, use of decellularized ECM is compounded by problems of tissue supply and variability, and therefore some investigators have begun to test the outcome of using synthetic biocompatible matrices in the generation of RTOC.

The Rosenzweig group published two studies that used synthetic matrix to culture *ex vivo* thymic stroma, CellFoam and Cytomatrix® (Marshall *et al*., 2003; Poznansky *et al*., 2000).. Focusing on the later Cytomatrix® report, four- to six-week postnatal thymi were processed into two mm^3 explants and placed on top of the matrix. The stromal cells infiltrated the matrix

and, once at confluency, were irradiated before seeding with $Lin^{-}Sca^{+}$ haematopoietic progenitors from either the thymus or bone marrow. Given that the initial thymic explants contained haematopoietic cells, the authors used CD45.1 or CD45.2 to distinguish between the seeding populations. No effort was made to characterise effects of the culture system on the thymic stroma, with the authors focusing on thymopoiesis, which did not substantially improve compared to RTOC. Therefore, the use of a defined matrix did not improve the reliability of *in vitro* thymopoiesis over RTOC. A subsequent publication by Clark and colleagues (2005) that found that human keratinocytes and fibroblasts cultured within CellFoam, upregulated key TEC genes and gained the ability to mediate thymopoiesis including central tolerance. However, this was subsequently found to be unreproducible (Meek *et al*., 2011).

More recently, Pinto and colleagues (2013) tested the use of a hydrogel for culturing TEC, with the aim of identifying conditions for mTEC that preserved promiscuous gene expression. Jettex, a viscose, fibrous material, was supplemented with thrombin and fibrinogen and human dermal fibroblasts were encapsulated inside. The hydrogel was placed in a trans-well to separate it from the tissue culture medium, while allowing nutrient exchange through the porous membrane. mTEC from one- to seven-day postnatal mice were cultured on top of the hydrogel and were unable to infiltrate it during the culture. This allowed proliferation and maintenance of mTEC, on top of the hydrogel, with evidence of promiscuous gene expression. However, the authors did not present evidence of functionality, for instance by testing whether the target mTEC population could rescue the *aly/aly* phenotype in kidney grafting experiments (Akiyama *et al*., 2016; Sekai *et al*., 2014).

Thus, whilst there has been effort to incorporate defined scaffolds into *in vitro* thymopoiesis assays, the studies reported to date do not show conclusive improvements over classical RTOC, although direct side-by-side comparison was not presented in all the above studies.

Two papers have reported that TEC progenitors can be cultured in spheres of clonally expanded cells and could differentiate into cTEC and mTEC progeny (McQualter *et al*., 2010; Ucar *et al*., 2014; Wong *et al*., 2014). These papers reported that the sphere-initiating

cells originated from fundamentally different starting populations. Ucar and colleagues (2014) claimed this population was FOXN1^{-}EpCAM^{-} while Wong and colleagues (2014) claimed that the starting cell population was FOXN1^{+}EpCAM^{+}. With respect to the former publication, a recent study failed to confirm the main findings, concluding instead that the FOXN1^{-}EpCAM^{-} population was mesenchymal and recruited bystander TEC into the spheres from the heterogeneous starting population (Sheridan *et al*., 2017). The FOXN1^{+}EpCAM^{+} population reported by Wong and colleagues (2014) displayed limited ability to be passaged, but could contribute to gRTOC when mixed with fetal thymic tissue. Further functional characterisation of TEC cultured in this system was not explored.

Therefore, FTOC and RTOC are still the only tissue culture techniques that successfully emulate thymic function. Notably this includes maintenance of *Foxn1* expression within TEC, which is not observable in monolayer conditions (Mohtashami and Zúñiga-Pflücker, 2006). The mechanism via which RTOC maintain *Foxn1* expression is not characterised. However, it is known that tissue age and ability to successfully form RTOC is negatively correlated (Rossi *et al*., 2007; Ueno *et al*., 2005). Whether that is due to a change intrinsic to TEC or within the environment is also unclear but exposure of embryonic tissue to postnatal ECM reduced *Foxn1* expression in TEC and biased differentiation toward the medulla lineage, (Hun *et al*., 2017).

1.3.B. Notch-Engineered Feeder Cell lines

In 2002, a novel methodology was published by Schmitt and Zúñiga-Pflücker that allowed *in vitro* thymopoiesis without *ex vivo* TEC. This circumvented key technical limitations associated with RTOC: namely, the scarcity of TEC and the technical difficulty and resulting inconsistency associated with preparing RTOC. In brief, these investigators utilised the mouse bone marrow stromal cell line OP9, that expresses key factors for thymopoiesis, including IL-7, CXCL12 and KIT-L but not bone marrow associated factors essential for other haematopoietic lineages such as Colony Stimulating Factor 1 (CSF1) (Smith *et al*., 2015), and was known to support B cell development from haematopoietic progenitors (Carlyle *et al*., 1997). They engineered this line to ectopically express the NOTCH ligand DLL1, since

NOTCH signalling was known to dictate T-cell lineage commitment (Radtke *et al*., 1999), and tested whether this would confer the capacity to support T cell development on the OP9 cells. This proved to be the case: in 2D co-culture, the OP9-DLL1 system was able to confer T-cell lineage commitment upon HSC, and to support efficient T cell differentiation up to the DP stage of development, with some SP8s being generated. Note that SP4 cells are not generated as the OP9 line does not express MHC2, a unique feature of TEC outside the haematopoietic system. Subsequently, the OP9-DLL1, and the more recently developed OP9-DLL4, systems have been at the forefront of investigation of thymopoiesis *in vitro*, with T-cells being generated from a range of starting cell types ranging from HSCs and ETPs to embryonic stem cells and induced pluripotent stem cells in both mouse and human (Brauer *et al*., 2016).

In an extension of this strategy, Seet and colleagues (2017) engineered the mouse bone marrow stromal cell line MS5 to ectopically express human-DLL1. Unlike OP9-DLL1, the MS5-hDLL1 system was inefficient at generating T-cells in a monolayer culture system. Therefore, the authors applied the cell line to an RTOC-inspired reaggregation and culture method. The resulting culture was termed an artificial thymic organoid (ATO) and demonstrated a markedly improved efficiency in generating $CD3^+$ SP4 and SP8 T-cells from human HSCs compared to the monolayer OP9-DLL1 system.

As discussed above, thymopoiesis can be broken into four parts: T-cell lineage commitment, β-selection, positive-selection and central tolerance induction/negative selection and the thymus has evolved specialised molecular mechanisms that are essential mediators of positive selection and negative selection. Both the OP9-DLL1 and MS5-hDLL1 systems can mediated lineage commitment and β-selection. However, effective negative selection requires promiscuous gene expression to remove TCRs that recognise tissue-restricted antigens (TRA) (Lopes *et al*., 2015), and which, as discussed above, depends on the expression of *AIRE* and *FEFZ2* in mTEC. The capacity for promiscuous gene expression is not present in OP9 or MS5 cells and, as T-cells generated in these systems will not be exposed to the full range of peptides present in the native thymic medulla, these systems will

produce T cell repertoires that contain autoreactive T-cells, similarly to mice with dysfunctional promiscuous gene expression (*Aire*$^{-/-}$) (Ramsey, 2002).

Once a thymocyte has completed its αβTCR, interactions with cTEC mediate positive selection and lineage fate decision (Figure C1.1). TCR activation minimally requires a peptide:MHC interaction from cTEC. Whether the OP9-DLL1 and MS5-hDLL1 can generate appropriate self-peptide pools will be discussed later. Firstly, whether OP9-DLL1 and MS5-hDLL1 express appropriate MHC will discussed and how this related to thymocyte fate decision. The MS5 and OP9 are both cell lines created from the murine bone marrow stroma and do not express MHC2 (Schmitt and Zúñiga-Pflücker, 2002; Seet *et al*., 2017). Without interactions with peptide:MHC2 to provide constant TCR signalling, it is not possible for a thymocyte to a adopt the SP4 lineage (Brugnera *et al*., 2000; Littman, 2016; Taniuchi, 2018). However, both systems report mediation of SP4 thymocyte generation. In the MS5-hDLL1 paper, Seet and colleagues hypothesise that a small population of DC are created from the input human haematopoietic progenitors. This population slowly accumulates, which describes the relatively slower emergence of SP4 thymocytes, and begins to provide peptide:MHC2 interactions that mediate both the active TCR signalling for positive selection and lineage diversion of SP4 thymocytes (Seet *et al*., 2017). Furthermore, this protocol used a human haematopoietic system, in which DP thymocytes also express MHC2, which will further contribute to haematopoietic – thymocyte TCR activation (Zinkernagel and Althage, 1999). This mechanism reflects those found within xenografted thymi, in which a recipient haematopoietic system can complete thymopoiesis in a donor thymus, interact with TEC expressing donor MHC complexes but emerge restricted to- and tolerant of- both donor and recipient MHC. Evidence was observed that the selection processes, which produced restriction to- and tolerance of- recipient peptide:MHC arose between haematopoietic-derived, recipient cells, while restriction to- and tolerance of- donor peptide:MHC arose through the canonical TEC-thymocyte interaction (Van Coppernolle *et al*., 2009; Zinkernagel and Althage, 1999). Therefore, this explanation is plausible. However, while the functional consequences of this remains to be characterised, it must be reinforced that in this process

the OP9-DLL1 and MS5-hDLL1 are not recapitulating cTEC mediated-positive selection (Takada *et al*., 2017).

How relative differences in peptide processing between cTEC and the OP9-DLL1 and MS5-hDLL1 systems affects the avidity of TCR-peptide:MHC can be understood by looking a knockout models, in which the peptide processing machinery of the cTEC are disturbed (Honey *et al*., 2002; Hsieh *et al*., 2002; Kincaid *et al*., 2016; Murata *et al*., 2007; Nakagawa *et al*., 1998). This has been discussed in detail above and it is likely that absence of key proteins β5t, TSSP and cathepsin L, will compromise the efficiency of positive selection and the functionality of generated thymocytes (Takada *et al*., 2017).

Although the engineered cell-line based methods described above overcome limitations associated with tissue availability to partially support *in vitro* thymopoiesis, these systems do not faithfully recapitulate the specialist thymus functions needed for physiological positive selection or central tolerance induction. Without promiscuous gene expression T-cells generated in this fashion cannot be tolerant to TRA. There are also substantial differences in peptide processing between OP9, MS5 and cTEC, which should reduce the efficiency of positive selection and peripheral T-cell functionality in T cell repertoires generated on these cell lines.

This does not diminish the important contributions to understanding T-cell lineage development that these systems have made. Additionally, there is increasing clinical interest in these technologies for producing T-cell lineage-restricted progenitors for transplantation. Evidence has indicated that transplantation of pro-T-cells improves thymic rebound after total body irradiation, and it is often argued that *in vitro* T-cell generation has potential for Chimeric antigen receptor T-cells (Montel-Hagen *et al*., 2019; Singh and Zúñiga-Pflücker, 2018). In a follow up paper focusing on potential clinical applications of the MS5-hDLL1 system, Montel-Hagen and colleagues (2019) demonstrated the ability of the ATO to produce SP8 T-cells from transgenic TCR-derived induced pluripotent stem cells. Furthermore, further developments from these methodologies that can support T-cell lineage commitment and hence generate large number of proT-cells in feeder cell-free systems are

now becoming available (Gehre *et al*., 2015; Shukla *et al*., 2017; Simons *et al*., 2018). This eliminates both the complications highlighted here as the target pro-T-cell population exists before positive or negative selection is executed.

1.3.C. Cellular Reprogramming Strategies

1.3.C.I. Directed Differentiation

Understanding thymic organogenesis has led to development of directed differentiation strategies to generate target cell populations from pluripotent stem cells (Li *et al*., 2017). This process has the aim of overcoming the scarcity of TEC and also generating patient-specific cells for personalised medicine (Lai *et al*., 2011). The first attempt to differentiate murine Embryonic Stem Cells (mESC) into TEPC was published by Lai and Jin in 2009. Subsequently, some progress towards making TEC from human Pluripotent Stem Cells (hPSC) has been reported (Parent *et al*., 2013; Soh *et al*., 2014; Su *et al*., 2015; Sun *et al*., 2013). Focusing on the human Embryonic Stem Cells (hESC) protocols, all involve initial differentiation into definitive endoderm-like cells using Activin A either alone or in combination with WNT3a. Methodologies then focus on upregulating *FOXN1* and *HOXA3*, akin to native thymic development. All studies used retinoic acid and BMP4, with Sun and colleagues (2013) providing IWR1 (WNT1 inhibitor); Parent and colleagues (2013) also supplemented with WNT3a, FGF8, Cyclopamine (SHH inhibitor) and LY364947 (TGFβ inhibitor) and Su and colleagues (2015) used FGF7, FGF10, and EGF to compensate for loss of mesenchymal signalling in the culture. However, only Parent and colleagues (2013) provided direct evidence of functionality, showing that T cells generated in the grafts were able to mediate alloreactive skin graft rejection. Of note, all methods produced cells that did not remain viable for substantial lengths of time, reported substantial variability in the differentiation protocols and required engraftment. These present large technical obstacles to clinical application.

1.3.C.II. Induced Thymic Epithelial Cells

In a distinct approach, our laboratory used direct lineage reprogramming to enforce *Foxn1* expression in MEFs, which mediated reprogramming and resulted in conversion of the MEFs

to a TEC phenotype (Bredenkamp *et al*., 2014). The induced TEC (iTEC) used a genetic reprogramming strategy. A *CreERt2* fusion protein was knocked into the parental Rosa26 allele while *Foxn1* and *GFP,* separated with an internal ribosome entry site, were knocked into the maternal Rosa26 allele with a floxed transcriptional pause site allowing Cre-mediated activation of the transgene (*Rosa26*^{CreERt2}*:Rosa26*^{iFoxn1}) (Bredenkamp *et al*., 2014). Notably, this process did not necessitate gRTOC to complete reprogramming, which allowed for investigation of the iTEC phenotype *in vitro*. iTEC were co-cultured with embryonic ETPs in a monolayer. After 12-days, the ETPs had progressed into DP, SP4 and SP8 thymocytes complete with up regulation of CD3ε and TCRβ. However, unlike both the OP9-DLL1 and MS5-hDLL1 systems, iTEC were shown to express β5t and MHC2. Therefore, iTEC utilised the thymoproteasome and native MHC2 expression to mediate peptide processing and presentation, respectively, which likely recapitulated the native processes in positive selection. When incorporated into a gRTOC methodology to replace the *ex vivo* TEC component, iTEC were able to form an organised and functional thymus. Cortical and medulla regionalisation of recovered gRTOC were shown using the cortical markers CD205 and β5, alongside medullary markers cytokeratin 14 (K14) and UEA1. The medullary phenotype was reinforced by finding evidence of promiscuous gene expression in AIRE^{+} iTEC. Analysis of the thymocyte populations of the graft demonstrated that iTEC were competent to mediate the generation of DP, SP4 and SP8 thymocytes when engrafted onto the kidney capsule and that recipient blood vasculature infiltrated the graft to facilitate the emigration of T-cells in the periphery. However, the differentiation capacity of iTEC *in vitro* were not defined, with no evidence of the system being able to produce cells capable of promiscuous gene expression. Furthermore, cortical function was only compared to the OP9-DLL1 system, which as discussed above does not aim recapitulate native TEC. There was no direct comparison between iTEC and *ex vivo* TEC and therefore as it stands the *in vitro* potential of the system in undefined.

1.3.D. Conclusion

In conclusion, currently, the approach that most faithfully emulates native TEC function *in vitro* is RTOC. Tissue scarcity and practical difficulties associated with this system provided

motivation for generating cell line based *in vitro* systems. The best of these are currently the OP9-DLL1/OP9-DLL4 and MS5-hDLL1 systems. However, these systems do not faithfully recapitulate positive selection or central tolerance induction. Directed differentiation and reprogramming strategies have aimed to generate large numbers of TEC *in vitro* and thus overcome the limitation of both techniques. Of these, currently, only the iTEC protocol has been shown to support generation of an intact thymus in the absence of any WT 'carrier' TEC. Tissue engineering aims to created functional organotypic systems for that either recapitulate key behaviours *in vitro* or can be implanted in the body and provide a source of transplantable material. The iTEC remains the system with the most potential for tissue engineering techniques that aim to recapitulate thymopoiesis *in vitro* and to scale up the size of engineered tissue to be suitable for transplantation in the human body.

1.4. Thesis Aims

The overall aim of the work performed in this thesis was to test the hypothesis that iTEC in conjunction with synthetic matrices, could be used generate thymic organoids that recapitulate the fundamental processes via which TEC mediate T cell differentiation and repertoire selection.

Specifically, I set out to test the following hypotheses:

In Chapter Three, I tested the hypothesis that the iTEC system could produce a large quantity of cells competent to recapitulate *ex vivo* TEC function *in vitro*. The work described addresses this hypothesis in two phases - firstly, maximising the scale-up capacity of iTEC, whilst focusing on generating standardised batches of cells, and secondly, testing the extent that this optimised iTEC system can recapitulate *ex vivo* TEC when cultured as RTOC.

In Chapter Four, I investigated the hypothesis that using defined culture substrates could create a more consistant iTEC phenotype, with respect to the essential functions of TEC. To achieve this, I identify synthetic polymers able to bind to both iTEC and *ex vivo* TEC and then to compare the effect selected polymers had on both cell types as a measure of emulating thymic functions *in vitro*.

In Chapter Five, I tested the hypothesis that miniaturising the RTOC process could be conducive to creating a culture system for thymus biology that is amenable to high throughput screening applications. Chapter Five establishes a novel method that aims to reduce tissue and improve consistency between conditions and beings to evaluate the compatibility of the novel system with *ex vivo* TEC and iTEC.

2. Chapter Two: Materials and Method

2.1. Mice

2.1.A. Facilities

Mice were housed at the animal unit within the Medical Research Councils' Centre for Regenerative Medicine, University of Edinburgh. Wild type mice refer to C57BL/6 originally acquired from the Jackson Laboratory and maintained at the MCR Centre for Regenerative Medicine (Jax SCRM). Three transgenic strains were used in this thesis: *Foxn1*^{G} (O'Neill *et al*., 2016) (Transgene outlined in Figure C4.12); iFoxn1 (Bredenkamp *et al*., 2014) and Rosa26:CreERt2 (Hameyer *et al*., 2007) (Transgene outlined in Figure C3.1) . All colonies were maintained by crossing a transgenic mouse, heterozygous with the relevant transgene, with a wild type (WT) C57BL/6 Jax SCMR mouse. Animal husbandry and treatments were carried out in accordance with Animal (Scientific Procedures) Act 1986 and performed in accordance with the institution and ethical guidelines of the University of Edinburgh.

2.1.B. Timed Mating

Embryos were produced by pairing mice overnight. The following morning, females with a vaginal plug were classified as E0.5. WT tissues were the result of $\mathrm{C57BL/6\ Jax\ SCRM} \times \mathrm{C57BL/6\ Jax\ SCRM}$ crosses; *Foxn1*^{G} tissues were produced using $\mathrm{C57BL/6\ Jax\ SCRM}$ (♀) × $Foxn1^{\mathrm{G}}$ (♂) and iFoxn1 tissues were generated by pairing $\mathrm{iFoxn1}$ (♀) × $\mathrm{Rosa26{:}\ CreERt2}$ (♂).

2.1.C. Isolation of Genomic Deoxyribonucleic Acid

Mice were weaned at fourteen days of age. At this point, ear clips marked each mouse with a unique identification number. The surplus tissue was collected to isolate genomic Deoxyribonucleic Acid (DNA). To isolate genomic DNA from embryos, the head of each embryo was collected. Tissue was digested overnight using tissue lysis buffer and 400 µg / ml Proteinase K (Promega), heated to 55°C in an agitated water bath. After a minimum of eight hour and a maximum 16 hours, the reaction was heat inactivated at 95°C for ten minutes and centrifugated for ten minutes at 2×10^4 rfc to pellet contaminating material, purifying the DNA in the supernatant. Genomic DNA was stored at 4°C.

2.1.D. Tissue Lysis Buffer

- 10mM Tris-HCL, pH 8.3 (Roche)
- 2.5mM Magnesium Chloride (MgCl2)
- 50mM Potassium Chloride (KCl)
- 0.1mg / ml Gelatin
- 0.45% NP40
- 0.45% Tween20

2.2. Genotyping

All genotyping protocols used Taq polymerase and associated buffers (Quigen).

2.2.A. Rosa26:CreERt2

2.2.A.I. Master Mix

- 3 µl 10x buffer
- 0.5 µl Deoxyribonucleotide Triphosphate (dNTPs)
- 0.5 µl Taq
- 1 µl Forward CreERt2 primer
- 1 µl Reverse CreERt2 primer
- 19 µl DEPC-treated water
- 5 µl DNA

2.2.A.II. Thermocycling

- Five minutes at 94°C
- 30 cycles of:
    - 30 seconds at 94°C
    - 30 seconds at 58°C
    - 1 minutes at 72°C
- Seven minutes at 72°C
- Infinite hold at 4°C.

2.2.A.III. Product Size

269 base pairs

2.2.B. iFoxn1

2.2.B.I. Master Mix

- 3 µl 10x buffer
- 0.5 µl dNTPs
- 0.5 µl Taq
- 1 µl Forward iFoxn1 primer
- 1 µl Reverse iFoxn1 primer
- 6 µl Q buffer
- 19 µl DEPC-treated water
- 5 µl DNA.

2.2.B.II. Thermocycling

- Five minutes at 94°C
- 35 cycles of:
    - 30 seconds at 94°C
    - 30 seconds at 60°C
    - 1 minutes at 72°C
- 10 minutes at 72°C
- Infinite hold at 4°C.

2.2.B.III. Product Size

750 base pairs

2.2.C. *Foxn1*[G]

2.2.C.I. Master Mix

- 3 µl 10x buffer
- 0.5 µl dNTPs
- 0.5 µl Taq
- 1 µl Forward GFP primer
- 1 µl Reverse GFP primer
- 6 µl Q buffer
- 19 µl DEPC-treated water
- 5 µl DNA

2.2.C.II. Thermocycling

- Five minutes at 94°C
- 30 cycles of:
    - 30 seconds at 94°C
    - 45 seconds at 57°C1 minutes at 72°C
- 10 minutes at 72°C
- Infinite hold at 4°C.

2.2.C.III. Product Size

220 base pairs

2.3. Tissue Processing

2.3.A. Dissection of Embryos

Once gestation had reached the desired length, the female mouse was sacrificed by cervical dislocation. Embryos were removed from the uterus and collected in Phosphate-Buffered Saline (PBS) at 4°C. Using a dissection microscope (Zeiss), embryos were removed from the embryonic sack and beheaded.

2.3.B. Disassociation of Embryonic Thymus

To harvest embryonic thymus from beheaded embryos, incisions were created to remove the rib cage and expose the upper thorax. Embryonic thymic lobes of all ages were located by tracing the common carotid vessels leading to the pharyngeal arches. Early tissues have thymic lobes located closer to the third pharyngeal arch, while in later tissues the thymic lobes have coalesced above the heart. Thymic lobes were harvested, and care was taken to removed surrounding, supportive tissues. Thymic lobes were incubated in TrypLE Express Enzyme (life technologies #12604013) for five minutes in a thermomixer set to 1400 rpm and 37°C. To complete disassociation, the suspension was triturated with a P1000 for a further 60 seconds to apply mechanical force to the lobes. To inactivate the reaction, the suspension was chilled to 4°C and washed twice using centrifugation and resuspension in 2% Fluorescence Activated Cell Sorting (FACS) buffer. All cellular centrifugation steps used 500 relative centrifugal force (rcf) for five minutes. Embryonic tissues are processed in 2% FACS buffer.

2.3.C. Establishment of Murine Embryonic Fibroblasts

Murine Embryonic Fibroblasts (MEFs) were routinely established from E13.5 beheaded embryos, the head being used for genomic DNA collection. All internal organs were stripped away from the embryo and the arms, legs and tail removed. The remaining tissue was homogenised by compression with a 18G syringe and enzymatically disassociated in 0.25% trypsin EDTA (Invitrogen) for 10 minutes at 37°C. Finally, tissue was further triturated with a 23G syringe before seeding into a gelatinised T75 (Corning #CLS430641U).

2.3.D. Isolation of Adult Thymocytes

To isolate thymocytes from the postnatal thymus, a four-week female mouse was sacrificed using cervical dislocation. The thymus was harvested by removing the rib cage to expose the upper thorax. Once collected, the thymus was compressed to mechanically remove the thymocytes. Adult thymocytes were processed in 0.2% FCS containing FACS buffer at 4°C.

2.3.E. Isolation of Adult LSK Haematopoietic Stem Cells

To isolate Lineage^{-}SCA-1^{+}c-KIT^{+} haematopoietic stem cells (LSKs) from the postnatal bone marrow, a six-week male mouse was sacrificed using cervical dislocation. The tibia and

femur were harvested and crushed to release the bone marrow. Bone marrow was processes in 0.2% FACS buffer at 4°C.

2.3.F. Magnetic Enrichment of C-KIT Expressing Thymocytes

Given the scarcity of early thymocyte progenitors (ETPs) within the four-week postnatal murine thymus and LSKs within the six-week postnatal bone marrow, magnetically conjugated beads were used to enrich the population before FACS sorting. Cells were stained with antiCD117-magentic bead conjugates concurrently to the rest of the panel and stained at 4°C for 15 minutes. This process was optimised as this results in competition between the antiCD117-magnetic bead conjugate and the antiCD117-Pe/Cy7 conjugate for available epitopes. Note that optimisation between batches of beads was required to maintain consistency. To remove excess and unbound antibody, cells were washed twice by centrifugation and resuspension in FACS buffer. The magnetically labelled cells were separated from the rest of the sample using the QuadroMACs Separator and LS columns (Miltenyi Biotechnologies). LS columns were washed with three ml FACS wash before application of cells and unlabelled cells were washed out of the column with nine ml of FACS wash after application of cells. To collect the CD117 expressing fraction, the LS columns were removed from the magnetic field allowing labelled cells to be washed out. This preparation was resuspended at 1×10^7cells / ml and FACS sorted.

2.4. Flowcytometry

2.4.A. Antibody staining protocol

Antibodies directly conjugated to fluorophores were used for flow cytometry. To stain surface markers, cells were resuspended in FACS buffer with pre-defined concentrations of antibody. All concentrations of antibodies were rigorously optimised when designing panels. Antibody – antigen interactions were incubated for 15 minutes at 4°C. To remove excess and unbound antibody, cells were washed twice by centrifugation and resuspension in FACS buffer. A membrane impermeable nuclear dye was used to discriminate between dead and alive cells and was added just before initiation of analysis or FACS sorting. This was 4′,6-diamidino-2-phenylindole (DAPI) or 7-Aminoactinomycin D (7AAD) depending on the panel

design. Flow cytometry panels were compensated using Ultracomp beads (Invitrogen) for all fluorophores except for the nuclear dye, which used a small proportion of unstained cells. Compensation matrices were always manually checked post-acquisition. When necessary, fluorescence minus one (FMO) samples were used to set gates.

2.4.B. Acquisition

All FACS sorting was performed by the Centre for Regenerative Medicine's FACS facility using BD FACS Arria II or Fusion running FACS Diva 4.1 (BD Biosciences). All flowcytometry was completed on a Novocyte running NovoExpress 1.3.0 (ACEA). All post-acquisition analysis was performed with FCSexpress 6 (De Novo Software).

2.4.C. Fluorescence Activated Cell Sorting Buffers

- 2% or 0.2% FCS (Life Technologies #10270106) for embryonic and adult tissue, respectively
- PBS without calcium and magnesium (Sigma)
- 0.05 mg / ml DNase1 (Lorne Laboratory).

2.5. Immunohistochemistry

2.5.A. Tissue Fixation and Sectioning

Tissues for whole mount staining were fixed in 4% paraformaldehyde (PFA) overnight at 4°C on an agitator. This includes monolayers, microarrays and miniaturised-reaggregate thymic organ culture (MTOC) in addition to whole thymic lobes. Tissue for sectioning was embedded in OCT (VWR) and snap frozen on dry ice. OCT blocks were stored at -80°C until cryo-sectioning (Leica CM3050 S or CM1950) into 7 µm sections, which were transferred on to 1.5 mm polystyrene glass microscopy slides (VWR). Slides were stored -80°C until fixation and staining. Immediately prior to staining, a hypophonic pen was used to draw a ring around sections. Once dry, 4% PFA (Sigma) was applied to the ring for 15 minutes at room temperature to fix tissue. Note that the total volume of PFA, and subsequent staining buffers, required is proportional to diameter of hydrophobic ring.

2.5.B. Types of Immunohistochemistry Samples

There were three types of sample that were taken for staining based on what the samples were stored in. The protocol remained the same. However, application of solutions had to be performed differently based on format:

1. The microarray and sections were on glass microscopy slides. Staining solutions were pipetted onto samples that were encapsulated in a hydrophobic ring
2. MTOC and monolayers of cells, such as the focused polymer arrays were in tissue culture plates. Staining solutions were pipetted directly into each well.
3. Whole, fixed thymic lobes were in a trans-well with 8 μm pores that was transferred between wells containing the various staining solutions in a 48-well plate.

2.5.C. Staining Protocol

Samples were blocked in Permeabilization and Block Buffer overnight at 4°C inside a humidity chamber. Primary antibodies were suspended in PtwH and centrifuged at 2×10^4 rcf for 10 minutes to remove antibody aggregates or contamination. The Permeabilization and Block Buffer was removed from the samples and the primary antibodies applied overnight at 4°C inside a humidity chamber with gentle agitation. The appropriate secondary antibodies and DAPI were suspended in PtwH and centrifuged at 2×10^4 rcf for 10 minutes to remove antibody aggregates or contamination. The sections were washed twice in PtwH to remove excess and unbound primary antibody. The secondary antibodies and DAPI were incubated with the samples overnight at 4°C inside a humidity chamber and gentle agitation. Samples were washed twice with PtwH to remove excess and unbound secondary antibody and airdried. Samples were stored in PBS 0.1% sodium azide until imaging except for the microarrays and sectioned samples, which were compatible with mounting agents. These samples were treated with Vectorshield hard set mounting medium (Vector Laboratories) and was mounted with a coverslip. Once dry, samples were stored at 4°C until imaging.

2.5.D. Staining Buffers

All staining buffers are taken from the iDisco^{+} protocol (Renier *et al*., 2016). All solutions contained 0.1 % sodium azide (Sigma) to prevent bacterial growth and were strained through a 0.22 µm filter before application to samples.

2.5.D.I. Permeabilization and Block Buffer

- 400 ml PBS (Sigma)
- 8 ml TritonX-100 (Sigma)
- 11.5g of Glycine (Sigma)
- 100 ml of Dimethyl Sulfoxide (DMSO) (VWR)
- 10% goat serum (Sigma) – added immediately prior to application

2.5.D.II. PtwH

- 1 L PBS
- 2 ml Tween-20 (Sigma)
- 1 mg Heparin (Sigma)
- 1 % goat serum - added immediately prior to application

2.6. Gene Expression Analysis

2.6.A. mRNA Acquisition and Preparation

2.6.A.I. Small Population Samples

2.6.A.I.a. mRNA Isolation

The CellsDirect (Invitrogen) protocol was employed to collect rare cell types for mRNA isolation. Populations of 50 cells were FACS sorted into PCR tubes containing 10 µl of CellsDirect 2X Reaction Mix and 0.2 µl SUPERase-in (Applied Biosystems). Once samples were collected, tubes were centrifuged briefly and stored at -80°C.

2.6.A.I.b. Reverse Transcription of mRNA into cDNA

Gene-specific reverse transcription was used to create cDNA for both small and large population mRNA isolation methods. For the small populations, the samples were mixed with 10 µl pre-amplification mix and then subjected to the thermocycling procedure.

2.6.A.I.c. Pre-Amplification Mix

- 5 µl primer pair mix. Forward and reverse primer pairs for each target gene were suspended in 5 µl DEPC-treated water (Life Technologies) at 0.2 µM.
- 4 µl DEPC-treated water
- 1 µl SuperScript III RT/Platinum Taq mix from CellDirect kit. To create a no reverse transcription control this was replaced with 1µl Taq (Qiagen).

2.6.A.I.d. Thermocycling Procedure for Reverse Transcription and Amplification of mRNA

- 15 minutes at 50°C
- 2 minutes at 95°C
- 18 cycles of:
    - 15 seconds at 95°C
    - Four minutes at 60°C
- Infinite hold at 4°C.

2.6.A.II. Large Population Samples

2.6.A.II.a. mRNA Isolation

RNEasy (Qiagen) was used to collect mRNA for large cell populations. Target cells were lysed with RLT lysis buffer before purification using affinity chromatography. A nanodrop (Thermo) was used to measure the concentration and purity of mRNA before storage at -80 °C.

2.6.A.II.b. Reverse Transcription of mRNA into cDNA

Gene-specific reverse transcription was used to create cDNA for both small and large population mRNA isolation methods. The SuperScript III First-Strand Synthesis System for Reverse Transcription-quantitative Polymerase Chain Reaction (RT-qPCR) (Invitrogen) kit was used to reverse transcribe mRNA collected from large populations. First, a standardised quantity of mRNA between samples was incubated with 0.2 μM of primer pairs and 10 mM of dNTPs in 10 μl DEPC-treated water for five minutes at 65°C. After cooling to 4°C for one minute, 10 μl of cDNA Synthesis Mix was added to each mRNA/primer sample. Reverse transcription was conducted at 50°C for 50 minutes before being terminated at 85°C for five minutes. After cooling to 4°C for one-minute, excess mRNA was removed by incubating 1 μl of RNase H to the cDNA samples at 37°C for 20 minutes. Manufactured cDNA was stored at -20°C.

2.6.A.II.c. cDNA Synthesis Mix

- 2 μl 10x RT buffer
- 4 μl 25 mM $MgCl_2$
- 2 μl 0.1 M DTT
- 1 μl RHaseOUT (40 Units / μl)
- 1 μl SuperScript III RT (200 Units / μl).

2.6.B. Reverse Transcription-Quantitative Polymerase Chain Reaction

2.6.B.I. Plate Loading

A white, 384-well plate (Roche) was loaded with 7.5 µl RT Gene Specific Master Mix and 2.5 µl cDNA in triplicate. The cDNA samples were diluted in DEPC-treated water to ensure enough for each plate. Note the quantity of cDNA in each well was specific to each plate and is comparable to other plates only as relative expression of target genes compared to house keepers.

2.6.B.II. RT Gene Specific Master Mix

- 5 µl 2x master mix (Roche)
- 0.1 µl UPL probe (Roche)
- 0.225 µl 20 µM forward and reverse primer pair (Sigma)
- 2.175 µl DEPC-treated water.

2.6.B.III. Real Time Fluorescence Detection

Completed 384-well plates were sealed (Applied Biosystems) and centrifuged at 1000 rcf for 1 minute at 4°C. A Lightcycler 480-II (Roche) was used to perform the PCR with real time detection of fluorescence.

2.6.B.IV. Thermocycling procedure for Reverse Transcription-Quantitative Quantitative PCR

- Five minutes at 95°C
- 45 cycles of:
    - 10 seconds at 95°C
    - 20 seconds at 60°C
    - Capture Fluorescent Signal
- 40°C – 10s.

2.6.B.V. Calculation of Relative Gene Expression

Triplicates were checked to ensure all replicates were with 1 Cq value of each other and outlies were removed. The numerical average for each triplicate was calculated. Each gene was then reported as a product of the housekeepers *Ywhaz*, *Hprt* and *Tbp*. It was assumed that each round of amplification doubled fluorescence output of unquenched probes. The following equation was used to calculate the expression of target express relative to the genomic mean of the three housekeepers:

Equation C2.1:

$$Gene\ epression\ realtive\ to\ house\ keepers\ = \frac{\left(2^{\mathrm{Ywhaz\ Cq}} \times\ 2^{\mathrm{Hprt\ Cq}} \times\ 2^{\mathrm{Tbp\ Cq}}\right)^{\frac{1}{3}}}{\left(2^{Target\ Gene\ Cq}\right)} =$$

2.7. Tissue Culture

2.7.A. Medium Formulation

2.7.A.I. Induced Thymic Epithelial Cell Medium

- Advanced DMEM/F12 (Life Technologies #12634010)
- 10% performance FCS, US origin (Life Technologies)
- 1% penicillin (10,000 Units / ml) and streptomycin (10,000 µg / ml) (Invitrogen #15140-122)
- 1% L-glutamine (200 mM) and sodium pyruvate (100 mM) (Invitrogen #25030-024 and #11360-039)
- 1% MEM non-essential amino acids (Invitrogen #11140-036)

2.7.A.II. 2% Medium

- Advanced DMEM/F12 (Life Technologies)
- 2% performance FCS, US origin (Life Technologies)
- 1% GlutaMAX (Life Technologies)

2.7.A.III. N2B27 Medium

- 10 ml DMEM/F12 (Life Technologies #31330-038)
- 10 ml Neurobasal medium (Life Technologies #21103-049)
- 200 µl N2 Supplement (Life Technologies #17502-048)
- 100 µl B27 Supplement (Life Technologies #17504044)
- 45.5 µl 2-Mercaptoethanol (Life Technologies #31350010)
- 440 µl L-glutamine (200 mM) and sodium pyruvate (100 mM) (Invitrogen)
- 100 µl penicillin (10,000 Units / ml) and streptomycin (10,000 µg / ml) (Invitrogen)
- 50 ng / ml BMP4 (Peprotech #315-27)
- 50 ng / ml FGF7 (Peprotech #100-19)
- 10 ng / ml EGF (Peprotech #315-09)

2.7.B. Expansion of MEFs

Once E13.5 tissues have been processed and seeded, each 10 ml induced Thymic Epithelial Cell (iTEC) medium was added to each T75. MEFs reached confluency within 24 hours. MEFs were washed twice in 10 ml of room temperature PBS, without magnesium and calcium, before incubation with 1 ml chilled 0.25% trypsin EDTA for one minute at 37°C. The reaction was quenched with MEF expansion medium. To begin P1, all T75s were seeded into a T150 (Corning #CLS430825) and 15 ml of iTEC medium was added to each. At confluency, MEFs were washed twice in 15 ml of room temperature PBS, without magnesium and calcium, before incubation with 3 ml chilled 0.25% trypsin EDTA for one minute at 37°C. Each T150 flask was seeded into three T150 flasks. Once at confluency, MEFs were passaged using the above protocol and each T150 was split into three cryovials

suspended in iTEC medium with 5% DMSO. The temperature of each cryovial was gently reduced to -80°C using the Mr Frosty propan-2-ol containers (Nalgene ThermoFischer). After 24 hours, cryovials were transferred to liquid nitrogen.

2.7.C. iTEC Reprogramming

Cryovials were thawed for three minutes at 37°C in a water bath. The DMSO was washed out and MEFs were seeded directly into a T150. After 48 hours, the flask was passaged and split into three T150s. After four hours, 0.1 μM 4OHT was administered to each flask. Fresh medium was added to the iTEC every two to three days for 18 days. iTEC were liberated from T150s using the above defined protocol. However, the trypsin incubation length was increased from one minute to five. For all experiments this process utilised iTEC medium, except the functionality assay detailed in chapter three and all MTOC experiments, which used 2% medium.

2.7.D. Coating Tissue Culture Flasks with Polymer

Glass-bottomed tissue culture plates were used to prevent the solvent from damaging the plates. To coat the plates, polymers were dissolved in acetone at 0.2 mg / mL and pipetted into wells in the appropriate layout. 15 μl was used to coat 384-well plates and 500 μl was used to coat 24-well plates, which was completed on an orbital shaker. The plates were airdried at room temperature to remove the acetone and then washed with water and PBS to remove any residual contaminates.

2.7.E. Microarray, Focused Arrays and *Ex Vivo* TEC Functionality Array

iTEC and TEC were cultured in iTEC medium, except for the N2B27 *ex vivo* TEC functionality array that used N2B27 medium. On all experiments, medium was changed every two to three days. Microarrays were cultured in 5 ml of medium using rectangular tissue culture flasks (ThermoFischer #167063). The focused polymer arrays and *ex vivo* TEC functionality arrays were performed in glass bottomed 384-well plates (ThermoFisher #164586). These smaller wells had the capacity for 100 μl of media.

2.7.F. Co-Cultures Cytokine Supplements

2.7.F.I. High Co-culture Cytokines

- 50 ng / ml FGF-7 (Peprotech #100-19)
- 5 ng / ml FLT3L (Peprotech #250-31L)
- 10 ng / ml IL-7 (Peprotech #217-17)
- 25 ng / ml KITL (Peprotech #250-03)

2.7.F.II. Low Co-culture Cytokines

- 50 ng / ml FGF-7
- 5 ng / ml FLt3L
- 1 ng / ml IL-7
- 5 ng / ml KITL

2.7.G. Monolayer Co-Cultures / iTEC Polymer Functionality Assay

FACS isolated iTEC and adult ETPs were seeded simultaneously in glass bottomed 24-well plates (CellVis #P24-1.5H-N). For the first four days, cells were cultured in 500 µl iTEC medium with high co-culture cytokines. For the final 10 days, cells were cultured in 500 µl iTEC medium with low co-culture cytokines. Medium was replaced every two to three days using a 50% change so the thymocytes would not be drawn off the monolayer.

2.7.H. Reaggregates Thymic Organ Culture

Reaggregates thymic organ culture (RTOC) were created using compact reaggregation (Sheridan *et al*., 2009). Briefly, target cell populations were suspended in 2% medium within a parafilm-sealed pipette tip. Centrifugation at 500 rcf, for five minutes, at room temperature created a cell pellet within the tip. The parafilm was removed and the cell pellet excised upon a porous membrane (Merck Millipore Corporation #ATTP01300) in a 24-well plate (Corning CLS3527). The membrane was floated on 1 ml of iTEC medium with low co-culture cytokines media. A 50% medium exchange was performed every two to three days.

2.7.I. Miniaturised-Reaggregates Thymic Organ Culture

Miniaturised-reaggregates thymic organ culture (MTOC) were created using the GRID3D system (Sun Biosciences). Target cell populations were suspended in 25 µl 2% medium and applied directly onto hydrogel. After one hour, 200 µl of 2% medium with low co-culture cytokines was added to the medium port of each well. This was replaced every two to three days using a 50% medium change.

2.7.J. Seeding Densities of Culture Methods

Table C2.1 :The Seeding Densities of Culture Methods.

This table shows seeding densities of cellular components used in a given experiment

Method	*iTEC*	*E15.5 TEC*	*Cre Only MEF*	*WT MEF*	*Adult ETP*	*Embryonic DN Thymocytes*
sevRTOC		600,000		100,000		100,000
iRTOC Chapter 3	600,000			100,000		100,000
Cre only RTOC			600,000	100,000		100,000
iTEC Microarray	200,000					
Cre only Microarray			200,000			
iTEC Focused Array	30,000 per well					
iTEC Functionality Array	200,00 per well					
iMTOC	1000 per well			12,000 per well	700 per well	
iRTOC Chapter 5	600,000			100,000	7,000	

2.8. Panels

The following panels describe the combination of antibodies used in either the flow cytometry or FACS procedures of in immunohistochemistry.

2.8.A. Flow Cytometry

2.8.A.I. Adult ETPs

Table C2.2: The Antibody Panel to Isolate ETPs for the Four-Week-Old Thymus. This table shows the name, associated fluorophore, supplier, clone and concentration of antibodies used to isolate ETPs in adult mice.

Antigen	*Clone*	*Fluorophore*	*Supplier*	*Catalogue Number*	*Dilution*
CD45	30-F11	APC/eflour780	Life Technologies	47-0451-80	1/1000
CD25	PC61	PE	BioLegend	102007	1/2000
CD44	IM7	APC	BioLegend	103011	1/2000
c-KIT	2B8	Pe/Cy7	BioLegend	105813	1/1000
Lineage:					1/800
CD3	145-2C11	FITC	BioLegend	100305	
CD4	RM4-5	FITC	BioLegend	100509	
CD8	53-6.7	FITC	BioLegend	100705	
CD11b	M1/70	FITC	eBioscience	11-0112-82	
CD11c	N418	FITC	eBioscience	11-0114-82	
B220	RA3-6B2	FITC	BioLegend	103205	
Gr-1	RB6-8C5	FITC	BioLegend	108405	
NK1.1	PK136	FITC	BioLegend	108705	
TER-119	TER-119	FITC	BioLegend	116205	
DAPI	-	-	Life Technologies	D1306	0.5 µg / ml

2.8.A.II. Embryonic DN Thymocytes and TEC

Table C2.3: The Antibody Panel to Isolate DN Thymocytes and TEC in E15.5 Mice. This table shows the name, associated fluorophore, supplier, clone and concentration of antibodies used to isolate DN thymocytes and TEC from E15.5 Embryos.

Antigen	*Clone*	*Fluorophore*	*Supplier*	*Catalogue Number*	*Dilution*
EpCAM	G8.8	PE	BioLegend	324205	1/3000
Lineage:					1/800
CD3	145-2C11	FITC	BioLegend	100305	
CD4	RM4-5	FITC	BioLegend	100509	
CD8	53-6.7	FITC	BioLegend	100705	
CD11b	M1/70	FITC	eBioscience	11-0112-82	
CD11c	N418	FITC	eBioscience	11-0114-82	
B220	RA3-6B2	FITC	BioLegend	103205	
GR-1	RB6-8C5	FITC	BioLegend	108405	
NK1.1	PK136	FITC	BioLegend	108705	
TER119	TER-119	FITC	BioLegend	116205	
CD45	30-F11	APC/eflour780	eBioscience	47-0451-80	1/1000
DAPI	-	-	Life Technologies	D1306	0.5 µg / ml

2.8.A.III. Thymopoiesis

Table C2.4: The Antibody Panel to Analyse Thymocyte Subsets in Co-culture Assay. This table shows the name, associated fluorophore, supplier, clone and concentration of antibodies used to analysis the thymocyte subsets found in co-culture assays. Note that the iTEC Polymer Functional Array omitted the CD25, CD44, CD62 and CD69 because they were not relevant to the readout.

Antigen	*Clone*	*Fluorophore*	*Supplier*	*Catalogue Number*	*Dilution*
Lineage: CD11b CD11c Gr-1 NK1.1 B220 EpCAM (or iFoxn1 GFP)	 M1/70 N418 RB6-8C5 PK136 RA3-6B2 9C4	 FITC FITC FITC FITC FITC FITC GFP	 eBioscience eBioscience BioLegend BioLegend BioLegend BioLegend	 11-0112-82 11-0114-82 108405 108705 103205 324204	1/800
CD4	RM4-5	Pe	BioLegend	100512	1/800
CD8	53-6.7	APC	BioLegend	100711	1/800
CD3e	145-2C11	BV786	BioLegend	100355	1/100
TCR-β	H57-597	Pe/Cy7	BioLegend	109222	1/100
CD62L	MEL-14	APC/FIRE	BioLegend	104450	1/800
CD25	PC61	BV650	BioLegend	102038	1/1000
CD44	IM7	BV510	BioLegend	103043	1/1000
CD69	H1.2F3	BV421	BioLegend	104528	1/100
7-AAD	-	-	BioLegend	420404	1/200

2.8.A.IV. Isolation of LKS Haematopoietic Stem Cells

Table C2.5: The Antibody Panel to Isolate Lineage$^-$SCA-1$^+$c-KIT$^+$ HSCs.
This table shows the name, associated fluorophore, supplier, clone and concentration of antibodies used to isolate Lineage$^-$SCA-1$^+$c-KIT$^+$ haematopoietic stem cells (LSKs) from murine bone marrow.

Antigen	*Clone*	*Fluorophore*	*Supplier*	*Catalogue Number*	*Dilution*
Lineage:					1/800
CD3	145-2C11	FITC	BioLegend	100306	
CD4	A20	FITC	BioLegend	110706	
CD5	53-7.3	FITC	BioLegend	100605	
CD11b	M1/70	FITC	eBioscience	11-0112-82	
Gr-1	RB6-8C5	FITC	BioLegend	108405	
B220	RA3-6B2	FITC	BioLegend	103205	
TER119	TER-119	FITC	BioLegend	116205	
SCA-1	D7	Pe	BioLegend	108107	1/1600
c-KIT	2B8	APC/Cy7	BioLegend	105826	1/1600
DAPI	-	-	Life Technologies	D1306	0.5 µg / ml

2.8.B. Immunohistochemistry

2.8.B.I. Microarray and Focused Array

Table C2.6: The Antibody Panel to Count iTEC/TEC in the Microarray and Focused Arrays.
This table shows the name, associated fluorophore, supplier, clone and concentration of antibody and DAPI used to count iTEC/TEC in the microarray and focused arrays.

Antigen	*Clone*	*Supplier*	*Catalogue Number*	*Dilution*	*Host*
Pan-Cytokeratin	-	Dako	Z0622	1/250	Rabbit
DAPI	-	-	Life Technologies	D1306	5 µg / ml

2.8.B.II. Selective Binding Assay

Table C2.7: The Antibody Panel to Count the Number of β5t$^+$ iTEC and to Quantify MHC2 Expression.
This table shows the name, associated fluorophore, supplier, clone and concentration of antibodies and Cell Mask Blue used to count the number of β5t$^+$ iTEC and to quantify MHC2 expression.

Antigen	*Clone*	*Supplier*	*Catalogue Number*	*Dilution*	*Host*
B5t	PD021	MBL	PD021	1 / 1000	Rabbit
MHC2	ER-TR3	Abcam	ab15630	1/250	Rat
Cell Mask Blue	-	Molecular Probes	H32720	1/1000	-

2.8.B.III. TEC Proliferation and mTEC Maintenance Assay

Table C2.8: The Antibody Panel to Observe Proliferation and mTEC within MTOC. This table shows the name, associated fluorophore, supplier, clone and concentration of antibodies and DAPI used observe proliferation and mTEC within MTOC.

Antigen	*Clone*	*Supplier*	*Catalogue Number*	*Dilution*	*Host*
EpCAM	G8.8	BioLegend	118201	1/1000	Rat
Ki67	SP6	Abcam	ab16667-500ul	1/100	Rabbit
Biotinylated Ulex Europaeus Agglutinin I (UEA I)	-	Vector Laboratories	B-1065	1/500	-
DAPI	-	-	Life Technologies	D1306	5 µg / ml

2.8.B.IV. Secondary Antibodies

Table C2.9: The Secondary Antibodies used in all Experiments.
This table shows the name, associated fluorophore, supplier, clone and concentration of antibodies and cell mask blue used observe proliferation and mTEC within MTOC.

Specificity	*Fluorophore*	*Host*	*Supplier*	*Catalogue Number*	*Dilution*
Rabbit	Alexa Fluor (AF)-488	Goat	Thermo	A-11001	1/500
Rat	AF-568	Goat	Thermo	A-11031	1/500
Streptavidin	AF-647	Goat	Thermo	S21374	1/500

2.9. Primers

2.9.A. Designing Primers

The Universal Probe Library (Roche) primer design software was used to create all primer pairs. When possible, intron spanning primers were used. Primers were judged based on the internal sore assigned by the software and the primers with the highest score were selected for use. All primers were ordered from Sigma as standard DNA oligonucleotides.

2.9.B. Genotyping Primers

Table C2.10: The Oligonucleotide Sequences used to Genotype Mice.
This table shows the name, orientation and sequences of primers for genotyping mice.

Transgene	*Orientation*	*Sequence*
Rosa26:CreERt2	Forward	GCA TAA CCA GTG AAA CAG CAT TGC TG
	Reverse	GGA CAT CAG GGA TCG CCA GGC G
iFoxn1	Forward	GGG AGC AGC TGA AGG ATG AC
	Reverse	CGC TTG AGG AGA GCC ATT TG
Foxn1^{G}	Forward	TAT ATC ATG GCC GAC AAG CA
	Reverse	GAA CTC CAG CAG GAC CAT GT

2.9.C. Reverse Transcription-Quantitative-PCR Primers

Table C2.11: The Oligonucleotide Sequences used to Genotype Mice.
This table shows the name, orientation and sequences of primers for RT-qPCR experiments and the associated UPL probe number (Roche).

Gene	*Orientation*	*Sequence*	*UPL Probe*
Endogenous *Foxn1*	Forward	CTTAAAGGTCAAAGAAGGAAAACACT	68
	Reverse	GGCTAACAAATAAGTTGGCTGA	
Total *Foxn1*	Forward	TGACGGAGCACTTCCCTTAC	94
	Reverse	GACAGGTTATGGCGAACAGAA	
Dll4	Forward	AGGTGCCACTTCGGTTACAC	106
	Reverse	GGGAGAGCAAATGGCTGATA	
Dll1	Forward	ACAGAGGGGAGAAGATGTGC	20
	Reverse	CCCTGGCAGACAGATTGG	
Aire1	Forward	GGTTCCTCCCCTTCCATC	45
	Reverse	GGCACACTCATCCTCGTTCT	
Psmb11 (β5t)	Forward	CAGGGTTAGTTCTGGGAGCA	21
	Reverse	CAAAGCAGGAAACCCAAAAG	
CTSL1 (Cathepsin-L)	Forward	CAAATAAGAATAAATATTGGCTTGTCA	60
	Reverse	TGTAGCCTTCCATACCCCATT	
Il-7	Forward	CGCAGACCATGTTCCATGT	27
	Reverse	TCTTTAATGTGGCACTCAGATGAT	
KitL	Forward	TCAACATTAGGTCCCGAGAAA	71
	Reverse	ACTGCTACTGCTGTCATTCCTAAG	
Flt3L	Forward	CCTAGGATGCGAGCCTTGT	102
	Reverse	TGTTTTGGTTCCCAACTCG	
Ccl25	Forward	GAGTGCCACCCTAGGTCATC	9
	Reverse	CCAGCTGGTGCTTACTCTGA	
Cxcl12	Forward	GGTTCTTCGAGAGCCACATC	21
	Reverse	TGTTCTTCAGCCGTGCCAA	
MHCIIEβ	Forward	CCTCCAGTGGCTTTGGTC	109
	Reverse	CCGTTGTAGAAATGACACTCAGA	
Ywhax	Forward	CTTCCTGCAGCCAGAAGC	74
	Reverse	GGTTTCCTCCAATCACTAG	
Hprt	Forward	TCCTCCTCAGACCGCTTTT	95
	Reverse	CCTGGTTCATCATCGCTAATC	
Tbp	Forward	GGGGAGCTGTGATGTGAAGT	97
	Reverse	CCTGGTTCATCATCGCTAATC	
Wnt4	Forward	TCATGAATCTTCACAACAACGA	4
	Reverse	CCCCGTGACACTTGCACT	

3. Chapter Three: Optimisation of the Induced Thymic Epithelial Cell Reprogramming Protocol into a Standardised and Scalable Tool

3.1. Introduction and Aims

In 2014, this laboratory published a method of direct reprogramming of murine embryonic fibroblasts (MEFs) into induced thymic epithelial cells (iTEC). Reprogramming into iTEC uses a genetic method to enforce transgenic *Foxn1* expression once the system has been exposed to 4-hydroxy tamoxifen (4OHT). Two transgenes are required to elicit this effect which are both knocked into the Rosa26 locus. The transgene in the maternal allele, contains *Foxn1* and *GFP*, with are produced as discrete proteins using an internal ribosome binding site. In the absence of CRE recombinase, this transgene is functionally inactive due to a *floxed* element, which when present, produces a transcriptional pause. This transgene is referred to as the induced FOXN1 (iFoxn1) transgene and is depicted in Figure C3.1A. The CreERt2 fusion protein is knocked into the paternal Rosa26 allele. The CreERt2 protein mediates activation of the iFoxn1 transgene by excising the transcriptional pause in the presence of 4OHT. In the absence of 4OHT, CreERt2 is localised to the cytoplasm, where it is functionally inactive, while in the presence of 4OHT, CreERt2 translocates to the nucleus where it can mediate excision of the transcriptional pause and hence activation of the iFoxn1 transgene.

The CreERt2 transgene is also represented in Figure C3.1A. Strikingly, iTEC were able to support T-cell differentiation *in vitro*, including production of $\beta TCR^{+}CD4^{+}$ and $CD8^{+}$ single positive (SP) T cells and $Foxp3^{+}$ T_{regs}, and upon transplantation were able to generate an organised and functional thymus (Bredenkamp *et al.*, 2014). Whilst this was a significant step toward generating a source of transplantable TEC for clinical application, the original protocol did not meet the scale up requirements necessary for larger experiments. Therefore, optimisation of the protocol into a scalable and standardised process was required.

This chapter details a series of experiments through which I optimised the expansion and reprogramming of iFoxn1 MEFs into iTEC (Figure C3.1A), such that a single embryo can produce in excess of 1×10^8 iTEC for experimentation, with a cryopreservation step. The experiments described include medium selection, titration of 4OHT and altering the duration

of the reprogramming protocol. This chapter also demonstrates that iTEC generated using the improved protocol upregulate key genes associated with thymic epithelial cell (TEC) function and compares the functionality of these optimised iTEC to *ex vivo* TEC and the native thymus.

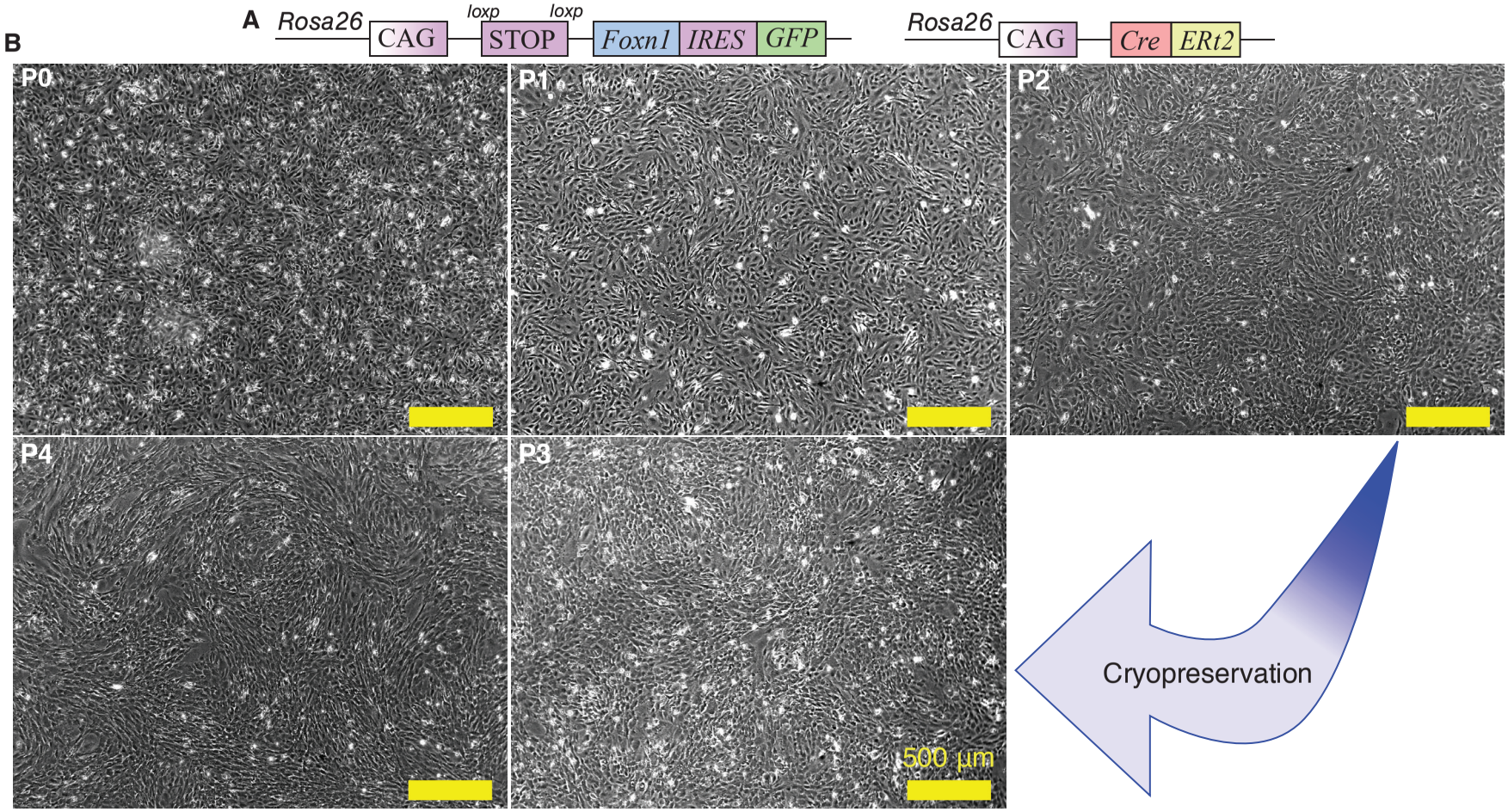

Figure C3.1: Generating a Bank of Cryopreserved iFoxn1 MEFs

A. Schematic of iFoxn1 MEF transgenes. **B**. Representative images of iFoxn1 MEFs at different time points during the expansion protocol. Between P2 and P3, MEFs were stored in liquid nitrogen and thawed for a final, expansion passage. At P4 MEFs were treated with 4OHT to induce expression of transgenic *Foxn1*. At all passages MEFs were diluted one-in-three and became confluent within 24 hours.

3.2. Creating a Bank of Cryopreserved MEFS

At the starting point of my thesis, it was routine to establish fresh iFoxn1 MEFs to generate each batch of iTEC for each individual experiment and induce reprogramming in MEFs after one passage (P). This practice limited the number of MEFs that could be feasibly expanded from each embryo and prevented each batch of MEFs from being used in more than one experiment. The timeline of the original protocol in detailed in Table C3.1.

To standardise the input population of MEFs for reprogramming and remove dependence on timed matings, I therefore set out to investigate whether iTEC could be generated from expanded and cryopreserved MEFs, since cells stored in liquid nitrogen can be reliably prepared for reprogramming within a short timeframe. There is evidence that extended passaging of cells in culture perturbs cellular growth, metabolism and introduces genetic abnormalities in a range of primary cell types, including MEFs (Hayflick, 1965). Given the sensitivity of reprogramming strategies to variation, it is reasonable to assume that populations of MEF established concurrently and using a standardised protocol should reduce batch-to-batch variability in generation of the target reprogrammed cell population. MEFs are a commonly used cell type in reprogramming assays, so the literature details common limitations of expansion (Amand *et al*., 2016). As it was reported that MEFs display the characteristic abnormalities associated with culture after P5 – 7, I decided to avoid this upper limit by initiating reprogramming at P4 (Amand *et al*., 2016; Hayflick, 1965). The passage at which expanded MEF display abnormalities is dependent upon environmental factors, most notably the severity of the passaging process. In setting out to test whether cryopreserved MEFs could be used to generate iTEC, I therefore employed a gentle passaging process: minimising exposure of the MEFs to trypsin and seeding tissue culture flasks with one third of the flask's maximum potential.

After each passage, bright field imaging was used to evaluate changes to cellular morphology, size and time taken to reach confluency. MEFs were cultured to P4, with a cryopreservation step between P2 and P3, without overt changes in size or morphology (Figure C3.1B). To prepare the MEFs for cryopreservation, each vial was seeded with one

third of the cells harvested from a confluent T150 tissue culture flask, which was approximately 5×10^6 cells. MEFs were frozen in 5% Dimethyl Sulfoxide (DMSO), with an overnight equilibration to -80°C using a Mr Frosty® container to surround cells in propan-2-ol. At all passages MEFs become confluent by 24 hours after seeding at a one-in-three dilution, at a confluent concentration of 1×10^4 MEFs per cm^2.

Therefore, I was able to produce large quantities of MEFs for reprogramming. Before progressing, I needed to ensure increasing the passage number of MEFs did not compromise their ability to undergo reprogramming into iTEC.

Table C3.1: Comparison Between the Timelines of the Original and Optimised Protocols to Generate iTEC.

A table comparing the original protocol to reprogram iFoxn1 MEFs into iTEC to the one detailed in this chapter. Note X denotes the day iFoxn1 MEFs were removed from storage.

Day	*Original*	*Optimised*
0	Establish P0 MEFs	Establish P0 MEFs
1	Change Medium, Genotype	-
2	-	Passage P1 MEFs 1/3
3	Passage P1 MEFs 1/9	Passage P2 MEFs 1/3 For cryopreservation
4	Change Medium on P1 MEFs	-
6	Add 1 μM 4OHT	-
8	Wash off 4OHT and change medium	-
10	FACS to isolate GFP^+ MEFs	-
X0	-	Thaw P3 MEFs
X1	-	Passage P3 MEFs and add 0.1 μM 4OHT
X3	-	Wash off 4OHT and change medium
X19	-	FACs to isolate GFP^+ MEFs

3.3. Expanded iFoxn1 MEFs Successfully Initiate Programming

iFoxn1 MEFs expanded in the above fashion and exposed to 4OHT displayed evidence of reprogramming into iTEC. MEFs were exposed to 3 μM 4OHT for 48 hours and left to reprogramme for a total of eight days (Bredenkamp *et al*., 2014). Fluorescence activated cell sorting (FACS) was used to observe whether CreERt2-mediated excision of the floxed transcriptional pause had activated GFP expression, and to collect GFP^+ and GFP^- fractions for mRNA preparation. Collection of both fractions controlled for expression of transgenic *Foxn1* as GPF^- MEFs contained the inactive iFoxn1 transgene and could not express transgenic *Foxn1*. The expression of key genes was then quantified using E13.5 thymic epithelial progenitor cells (TEPC) as positive controls, and GFP^- MEFs as negative controls. TEPC were defined as $EpCAM^+PLET1^+$. Furthermore, both the GFP^+ and GFP^- MEFs were cultured in the same tissue culture flask, so the environment was consistant, and both arose from the same starting MEF population, so any genetic abnormalities introduced during the expansion process were shared.

A panel of genes was selected to encompass a range characteristic of TEC identity (Figure C3.2). Total *Foxn1* quantified the amount of mRNA contributed from both transgenic and endogenous loci and expression of endogenous *Foxn1* was also quantified. This is important to understand whether reprogramming promotes transcription of the endogenous locus but to also calculate the amount of transgenic mRNA. *Wnt4* was included as there is evidence that it is important for thymic organogenesis, it is both regulated by FOXN1and also acts as a negative regulator of *Foxn1* expression (Bredenkamp *et al*., 2014; Swann *et al*., 2017b). *Dll4* and *Psmb11* were included as they represent functional targets that are directly regulated by FOXN1 (Hozumi *et al*., 2008; Takada *et al*., 2017; Žuklys *et al*., 2016). Finally, *Il-7* was included as it represents an important factor for thymopoiesis and thymus organogenesis, but is not a direct target of FOXN1 (Zamisch *et al*., 2005).

Unpaired t-tests were used to compare the relative level of expression in GFP^- and GFP^+ iFoxn1 MEFs eight days after administration of 4OHT. Data were evaluated for homogeneous variance using Levene's test and normality using the Shapiro-Wilks tests.

Data that failed assumptions were analysed using Welch corrected t-test or Mann-Whitney tests, respectively. This reverse transcription- uantitative polymerase chain reaction (RT-qPCR) provided evidence that GFP^+ MEFs had initiated reprogramming with significantly greater expression of transgenic *Foxn1.* This led to increased *Wnt4* and *Dll4* but GFP^+ MEFs had not completed reprogramming as indicated by similar expression of *Psmb11* and *Il-7,* compared to GFP^- MEFs (Figure C3.2).

There were two caveats to this readout. Firstly, it could be argued a one-way Analysis of Variance (ANOVA) was better suited to analyse the data as it would allow comparison of both MEF groups to the positive control, E13.5 TEPC. This was decided against as the TEPC introduced a large amount of variation to the ANOVA. Given that TEPC are a rare cell type, a small cell population method was used to collect mRNA for the positive controls. Whilst this overcomes tissue limitation, it also promotes sampling bias. This is most evident in the total *Foxn1* data set. One biological replicate reported ~500% greater expression than the remaining two replicates. Ultimately the ANOVA was associated with an R^2 value of 0.5 and as result the ANOVA was a poor comparison between groups. Therefore, it was decided to test the more specific hypothesis that GFP^+ MEF expressed greater amounts of TEPC associated genes than GFP^- MEFs as this could be queried more robustly. It is possible to test the hypothesis that GFP^+ MEFs have a similar gene expression profile to TEPCs by increasing the number of cells analysed in each condition to remove the sampling bias. Over a larger sample the average gene expression profile of TEPC would be more similar. However, this hypothesis ultimately aims to make indirect assertions regarding the behaviour of GFP^+ MEFs compared to TEPC, which can be, and was, explored directly. Secondly, it could be argued that it is important to investigate the effect the expansion process had upon reprogramming by using a repeated measure design and collecting mRNA from the same batch of MEFs at P1 and P4.

Therefore, I established that increasing the passage number did not prevent MEFs from instigating the reprogramming. The next step was to optimise the reprogramming stage.

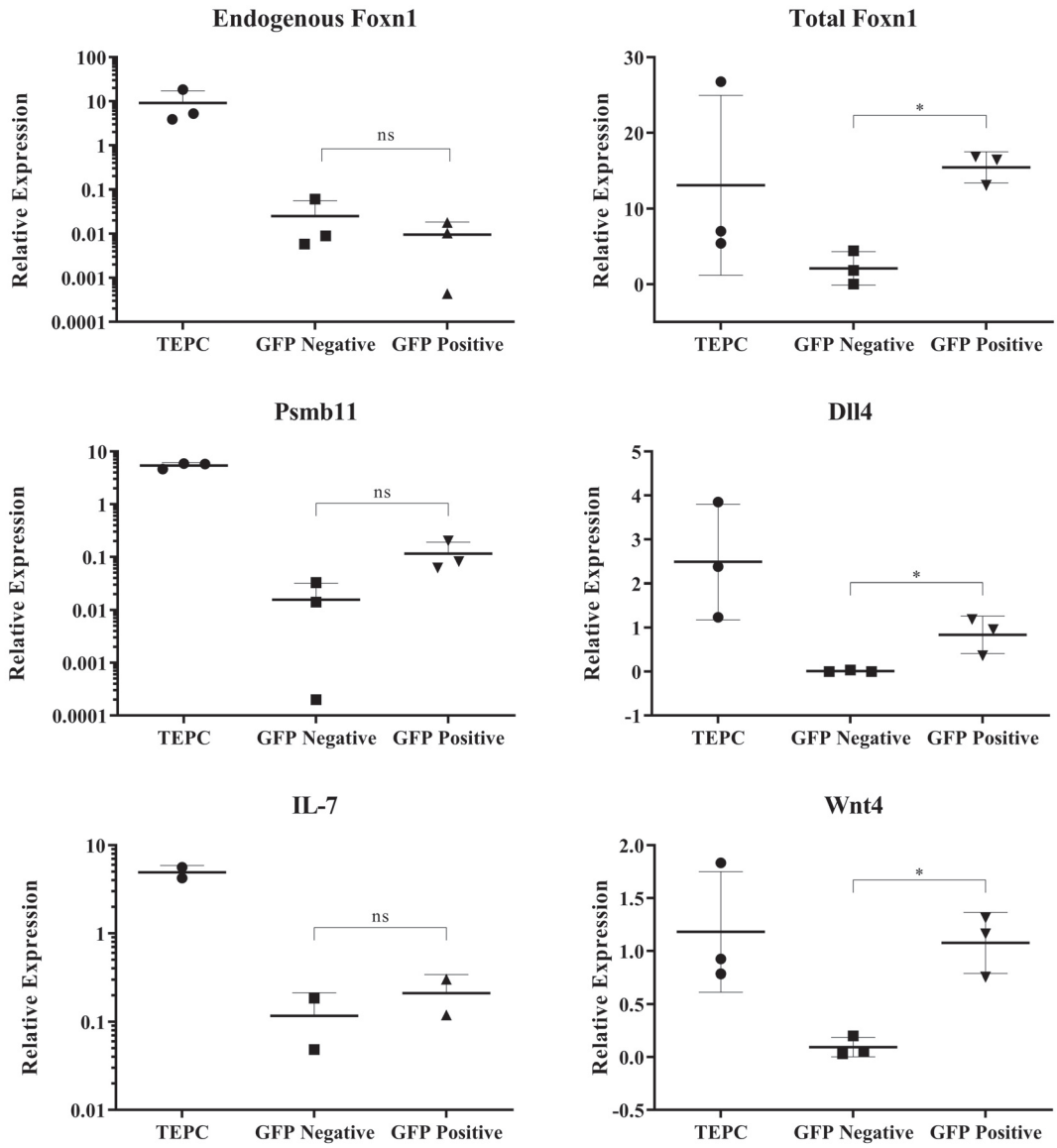

Figure C3.2: iTEC Display Upregulation of Key TEC Genes

RT-qPCR data showing initiation of reprogramming in GFP$^+$ MEFs into iTEC eight days after treatment with 4OHT. Expression of GFP marks those MEFs that have activated expression of the iFoxn1 transgene. Both the GFP$^+$ and GFP$^-$ fractions were isolated from the same iFoxn1 MEF preparations using FACS.

The endogenous *Foxn1* and total *Foxn1* gene expression measurements utilised two sets of primers that distinguished between transcripts that originated from the transgenic allele and the endogenous *Foxn1* locus. The primer pair responsible for measuring total *Foxn1* expression bind to both transgenic and endogenous *Foxn1* transcripts. However, the primer pair that measured just endogenous *Foxn1* was unable to bind to the *Foxn1* transcripts originating from the transgenic allele due to the presence of the IRES system found at the 3' end.

Gene expression is shown relative to three housekeeping genes, *Hprt*, *Ywhaz* and *Tbp*.* denotes significance. The Y-axis for the genes Endogenous *Foxn1*, *Il-7* and *Psmb11* use a logarithmic scale. This experiment was performed three times using iFoxn1 MEFs established from unique embryos. Note that due to the low expression of *Il-7*, one biological replicate was unable to provide a measurement. Each biological replicate produced one sample of mRNA that was quantified in three technical replicates by RT-qPCR.

3.4. Optimisation of 4OHT concentration

3.4.A. 0.1μM 4OHT Applied to Proliferating MEFs in Advanced DMEM/F12 is Optimal for Reprogramming

Once a method was optimised to establish a bank of cryopreserved iFoxn1 MEFS, with the potential to initiate reprogramming into iTEC, using a standardised strategy, it was necessary to optimise the reprogramming protocol. Three key variables were identified for this process: confluency, cell culture medium and concentration of 4OHT (Figure C3.3).

It was assumed that a significant environmental variable within a single tissue culture flask is confluency. Once cells reach a certain density, they dramatically inhibit their proliferative behaviour via Yes-associated protein (YAP) inactivation and the Hippo signalling pathway (Eagle and Levine, 1967; Zhao *et al*., 2007). Therefore, I tested the effect of initiating reprogramming in proliferating or confluent MEFs. Additionally, since different cells require different cell culture medium to reflect their native environment (McKee and Komarova, 2017) and thus to maintain their identity, two media conditions were tested. These were DMEM (Gibco #42430025), which was used in the original publication and is commonly cited as the preferred medium for MEF expansion; and Advanced DMEM/F12 (Gibco #12634-028), which this lab reported to be beneficial in RTOC (Sheridan Thesis, 2007; Bredenkamp *et al*., 2014; Amand, Hanover and Shiloach, 2016). It was hypothesised that reprogramming MEFs in medium associated with improving *ex vivo* TEC culture, would be conducive to producing more TEC-like iTEC. Finally, the concentration of 4OHT was optimised to avoid adverse reactions, as it has established toxic properties (Hodges *et al*., 2003).

To examine the influence of these variables, 1×10^5 CreERt2$^+$iFoxn1$^+$ (“iFoxn1”) MEFs and CreERt2$^+$iFoxn1$^-$ (“CreERt2 only”) control MEFs were seeded into 24-well plates and were assigned to conditions in triplicates. 4OHT was administered to the wells after 2 hours in the proliferating group and after 48 hours for those in the confluent group (Figure C3.3). After four days, MEFs were liberated from the wells with trypsin and the percentage of GFP$^+$ MEFs determined using flow cytometry. An unbiased gating strategy was developed that treated the 0 (vehicle only) 4OHT group as a GFP Fluorescence-Minus-One (FMO) control (Figure C3.3). To ensure the iFoxn1 transgenes was responsible for producing GFP$^+$ MEFs,

CreERt2 only MEFs were treated alongside iFoxn1 MEFs, and GFP was not observed at any concentration of 4OHT in these CreERt2 only controls (data not shown).

A three-way ANOVA was used to compare effects between mean proportion of MEFs expressing GFP. The three independent variables compared were 4OHT concentration, medium condition and confluency (Table C3.2). The greatest and only statically significant contributor of variation within the experiment arose between the vehicle only control and other concentrations of 4OHT (Table C3.3). As no significant difference in reprogramming efficiency between 4OHT concentrations was found, the 0.1 μM concentration was used in subsequent experiments based on the assumption that reducing the concentration of 4OHT would reduce the probability of side effects causing adverse consequences (Figure C3.4). Application of 0.1 μM 4OHT to proliferating MEFs produced less variance, reported as the Coefficient of Variation (CoV), than application to confluent MEFs (Table C3.4). Given the aim of reducing variance within the reprogramming protocol, this was taken as enough evidence to apply 4OHT to proliferating cells in all subsequent experiments.

The basal DMEM medium preparation did not have a significant effect on the reprogramming efficiency, so both, DMEM and advanced DMEM/F12 were taken forward for further experimentation to evaluate their effects on the proliferation of iFoxn1 MEFs undergoing reprogramming. MEFs were seeded into four 150 cm^2 tissue culture flasks and two were assigned to the DMEM group and two to the Advanced DMEM/F12 group. After two hours, 0.1 μM 4OHT was applied. On day four and day 18, the total MEFS from one of the flasks from each group were counted. A one-way ANOVA found there were significantly more cells in the Day 18, Advanced DMEM/F12 than at day 4, whilst there was no difference in the DMEM group. MEFs in Advanced DMEM/F12 proliferated during the reprogramming phase whilst those in DMEM did not. This analysis returned a satisfactory R^2 of 0.8653 and Advanced DMEM/F12 was therefore judged superior, given the objective of the experiment to create a scalable protocol to generate iTEC, and was used in all subsequent experiments (Figure C3.5).

Therefore, I was able to improve the reprogramming conditions to produce a larger number of iTEC than previously achievable. Now I need to ensure that the changes I made to the protocol did not comprise iTEC ability to function. The main function of the thymus is to generate T-cells, so I investigated whether iTEC where able to mediate T-cell differentiation.

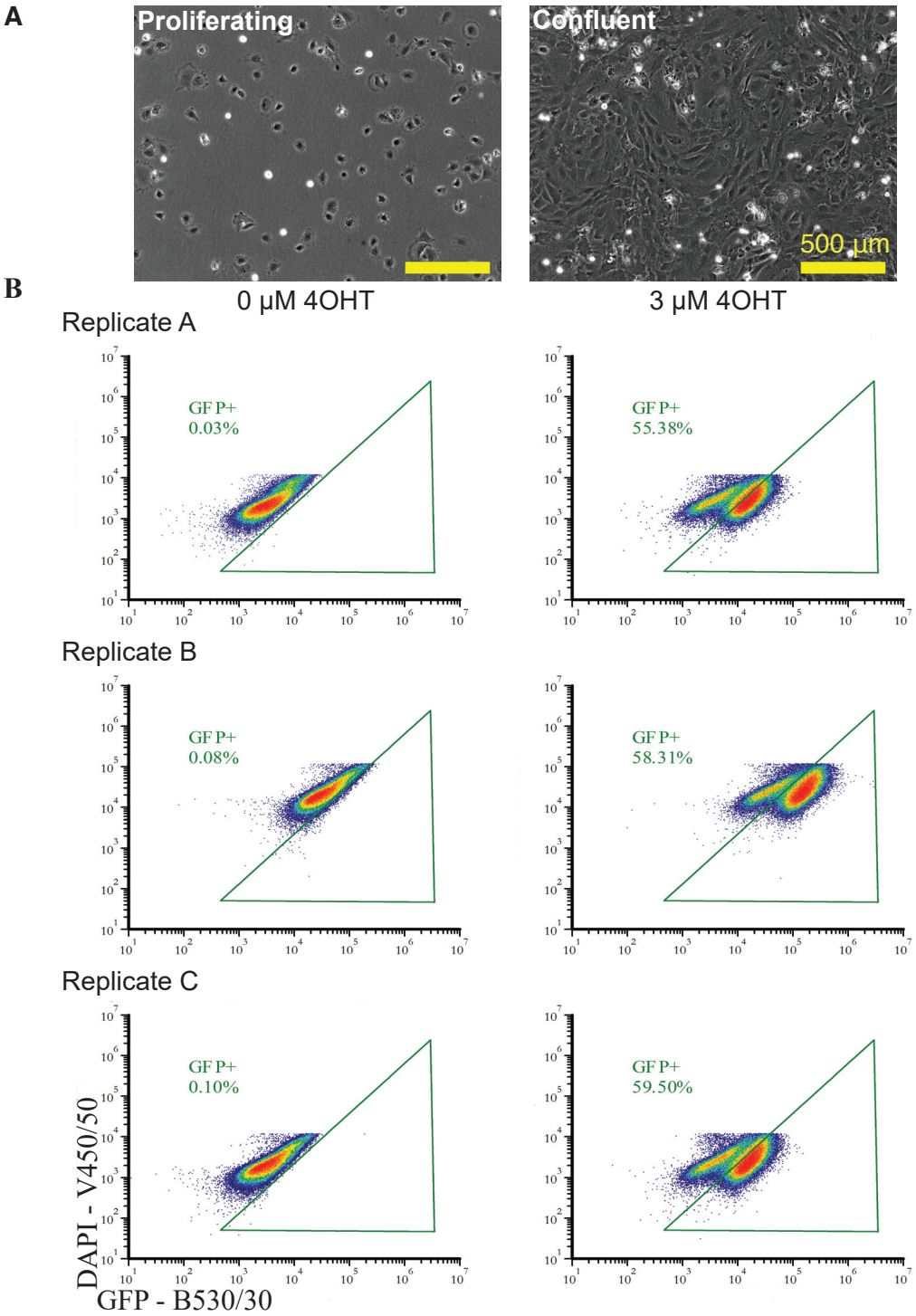

Figure C3.3: Method to Determine Optimal 4OHT Concentration

A. Bright field images of MEFs before reprogramming. 4OHT was applied to proliferating MEFs two hours *(left)* and confluent MEFs 48 hours after seeding *(right)*. **B**. The gating strategy used to measure effect of 4OHT concentration on the proportion of MEFs expressing GFP. Representative plots shown from a single experiment using Advanced DMEM/F12 media. The experiment was performed in triplicate using MEFs established from unique embryos and for each condition three technical replicates were used. Gate was set to a maximum of 0.1% error across all three technical replicates on untreated control MEFs, which was treated as an FMO.

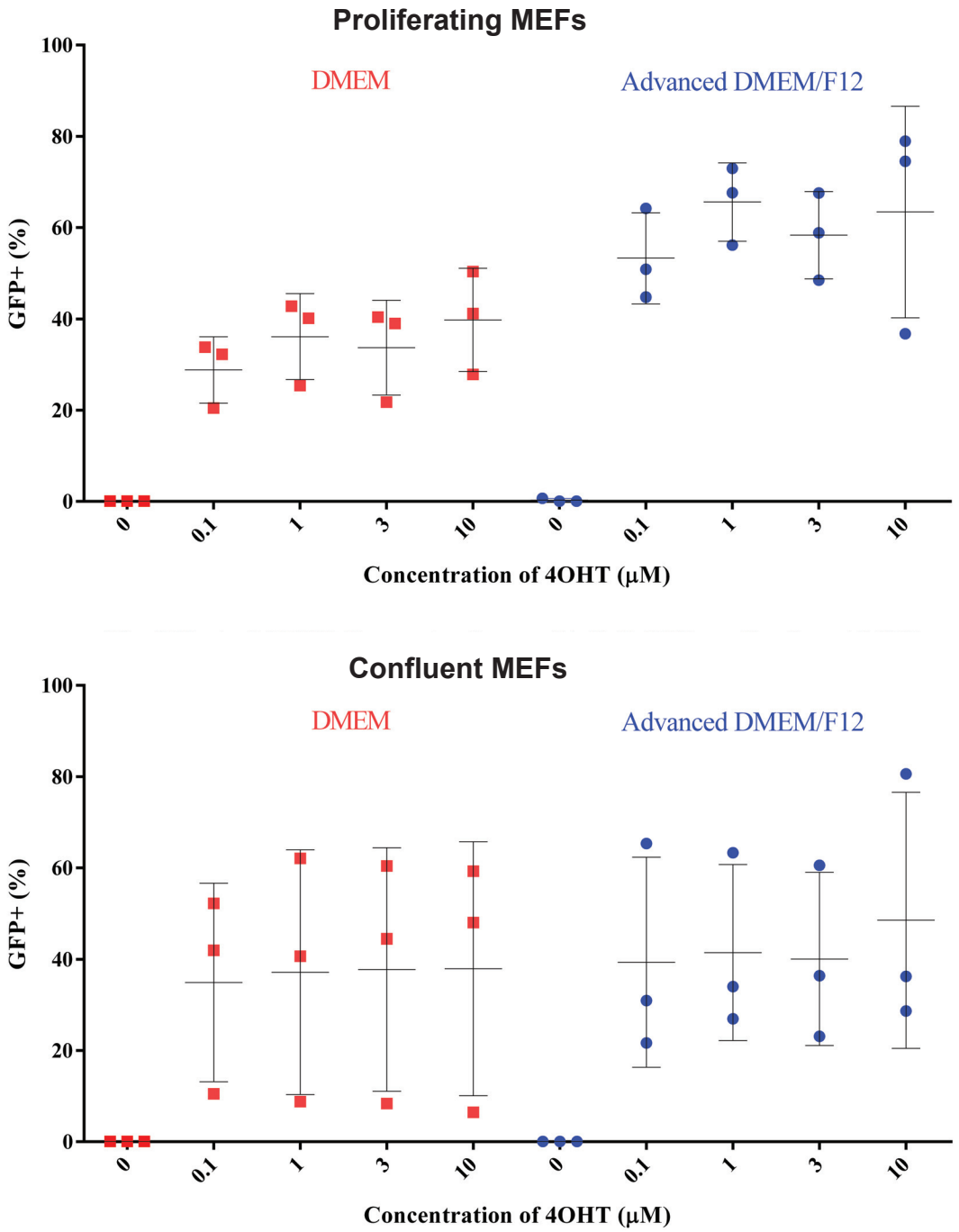

Figure C3.4: Results of Optimising 4OHT Concentration for iFoxn1 MEF Reprogramming

Graphs depicting the percentage of GFP expressing MEFs when exposed to a range of 4OHT concentrations when cultured in DMEM (red) and Advanced DMEM/F12 (blue). 4OHT was added to MEFs when during proliferation (left) and at confluency (right). The experiment was perfromed in triplicate using MEFs established from three unique embryos. Each biological replicate, represented as a data point above, represents the mean of the three technical replicates used in each condition.

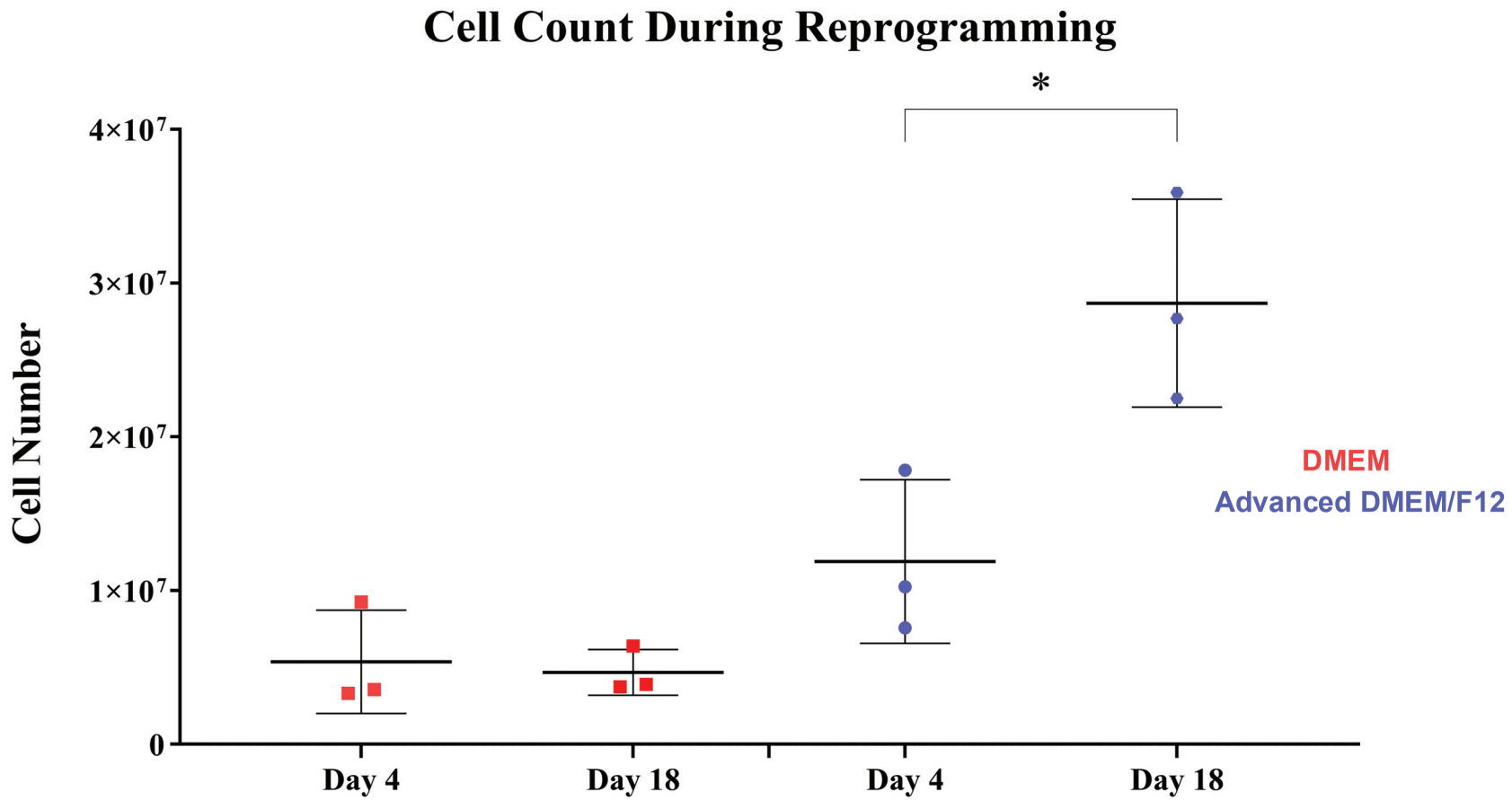

Figure C3.5: Advanced DMEM/F12 Stimulated iFoxn1 MEF Proliferation During Reprogramming

Graph depicting the cell counts of iFoxn1 MEFs during reprogramming when cultured using DMEM *(red)* and Advanced DMEM/F12 *(blue)*. A one way ANOVA compared means from three independent experiments each representing a reprogramming of a different preparation of MEFs established from a unique embryo. * denotes significance.

Table C3.2: Optimising the Application of 4OHT, Raw Data.
Table shows the portion of GFP^+ MEFs found in a 24well. Each condition was produced in triplicate across confluence, 4OHT concentration and medium condition. The results are shown as the mean and CoV of the triplicate wells.

Medium	*Confluency*	*40HT Concertation (μM)*	*Mean % GFP^+*	*CoV (%)*
DMEM	Confluent	0	0.07	4.761
		0.1	34.9	62.24
		1	37.17	72.09
		3	37.76	70.62
		10	37.91	73.31
DMEM	Proliferating	0	0.7556	14.18
		0.1	28.85	25.22
		1	36.13	26.01
		3	33.73	30.77
		10	39.8	28.38
Advanced DMEM/F12	Confluent	0	0.09	7.408
		0.1	39.33	58.47
		1	41.45	46.5
		3	40.05	47.35
		10	48.52	57.83
Advanced DMEM/F12	Proliferating	0	0.28	123.7
		0.1	53.29	18.67
		1	65.59	13.12
		3	58.31	16.42
		10	63.43	36.51

Table C3.3: Optimising Application of 4OHT, Results of Three-Way ANOVA.
Table shows the proportion of contribution of each variable to the total variation. The ANOVA also includes the variation produced through the interaction of these variables. The technical variation is termed “Technical Replicates” as this represents variation between replicates.

Source of Variation	*Percentage of Total Variation (%)*	*P value*
4OHT Concentration	52.47	<0.0001
Medium	1.646	0.4850
Confluency	6.524	0.1831
4OHT Concentration x Medium	0.6505	0.6731
4OHT Concentration x Confluency	1.686	0.2181
Medium x Confluency	2.765	0.3705
4OHT Concentration x Medium x Confluency	0.8469	0.5548
Technical Replicates	24.57	N/A

Table C3.4: The CoV within the 0.1 µM 4OHT Condition.
This table shows the variation in the proportion of GFP^+ MEFs in the proliferating group compared to the confluent group. The proliferating group was associated with less variation, which made it the preferable condition.

Condition	*DMEM* CoV (%)	*Advanced DMEM/F12* CoV (%)
Proliferating	25.22	18.67
Confluent	62.24	58.47

Table C3.5: iTEC Proliferation during Reprogramming, Raw Data.
Table shows the number of MEFs liberated from a T150. This study compared the number of MEFs produced after four and 18 days after activation of the iFoxn1 transgene in both DMEM and Advanced DMEM/F12. Advanced DMEM/F12 medium mediated an increase in the number of MEFs from day four to 18 and was the preferred condition.

Condition	*Day 4 Mean Cell Number*	*Day 4 CoV*	*Day 18 Mean Cell Number*	*Day 18 CoV*
DMEM	5373667	62.51%	4676667	31.87%
Advanced DMEM/F12	11891667	44.75%	28700000	23.54%

3.5. Assessment of iTEC Functionality

3.5.A. Method

The ability to mediate T-cell differentiation was used to evaluate whether iTEC manufactured in the optimised protocol detailed above were successfully reprogrammed and competent to recapitulate TEC functionality. Reaggregate thymic organ culture (RTOC) was used to compare the functionality of iTEC to *ex vivo* TEC as it is currently the best available method for culturing functional *ex vivo* TEC (Anderson *et al*., 1993). RTOC generation was performed as outlined by Sheridan and colleagues, using the 'compaction reaggregation' technique (Sheridan *et al*., 2009).

Thus, defined numbers of iTEC or *ex vivo* TEC were reaggregated into RTOC, along with defined numbers of $CD4^-CD8^-$ double negative (DN) thymocytes and wild type (WT) MEFs to form RTOC, which were then cultured for two weeks (Figure C3.6). WT MEFs were C57BL/6 background and were expanded and cryopreserved using the above defined process. Both DN thymocytes and TEC were isolated simultaneously from the embryonic day (E) 15.5 thymus. DN thymocytes were defined as: $CD45^+EpCAM^-CD3\varepsilon^-CD4^-CD8^-CD11b^-CD11c^-TCR\beta^-TCR\gamma\delta^-B220^-GR\text{-}1^-NK1.1^-TER\text{-}119^-$. TEC were defined: as $EpCAM^+CD45^-$ (Figure C3.7). Each RTOC contained 6×10^5 iTEC, TEC or CreERt2-only MEFs, reaggregated with 1×10^5 DN thymocytes and 1×10^5 WT MEFs.

RTOC were cultured for 14 days at the gas/liquid interface, on a porous membrane, after which thymocytes were recovered from the RTOC for analysis by squashing the structure with a syringe. RTOC were mechanically disassociated to prevent disruption of target antigens with enzymatic treatment. However, while this increased the probability of losing cells during the preparation, this loss was assumed to be constant and proportional. Advanced DMEM/F12 was used as the culture medium and was supplemented with FGF7, FLT3L, KITL and IL-7. A positive staining control was produced for each experiment using thymocytes harvested from a four-week postnatal mouse as a reference to determine thymocyte developmental progression in the RTOC (Figure C3.8). Finally, comparison to RTOC in which CreERt2 only MEFs replaced the iTEC or TEC component, was included to

control for the effect of the iFoxn1 transgene and contaminating, differentiated thymocytes within the DN thymocytes pool proliferating in the RTOC.

The RTOC were then analysed using flow cytometry designed to interrogate thymocyte development. This panel was inspired by Xing and colleagues (2016) with the notable omission of C-C motif receptor (CCR) 7 and major histocompatibility class I (MHC1) due to the physical limitations of the selected flow cytometer. The Novocyte (ACEA) was used for the experiment as capturing information regarding cell numbers was considered more important than quantifying expression of more than ten markers. The addition of anti-CD117 (cKIT) would have allowed identification of DN thymocytes within the DN1 subpopulation (Figure C3.4); the addition of CCR7 would have allowed gating on to positively selected thymocytes that are moving from the cortex into the medulla and observations on the expression of MHC1 would have provided further understanding of the single positive (SP) phase (Xing *et al*., 2016).

In this analysis, CD4 and CD8 provide information on thymocyte differentiation. CD25 and CD44 define the DN phase (Godfrey *et al*., 1993). CD3ε marks the completion of β-selection, and then is upregulated both after completion of the αβTCR and lineage commitment (Wang *et al*., 1999). TCRβ was intended to mirror CD3ε but in practice marked expression of the αβTCR. CD69 is a marker of T-cell activation and during thymopoiesis, marks positive selection. CD62L is upregulated prior to thymic egression and was used as a loose marker (given the omission of CCR7 and MCH1) of the completion of thymopoiesis. In practice, CD62L was also upregulated during transition from the DN to double positive (DP) phases. The lineage cocktail removed non-T-cell, blood cell lineages, iTEC and TEC.

To make valid inferences regarding the capacity of iTEC to mimic native TEC function, a two-step comparison was used: firstly, between native thymopoiesis and sorted *ex vivo* TEC based RTOC (sevRTOC) to observe the effects of the culture method; secondly, by comparing iTEC and *ex vivo* TEC in RTOC to identify the differences between the cell types. In this regard, over the 14 day co-culture, the absence of thymic immigration was not predicted to be a problem given that early thymic precursors (ETPs), presence within the

input DN thymocyte pool, can maintain the thymus for extended periods when trafficking of thymus seeding precursors (TSPs) to the thymus is perturbed (Zlotoff *et al*., 2010). However, it must be stated that RTOC lack regulated egression of thymocytes and therefore it was assumed there would be a build-up of mature SP thymocytes. All data were acquired concurrently as it was important to compare RTOC within a repeat measures experimental design to account for changes in culture environment and DN pool.

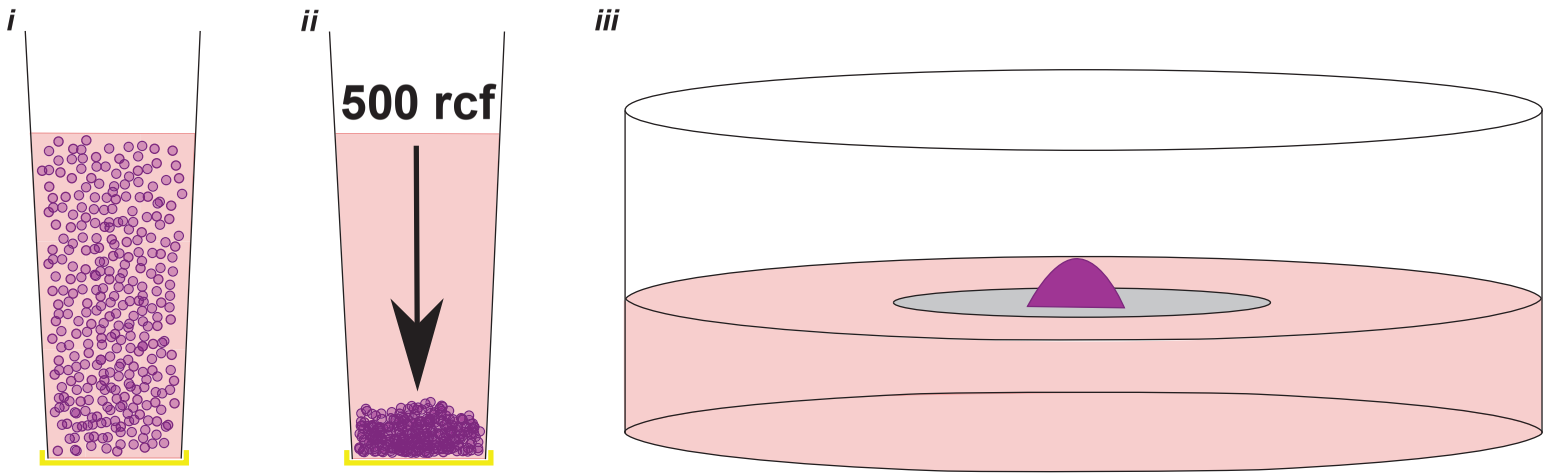

Figure C3.6: Method For iTEC Functionality Test

Schematic of RTOC preparation: RTOC generation was performed as outlined by Sheridan and colleagues (2009). In brief, centrifugation was used to pellet a suspension of iTEC or *ex vivo* E15.5 TEC with MEFs and DN thymocytes within a parafilm-sealed pipette tip. The pellet was then extruded from the tip cultured at the gas/liquid interface for 14 days.

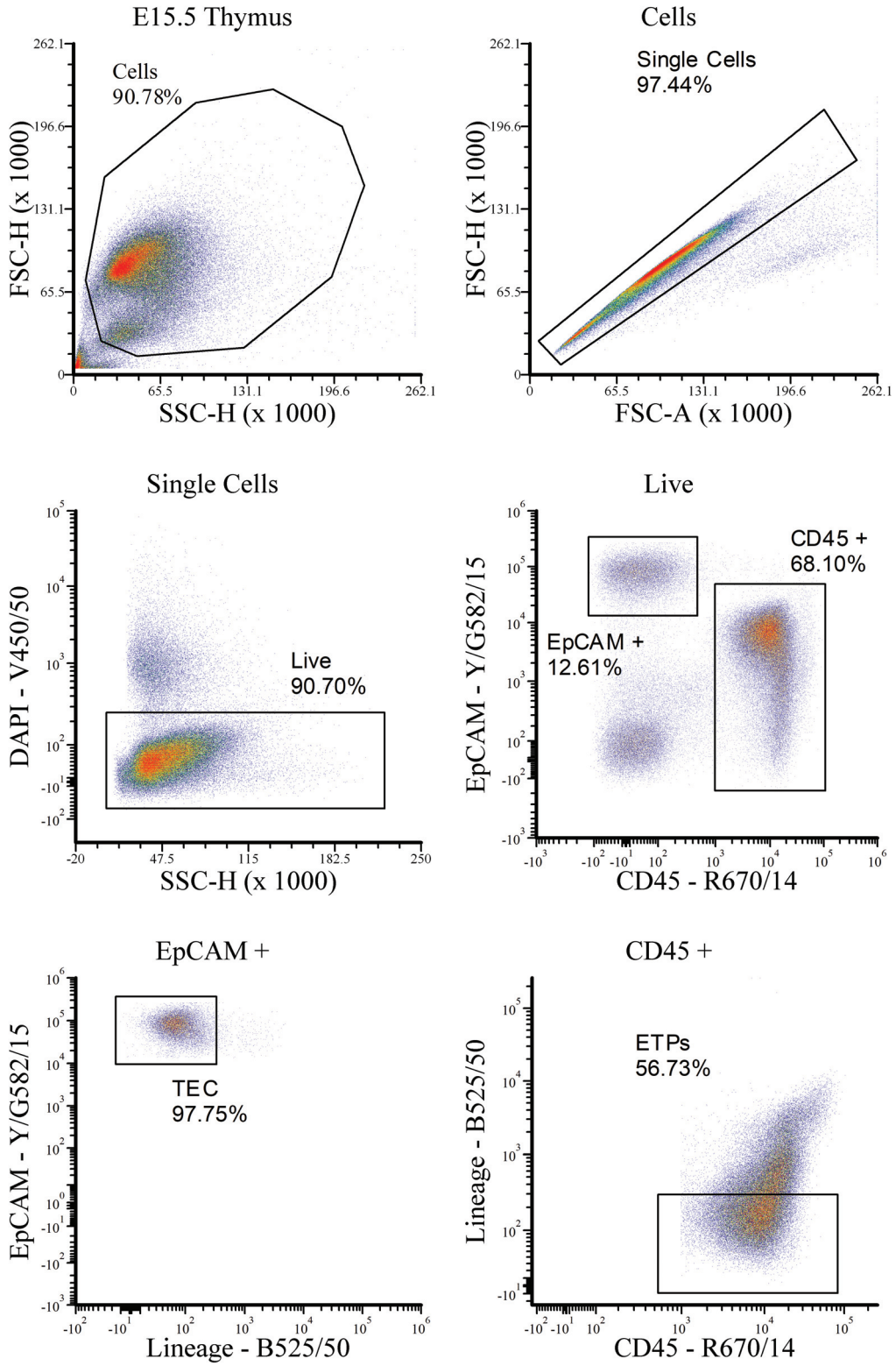

Figure C3.7: Sorting Strategy for E15.5 TEC and DN Thymocytes

Images depict the sorting strategy for E15.5 thymus to isolate TEC and ETPs. Lineage cocktail included: CD3ε, CD4, CD8, CD11b, CD11c, TCRβ, TCRγδ, B220, Gr1, Nk1.1, Ter119. DN thymocytes were defined as $CD45^{+}EpCAM^{-}Lineage^{-}$. TEC were defined as $CD45^{-}EpCAM^{+}Lineage^{-}$.

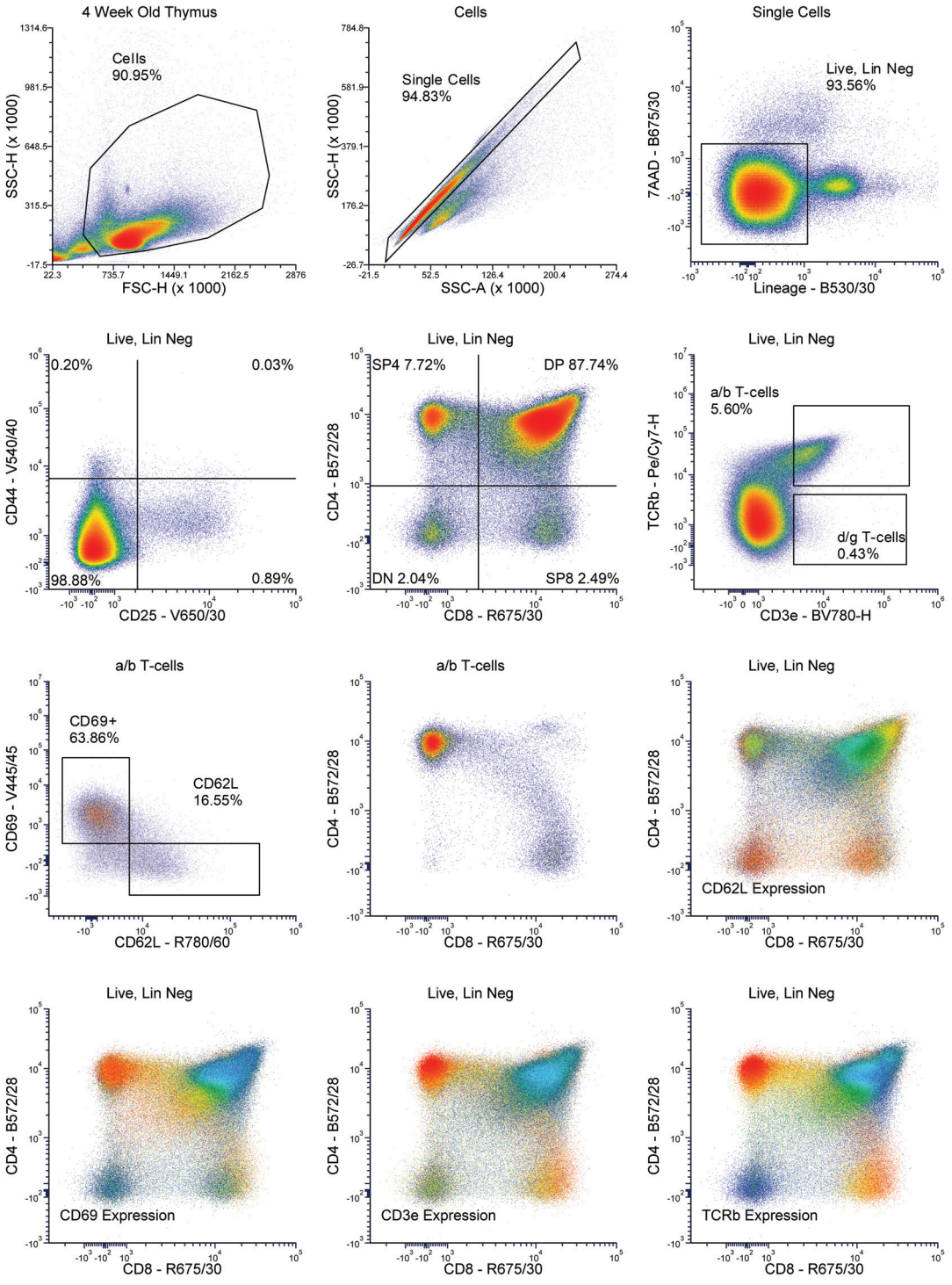

Figure C3.8: Profile of Thymopoiesis in The Native Thymus

The flow cytometry profile used to characterise thymopoiesis in this chapter. Here it is demonstrated using thymocytes isolated from a four-week old thymus. The warmer the colours the greater the expression of the stated marker. The title of each plot describes where the cells are gated from. To gain temporal resolution of specified markers, its expression was overlaid on the CD4 and CD8 prolife in a flame UTI. Lineage cocktail = CD11b, CD11c, B220, Gr-1, Nk1.1, EpCAM, Ter119.

3.5.B. Native Thymopoiesis

3.5.B.I. Overview of Native T-cell Differentiation

Native thymopoiesis was described in detail in Chapter One and is presented here with respect to the markers used for flow cytometry in Figure C3.8. Here is a brief description using the selected markers: the early thymocytes are DN, referring to $CD4^{-}CD8^{-}$ thymocytes. This population is then segmented using CD44 and CD25 (Godfrey *et al*., 1993). $CD44^{+}CD25^{-}$ cells represent the earliest thymocyte population and is termed DN1. This subpopulation is heterogeneous and contains the ETP (defined as $Lin^{-}CD25^{-}c\text{-}Kit^{+}$), which amongst DN1 cells is the canonical T cell progenitor (Prockop and Petrie, 2004). Thymocytes then progress into DN2 by upregulating CD25 and to DN3 by downregulating CD44. TCR variable (diversity) joining (V(D)J) recombination begins during DN2. Focusing solely on αβ T-cells, only thymocytes that are able to produce a T-cell receptor (TCR)β chain are allowed to continue through thymopoiesis, this process is called β-selection (Petrie *et al*., 1995). Thymocytes downregulate CD25 to enter the DN4 stage, here thymocytes undergo a second round of V(D)J recombination to generate a unique TCRα chain that heterodimerises with the previously created TCRβ chain to form the αβTCR. During this process, thymocytes upregulate both CD4 and CD8 and initiate the DP phase (Koch and Radtke, 2011).

Note the CD25 stain in this experiment was taken to be a technical failure as the proportion of $CD25^{+}$ were much lower than expected and not representative of previous experiments (Figure C3.8). This means that analysis of DN thymocytes within any experimental condition are likely to be confounded and this analysis was not performed. Analysis was only performed using CD4 and CD8 with markers CD69, CD62L, TCRβ and CD3ε. DP thymocytes enter positive selection, in which thymocytes communicate with TEC through cognate TCR-peptide:MHC interactions. Within the thymocytes, TCR activation is marked with expression CD69 and downregulation of either CD4 or CD8 to become SP thymocytes and enter the thymic medulla for negative selection. During negative selection, thymocytes downregulate CD69 and upregulate CD62L for thymic egression.

3.5.B.II. Initiation of Positive Selection

The expression of the above markers was plotted onto the CD4 and CD8 profile to provide a temporal map of their expression (Figure C3.8). Focusing on the αβ T-cells, it is interesting to note that TCRβ (clone #H57-597) was only detectable in the DP phase, which was unexpected (Petrie *et al*., 1995). Whether this reflects the true expression pattern on the cellular membrane, or the antibody is specific to an epitope of the C region of the TCRβ chain that only becomes available once the αβTCR becomes available or recognises the TCRα chain is unclear. Instead of mirroring CD3ε, TCRβ expression was observed to mirror CD69 expression, which likely represents that at this stage thymocytes receive active TCR signalling for positive selection and lineage fate decision (Brugnera *et al*., 2000). This process occurred alongside a small downregulation in CD4 and CD8, flagging the start of positive selection. CD69 expression itself adhered to the kinetic signalling model with expression shifting over to $CD4^{med}CD8^{low}$ thymocytes, which do not yet express CD62L (Brugnera *et al*., 2000). CD62L was dynamically expressed through thymopoiesis. It was expressed during DN to DP and represents the migration of thymocytes from the CMJ to the subcapsular region. CD62L is also expressed in thymocytes that have finished the lineage specification begin to downregulate CD69, in which CD62L mediates thymic egression (Xing *et al*., 2016).

3.5.C. sevRTOC Recapitulated T-cell Differentiation

As expected, the sevRTOC effectively mediated T-cell differentiation with all CD4 an CD8 subpopulations being present (Figure C3.9). However, expression of CD69, CD62L and TCRβ were largely dissimilar in DP thymocytes compared to those in the native thymus, in which thymocytes entering positive selection downregulated both CD4 and CD8 a small degree and upregulated TCRβ and CD69. Within the RTOC, this slight downregulation of CD4 and CD8 and the accompanying upregulation of TCRβ and CD69 was not evident and may represent that the majority of thymocytes capable of positive selection had already passed through or that positive selection was disrupted. However, it is likely that thymocytes effectively transitioned into the SP phases as there is the incremental increase in CD3ε and TCRβ between the DN, DP and SP thymocytes that was observed in the native thymus.

Finally, there was a build-up of SP thymocytes in the sevRTOC but this was attributed to an inability of thymocytes to egress from the structure.

Therefore, by analysing the ability of *ex vivo* TEC to mediate T-cell differentiation, we can infer what can maximally be expected of the iTEC system. SevRTOC mediated generation of all CD4 and CD8 thymocyte subsets with evidence of correct transition from the DP into the SP phase. However, there were some differences between sevRTOC and the native thymus: there was a relative increase in γδ T-cells and an accumulation of SP thymocytes.

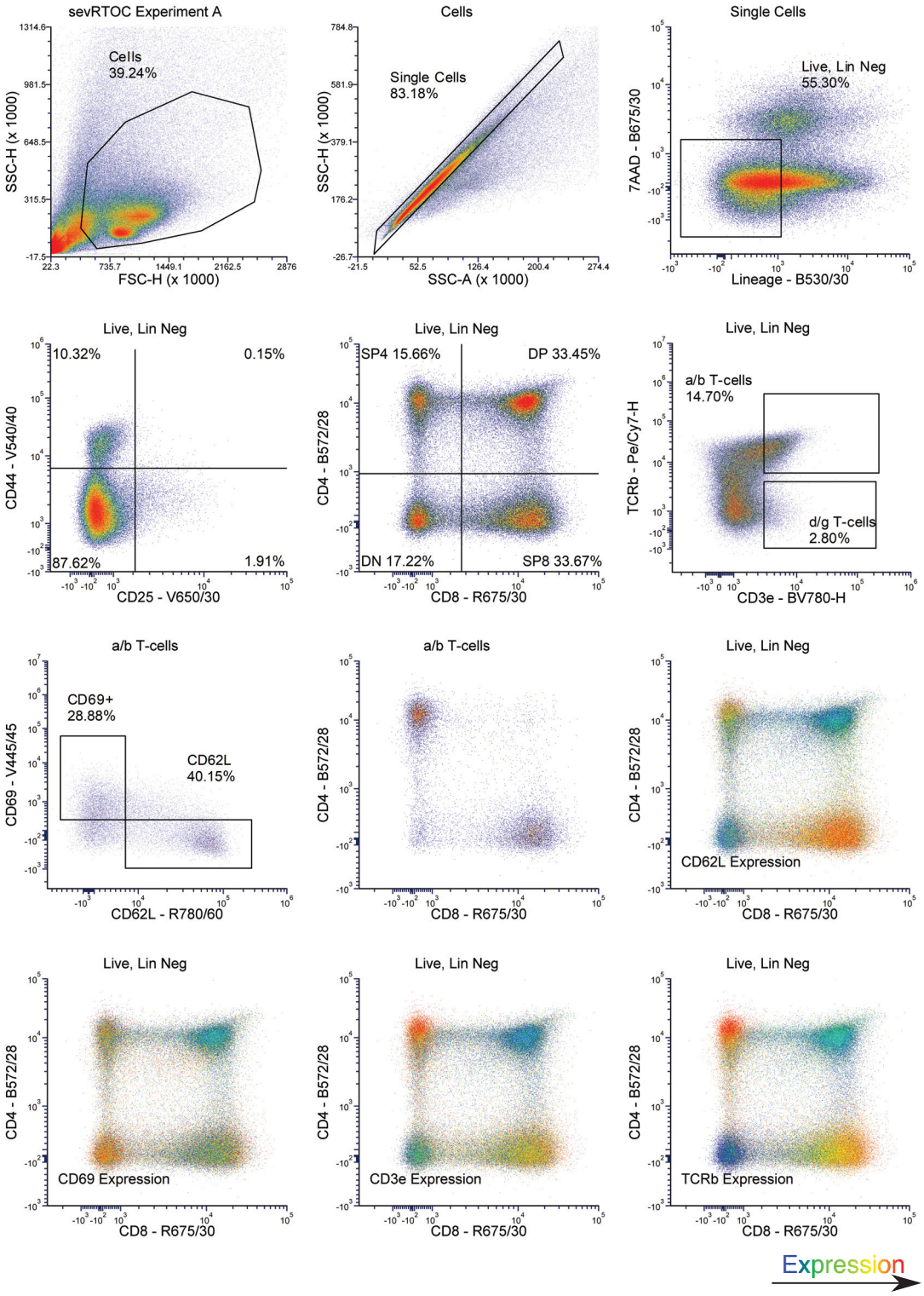

Figure C3.9: Profile of Thymocyte Subsets in sevRTOC

Thymopoiesis profile of a sevRTOC from experiment A. When specified, expression of a marker is overlaid upon the CD4 and CD8 plot as a flame UTI to provide temporal resolution. The warmer the colours the greater the expression of the stated marker. The title of each plot describes where the cells are gated from. Lineage cocktail = CD11b, CD11c, B220, Gr-1, Nk1.1, EpCAM, Ter119.

3.5.D. iTEC Mediate T-cell differentiation but with Perturbed Positive Selection

Analysis of the thymocyte subsets in iTEC-based RTOC (iRTOC) cultured concurrently to the above described sevRTOC demonstrated that iRTOC supported T cell differentiation from the DN input population, but that the outcome exhibited variability. Three examples are shown herein. Figure C3.10 presents an iRTOC with a bias towards SP8 thymocytes; Figure C3.11 represents iRTOC with a bias toward the SP4 lineage and Figure C3.12 shows data from an iRTOC that performed weakly as judged by the absolute cell counts of each thymocyte subset (Table C3.6 and C3.7). All three experiments were performed concurrently using the same pool of iTEC, MEFs, DNs.

Flow cytometric analysis confirmed that iTEC were able to mediate T-cell differentiation because all CD4 and CD8thymocyte subsets were present in the iRTOC. This suggests that the iTEC could activate Notch signalling effectively in thymocytes and mediate upregulation of CD4, CD8, CD3ε and TCRβ. However, the overall kinetics of thymopoiesis were slower in iRTOC as the build-up of SP thymocytes, caused by the absence of thymic egression, was not as pronounced as in sevRTOC. Comparatively, there was a greater proportion of DP thymocytes, so it is likely that the transition from DP to SP phases was slower in the iRTOC.

Once T-cell lineage has been enforced, thymocytes undergo positive selection and the lineage fate decision. These processes were dramatically different between iRTOC and sevRTOC. Notably, expression of CD3ε and TCRβ in the sevRTOC and native thymus increased incrementally from DN to DP and then SP stages. This pattern was not shown in the iRTOC, in which expression of these markers decreased between DP and SP thymocytes, suggesting a perturbation in positive selection. iTEC appeared to be selecting for SP thymocytes with lower TCR expression. Furthermore, in the native thymus and sevRTOC, CD69 expression increased between the DP and SP thymocytes. In the iRTOC this did not occur and expression of CD69 decreased between DP and SP thymocytes, which may reflect weaker TCR activation, or a failure of thymocytes to produce a TCR.

This may represent the absence of a medulla within the iRTOC. In effect, thymocytes completing positive selection become stuck at the transitional phase when thymocytes become licenced to migrate to the medulla because there are no mTEC to establish the necessary chemokine gradient for migration. The CD62L stain provides evidence for mechanism. In the native thymus and sevRTOC, CD62L is upregulated in DP to SP transition, while in iRTOC this is absent. Providing more detail on this mechanism is outside the limits of the flow cytometry panel that was designed to focused on cortical thymopoiesis. It would be interesting to compare CCR4 and CCR7 expression, and whether thymocytes undergo the VCAM-1 to ICAM-1 switch that characterises this section of thymopoiesis. Furthermore, interesting future experiments could determine whether *ex vivo* mTEC supplemented into iRTOC can rescue this phenotype, making it more like the sevRTOC.

Overall, iRTOC was able to mediate T-cell differentiation and produce all subsets of thymocyte based upon CD4, CD8 TCRβ and CD3ε and this was taken as evidence of iTEC functionality. However, the kinetics of this mechanism were slower in iRTOC that sevRTOC. In addition, once T-cell lineage was enforced on thymocytes, the transition between DP to SP phases did not reflect that in sevRTOC or the native thymus

Finally, CreERT2 only MEF-based RTOC were unable to support T-cell differentiation (Fig 3.13). Therefore, the above effects result from expression of the iFoxn1 transgene in MEFs and the pool of DNs were not contaminated with any pre-specified thymocytes able to proliferate within the system.

Therefore, we can conclude that within this single experiment iTEC produced using the above described protocol were functional, in which they were able to mediate T-cell differentiation. The total absolute counts of each thymocyte subset are shown for every iRTOC in Figure C3.14. However, further evidence was required from multiple experiments before this conclusion could be generalised to all future produced iTEC.

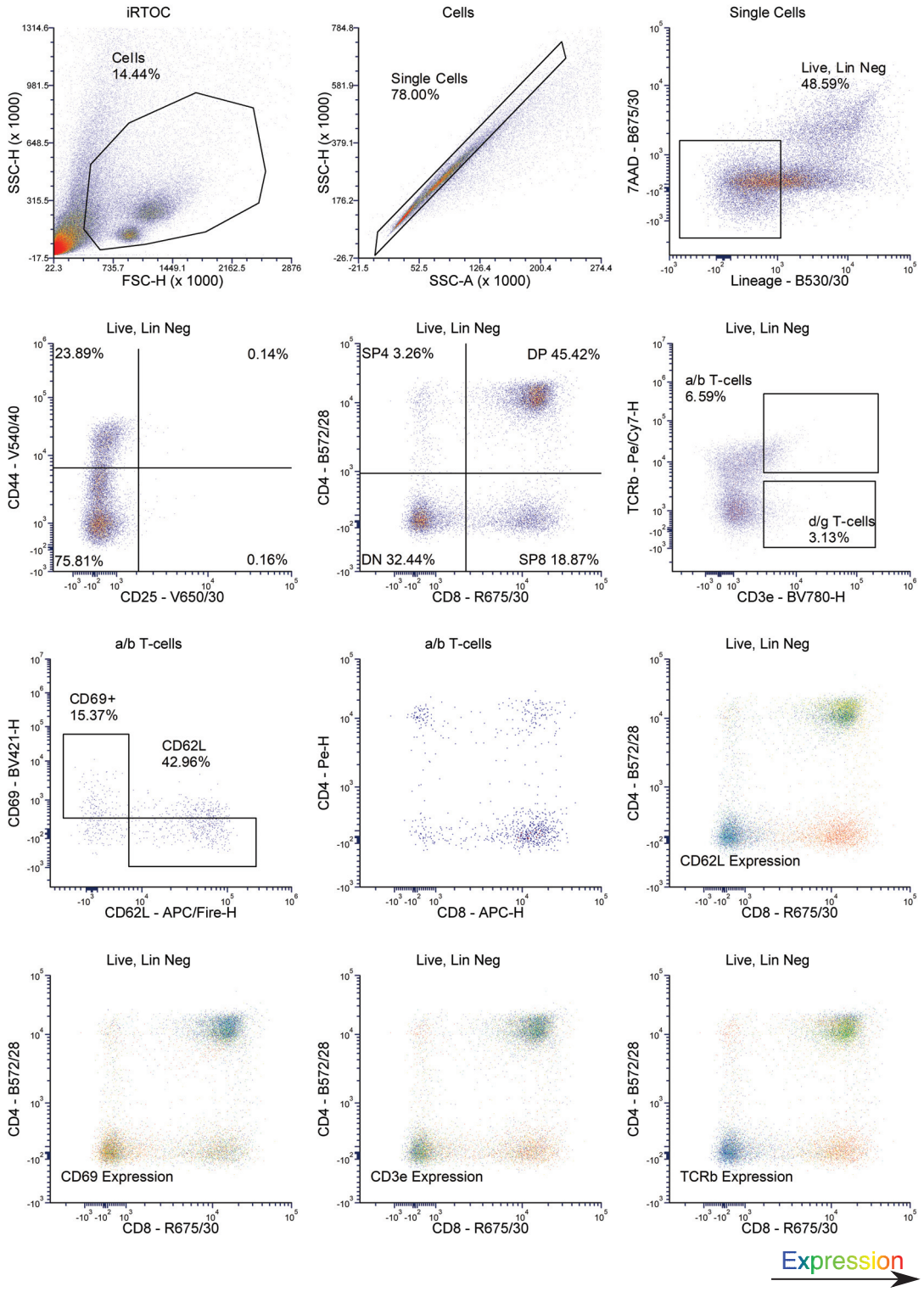

Figure C3.10: Profile of Thymocyte Subsets in iRTOC with CD8 Bias

Thymopoiesis profile of iRTOC with CD8 bias. When specified, expression of a marker is overlaid upon the CD4 and CD8 plot as a flame UTI to provide temporal resolution. The warmer the colours the greater the expression of the stated marker. The title of each plot describes where the cells are gated from. Lineage cocktail = CD11b, CD11c, B220, Gr-1, Nk1.1, EpCAM, Ter119. See table C3.6 and C3.7 for information on relative cell abundances and proportions.

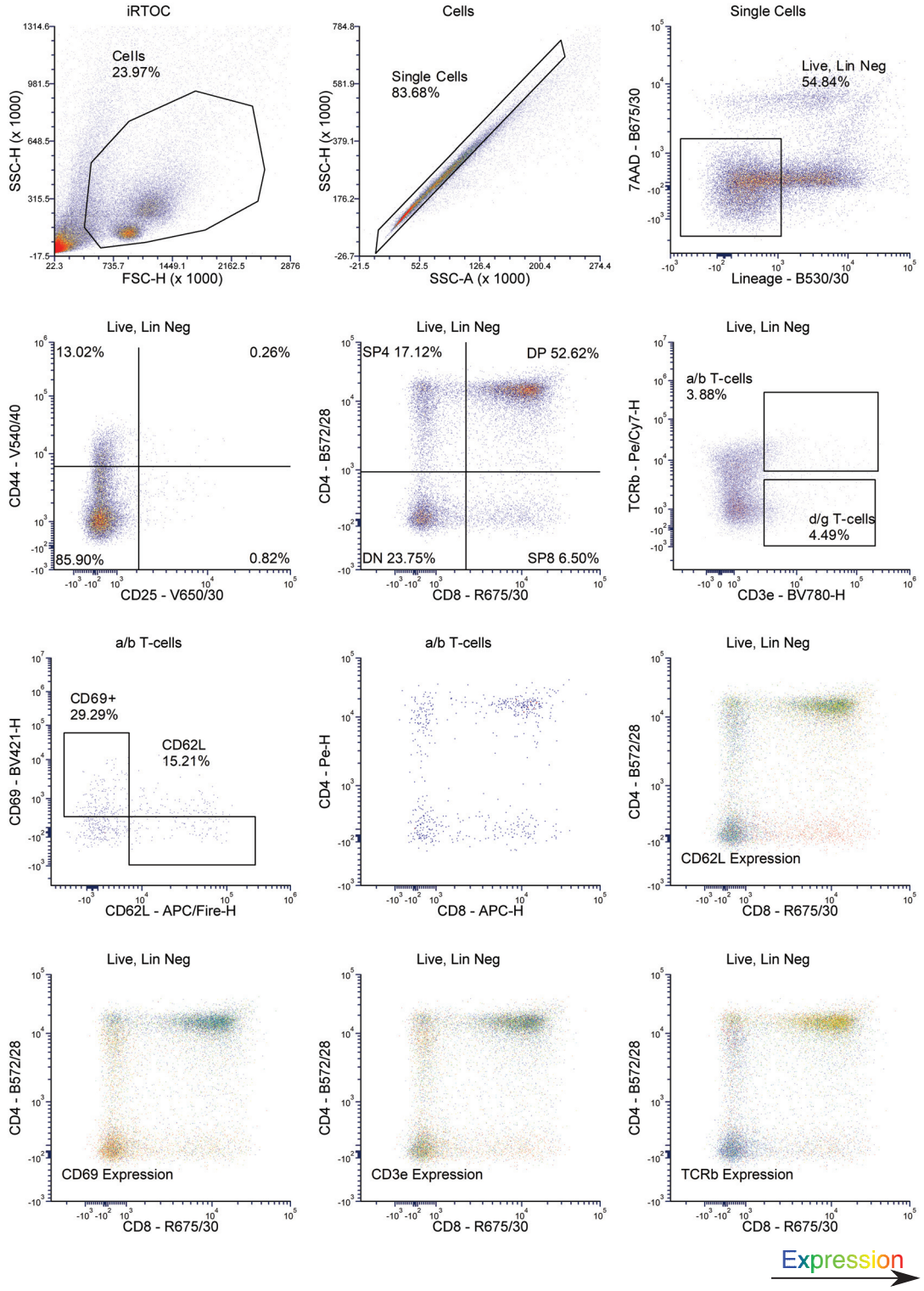

Figure C3.11: Profile of Thymocyte Subsets in iRTOC with CD4 Bias

Thymopoiesis profile of iRTOC with CD8 bias. When specified, expression of a marker is overlaid upon the CD8 and CD4 plot as a flame UTI to provide temporal resolution. The warmer the colours the greater the expression of the stated marker. The title of each plot describes where the cells are gated from. Lineage cocktail = CD11b, CD11c, B220, Gr-1, Nk1.1, EpCAM, Ter119. See table C3.6 and C3.7 for information on relative cell abundances and proportions.

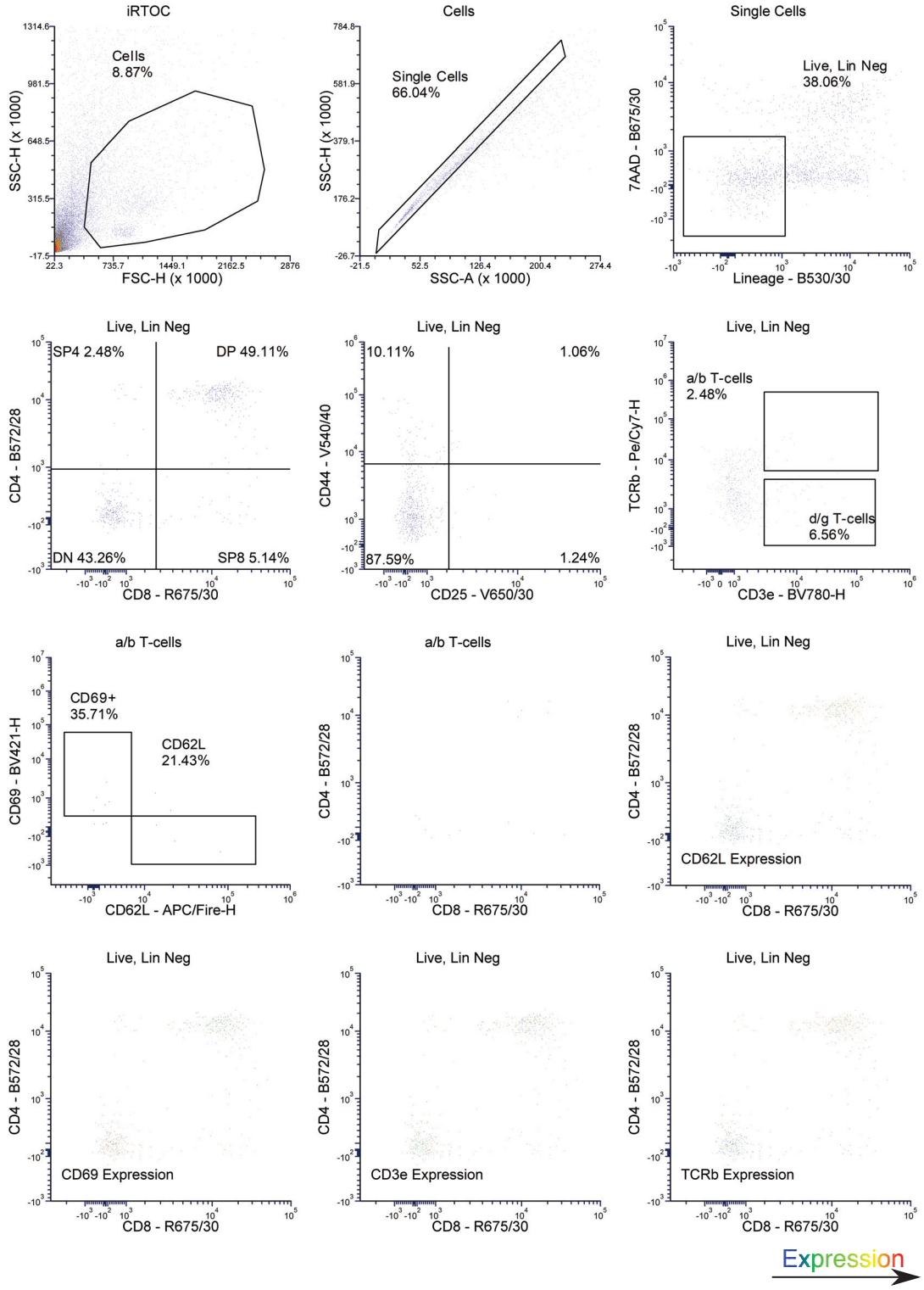

Figure C3.12: Profile of Thymocyte Subsets in Weakly Performing iRTOC

Thymopoiesis profile of weakly performing iRTOC. When specified, expression of a marker is overlaid upon the CD4 and CD8 plot as a flame UTI to provide temporal resolution. The warmer the colours the greater the expression of the stated marker. The title of each plot describes where the cells are gated from. Lineage cocktail = CD11b, CD11c, B220, Gr-1, Nk1.1, EpCAM, Ter119. See table C3.6 and C3.7 for information on relative cell abundances and proportions.

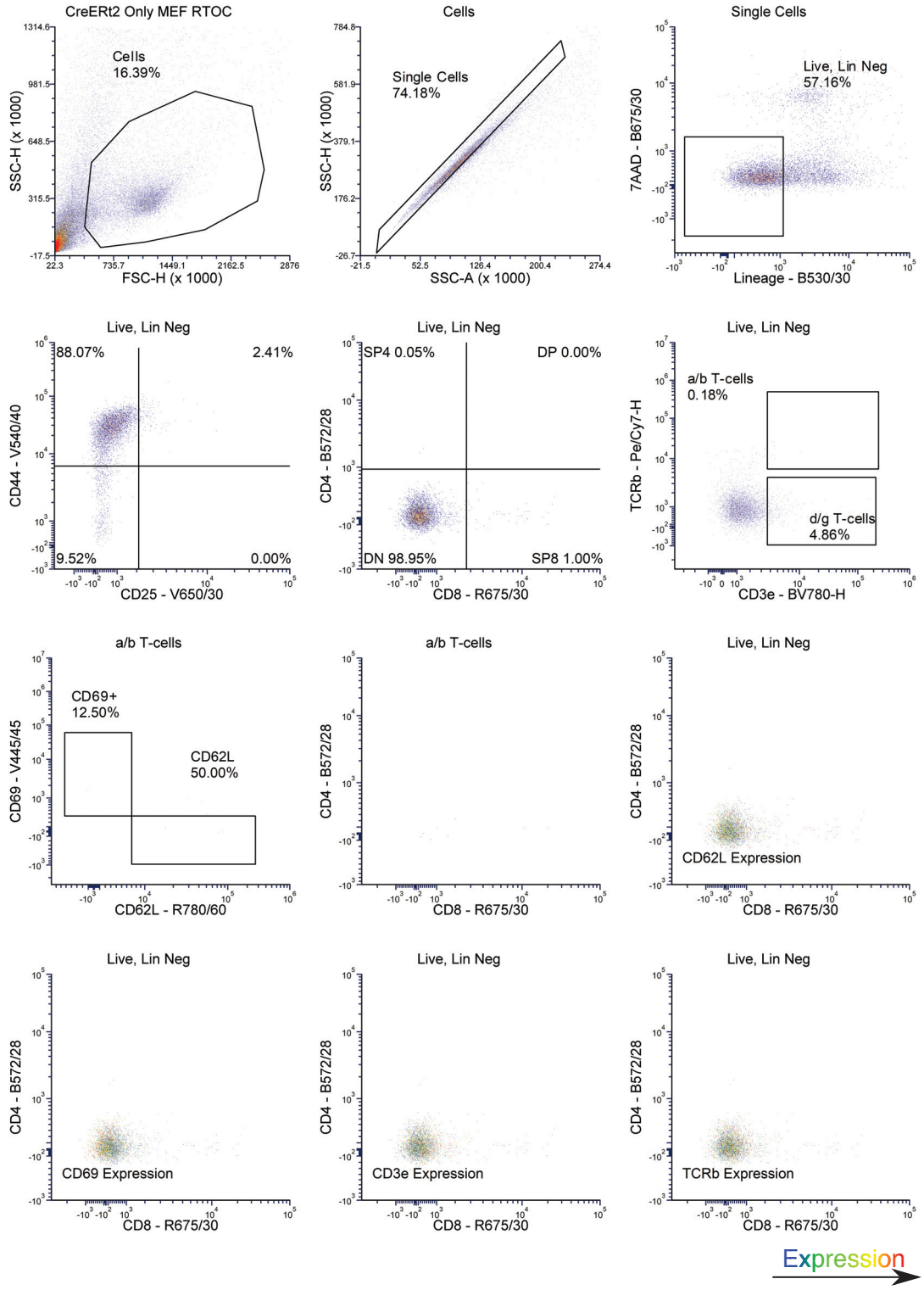

Figure C3.13: Profile of Thymocyte Subsets in Cre Only MEF Control RTOC

Thymopoiesis profile of the control RTOC that replaced iTEC/TEC component with Cre Only MEFs. When specified, expression of a marker is overlaid upon the CD4 and CD8 plot as a flame UTI. The warmer the colours the greater the expression of the stated marker. The title of each plot describes where the cells are gated from. Lineage cocktail = CD11b, CD11c, B220, Gr-1, Nk1.1, EpCAM, Ter119.

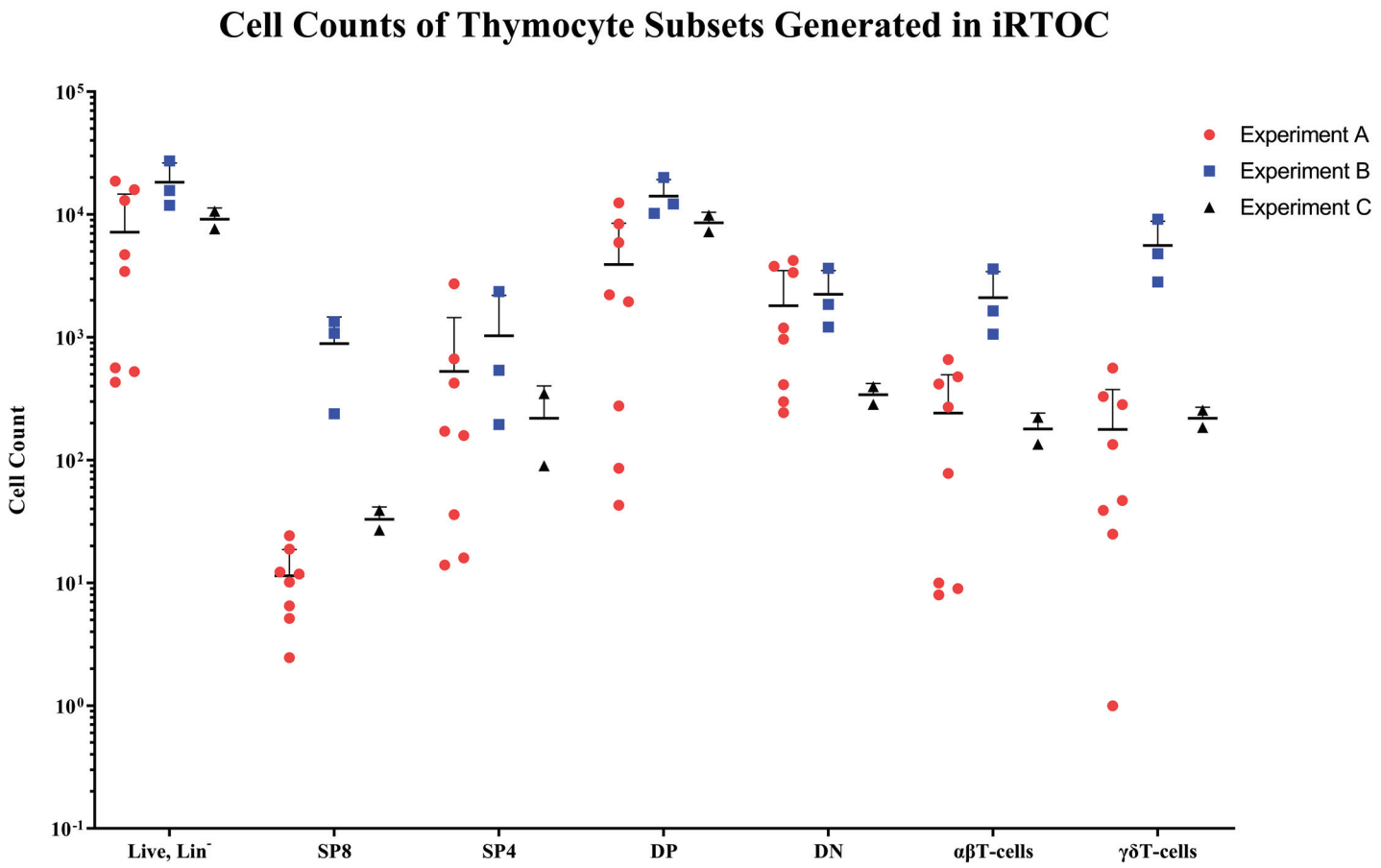

Figure C3.14: The Absolute Cell Counts of Thymocyte Subsets Generated in all Three Experiments

Graph depicting the cell counts of the various thymocyte populations generated in iRTOC. εβ T-cells refers to $CD3\gamma^{+}TCR\delta^{-}$ thymocytes. Note that the y-axis is a logarithmic ^{10} scale. See Table C3.6 for relevant proportions of each population and Table C3.7 for abolute cell counts. Each data point represents the one iRTOC. Those from Experiment A are red circles, B are blue squares and C are black triangles.

Table C3.6: Percentages of each iRTOC from the Live, Lineage Negative Gate.
The table shows the relative proportions (%) of each thymocyte subset from the total cells gated as Live and Lineage Negative

Replicate	*% Live, Lineage*	*% SP4*	*% DP*	*% SP8*	*% DN*	*% αβT-cells*	*% γδ T-cells*
A	43.45	8.35	9.74	12.53	69.37	1.86	9.05
A*	48.59	3.26	45.42	18.87	32.44	5.06	2.17
A	62.89	5	56.72	10.18	28.1	2.27	1.37
A	47.53	3.37	47.14	24.22	25.28	5.74	2.84
A***	38.06	2.48	49.11	5.14	43.26	1.77	4.43
A	58.83	3.57	66.65	11.8	17.98	2.23	1.76
A	41.93	3.04	16.32	2.47	78.18	1.71	0.19
A**	54.84	17.12	52.62	6.51	23.75	3	3.53
B	45.68	2	1.64	10.23	86.13	8.91	23.78
B	57.62	4.91	8.62	13.32	73.15	13.17	33.46
B	57.02	6.9	3.44	11.82	77.84	10.49	30.59
C	28.69	0.35	1.18	3.73	94.74	1.77	2.42
C	40.07	0.37	3.26	3.73	92.65	2.1	2.39
* iRTOC represented in Figure C3.10							
*** iRTOC represented in Figure C3.11							
** iRTOC represented in Figure C3.12							

Table C3.7: Absolute Cell Counts from each iRTOC from the Live, Lineage Negative Gate.
The table shows the absolute cell counts of each thymocyte subpopulation in all iRTOC in all three experiments

Replicate	*Live, Lineage*	*SP4*	*DP*	*SP8*	*DN*	*Aβ T-cells*	*γδ T-cells*
A	431	36	42	54	299	8	39
A*	13035	425	5921	2460	4229	659	283
A	3438	172	1950	350	966	78	47
A	4720	159	2225	1143	1193	271	134
A***	564	14	277	29	244	10	25
A	18711	668	12470	2208	3365	417	330
A	527	16	86	13	412	9	1
A**	15943	2729	8389	1038	3787	478	563
B	11896.5	238.5	195	10246.5	1216.5	1060.5	2829
B	27370.5	1344	2358	20022	3646.5	3604.5	9159
B	15684	1081.5	540	12208.5	1854	1645.5	4798.5
C	7636.5	27	90	7234.5	285	135	184.5
C	10666.5	39	348	9882	397.5	223.5	255
* iRTOC represented in Figure C3.10							
*** iRTOC represented in Figure C3.11							
** iRTOC represented in Figure C3.12							

3.5.E. Variation Between Independent Experiments

Whilst it was pertinent to perform the above analysis within one experiment to standardise stochastic variation produced from differences between input populations and environmental factors, it was also important to observe gross changes over multiple independent experiments, given the aspiration of standardising iTEC. Table C3.6 and C3.6 and Fig 3.14 present data collected from iRTOC in three biological replicate experiments. Although the above discussion comparing iRTOC and sevRTOC used evidence provided exclusively from replicate A, the patterns highlighted were observed in all experiments. Note that different numbers of iRTOC were created in each experiment for technical reasons (FACS sorting availability). A minimum of three iRTOC was set up in each experiment but, in experiment C, one of these resulted in a technical failure so no data were collected. Comparison between iRTOC from these independent experiments simultaneously emphasises biological differences in iTEC, but also thymocytes and WT MEFs, and environmental factors such as cytokine batch and variation in manufacturing RTOC, with little ability to differentiate the contributions of these sources of variation from each other. However, on the assumption that *ex vivo* TEC are less variable than iTEC, a comparison between sevRTOC from each experiment isolates the iTEC/TEC variation to provides information on differences in thymocytes, WT MEFs and environment. Note, due to the scarcity of E15.5 TEC, only one sevRTOC was produced in each experiment (Figures C3.9, C3.15 and C3.16).

iRTOC manufactured for experiment B produced more γδ T-cells than in the other replicates. This is likely to be a related to the iTEC as this phenotype was not shown in the sevRTOC control. The mechanics underscoring the αβ vs γδ lineage decision are not completely understood. There is some evidence of IL-7 involvement (Huang *et al*., 2001; Ye *et al*., 2001). However, it should be noted that in this experiment IL-7 was supplemented at consistant levels. Therefore, this observation provides evidence against the fate decision being completely independent of environment, the effect was likely to have arisen from the iTEC, or the same bias would have been present in the sevRTOC. Strikingly, regardless of γδ T-cells, sevRTOC B performed weakly. SevRTOC A and C look very similar, with respect to cellular proportions and expression of CD69, CD62L, CD3ε and TCRβ, while in sevRTOC

B these were more reminiscent of iRTOC. It maybe that either the DN thymocyte or WT MEF population, or an environmental factor, rather than the iTEC, reduced the efficacy of experiment B, which in turn may explain why the iRTOC were unable to generate many DPs thymocytes. A notable difference between iRTOC and sevRTOC in experiment B is that the sevRTOC did not generate aberrant SP thymocytes, with respect to the relative expression levels of TCRβ and CD3ε, which is further evidence that this abnormality is likely to be associated with iTEC. The same cannot be said for iRTOC generated in experiment C, which demonstrated very poor ability to mediate thymopoiesis while the concurrent sevRTOC performed well.

Therefore, despite efforts to create a standardised process to reprogram iTEC, there was dramatic variablity between preparations of iTEC that appears not to be due to other the cellular compartments or environmental factors. This variation existed within batches, as demonstrated between iRTOC within experiments and between batches as shown by comparing the above three independent experiments. Future work is necessary to further reduce the variability in the iTEC system.

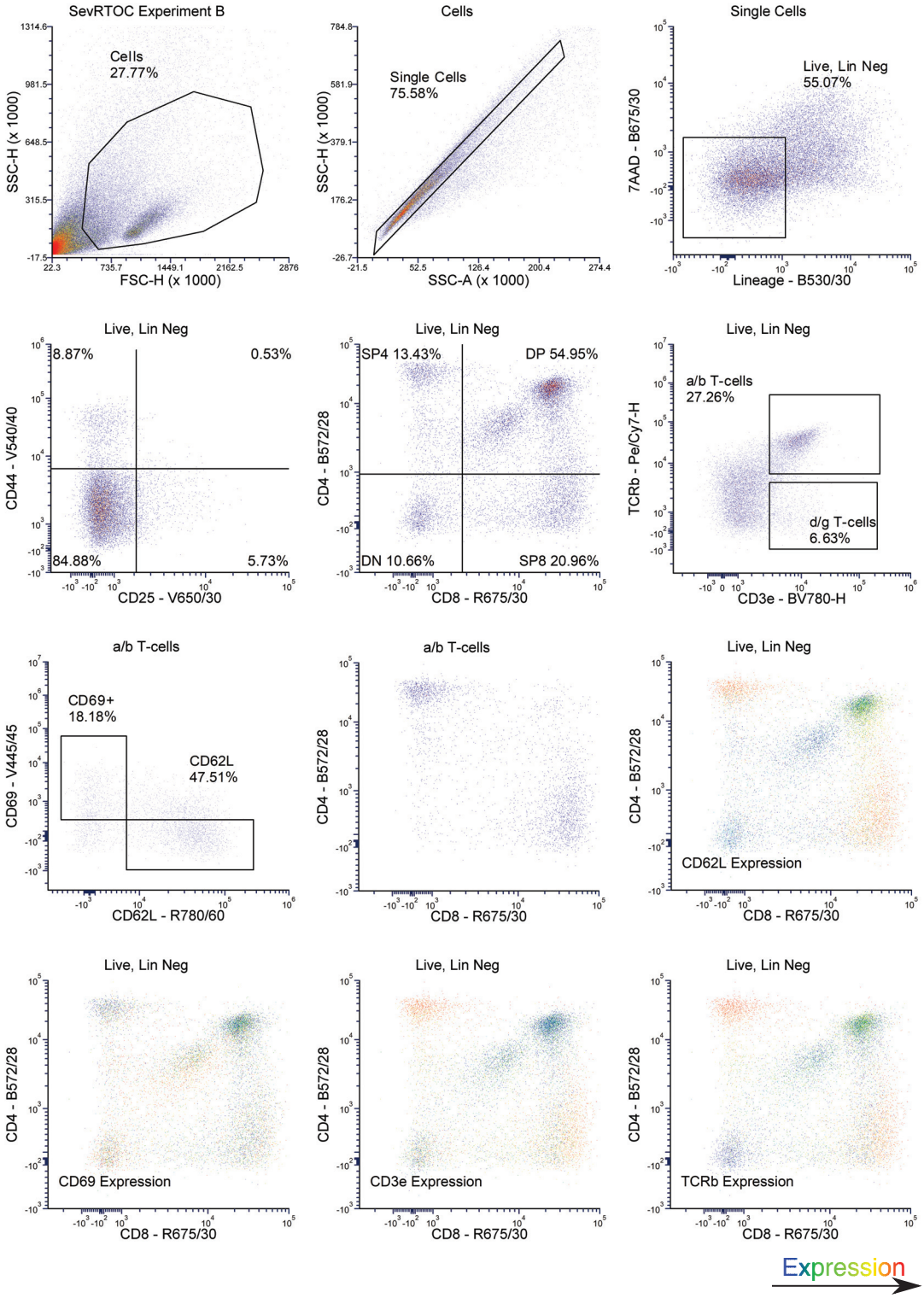

Figure C3.15: Profile of Thymocyte Subsets in sevRTOC from Experiment B

Thymopoiesis profile of sevRTOC from experiment B. When specified, expression of a marker is overlaid upon the CD4 and CD8 plot as a flame UTI to provide temporal resolution. The warmer the colours the greater the expression of the stated marker. The title of each plot describes where the cells are gated from. Lineage cocktail = CD11b, CD11c, B220, Gr-1, Nk1.1, EpCAM, Ter119.

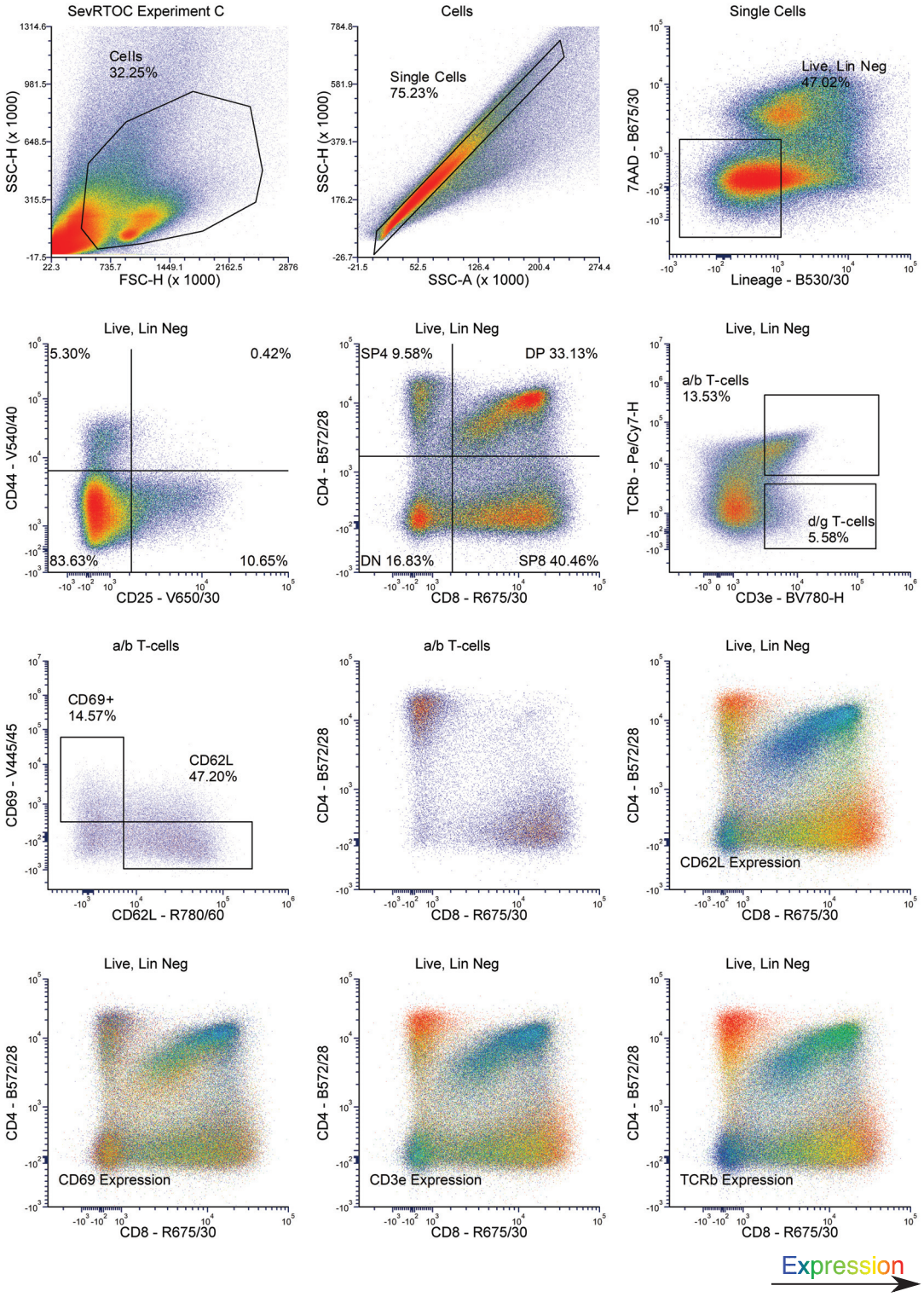

Figure C3.16: Profile of Thymocyte Subsets in sevRTOC from Experiment C

Thymopoiesis profile of sevRTOC from experiment C. When specified, expression of a marker is overlaid upon the CD4 and CD8 plot as a flame UTI to provide temporal resolution. The warmer the colours the greater the expression of the stated marker. The title of each plot describes where the cells are gated from. Lineage cocktail = CD11b, CD11c, B220, Gr-1, Nk1.1, EpCAM, Ter119.

3.5.F. Comparison between sevRTOC and Unsorted RTOC

iTEC are intended to recapitulate only the epithelial component of thymic stroma. It is pertinent to compare the sevRTOC to an RTOC created using the entire range of thymic stroma to set realistic, evidence-driven goals for iTEC. A comparison between the successful sevRTOC from experiment C and a control created by dissociating and reaggregating six whole E15.5 thymic lobes, with appropriate proportions of WT MEFs, allowed resolution of the effect of the non-epithelial thymic stroma on RTOC functionality (Figure C3.17). Note the caveat of this control is that the input thymocyte population was not DNs but already contained differentiating thymocytes (Klug *et al*., 2002; Petrie and Zúñiga-Pflücker, 2007). Interestingly, the unsorted RTOC did not display the abnormal expression pattern of CD69 observed in sevRTOC but an expression pattern much more in keeping with the kinetic signalling model (Brugnera *et al*., 2000). Thymocytes within the unsorted RTOC, downregulated CD69 appropriately after an initial and, with respect to SP8 thymocytes, transient SP4 phase. This lends evidence to the hypothesis that non-epithelial stromal cells supported TEC to mediate positive selection. The other striking difference is that the unsorted RTOC did not accumulate SP thymocytes to the extent that the sevRTOC did, particularly for SP8 thymocytes. Whether this reflects SP thymocytes leaving the structure, or a better regulation of thymocyte proliferation, is unclear. Whilst understanding these differences is not relevant to the main aims of this thesis, it remains an interesting future experiment to test how the non-epithelial thymic stromal cells effect RTOC organisation. A notable experiment would be to compare sevRTOC to 2′-Deoxyguanosine treated unsorted RTOC and fetal thymic organ culture that had been seeded from a common pool of DN thymocytes. Therefore, it may be unrealistic to expect iTEC to mediate positive selection without support from key non-epithelial thymic stromal cells.

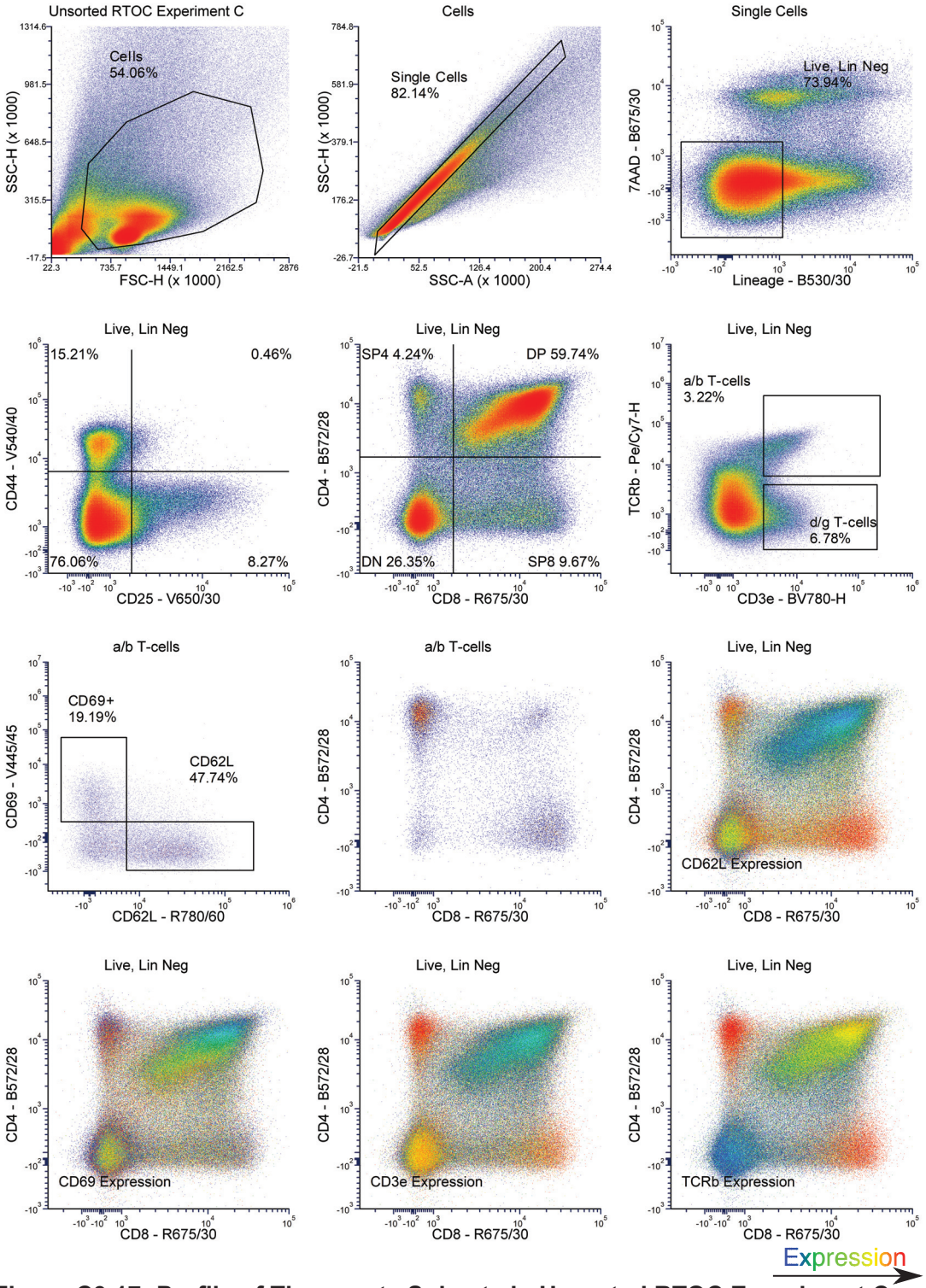

Figure C3.17: Profile of Thymocyte Subsets in Unsorted RTOC Experiment C

Thymopoiesis profile of an RTOC created by dissociating six thymic lobes and reaggregating the cells without sorting with WT MEFs into RTOC. When specified, expression of a marker is overlaid upon the CD4 and CD8 plot as a flame UTI. Note that the greater than expected expression of CD3ε and CD69 within the $CD4^{-}CD8^{-}$ population is due to the increased γδ T-cell population. The title of each plot describes where the cells are gated from. Lineage cocktail = CD11b, CD11c, B220, Gr-1, Nk1.1, EpCAM, Ter119.

3.6. Conclusion

From these data, I concluded that iTEC generated using the protocol optimised in this chapter were able to mediate T-cell differentiation, but that additional work was required standardise results between batches. Additionally, by probing thymocyte differentiation in iRTOC in more detail than previously reported, I identified differences in the capacity of iTEC to support thymocyte development compared to *ex vivo* TEC, particularly at the $CD4^+$ / $CD8^+$ lineage commitment and/or positive selection stages. However, evidence was presented that these processes may be perturbed in sevRTOC, with iTEC further confounding these problems. These effects are likely due to differences in TCR activation between the systems; iTEC instigating weaker activation than their native counterparts. Overall, these data validated iTEC as an alternative source of TEC to generate the *in vitro* thymus. However, improvements are required, particularly when enforcing positive and negative selection. Whether this phenotype can be rescued by including additional populations in the RTOC, notably the non-epithelial stromal cells and mTEC, or upon grafting, remains an open question.

4. Chapter Four: Screening Synthetic Polymers for Capacity to Bind and Support Thymic Epithelial Cells

4.1. Introduction and Aims

It is well established that thymic epithelial cells (TEC) rapidly downregulate *Foxn1* when culture *in vitro*, which ultimately leads to an inability to mediate thymopoiesis (Anderson *et al*., 1998). A study in 2006 found that loss of *Foxn1* led to downregulation of the Notch ligands DLL1 and DLL4, which are essential for T-cell lineage commitment and some subsequent stages of T cell differentiation (Mohtashami and Zúñiga-Pflücker, 2006). The authors showed that TEC cultured in reaggregate thymic organ culture (RTOC) maintained *Foxn1* expression, while those cultured in monolayers did not. It was therefore concluded that the three-dimensional (3D) structure of RTOC may have contributed in maintaining FOXN1 expression and thus TEC function *in vitro* (Mohtashami and Zúñiga-Pflücker, 2006).

An essential component of any 3D structure is the extracellular matrix (ECM), which is the macromolecular network that creates the structure between cells. ECM is composed of a wide range of proteins and polysaccharides that form hydrophilic gels (Lam *et al*., 2019). Cells are both supported by and contribute to these structures, which become an essential part of cell-to-cell interactions by potentiating soluble factors and mediating mechanotransduction (Lam *et al*., 2019). ECM components, when added to *in vitro* culture systems, can affect cellular proliferation and function. In a recent example, Lam and colleagues show that supplementing neural networks with ECMs accelerated the formation of the networks, without affecting the functional properties compared to culture on Poly-D-Lysine alone (Lam *et al*., 2019). Furthermore, fabricating synthetic 3D hydrogels with select ECM elements have been shown to affect the balance of self-renewal and differentiation in stem cells (Ranga *et al*., 2014). However, addition of currently available ECMs to *in vitro* monolayer cultures is associated with limitations including efficacy and reproducibility and can also be expensive (Tourniaire *et al*., 2006).

These concerns have led to the development of the synthetic polymers that can be used to mimic the physicochemical properties of the ECM, for applications in cell culture systems (Sakiyama-Elbert and Hubbell, 2002). In turn, the ability to manipulate polymers to produce a

wide range of chemical and physical properties led to the development of polymer microarrays. These microarrays provide a means of screening cells against libraries of different polymers containing many different functional properties, in order to find those most compatible with a given cell type (Anderson *et al*., 2004; Tourniaire *et al*., 2006). This technique was developed by the Langer and Bradley groups and, since publication, has been applied to both the isolation and culture of tissue-specific cell types, including hepatocytes, mesenchymal stromal cells and osteoblasts, and for creating completely defined conditions for embryonic stem cell culture (Duffy *et al*., 2014a; Hay *et al*., 2011; Mei *et al*., 2010a, 2010b; Melkoumian *et al*., 2010; Tare *et al*., 2009). The rationale was that such polymers could form a component of a defined culture system suitable for propagating TEC or induced TEC (iTEC) monolayers and could potentially be further developed as components of engineered RTOC.

Therefore, in this chapter I aimed to employ a two-step approach to first identify polymers that facilitate the adhesion of TEC and then to evaluate whether TEC cultured upon the selected polymers can more closely emulate native behaviours. To created testable outcomes that assay of the effect of polymers on TEC behaviour, I chose to address a set of objectives that analysed three discrete thymic functions:

A. Determine whether candidate polymers can improve maintenance of *Foxn1* expression in cultured TEC.

B. Determine whether candidate polymers improve the ability of *ex vivo* TEC and iTEC to mediate T-cell differentiation compared to standard culture methods, such that thymocyte development in monolayer cultures more closely resembles that observed in the native thymus.

C. Determine whether candidate polymers promote differentiation of iTEC into mTEC-like TEC, with evidence of promiscuous gene expression.

These objectives were selected because a culture system that met all the above criteria would be superior to currently available technology. Moreover, they were each technically feasible and created a non-redundant and sequential structure.

Objective A was evaluated using transgenic embryonic TEC from a *Foxn1* reporter mouse line in which expression of *Foxn1* can faithfully tracked based on GFP fluorescence intensity (*Foxn1*^{G} mice: O'Neill *et al*., 2016). Of note is that this criterion was assumed not to be relevant to iTEC as the iFoxn1 transgene enforces continuous *Foxn1* expression. Testing of murine TEC was prioritised for this experiment as a suitable reporter line was already available.

Objective B was inspired by the systems OP9-DLL1 and MS5-hDLL1 systems, in which enforced expression of the Notch signalling ligands delta-like-ligand (DLL)1 or DLL4 in the bone marrow-derived OP9 or MS5 cell line confers the capacity to partially support T cell development (Schmitt and Zúñiga-Pflücker, 2002; Seet *et al*., 2017; Montel-Hagen *et al*., 2019). Both systems support commitment of haematopoietic progenitors to the T-cell lineage, and efficiently mediate the progression of ETPs and other haematopoietic progenitors into TCRβ^{+}CD3^{+}CD4^{+}CD8^{+} thymocytes (Schmitt and Zúñiga-Pflücker, 2002; Schmitt *et al*., 2004). However, these systems cannot currently support physiological positive selection or production of TCRβ^{+}CD3^{+}CD4^{+} thymocytes given they cannot present peptides in the context of major histocompatibility class 2 (MHC2) (Takada, Kondo and Takahama, 2017).

Objective C asks whether the candidate polymers can support a monolayer system in which some cells adopt mTEC fates and exhibit promiscuous gene expression. This represents a reductionist readout for the ability to support negative selection. Given that OP9-DLL1 and MS5-hDLL1 cells are not able to do this, Objective C represents a novel aspiration for *in vitro* thymopoiesis.

4.2. Identifying Polymers that the Facilitated TEC Adhesion

4.2.A. Primary iTEC-based Screen of 367 Polymers

4.2.A.I. Experimental Design

To identify TEC-specific polymers, I employed a similar method to that originally described by Bradley and colleagues (Tourniaire *et al*., 2006). The polymers used in this chapter were synthesised by to Dr C. Duffy and Dr S. Venkateswaran in the Bradley laboratory, who also helped me manufacture and image the initial microarrays. To produce the microarrays, a microscope slide was coated in 2% agarose to prevent cellular adhesion to the glass. On top of this, polymers were contact printed in quadruplicate to create a matrix of polymer spots (Figure C4.1A).

Microarrays of 367 different polymers were fabricated using polymers selected to encompass a range of physical properties, and including polymers already identified as supporting other cell types via previous library screening experiments (Pernagallo *et al*., 2009). The result was a microarray that presented a range of functional groups, wettability, charge, nano-topography, integrin contact point density and lipophilicity in polymer compositions with a proven history of success on other cell types (Duffy *et al*., 2014a).

In the primary microarray screen, I elected to use iTEC as a surrogate for TEC, based on the validation of this reprogrammed cell-type documented in Chapter Three, and due to the scarcity of the native tissue. The screen was designed such that, once initial candidate polymers were identified, these were subject to a focussed secondary screen in which both cell types were tested in parallel on a scale appropriate to the scarcity of *ex vivo* tissue.

In the initial screen, microarrays of either iTEC or CreERt2^{+}iFoxn1^{-} (Cre Only) MEFs were performed in parallel. iTEC were defined as Green Fluorescent Protein (GFP)$^{+}$ CreERt2^{+}iFoxn1^{+} (iFoxn1) MEFs that were purified eight days after exposure to 4OHT. A hydrophobic pen was used to draw a ring around the array to concentrate cells onto the polymers.

The microarrays were sterilized using ultraviolet light and placed inside rectangular tissue culture dishes. 2×10^5 of either cell type were seeded into the hydrophobic ring in 1 ml of iTEC medium and allowed to bind to polymers. After four hours, an additional 4 ml of iTEC medium (described in Chapter Three) was added to each microarray, fully submersing the

glass slide. A 50% medium change was performed every 2 days until the microarrays were fixed seven days after being seeded.

The number of cells adhered to each polymer spot was then manually counted using the nuclear stain 4′,6-diamidino-2-phenylindole (DAPI). On the microarrays seeded with iTEC, two measures were taken to ensure only successfully reprogrammed MEFs were counted. Firstly, the iTEC seeded on to the microarrays were isolated using fluorescence activated cell sorting (FACS) for expression of GFP, which reported expression of the iFoxn1 transgene, prior to seeding and secondly the slides were stained for the epithelial cell marker pan-cytokeratin and only nuclei surrounded by a positive cytokeratin stain were counted as iTEC (Figure C4.1B). On the microarrays that were seeded with Cre only MEFs, all nuclei were considered eligible for counting.

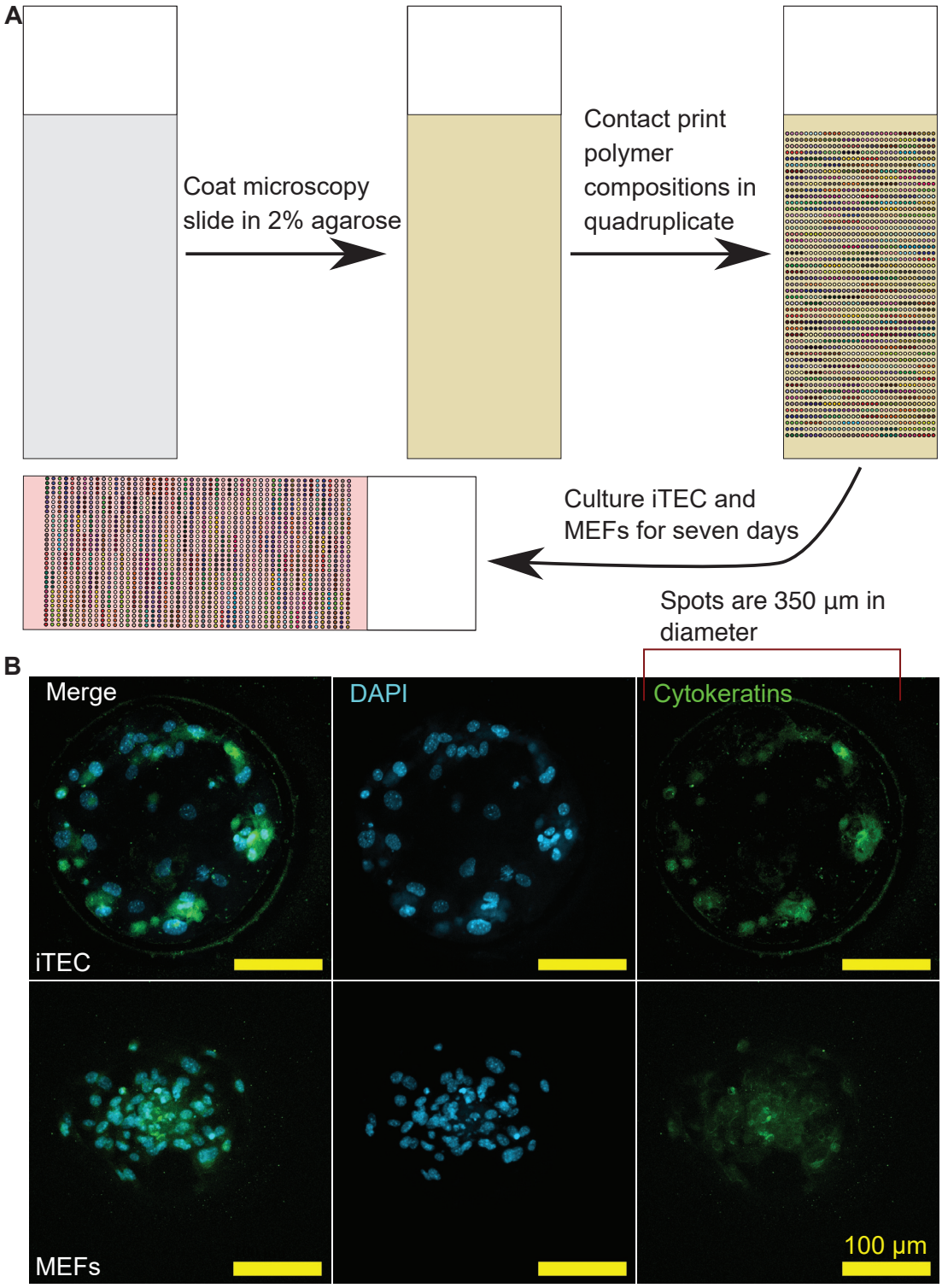

Figure C4.1: Screening a Microarray of 367 Polyacrylates and Polyurethanes for Polymers able to Bind iTEC

A. Representation of microarray manufacturing process. Glass microscope slides were coated in 2% agarose before 367 different polyacrylates and polyurethanes were contact printed on the surface. Each polymer was represented in quadruplicates at various positions on each slide. **B**. Representative images of a successful polymer spots with iTEC *(top)* or Cre only MEFs *(bottom)*. Average area of iTEC nuclei was 241 µm^2 while the area of the spot was 66,676 µm^2.

4.2.A.II. Results

The microarrays were imaged on a Nikon 50i microscope using pathfinder software (IMSTAR). Images of each polymer spot were taken to capture DAPI and Alexa Fluor (AF) 488 (Figure C4.1B). The number of cells was counted for each microarray (Figure C4.2). The area of one spot from each polymer quadruplicate was measured and the cell counts were normalised using:

Equation C4.1:

$$Area\ Normalised\ Cell\ Count\ = \frac{Cell\ Count}{Area\ in\ mm}$$ (Figure C4.3).

A high degree of variability was observed in the screen, and therefore polymers that met defined criteria, rather than statistical inference, were taken forward (Wasserstein *et al*., 2019). In this primary screen, type 2 statistical errors would have worse consequences than type 1 errors, since a type 2 error could mean that a potentially useful polymer was missed, while a type 1 error would simply result in a 'false-positive' polymer being subjected to another round of experiments, where it would be excluded. Therefore, all polymers that bound iTEC, MEF or both cell types across all four technical replicates in all three independent experiments were judged successful and are represented in Figures C4.2 and C4.3. The data presented in Figures C4.2 and C4.3 show only the polymers that bound iTEC alone (29/367 polymers), MEF alone (24/267 polymers), or both cell types (6/367 polymers).

Therefore, the primary screen identified polymers than bound either iTEC, MEFs or both cell types. However, given the variation found in the screen these needed to be re-tested using a in secondary screen.

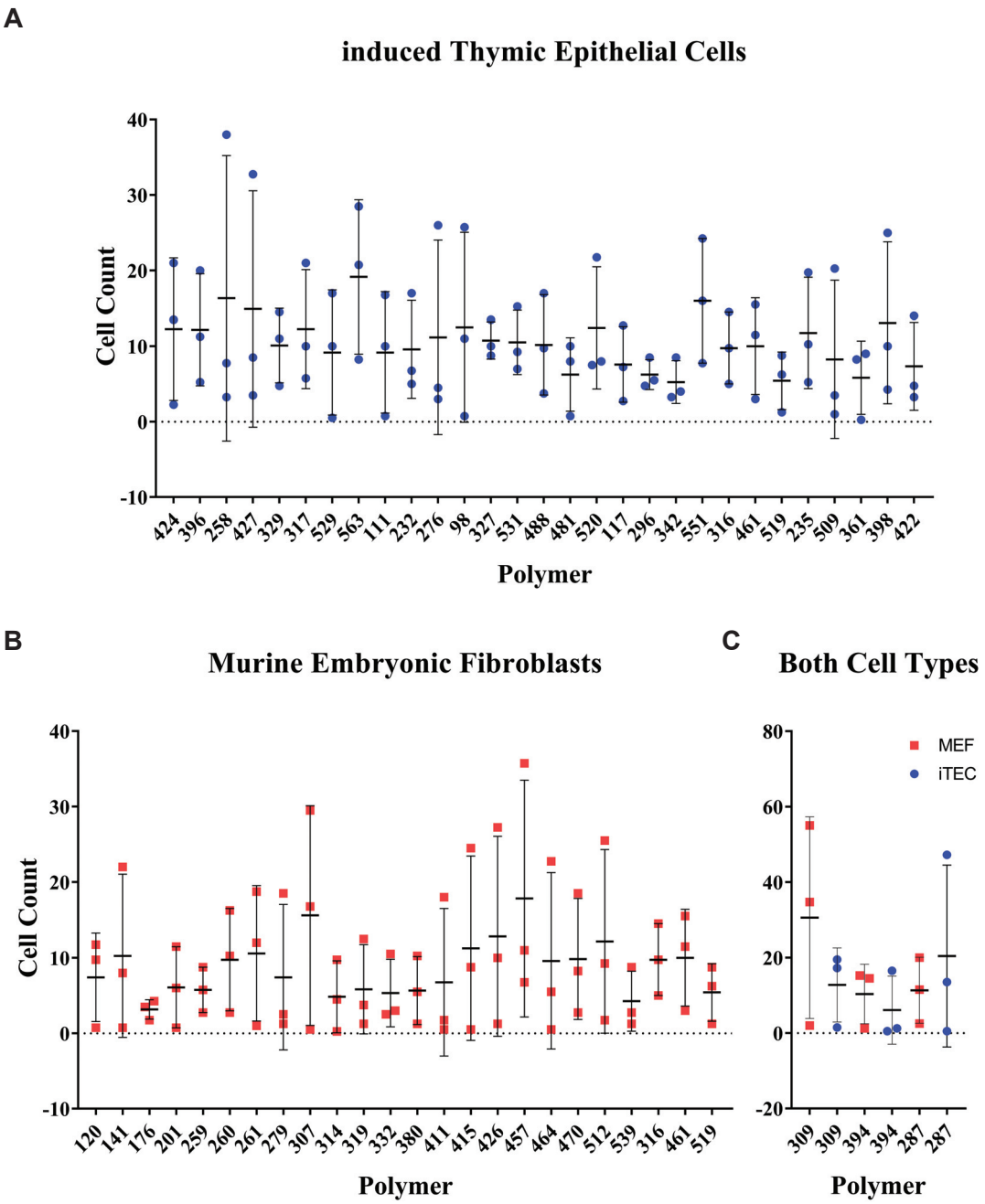

Figure C4.2: Results of Microarray Polymer Screen

Graphs depict the number of cells observed on each polymer spot **A**. Shows all polymers, of the 367, that could bind iTEC. **B**. Of all 367 polymers those that bound MEFs. **C**. Of all 367 polymers those that bound to both iTEC and MEFs. Polymers that did not bind any cells across all three independent experiments were excluded. Data points show the mean of three technical replicates.

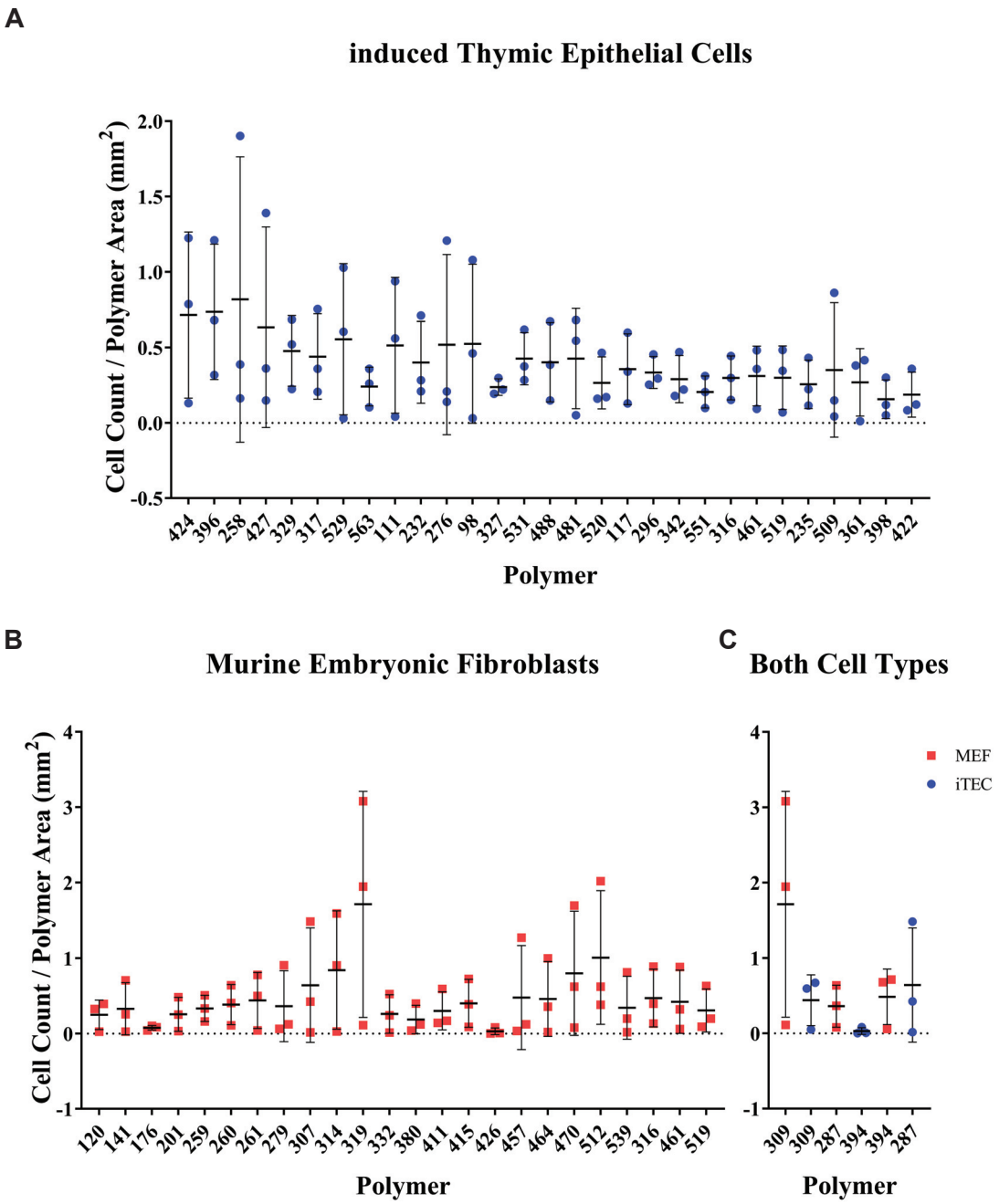

Figure C4.3: Area Normalised Results of Microarray Polymer Screen

Graphs depict the number of cells oberved on polymer spots divided by the total area of that polymer spot. **A**. Shows the polymers, of the 367 that could bind only iTEC. **B**. Of all 367 polymers those that bound only MEFs. **C**. Of all 367 polymers those that bound both iTEC and MEFs. Polymers that did not bind any cells across all three independent experiments were excluded. Data points show the mean of three technical replicates.

4.2.B. Secondary iTEC Screen on the Focused Array Format

4.2.B.I. Experimental Design

Given the high level of variance in the microarray experiments described above, all polymers that bound iTEC across all four technical replicates in all three independent experiments were taken forward for subsequent testing. This necessitated development of focused polymers arrays, which were designed to screen fewer polymer conditions but with greater precision.

A 384-well plate was used as it allowed testing of many conditions, without demanding an unreasonable amount of input tissue. To coat the plate, all selected polymers from the primary screen were dissolved in acetone at 0.2 mg / ml and pipetted into wells in the appropriate layout. The plates were airdried at room temperature to remove the acetone and then washed with water and phosphate-buffered saline (PBS) to remove any residual contaminates (Figure C4.4A).

Compatibility with this procedure was an essential criterion for identification of candidate polymers with work-up potential for routine laboratory use. Polymers that were unable to dissolve completely produced a thick and clumpy coating that impaired imaging. Acetone was considered a mandatory solvent as harsher solvents damage the silicon glue currently used to manufacture tissue culture plates. A potential alternative was to spin-coat glass cover slips with polymer and insert these into tissue culture flasks. This was decided against as it would impair future scale-up, an important component of clinical applicability, and makes the assay incompatible with high throughput imaging systems, which use refractive index to automatically focus objectives.

Overall, a total of 12 polymers were excluded from the panel at this stage due to poor solubility in acetone and were not used in subsequent experimentation. These were polymers 117, 232, 235, 276, 296, 317, 329, 342, 422, 424, 461 and 488. Polymer 369, which featured on the primary microarray but was not a “hit” candidate, was included as a negative control.

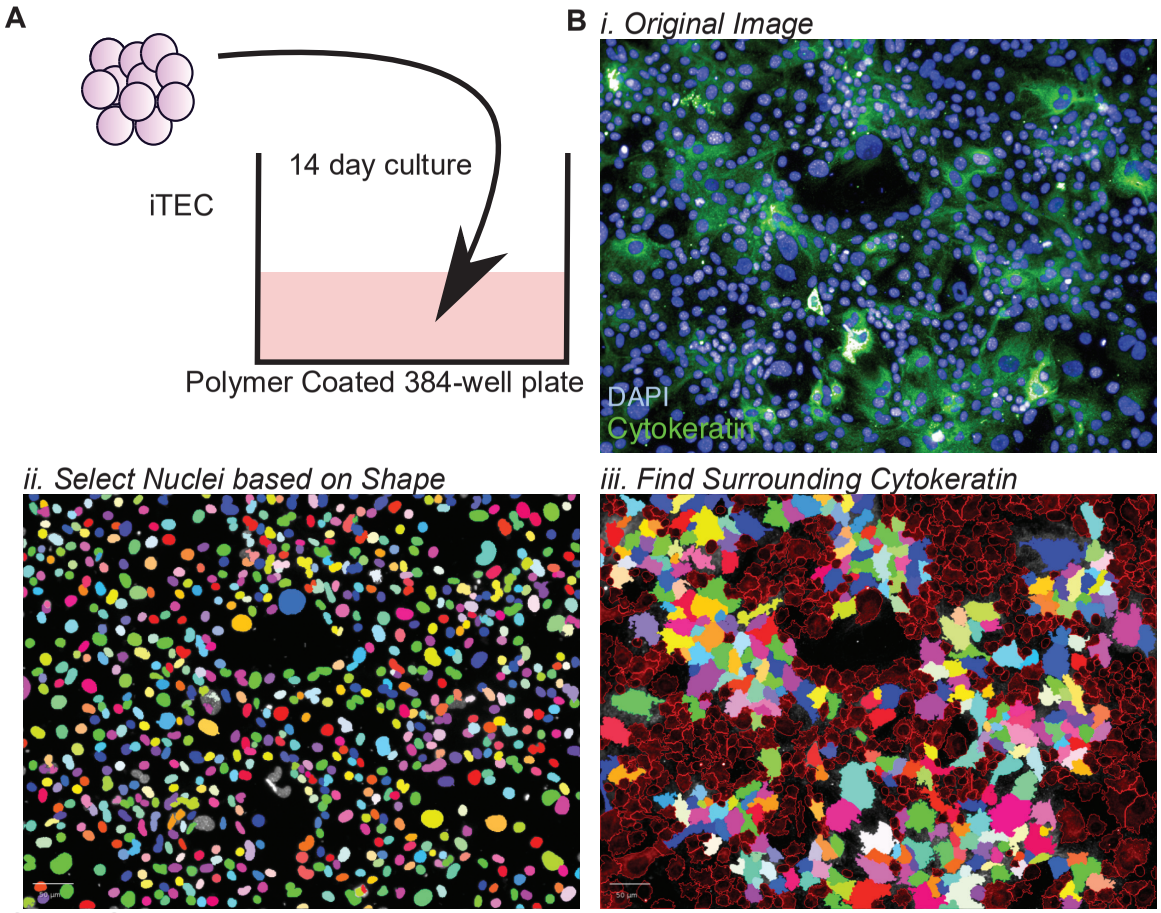

Figure C4.4: Method for iTEC Focused Polymer Array

A. iTEC were cultured for 14 days upon selected polymers identified in the Microarray screen. **B**.***i***. iTEC were stained for cytokeratins and nucleic acid. ***ii***. An automated pipeline selected larger nuclei associated with iTEC. Colours represent individual segmented elements ***iii***. Cells with cytoplasmic cytokeratin were selected and counted as iTEC, those with a greater than background expression were selected and are represented in different colours while those that are rejected are shown in red.

4.2.B.II. Results

The Focused Polymer Array aimed to test the same hypothesis as the microarray experiments, using a more precise methodology. iFoxn1 MEFs were treated with 4OHT to induce reprogramming and GFP$^+$ cells were FACS sorted at 18 days post-induction for use in the screen. A total of 3.03×10^4 iTEC were seeded into each well in iTEC medium, over a 14-day culture period, the medium was replaced every two to three days. Care was taken to wash off unbound cells before the plate was fixed and the iTEC were stained with DAPI and anti-cytokeratin to identify epithelial cells, as for the microarray above (Figure C4.4A).

An automated pipeline to was optimised to calculate the number of cytokeratin expressing cells in each well using the Columbus^{TM} software (PerkinElmer) (Figure C4.4B). First, DAPI$^+$ nuclei were segmented, on the assumption that one cell contained one nucleus, to form the basic cell count. To count the number of successfully reprogrammed iTEC, the area surrounding each nucleus, which was assumed to be the cytoplasm, was to be segmented into individual cells. Areas with variable brightness, with respect to the neighbouring region, were delineated and assumed to mark the boundary between cells, thereby pairing a nucleus with a surrounding delineated area, or cytoplasm, to create a whole cell. Note that by using a camera with a high bit depth, it was possible to use cellular autofluorescence to make this measurement. The mean fluorescence intensity (MFI) for each ‘cell’, which was simply a delineated area in the AF488 channel extending from a DAPI$^+$ spot, was calculated and those over a given threshold, which was set using a negative control, were counted as cytokeratin$^+$ iTEC.

The number of iTEC bound to each polymer, calculated using this pipeline, is shown in Figure C4.5. A high degree of variation was observed between biological replicates within this study (Table C4.1).

The two most probable sources of this variation were: biological variation within the iTEC, creating cells with heterogeneous adhesive properties; and inaccurate cell counting before seeding into wells. Given that all cell counts have associated precision errors, the later effect

was normalised against by reporting the cell counts with respect to the positive control, 0.1% gelatin (Figure C4.6).

Equation C4.2:

$$Normalised\ Cell\ Count = \frac{Cell\ Count\ on\ Polymer}{Cell\ Count\ on\ 0.1\%\ Gelatine}$$

With this equation applied, the major source of variation was likely to be biological with the caveat of the normalisation being that binding to 0.1% gelatin is assumed to be consistent across biological replicates i.e. if the same cell type was repeatedly seeded into 0.1% gelatin the same number of cells should consistently bind.

Once this normalisation was applied, the average coefficient of variation (CoV) for each condition was reduced from 95.7% to 79.95%, and polymers were evaluated using this metric (Figure C4.6). The normalised cell counts for each polymer were compared to the negative control 369. Logical criteria were used to judge successful candidates rather than statistical inference, because the experimental design was more forgiving of type 1 errors than type 2 errors as with interpretation of the primary screen (Wasserstein *et al*., 2019). The red line on Figure C4.6 indicates the mean plus + 1 standard deviation (SD) (0.08564) of the cell count for polymer 369. Any polymers with a mean ± 1 SD that intercepts this line were considered failures and removed from future tests.

Based on these criteria, polymers 111, 287, 396, 427, 509, 519, 520 and 563 were identified as able to bind iTEC. Now I had identified polymers that could bind iTEC, I could apply *ex vivo* TEC to the same test to determine whether iTEC shares a similar adhesion profile to TEC and whether using iTEC for the primary screen was a correct assumption.

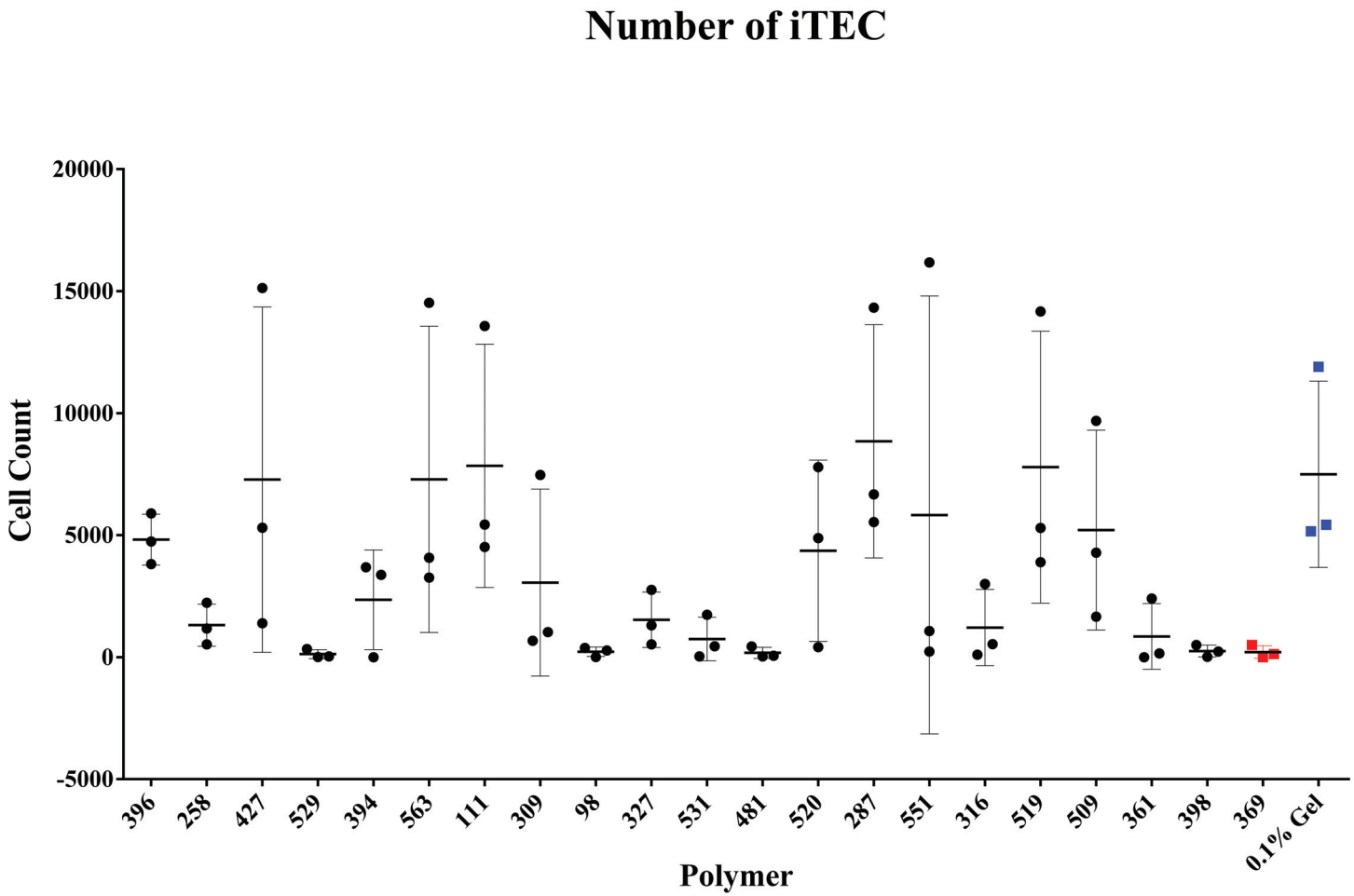

Figure C4.5: Results of iTEC Focused Polymer Array

Graph depicts the number of iTEC observed in each well. Each data point represents the mean of three wells. Negative control polymer 369 is shown red, while positive control 0.1% Gelatin is shown in blue.

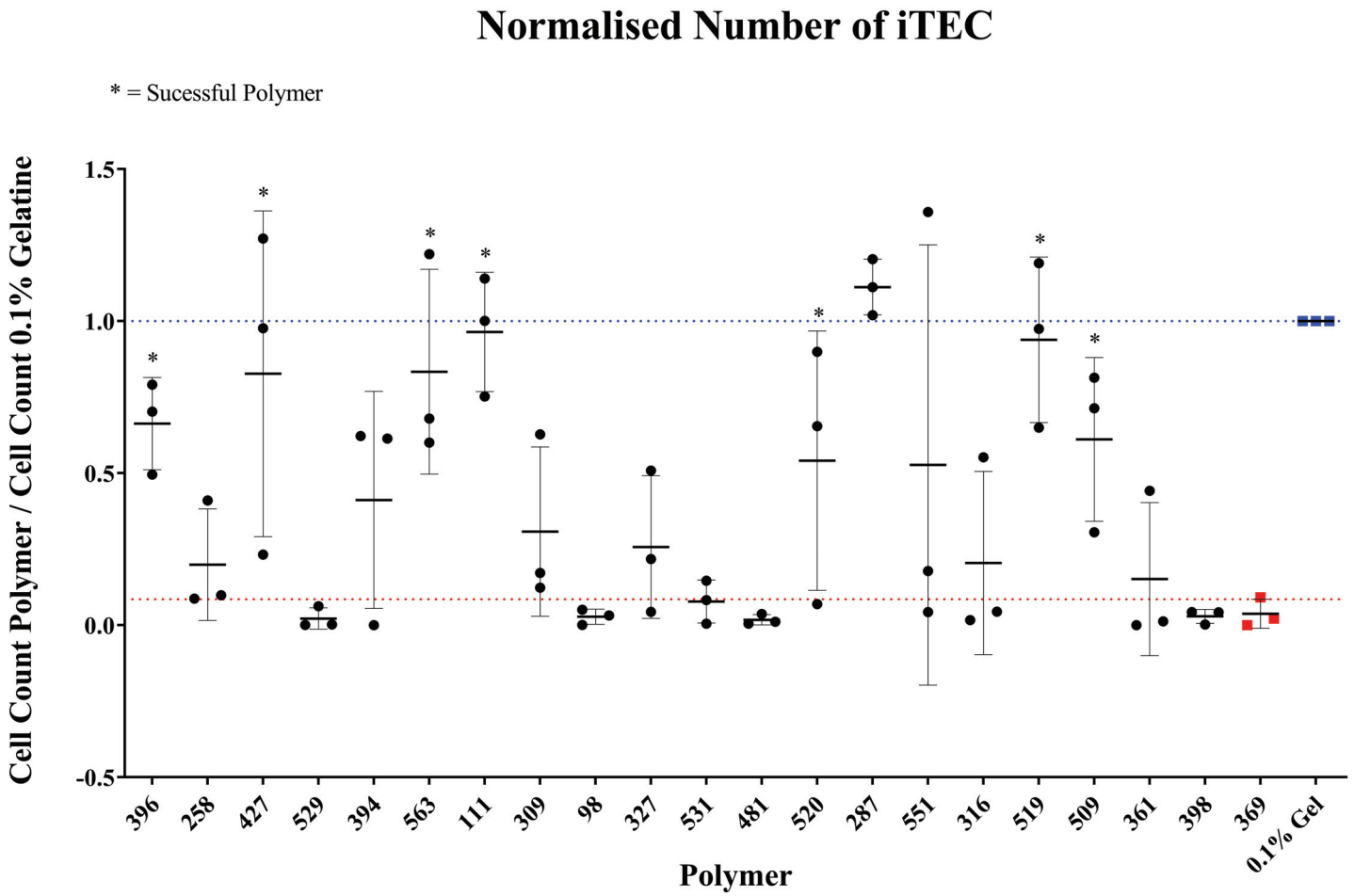

Figure C4.6: Initial Seeding Density Normalised Results of iTEC Focused Polymer Array

Graph depicts the number of iTEC observed in each polymer. Each data point represents the mean of three replicates. Red line shows the mean plus one standard deviation of the negative control polymer 369 and the failure threshold. 0.1% Gelatin is represented in blue.

Table C4.1: Biological Replicate Affected Cell Count in Focused Arrays.
Table depicts the mean number of iTEC counted in three conditions across three technical replicates. Data from three experiments are shown. The cell counts of each condition were variable across experiments despite using the same methodology.

Polymer	*Replicate A Count*	*Replicate B Count*	*Replicate C Count*
0.1% gelatin	5429	5155	11900
519	5294	3898	14170
287	5538	6670	14325

4.3. Primary *Ex Vivo* TEC Screen on the Focused Array Format

The screening strategy described above assumed that iTEC effectively mimicked native TEC and shared the same adhesion profile. To test this hypothesis, *ex vivo* embryonic murine TEC were screened on the successful polymers from the primary iTEC microarray. The experimental set up described above in the iTEC focused array was applied to *ex vivo* material, with the exception that tissue availability allowed for only one technical replicate per condition (Figure C4.7A).

Selecting the developmental age at which TEC were obtained for these experiments was a compromise between total TEC yield and TEC heterogeneity. TEC in the older embryonic thymus are more heterogeneous than TEC at younger developmental ages, as TEC differentiation actively progresses with age during thymic organogenesis. For example, from E13.5 to E15.5, PLET1 expression decreases in most fetal TEC, and patterning into $K5^+$ or $K8^+$ TEC, representing mTEC and cTEC respectively, also occurs during this time window (Bennett *et al*., 2002; Farley *et al*., 2013; Klug *et al*., 2002). I elected to use E13.5 and E14.5 murine TEC to balance tissue scarcity with increasing heterogeneity within the samples. Embryonic thymi were collected and dissociated before depletion of the CD45 compartment using magnetically conjugated beads. The resulting stromal cell preparation was seeded onto polymer coated wells and fixed after 16 hours to mitigate downregulation of *Foxn1* as a confounding variable (Figure C4.7A). Wells were stained with DAPI and anti-pan-cytokeratin and the automated pipeline described above was used to determine the number of cytokeratin expressing cells, assumed to be TEC, within each whole well (Figure C4.7B). The native murine TEC focused arrays were seeded with cells from 140 lobes per array, rather than a defined cell number because a cell count was assumed to be misleading given that whole thymic stroma was seeded into the arrays and only thymic epithelial cells would be counted in the readout (Figure C4.8). Since two developmental ages were used, the proportion of TEC within the total cellularity would not be consistant (Hirakawa *et al*., 2018). To remove this technical variation, the same strategy used in the iTEC focused array was used to normalise the count on each polymer to that of 0.1% gelatin (Figure C4.9):

Equation C4.3:

$$Normalised\ Cell\ Count = \frac{Cell\ Count\ on\ Polymer}{Cell\ Count\ on\ 0.1\%\ Gelatin}$$

This reduced the mean CoV from 60.53% to 49.14%. It is interesting to compare the mean CoV in the iTEC and *ex vivo* TEC focused array, which were 79.95% and 49.14%, respectively. Despite the iTEC using three technical replicates the system contained greater variation. The same criteria were set for polymers in the native TEC focused array as in the iTEC focused array: any polymer with a mean ± 1 SD that intercepted the mean plus + 1 SD (0.3362) of the cell count from polymer 369 was considered a failure (Figure C4.9).

On these criteria, polymers 111, 287, 394, 396, 427, 461, 519, and 563 were identified as able to bind *ex vivo* TEC. This highly similar binding pattern of *ex vivo* TEC and iTEC to the individual polymers present in the Focused Polymer Array (Table C4.2) validated the initial iTEC-based screening approach.

Additionally, I began to test whether *ex vivo* human fetal TEC would also bind these same polymers. Preliminary data were obtained using this approach, with human fetal TEC obtained from a fetus of week 11 of gestational age (Farley *et al*., 2013). However, the human screen was stopped after one experiment because of limitations in sourcing tissue. No normalisation was performed on these data as comparison between biological replicates was impossible. None-the-less, polymers with a higher TEC count than 0.1% gelatin are highlighted in Figure C4.10. These include polymers 111, 309, 396, 427, 461, 519, 520 and 531. The monomers used to create each selected polymer are represented in Table C4.3 and Figure C4.11.

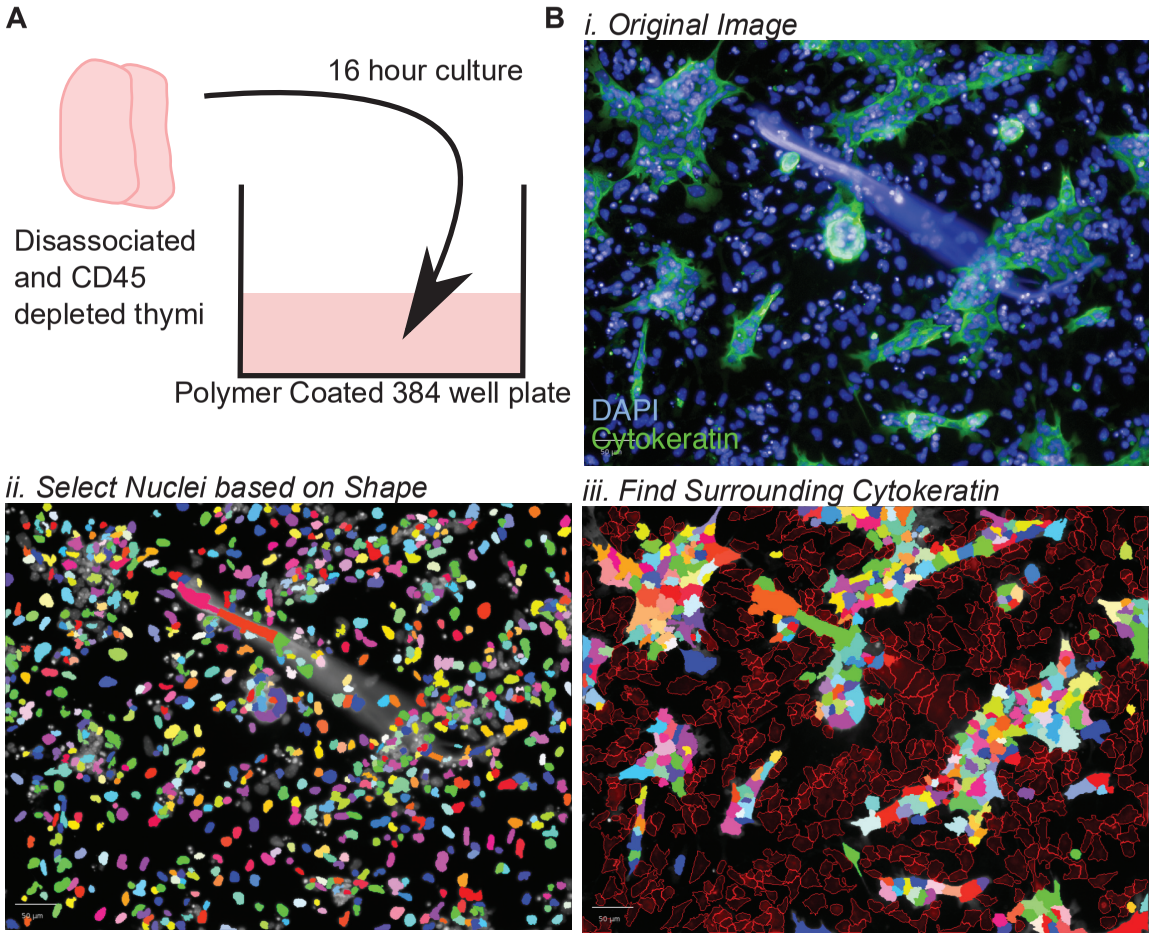

Figure C4.7: Method For *Ex Vivo* TEC Focused Polymer Arrays

A. Embryonic thymic disassociate was cultured for 16 hours on polymers selected from microarray screen. **B**. The automated pipeline to count the number of cytokeratin expressing cells. ***i***. TEC were stained for cytokeratins and nucleic acid. ***ii***. An automated pipeline selected nuclei based on size and shape of $DAPI^+$ spots. ***iii***. Cells with cytoplasmic cytokeratin were selected for and counted.

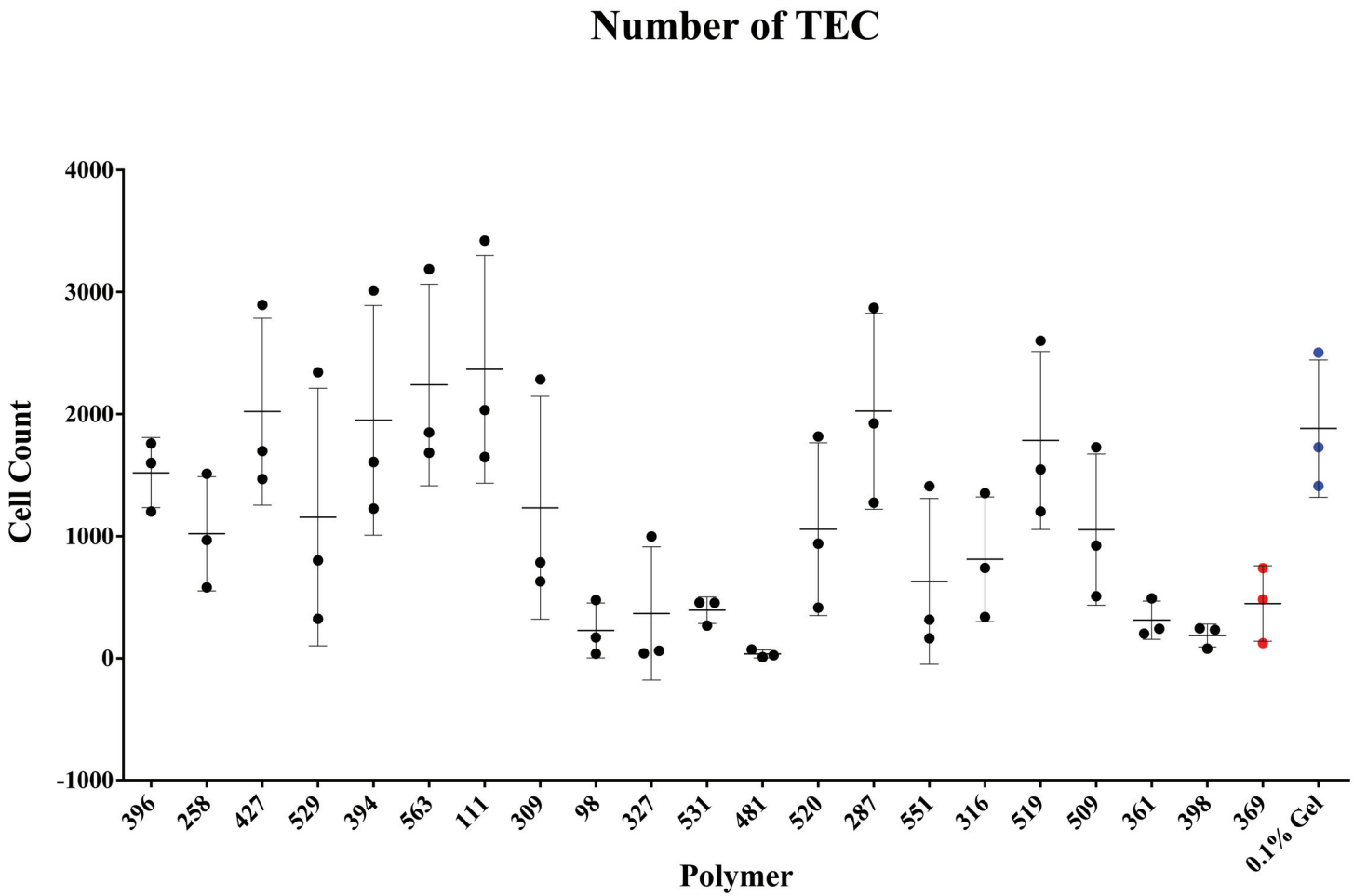

Figure C4.8: Results of *Ex Vivo* Murine TEC Focused Array

Graph depicting the number of E13.5 and 14.5 TEC that bound across all polymers. Each data spot represents one technical replicate. The negative control polymer 369 is in red while the positive control 0.1% Gelatin is in blue.

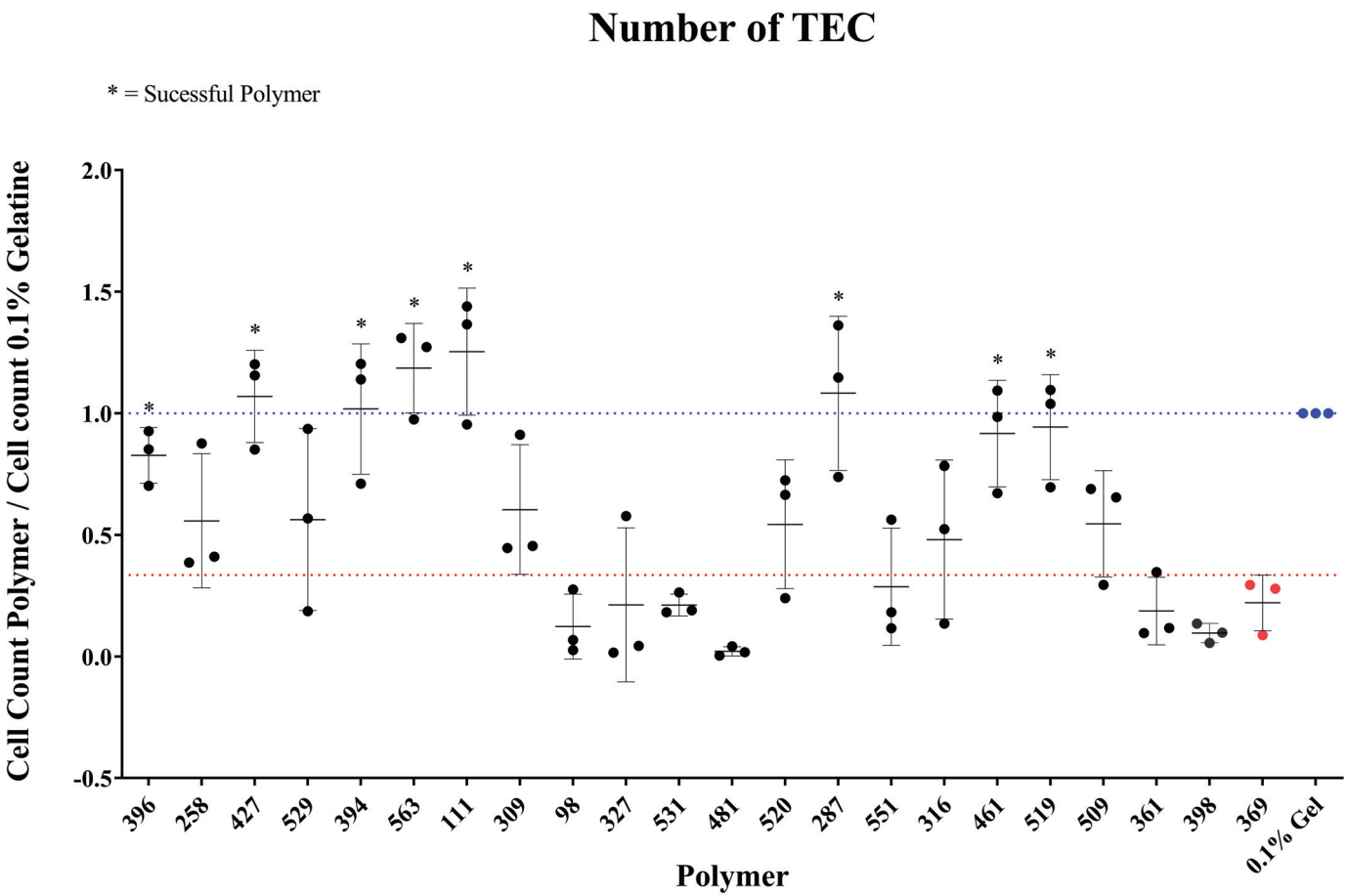

Figure C4.9: Initial Seeding Density Normalised Results of *Ex Vivo* Murine TEC Focused Array

Graph depicting the number of E13.5 and 14.5 TEC observed in each polymer coated well, 16 hours after seeding and normalised to the cell count of 0.1% Gelatin, which is represented in blue. The red line shows plus one SD from the mean of the negative control polymer 369 and the failure criterion for the screen. Each data spot represents one technical replicate.

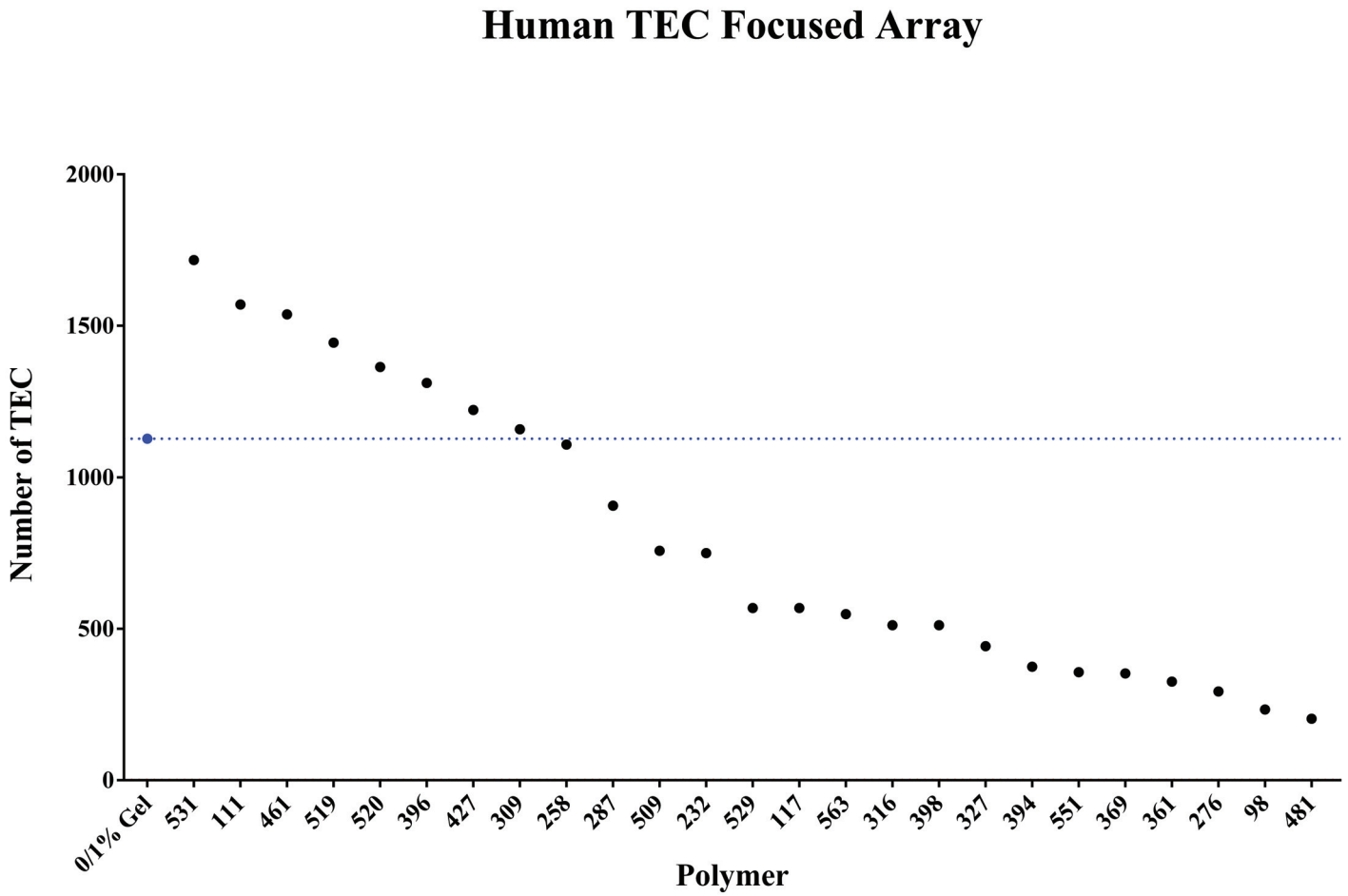

Figure C4.10: Results of *Ex Vivo* Human TEC Focused Polymer Array

Graph depicting the number of gestational week 11 human TEC that had adhered after 16 hours, across all polymers. Blue line represents the number of TEC observed upon 0.1% Gelatin, which is the postitive control. N=1. Each data spot represents one technical replicate.

Table C4.2: List of Successful Polymers in all Focused Arrays.
Table shows all successful polymers with respect to the cell type.

iTEC Candidates	*Murine TEC Candidates*	*Human TEC Candidates*
111	111	111
287	287	-
-	-	309
-	394	-
396	396	396
427	427	427
-	461	461
509	-	-
519	519	519
520	-	520
-	-	531
563	563	-

Table C4.3: List of Monomeric Structures of Successful Polymers in all Focused Arrays.
This table details the monomer composition of the selected polymers. Monomer structures are described in Figure C4.11. MEMA (methoxyethyl methacrylate); MMA (methyl methacrylate); EMA(ethly methacrylate); BAEMA (t-butly methacrylate); GMA(glycidyl methacrylate); DMAEMA (dimethylaminoethyl methacrylate); DEAEA (2-(diethylamino)ethyl acrylate); MAN (methacrylonitrile); BMA (N-butyl methacrylate); THFFMA (tetrahydrofurfuryl Acrylate); DAA (dihydroxyaluminum aminoacetate); DEAEMA ((diethylamino)ethyl methacrylate); St (styrene)

Polymer	*Monomer 1 (ratio)*	*Monomer 2 (ratio) Group*	*Monomer 3 (ratio) Group*	*Molecular Weight*
111	MEMA (90%)	BAEMA (10%) Amine	-	273000
287	MEMA (50%)	GMA (50%)	Man (>1%) Amine	>2,000,000
309	MMA (90%)	GMA (10%)	DnHA (>1%) Amine	1900000
394	EMA (70%)	DMAEMA (30%) Amine	-	120000
396	EMA (90%)	DEAEA (10%) Amine	-	123000
427	MEMA (60%)	DEAEA (10%) Amine	BMA (30%)	111000
461	MEMA (80%0	DEAEA (10%) Amine	THFFMA (10%)	152000
509	MEMA (80%)	DEAEA (10%) Amine	DAAA (10%) Amide	211000
519	MEMA (60%)	DEAEMA (10%) Amine	St (30%) St	86600
520	MEMA (60%)	DEAEMA (30%) Amine	St (10%) St	143000
531	MEMA (55%)	DEAEMA (45%) Amine	-	141000
563	MEMA (50%)	A-H (25%) Acid	DEAEMA (25%) Amine	107000

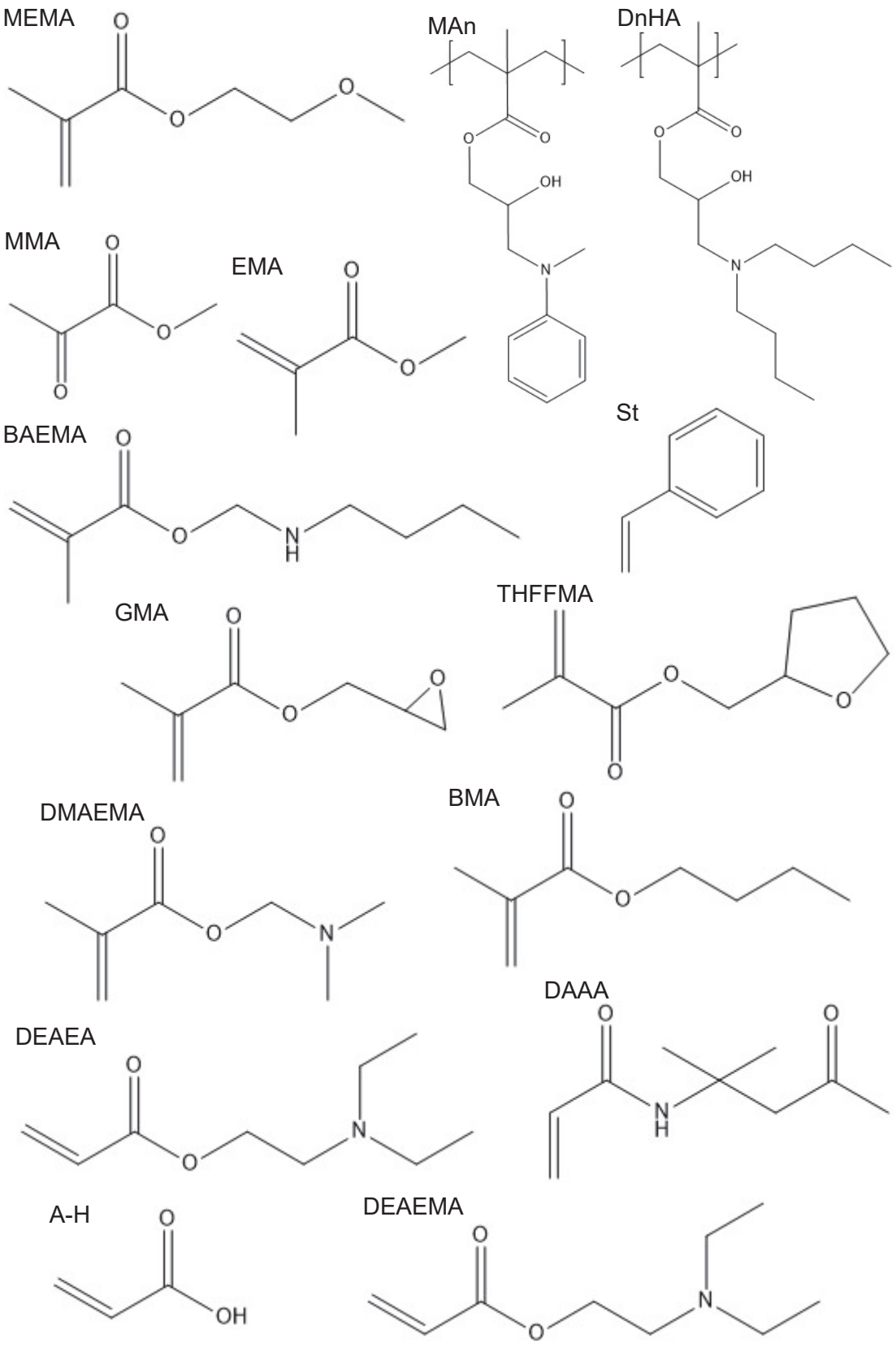

Figure C4.11: Monomer Structures of Candidate Polymers
Images depict the chemical structures of the monomer sub-units used to fabricate the polymers that were successful in the Focused Arrays.

4.4. Characterising the Functional Effects of Culturing *Ex Vivo* TEC on Selected Polymers

4.4.A. Experimental Design

The data presented above identify a set of 12 polymers that bound TEC, iTEC and human TEC as well as or better than 0.1% gelatin that were screened from a library of 367 candidates. These polymers therefore have potential for replacing gelatin and other animal derived ECMs, in TEC culture protocols. Next it was interesting to test whether these polymers identified above affected the behaviour of the cells bound as described into the introduction of this chapter.

Glass bottom 384-well plates were coated with candidate polymers as previously described. Matrigel was included in the screen as an addition control, representing a heterogeneous native ECM matrix. Note that in this experiment, 0.1% gelatin represents the negative control as it is known that TEC downregulate *Foxn1* in monolayer cultures in when plated on gelatin (Anderson and Jenkinson, 2007; Mohtashami and Zúñiga-Pflücker, 2006).

E12.5 and E13.5 tissue was dissected and dissociated, to obtain sufficient numbers to seed each well with 2×10^5 cells. The cell count was used to standardise conditions with the aim of minimising variability, since seeding density often affects cellular behaviour in culture. Given the relative high proportion of TEC to other cells within the thymic rudiment at these developmental ages, a cell count was assumed to reasonably capture information regarding total input TEC into each well (Hirakawa *et al*., 2018). However, it should be noted that the seeding population was a heterogenous mixture of TEC, mesenchymal cells and early haematopoietic colonising cells (Itoi *et al*., 2001). The decision not to sort the samples using FACS was justified because of the importance of the crosstalk during thymic organogenesis. It was assumed if all cell types within the thymus were seeded into the monolayer, crosstalk would make *ex vivo* TEC more likely to recapitulate native behaviour and maintain *Foxn1* expression. The mating strategy used to obtain embryos for microdissection was to backcross heterozygous *Foxn1*$^{G/+}$ to C57BL/6 mice, since *Foxn1*^{G} is a null allele. Therefore, only half of the cultured TEC had the capacity to express GFP (Figure C4.12A). However,

this was reasoned to not affect the readout based on the assumption that downregulation of *Foxn1* was relatively consistent between all TEC within a well. Furthermore, a no staining control was not required for the experiment as the wild type TEC in each well fulfilled this control.

After seeding, the plates were imaged in brightfield and for GFP after 2, 24 and 48 hours (Figure C4.12B). ImageJ was used to automatically threshold the GFP image set to 'Rényi entropy' mode, which segmented out objects brighter than the background using a single colour histogram (Kapur *et al*., 1985). The number of segmented objects were then filtered according to size and shape and this provided the number of GFP^+ TEC at each time point. The inclusion of dividing cells produced inconsistencies and therefore these cells were excluded from the cell count (Figure C4.12C).

Using only one colour for image segmentation was not ideal, as both selecting on the target population and quantifying fluorescence intensity had to be performed using one histogram. The total level of GFP could not accurately be measured down to zero, as GFP expression was used to select on cells and so cells without *Foxn1* expression could not be measured. This bias toward reporting false positive cells was further aggravated by the premise of segmenting cells using 'Rényi entropy' (Kapur *et al*., 1985). The mode actively looks for outliers by taking the upper proportion of the histogram as positive i.e. this mode will always find positive pixels based upon deviation away from the mean. In turn, this complicated direct testing of the null hypothesis that the fluorescence intensity of GFP, and therefore *Foxn1* expression, did not decrease over time. To test this hypothesis more rigorously, a dual reporter mouse would be required, such that one colour could be used to identify TEC and one to quantify *Foxn1* expression. This could have been achieved by using a triple transgenic mouse line in which a fluorescent reporter was expressed under the *Foxn1* promoter, Cre was knocked into the *Foxn1* locus, and an inducible fluorescent reporter was knocked into the Rosa26 locus (Hirakawa *et al*., 2018).

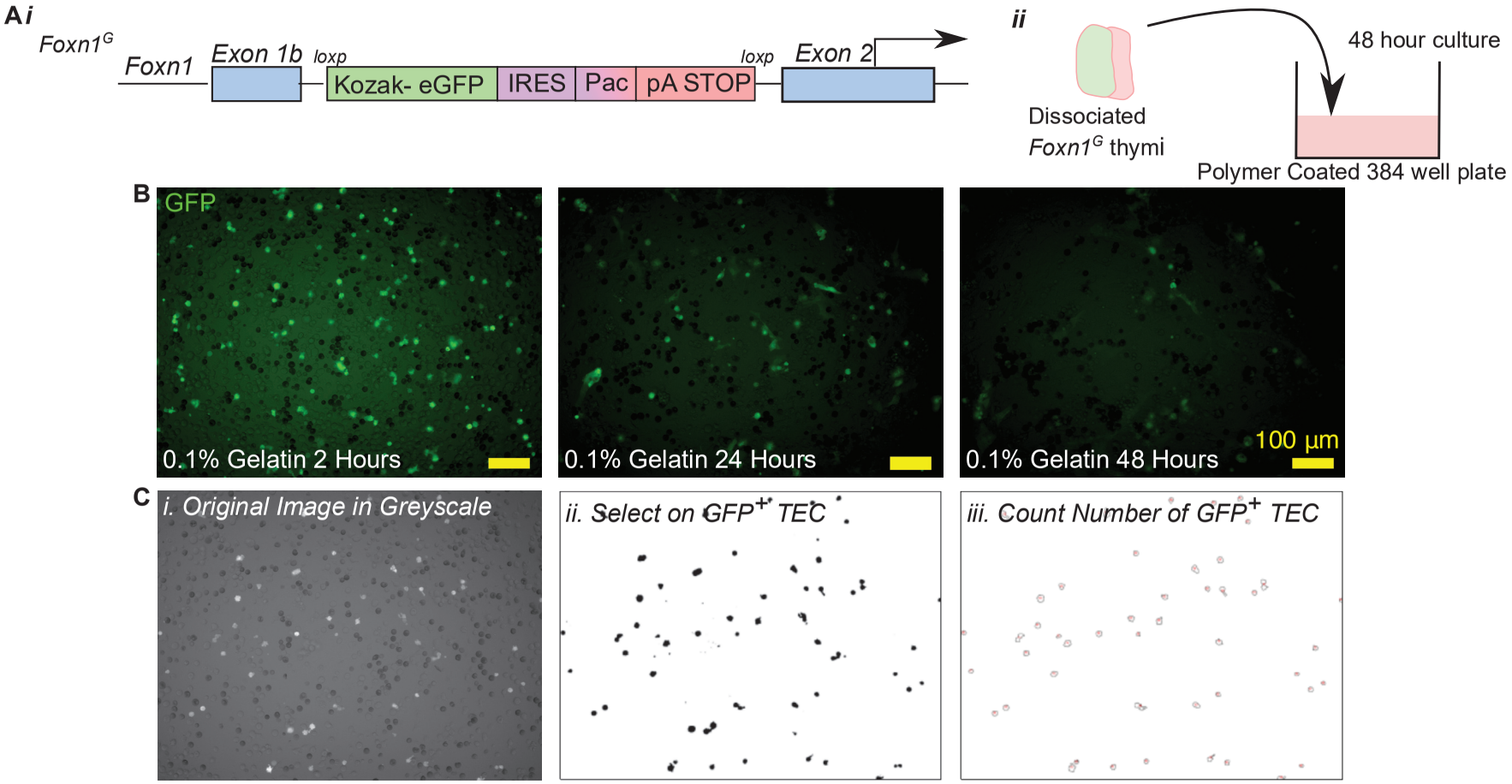

Figure C4.12: Method for *Ex Vivo* TEC Functionality Tests

A.***i***. The *Foxn1G* transgene. **A**.***ii***. Half of TEC contained the *Foxn1*^{G} transgene, these TEC expressed GFP in proportional to expression *Foxn1*. **B**. Images, in the GFP channel, of disassociated E12.5 and 13.5 thymi cultured on 0.1% Gelatin 48 hours after seeding. **C**.***i***. An original image taken in the GFP channel. ***ii***. Single colour segmentation strategy to select GFP^{+} TEC. ***iii***. Small debris were removed and the number of GFP^{+} TEC was counted.

4.4.B. Results

The number of GFP$^+$ TEC was recorded at each time point across three independent experiments (Figure C4.13). Given that there were two independent factors, which were polymer condition and time, associated *Foxn1* maintenance, and that time is a continuous variable, a second order polynomial (quadratic) regression was employed to calculate a curve of best fit and confidence intervals for all three replicates, in all polymer conditions and at all three time points.

The number of GFP$^+$ TEC decreased over time in all polymer conditions and there was a degree of variation between the biological replicates in the experiment. The variation between biological replicates can be represented by the R^2 of the quadratic regression and denotes how well the regression curve fits the three data sets simultaneously. Hypothetically, if the data from all three experimental replicates were the same, R^2 would equal 1. Similarly, to the focused arrays, there were two probable sources of variation: biological differences between TEC within wells and differences in starting cell densities. The latter was normalised for by reporting the cell count as a percentage of the initial cell count, as this normalised against having a different starting number of GFP$^+$ within each well (Figure C4.14):

Equation C4.4:

$$Normalised\ Cell\ Count = \frac{\boldsymbol{Number\ of\ Thresholded\ GFP^+\ TEC}}{\boldsymbol{Number\ of\ Thresholded\ GFP^+TEC\ at\ 2\ hours}}$$

This normalisation also created the assumption that the two-hour point must equal one, so a parameter constraint was included in the regression to enforce that B0 = 1. This raised the mean R^2 of the regression from 0.42852 to 0.74846. The null hypothesis that the quadratic regression was not statistically different from $y = 0x + 1$ was rejected (Figure C4.14). The number of TEC expressing detectable GFP decreased over time. This inference was used to conclude that *Foxn1* was downregulated over time on all substrates.

The other source of variation within this experiment was biological. This might result from using undefined culture medium containing fetal calf serum. The experiment was therefore repeated in serum-free N2B27 medium supplemented with BMP4, FGF7 and EGF (Figure

C4.15), since these conditions were previously shown to support growth of TEC *in vitro* (this laboratory, unpublished). BMP4 and FGF7 are implicated in thymic organogenesis and have also been used in a directed differentiation process to create TEC from human pluripotent stem cells (Farley, 2010; Jenkinson *et al*., 2007; Su *et al*., 2015; Swann *et al*., 2017a).

After following the same normalisation strategy to remove variation in the initial seeding density, the defined medium increased the average R^2 of the regression curves to 0.92662. The high value shows that the data points across all three independent experiments were regressed into similar curves of best fit for each polymer condition, as described above if all three curves of best fit were identical the hypothetical R^2 would equal 1, this can be used to infer that there was little technical variation between experiments and differences found in the study were due to the changes measured independent variables (polymer condition and time). The increase between the R^2 found in the experiment using serum compared to this serum free experiment shows that serum was introducing variation into the results. Again, the null hypothesis that number of detectable GFP^+ TEC did not change over time (and that the regression curves were not different from $y = 0x + 1$), was rejected (Figure C3.16). Thus, culture on none of the eight candidate polymers tested met Objective A, as *Foxn1* was not maintained in any of these culture conditions.

Given that *ex vivo* TEC were unable to maintain *Foxn1*, it was assumed that they will not be able to meet the second objective of this chapter, which was to mediate T-cell differentiation (Mohtashami and Zúñiga-Pflücker, 2006). No further testing of the effect of the polymers on TEC functionality was performed, given the technical limitation of polymers currently only being compatible with monolayer culture conditions. Therefore, this chapter identified eight defined polyacrylate substrates that allowed culture of *ex vivo* TEC and maintained *Foxn1* expression to the same extent as currently existing technologies. Now I wanted to investigate how culturing with the selected polymers affected iTEC behaviours.

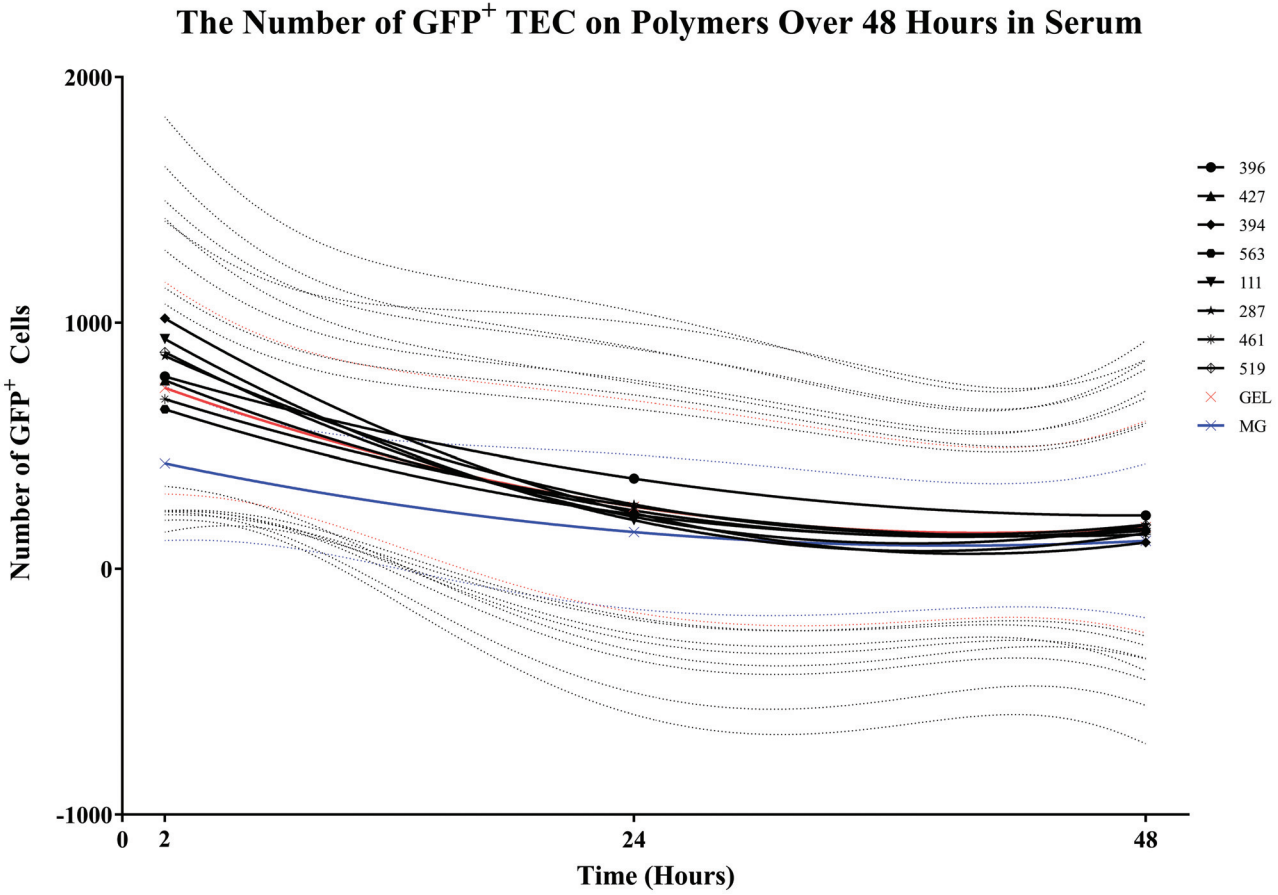

Figure C4.13: The Number of *Ex Vivo*, *Foxn1*^{G} TEC on Polymers Over 48 Hours, in Serum

Graph depicting the raw cell count of GFP^{+} E12.5 and E13.5 TEC over time, using the *Foxn1*^{G} transgene. The 95% confidence intervals were calculated using a quadratic regression and are are shown as dotted lines. Matrigel is represented in red and 0.1% Gelatin is shown in blue. Each data point represents the mean of three independent experiments.

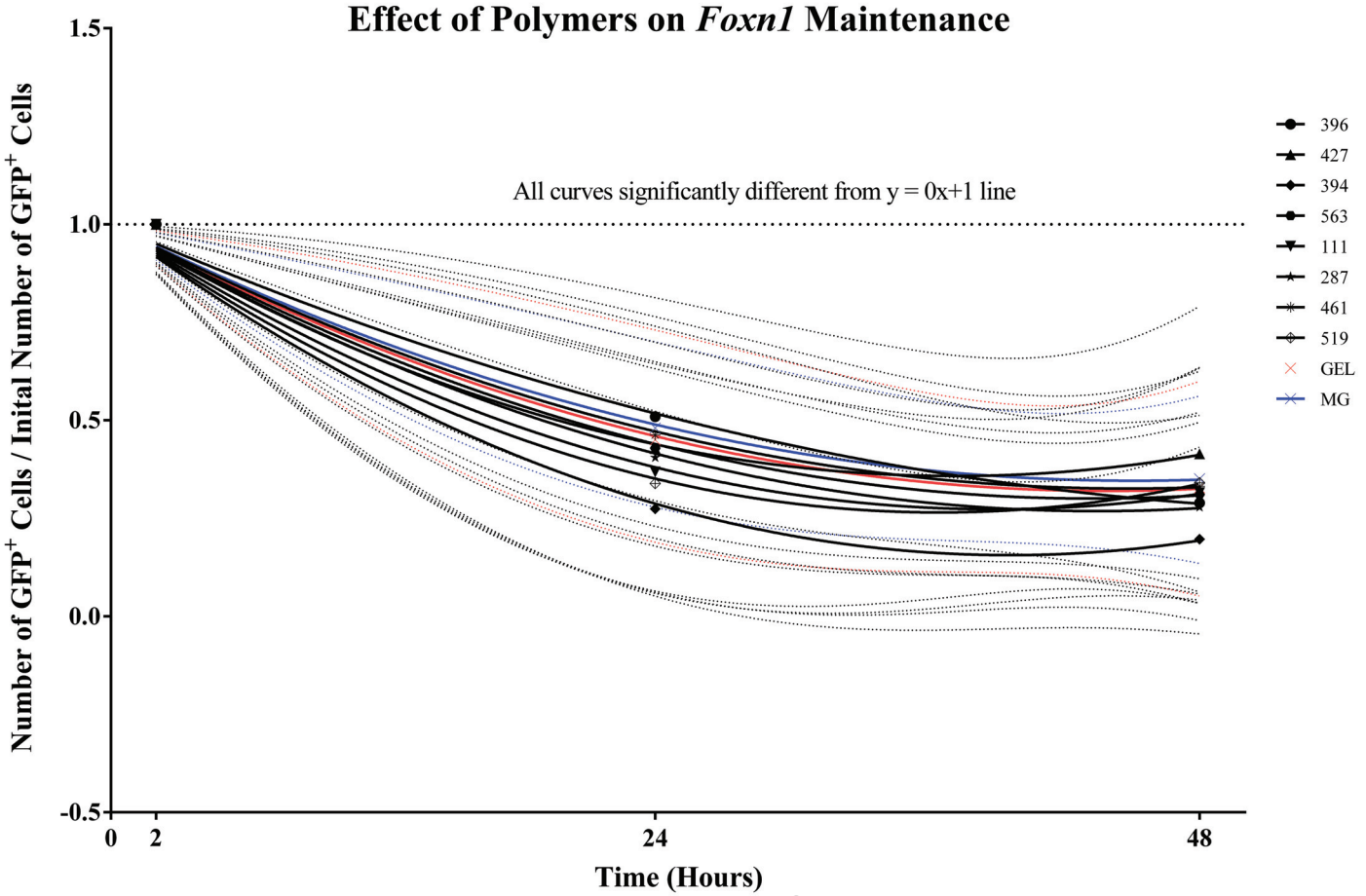

Figure C4.14: Polymers Did Not Affect Foxn1 Maintenance in *Foxn1*^{G} *Ex Vivo* TEC Over 48 Hours, Cultured in Serum

Graph depicting the ratio GFP^{+} TEC to the initial count of GFP^{+} TEC over 48 hours. A quadratic regression analysis calculated 95% confidence intervals, which are represented as dotted lines, and inferred all curves deviated significantly away from the hypothetical line representing no change in the number of GFP^{+} TEC over time. Matrigel is shown in red and 0.1% Gelatin is shown in blue.

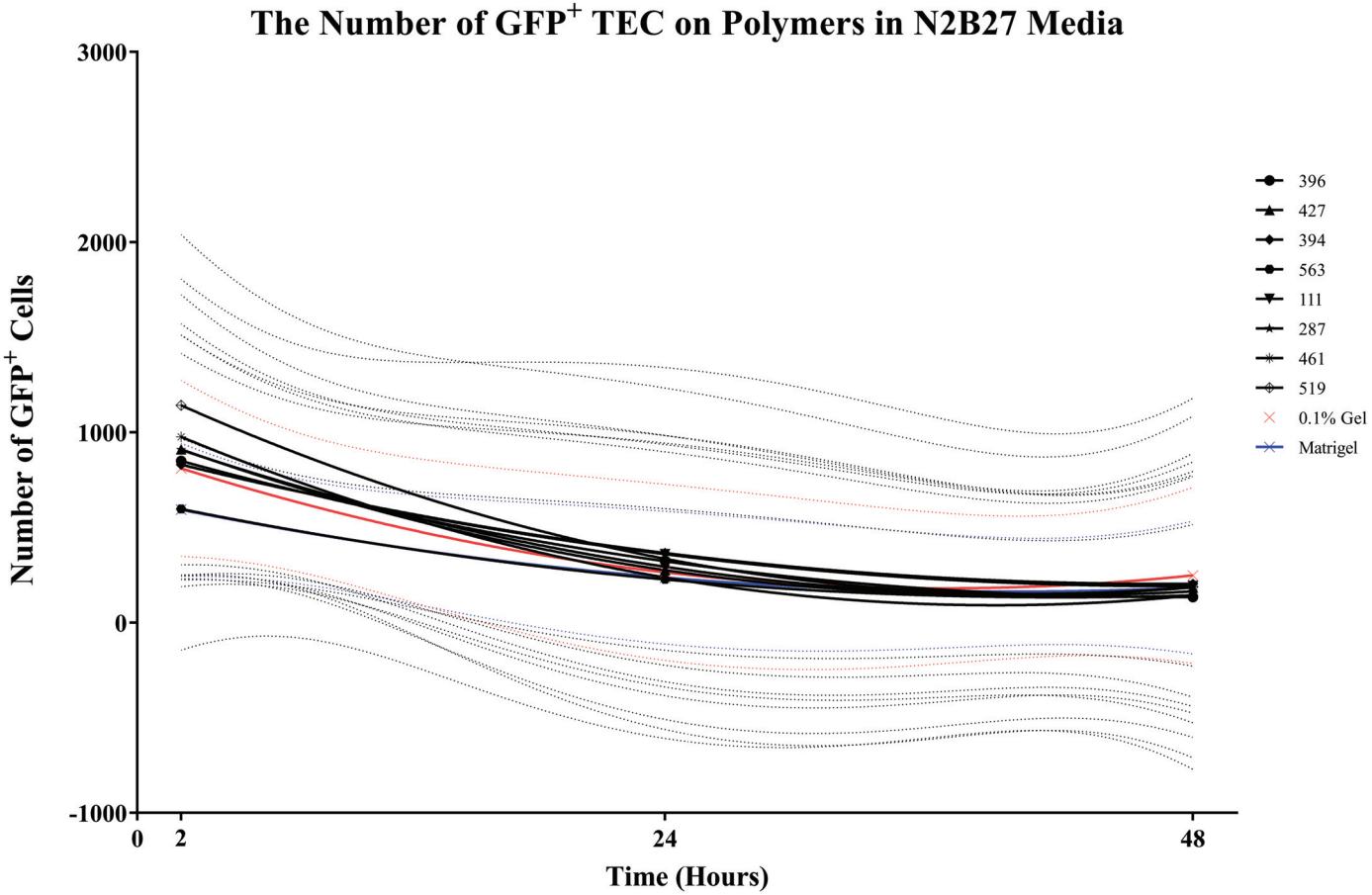

Figure C4.15: The Number of *Ex Vivo*, *Foxn1*^{G} TEC on Polymers Over 48 Hours, in N2B27 Medium

Graph depicting the raw cell count of GFP^{+} TEC over time, using the *Foxn1*^{G} transgene. Tissue culture was perfromed in defined N2B27 media. The 95% confidence intervals were calcualted using a quadratic regression and are are shown as dotted lines. Matrigel is represented in red and 0.1% Gelatin is shown in blue. Each data point represents the mean of three independent experiments.

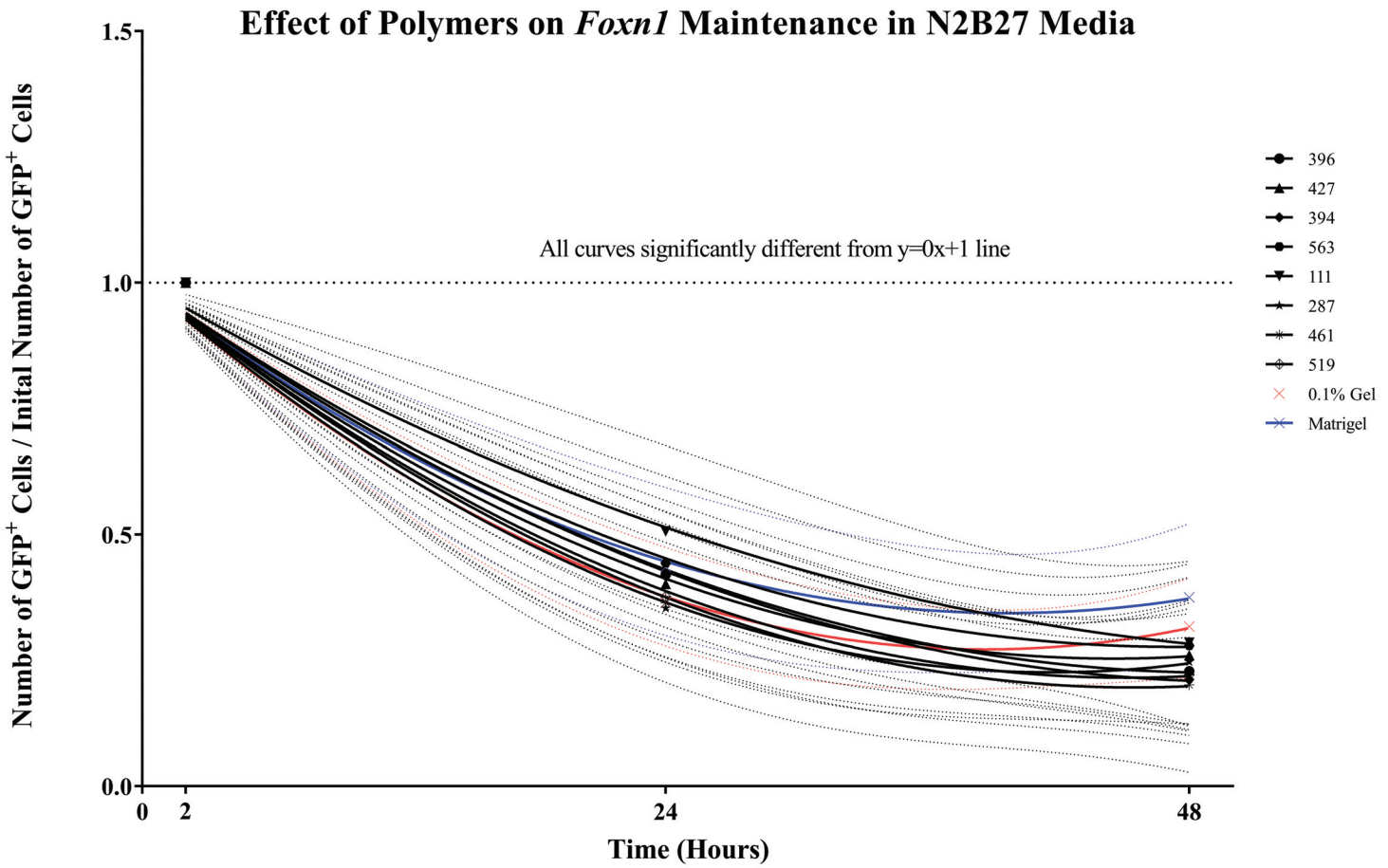

Figure C4.16: Polymers Did Not Affect Foxn1 Maintenance in *Foxn1*^{G} *Ex Vivo* TEC Over 48 Hours, in N2B27 Medium

Graph depicting the ratio GFP^{+} TEC to the initial count of GFP^{+} TEC in defined N2B27 Media. A quadratic regression analysis calculated 95% confidence intervals, which are represented as dotted lines, and inferred all curves deviated significantly away from the hypothetical line representing no change in the number of GFP^{+} TEC over time. Matrigel is shown in red and 0.1% Gelatin is shown in blue.

4.5. Determination of Whether Select Polymers Improved the Ability of iTEC to Mediate T-cell Differentiation Compared to Standard Culture Methods

4.5.A. Experimental Design

To investigate the effects of culture with the selected polymers on iTEC behaviour, I tested the second objective: investigation of whether culture on any of the polymers selected for iTEC culture resulted in an improved ability to mediate T-cell differentiation compared to standard culture methods. The first objective, that polymers were able to maintain *Foxn1* during culture was redundant in the iTEC system because *Foxn1* is genetically enforced through the reprogramming method.

To allow collection of enough thymocytes for flow cytometric analysis, these experiments were conducted in 24-well plates. The larger surface area of these wells necessitated a different coating strategy. 500 µl of 0.2 g / ml polymer solution was applied to each well on an orbital shaker and left to airdry. Agitation ensured that the centre of each well did not dry before the outer edge of the well, which would create a nonuniform coating of polymer. Gelatin (0.1%) was used as a positive control substrate given that it was used in the original publication of iTEC (Bredenkamp *et al*., 2014). Matrigel was also included as a control as this is a heterogeneous ECM-based substrate. Note that unlike previous experiments, Cre only MEFs were not included as a negative control as all polymers except 287 did not bind MEFs in the microarray.

In each well, 2×10^5 iTEC were co-cultured with 5×10^3 ETPs in iTEC medium supplemented with 50 ng / ml FGF-7, 5 ng / ml FLT3L, 10 ng / ml IL-7, 25 ng / ml KITL. 50% of the medium was replaced on day two or three and then, for all subsequent media changes that occurred every other day, IL-7 was reduced to 1 ng/ ml and KITL to 5 ng / ml. Of note is that in these experiments, ETP were isolated from the thymus of a four-week old female mouse and before isolation using FACS were enriched for c-KIT using magnetic beads to reduce the length of the FACs sorting session. ETPs were defined as: $CD45^+CD44^+c\text{-}Kit^+CD25^-CD3^-CD4^-CD8^-CD11b^-CD11c^-B220^-Gr\text{-}1^-Nk1.1^-Ter119^-$ (Figure C4.17).

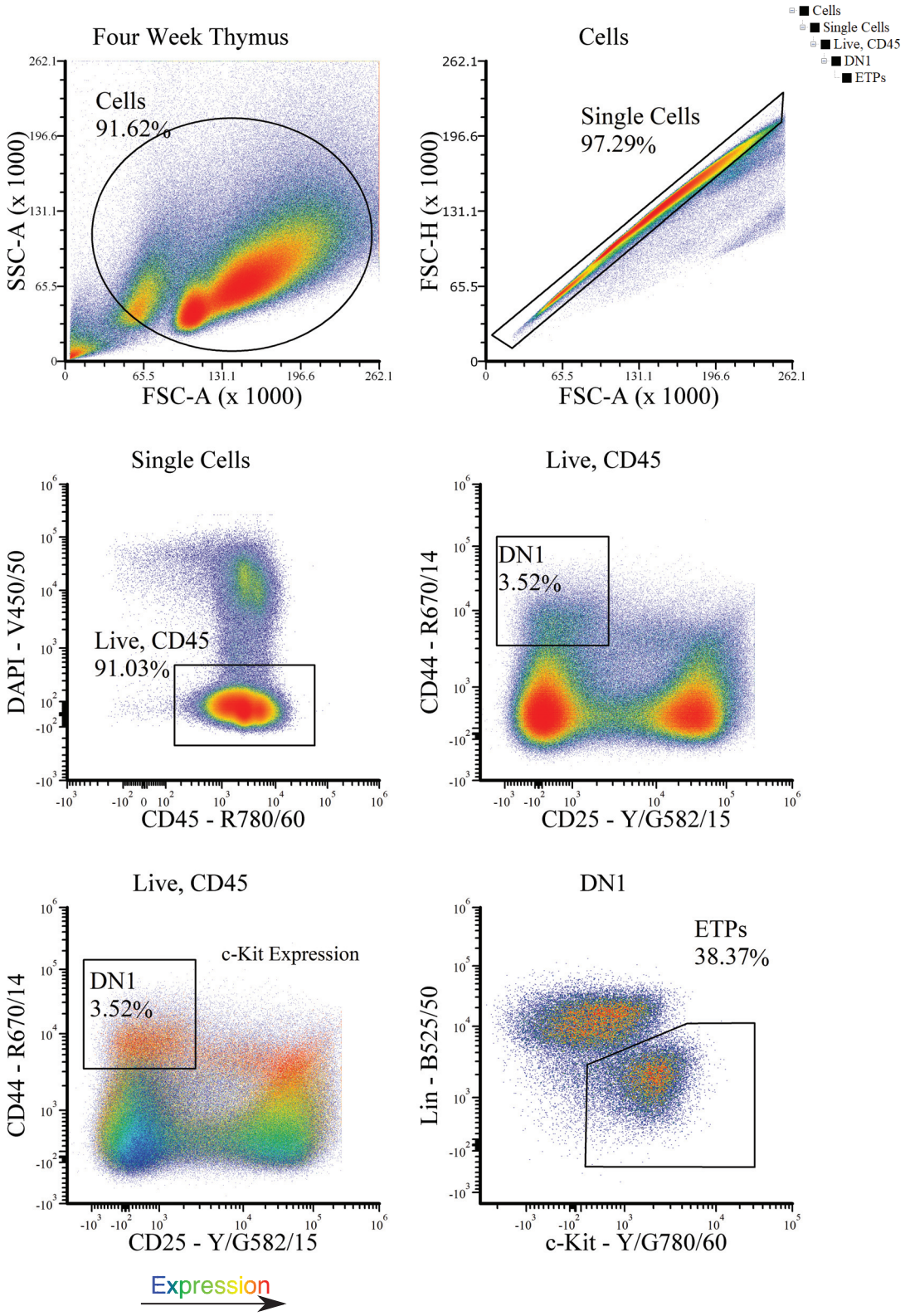

Figure C4.17: Sorting Strategy for c-KIT Enriched ETPs

Strategy for isolating ETPs after magnetic enrichment for c-Kit. The title of each plot shows which gate is active. c-Kit expression is shown on live, CD45 population as a flame UTI to justify the DN1 gate. The lineage cocktail was: CD3ε, CD4, CD8, CD11b, CD11b, Gr-1, Nk1.1, Ter119.

4.5.B. Results of Thymocyte Subset Analysis

After 14 days, the cells were separated using trituration, creating a single cell suspension of thymocytes and leaving the monolayer of iTEC in the well and the two cell types were subjected to different analyses. The changes to the iTEC were measured using reverse transcription-quantitative polymerase chain reaction (RT-qPCR) and immunohistochemistry, while progression of the thymocytes through thymopoiesis was quantified using flow cytometry. The absolute numbers of $CD4^+CD8^+$ (DP), $CD4^+CD8^-$ (SP4), $CD4^-CD8^+$ (SP8) and $TCR\beta^+CD3\varepsilon^+$ (T-cells) thymocytes from each well were counted using a standardised gating strategy (Figure C4.18). Note, that only 75% of each sample was collected so the absolute count had to be corrected for this. The data were collected and analysed without further normalisation; representative plots are shown in Figures C4.19-29; the mean cell counts are displayed in Table C4.4 and this is broken down into each experiment in Tables C4.5, C4.6 and C4.7. The mean proportions are presented in Tables C4.8 and the mean CoVs are shown in Table C4.9. The assumption used on previous normalisation methods, that the positive control was consistent, was not satisfactory. In this screen 0.1% gelatin had a higher co-efficient of variation than average for each thymocyte subset (Table C4.9).

Whether culture on any individual polymer resulted in improved iTEC functionality compared to culture on 0.1% gelatin was determined using a one-way ANOVA. Data were tested for normality using the Shapiro-Wilk test. Note that the Total T-cell count data failed this test and were analysed with the non-parametric Kruskal-Wallis test. The null hypothesis was accepted. No polymer condition was found to produce a significantly different number of thymocytes compared to 0.1% gelatin (Figure C4.30). However, the ANOVA was associated with an average R^2 of 0.338875. This is low and describes that most of the variance within the experiment was not captured within the analysis and arose from unmeasured sources of variation. This is probably due to technical variability in both the iTEC and co-culture methodologies and this ‘noise’ prevent resolution of the biological effect found between polymer conditions (Table C4.9). The variation between wells is shown in Figure C4.31. It is notable to highlight in this figure that there was no distinct pattern that could be used to normalise the data.

Overall, it was concluded that due to the large variation associated with the iTEC system in monolayer co-cultures it was impossible to find a significant effect between iTEC across polymer conditions. However, polymers 396 and 427 and, to a lesser extent, polymer 509 warranted further investigation and provided evidence that the overarching hypothesis of this chapter (outlined in Chapter One) was true, defined polymers were able to reduce variation in iTEC. Next, I characterised the direct changes in the iTEC of the co-culture.

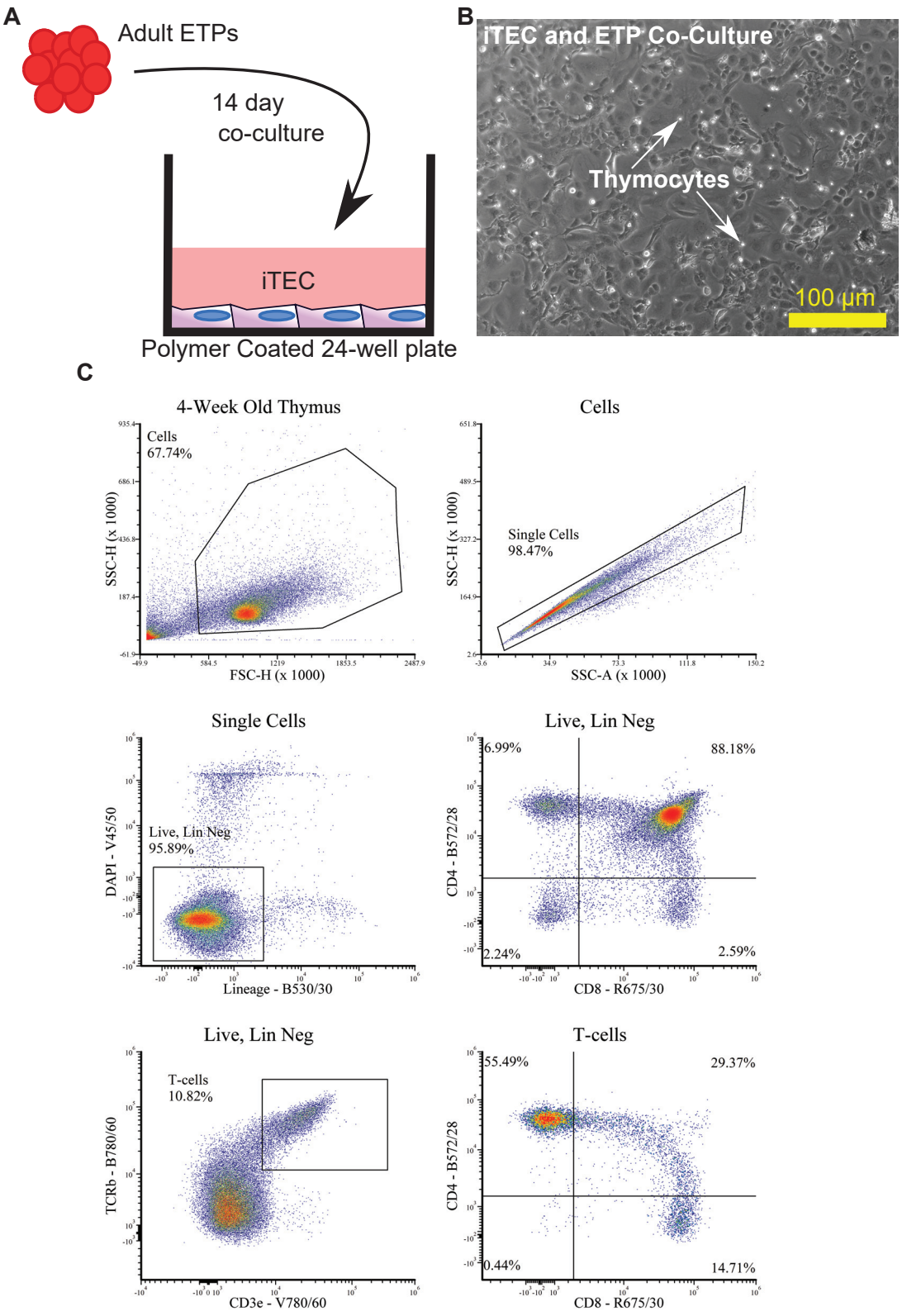

Figure C4.18: Method for iTEC Functionality Polymer Array

A. Representation of iTEC Functionality Array. **B**. Bright field image of iTEC and adult ETP co-culture after 14 days on 0.1% Gelatin. **C**. Gating strategy, demonstrated using thymocytes isolated from a four-week old thymus, to count cell numbers of T-cells and subsequent $TCR\beta^{+}CD3\varepsilon^{+}$ DP, SP4 and SP8 populations for analysis.

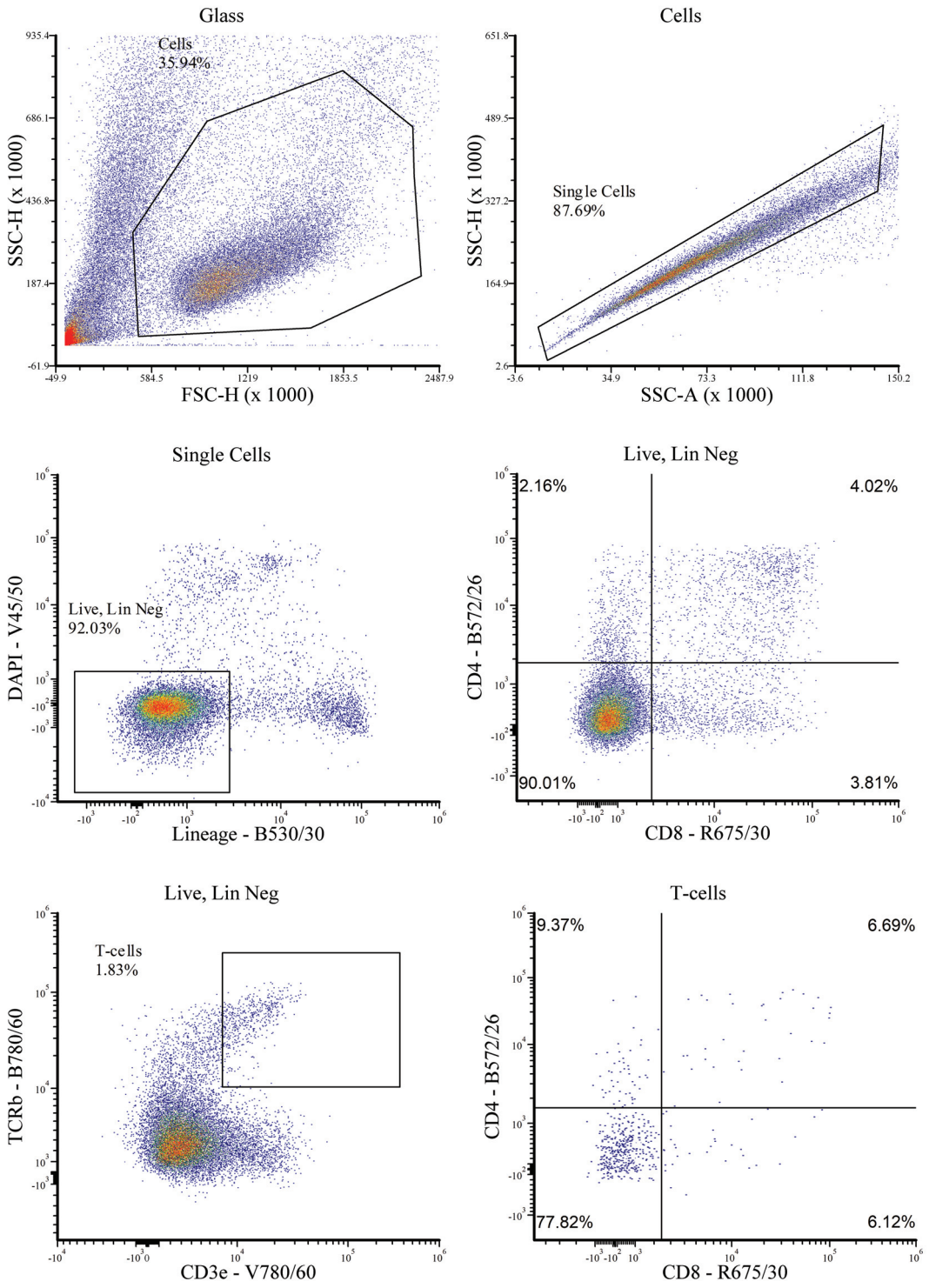

Figure C4.19: iTEC Functionality Polymer Array Representative Plots - Glass

Flow cytometric profile of a representative replicate in the iTEC Functionality Polymer Array. Lineage cocktail included: CD11b, CD11c, Gr-1,Nk1.1, B220, EpCAM, Ter119.

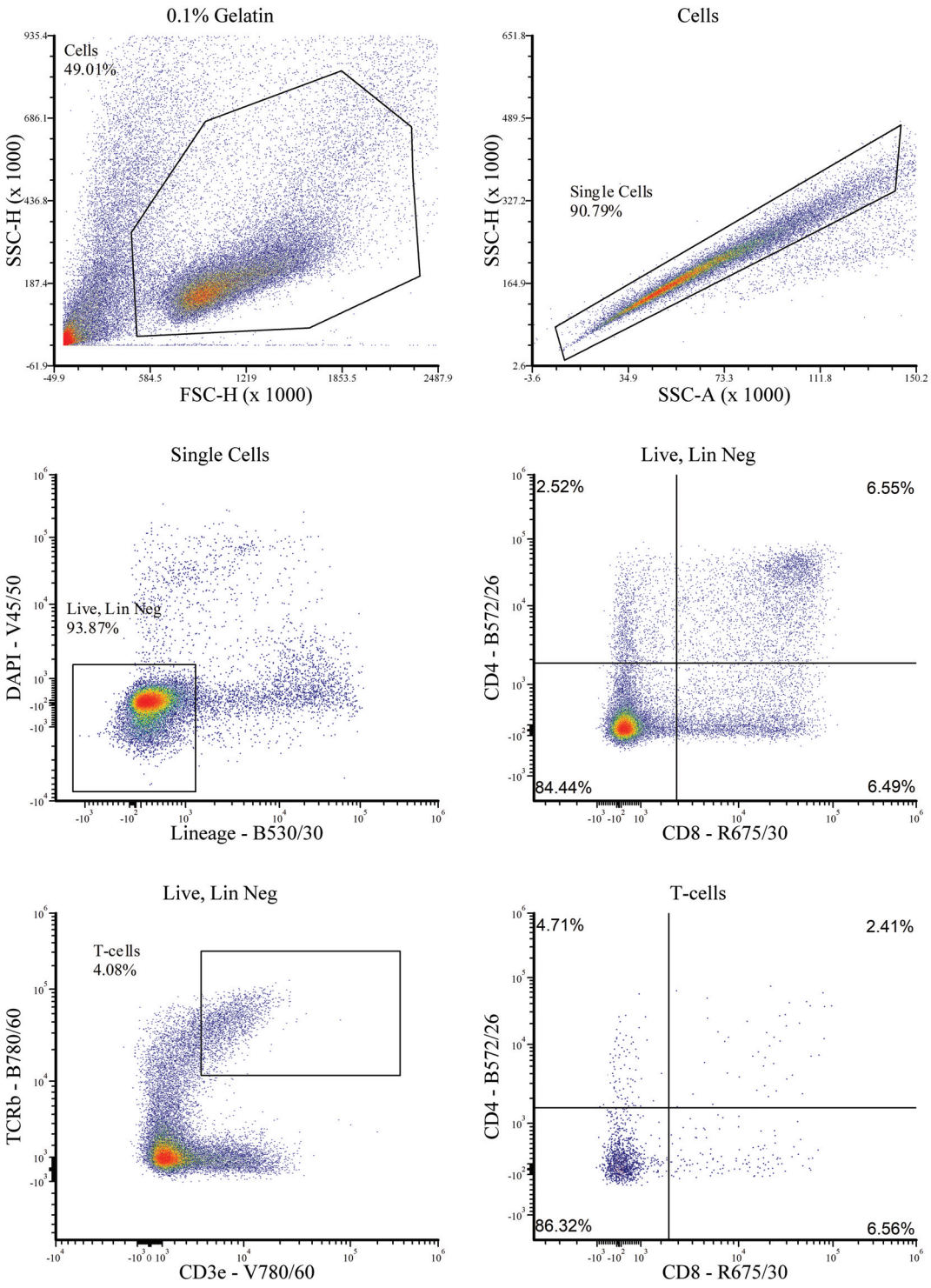

Figure C4.20: iTEC Functionality Polymer Array Representative Plots - 0.1% Gelatin

Flow cytometric profile of a representative replicate in the iTEC Functionality Polymer Array. Lineage cocktail included: CD11b, CD11c, Gr-1,Nk1.1, B220, EpCAM, Ter119.

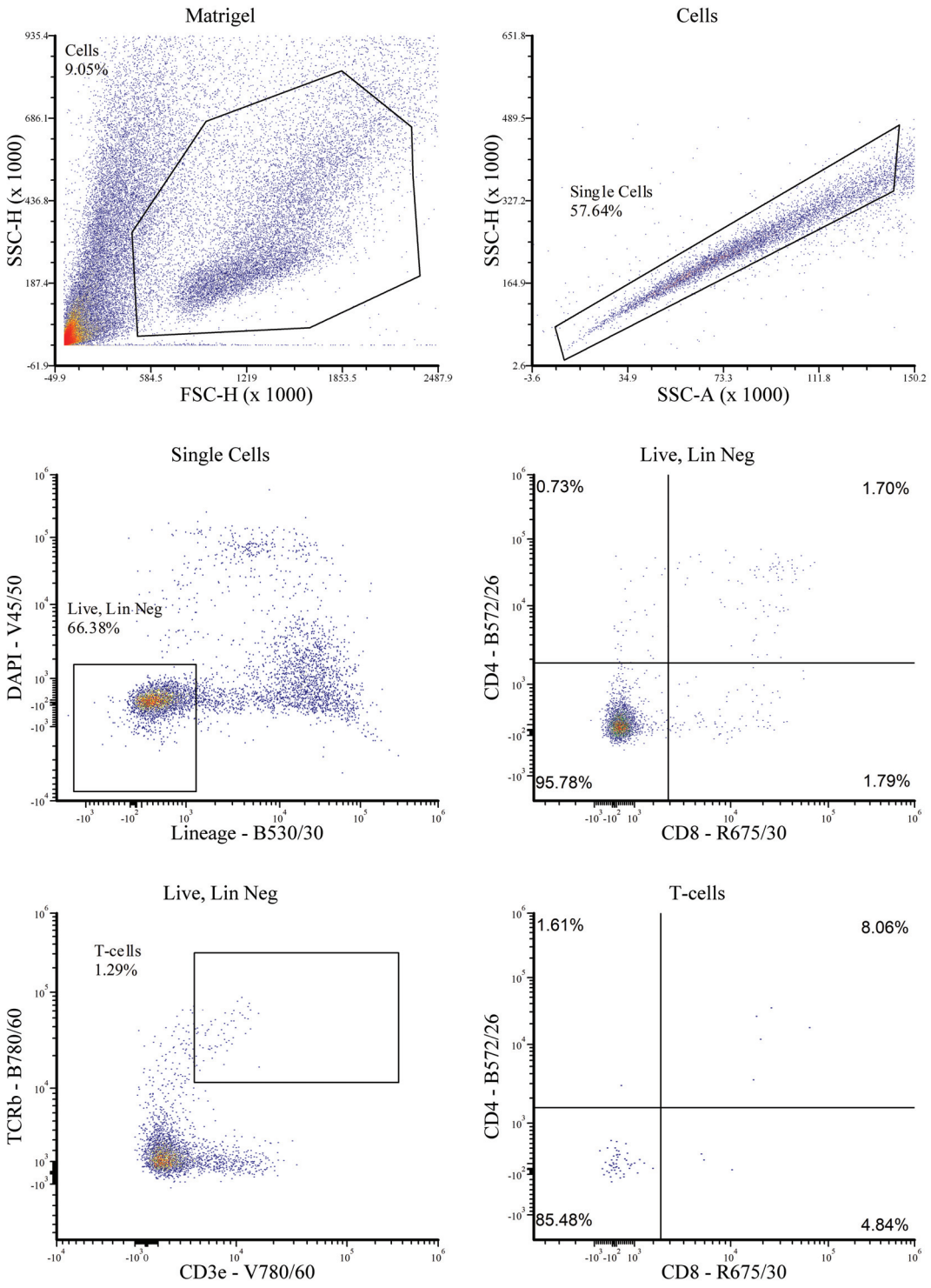

Figure C4.21: iTEC Functionality Polymer Array Representative Plots - Matrigel

Flow cytometric profile of a representative replicate in the iTEC Functionality Polymer Array.

Lineage cocktail included: CD11b, CD11c, Gr-1,Nk1.1, B220, EpCAM, Ter119.

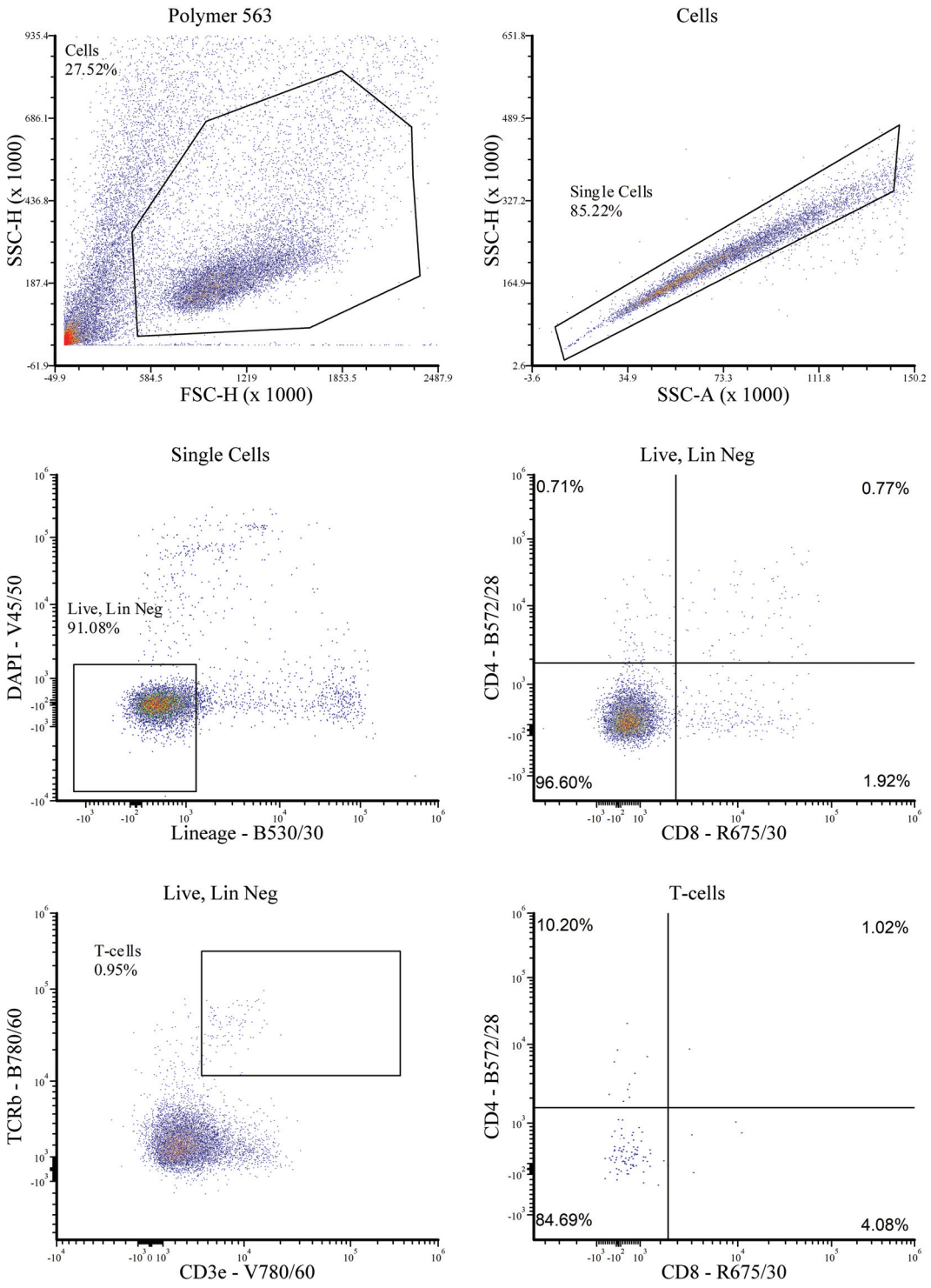

Figure C4.22: iTEC Functionality Polymer Array Representative Plots - Polymer 563

Flow cytometric profile of a representative replicate in the iTEC Functionality Polymer Array. Lineage cocktail included: CD11b, CD11c, Gr-1,Nk1.1, B220, EpCAM, Ter119.

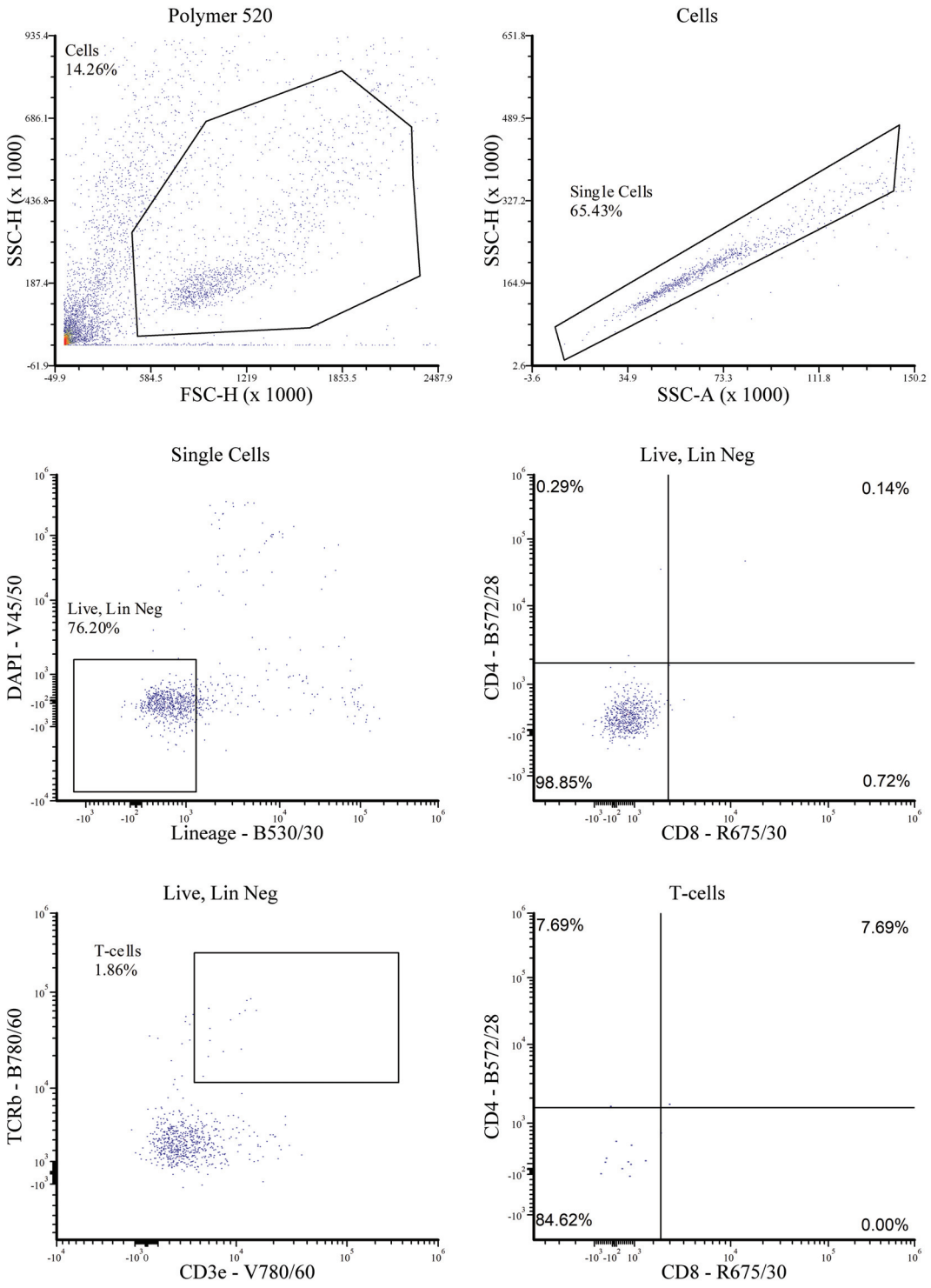

Figure C4.23: iTEC Functionality Polymer Array Representative Plots - Polymer 520

Flow cytometric profile of a representative replicate in the iTEC Functionality Polymer Array. Lineage cocktail included: CD11b, CD11c, Gr-1,Nk1.1, B220, EpCAM, Ter119.

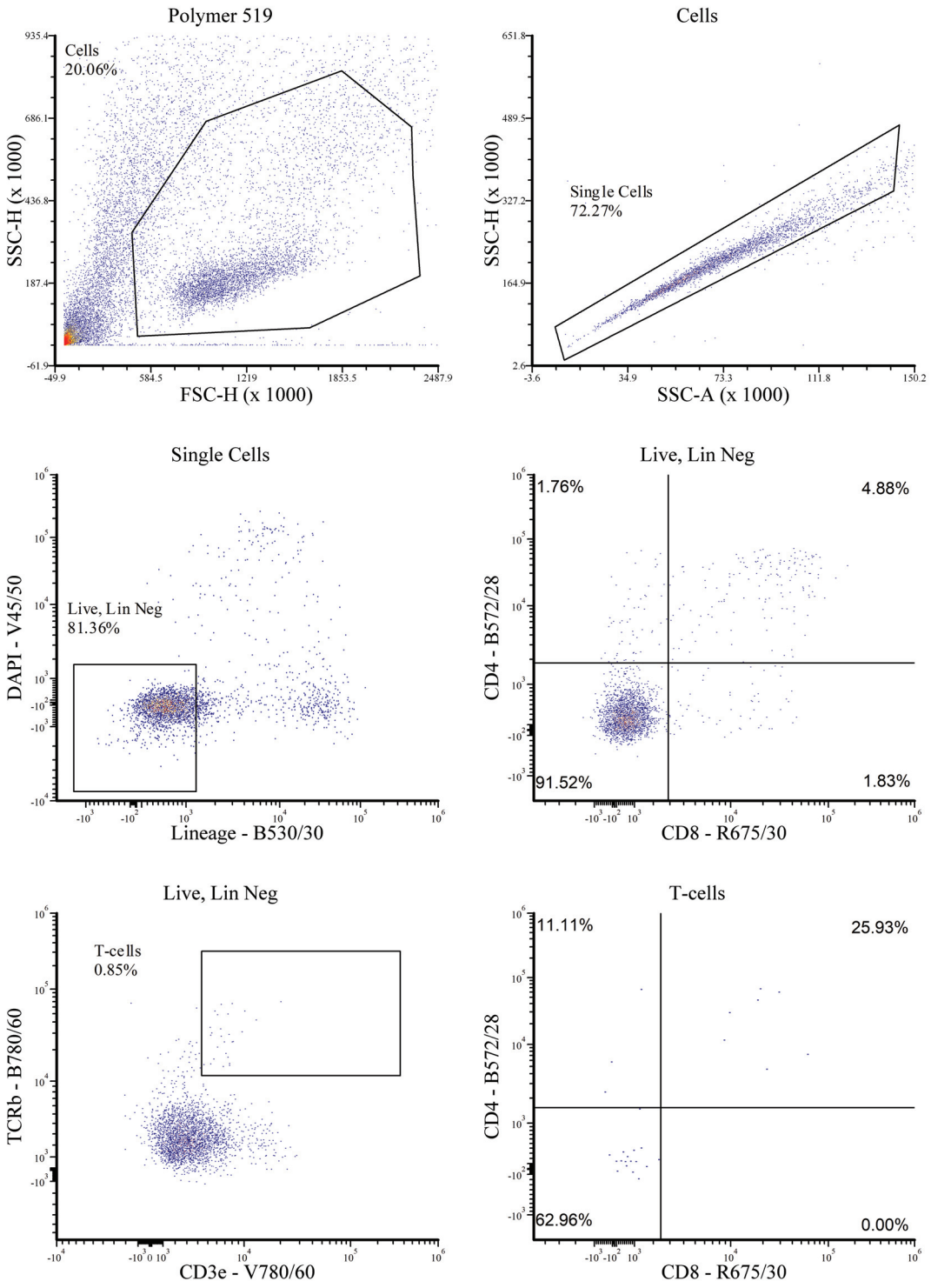

Figure C4.24: iTEC Functionality Polymer Array Representative Plots - Polymer 519

Flow cytometric profile of a representative replicate in the iTEC Functionality Polymer Array. Lineage cocktail included: CD11b, CD11c, Gr-1,Nk1.1, B220, EpCAM, Ter119.

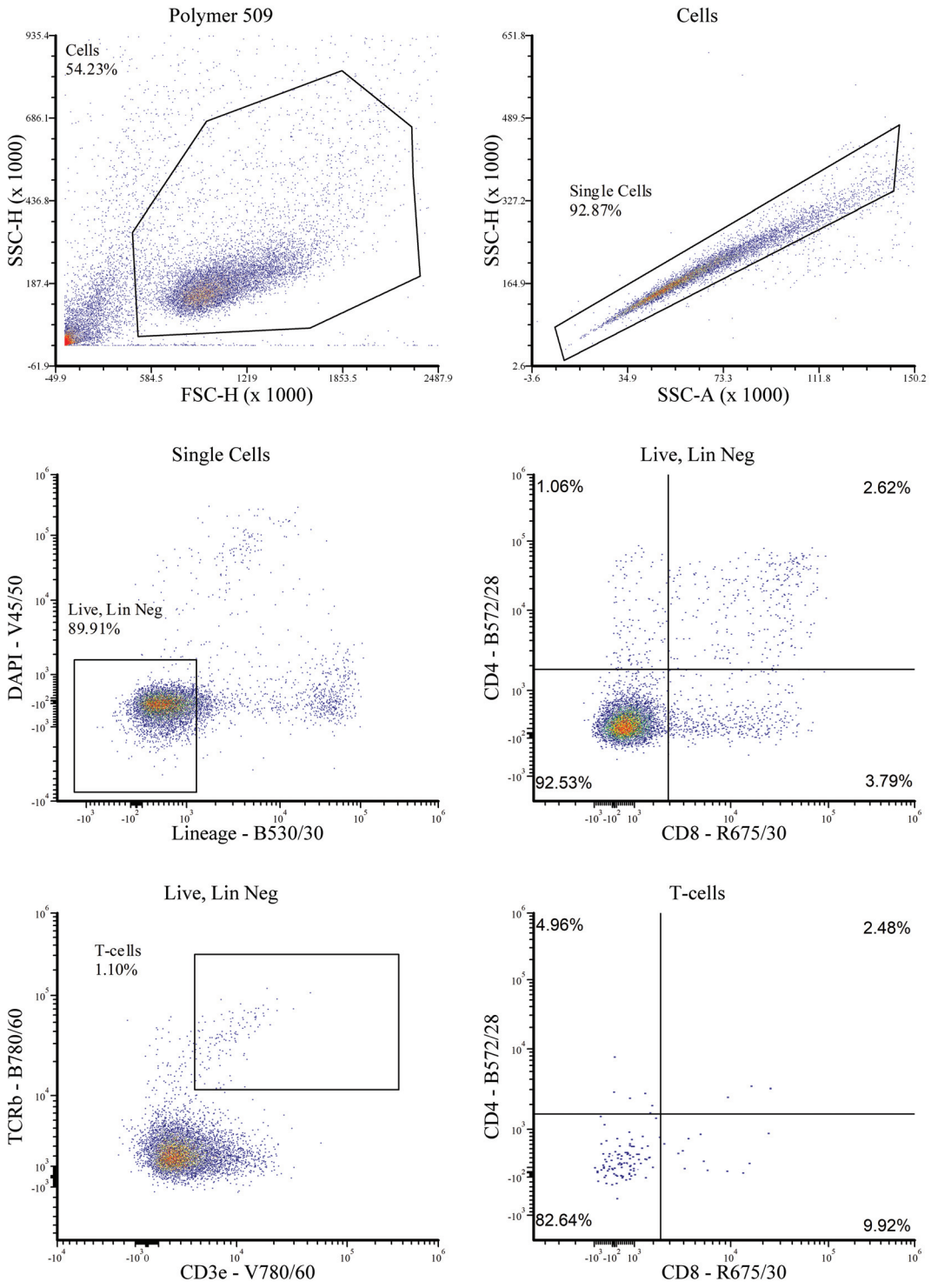

Figure C4.25: iTEC Functionality Polymer Array Representative Plots - Polymer 509

Flow cytometric profile of a representative replicate in the iTEC Functionality Polymer Array. Lineage cocktail included: CD11b, CD11c, Gr-1,Nk1.1, B220, EpCAM, Ter119.

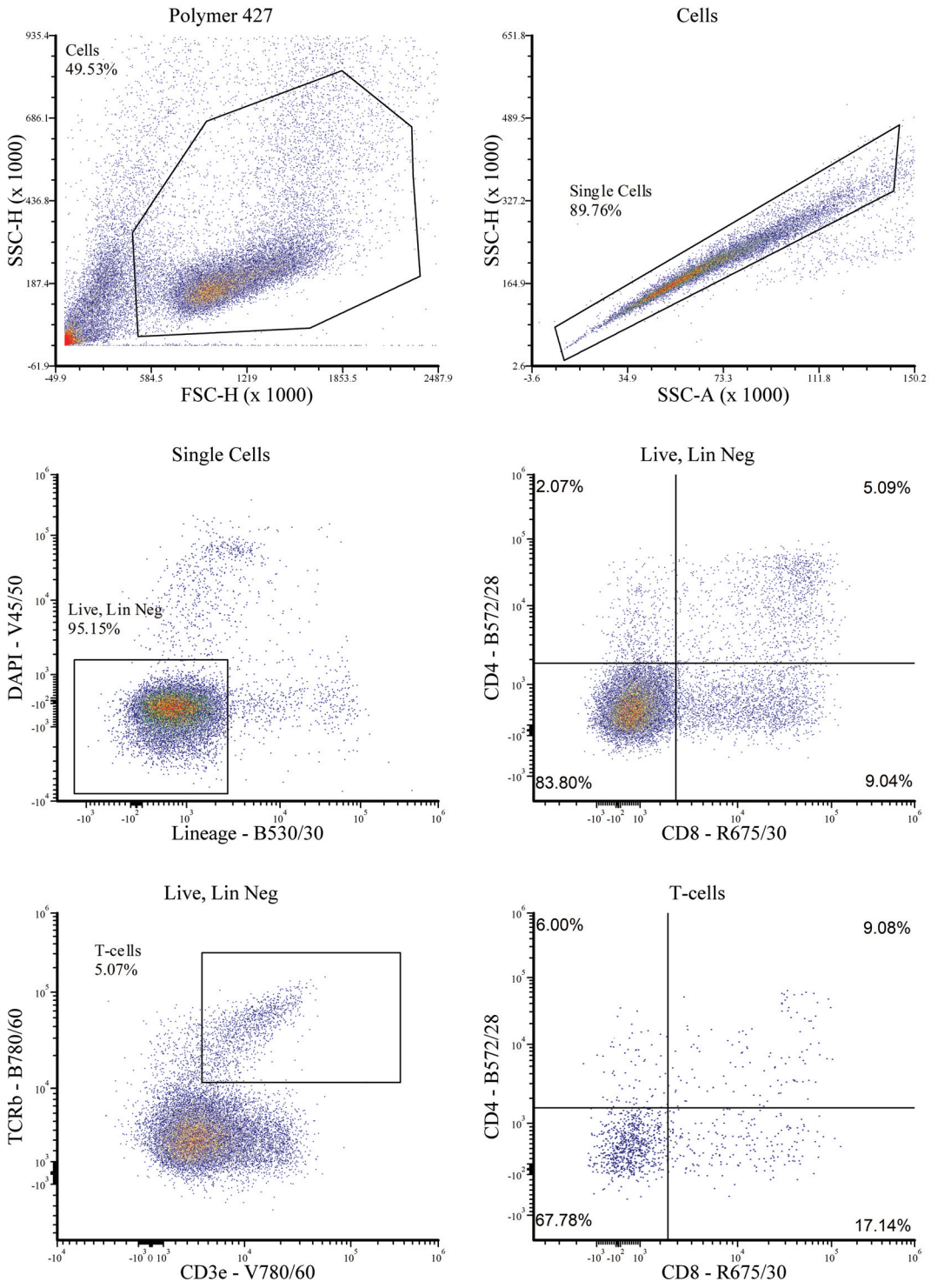

Figure C4.26: iTEC Functionality Polymer Array Representative Plots - Polymer 427

Flow cytometric profile of a representative replicate in the iTEC Functionality Polymer Array. Lineage cocktail included: CD11b, CD11c, Gr-1,Nk1.1, B220, EpCAM, Ter119.

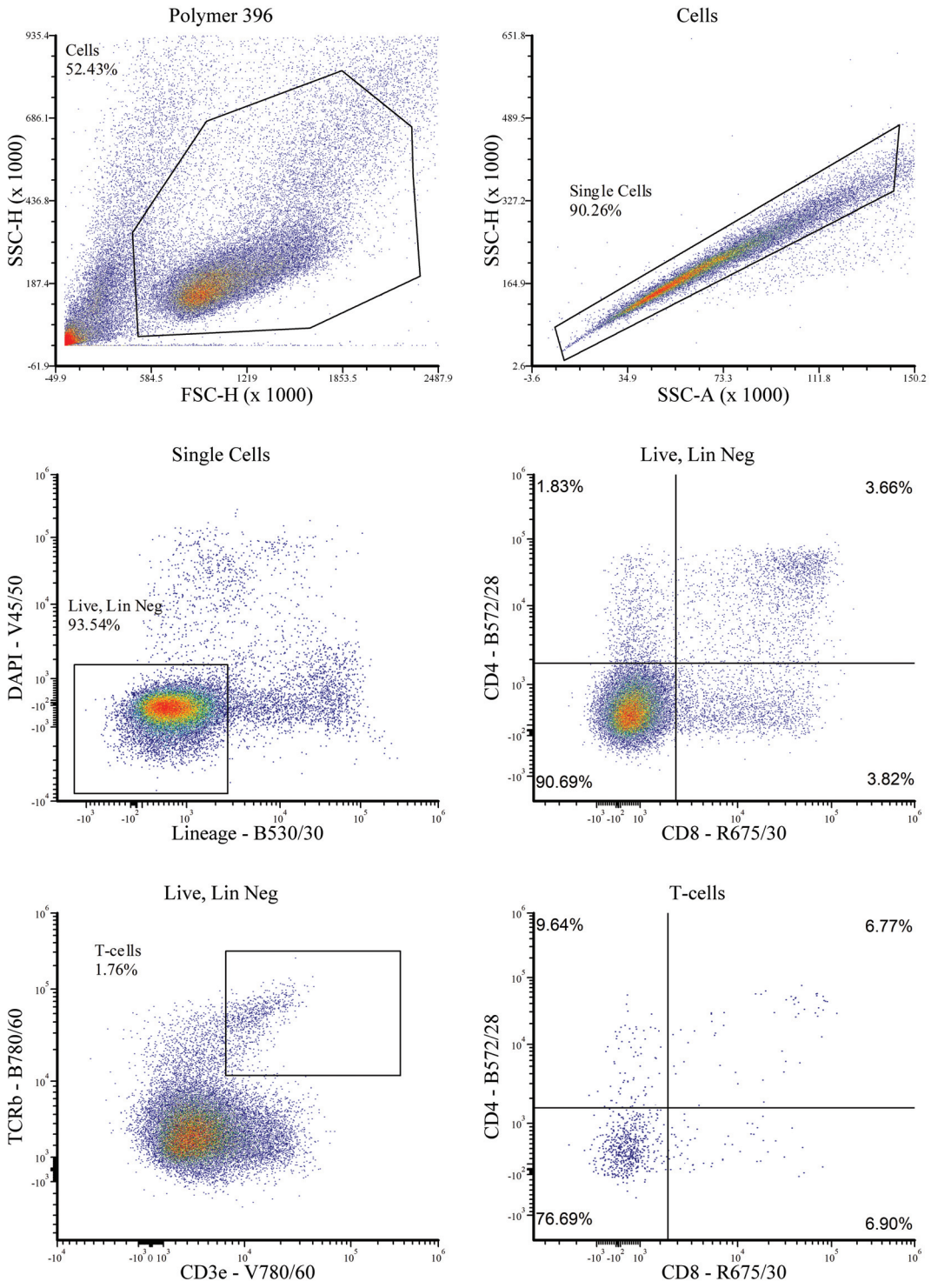

Figure C4.27: iTEC Functionality Polymer Array Representative Plots - Polymer 396

Flow cytometric profile of a representative replicate in the iTEC Functionality Polymer Array. Lineage cocktail included: CD11b, CD11c, Gr-1,Nk1.1, B220, EpCAM, Ter119.

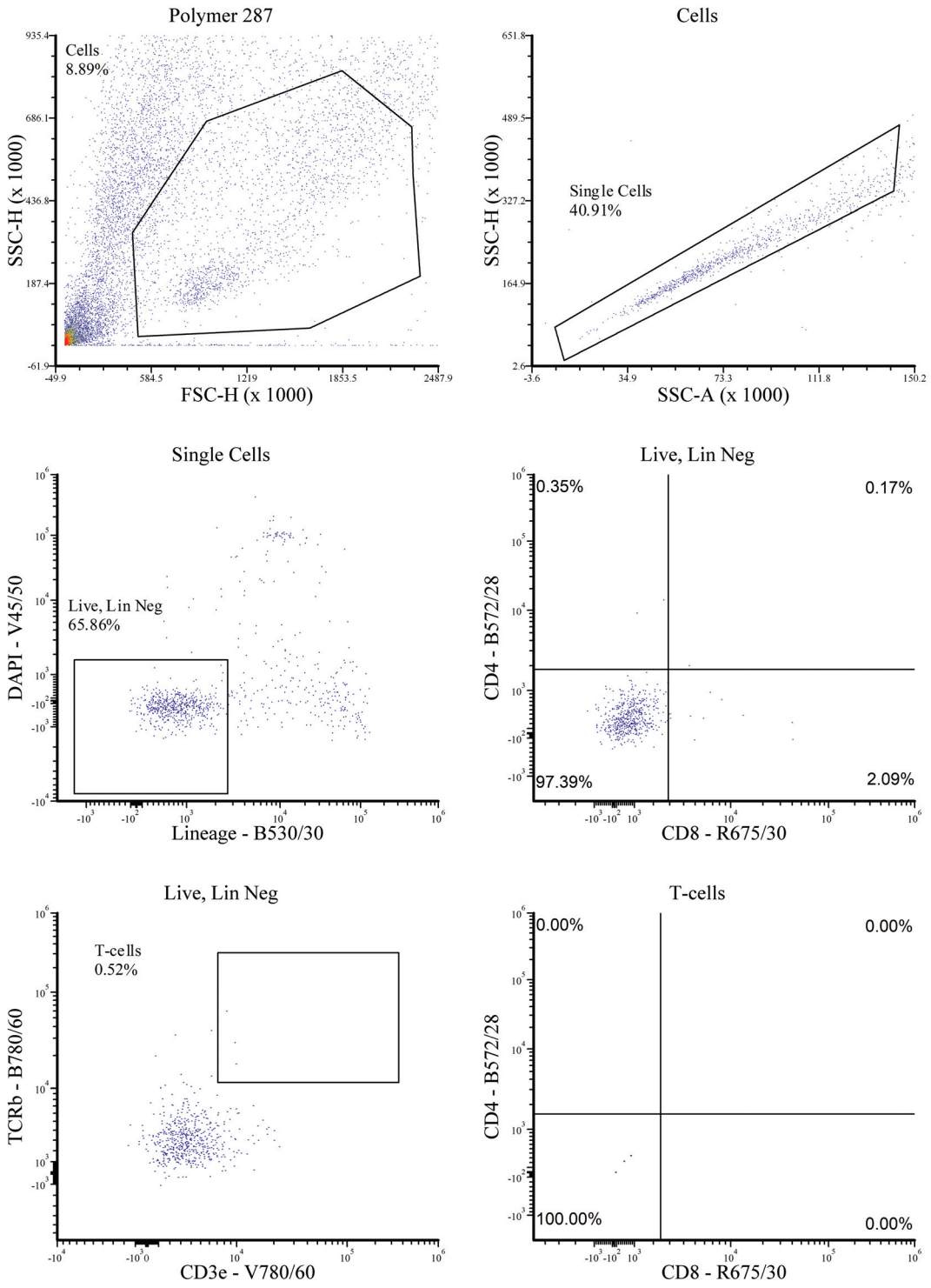

Figure C4.28: iTEC Functionality Polymer Array Representative Plots - Polymer 287

Flow cytometric profile of a representative replicate in the iTEC Functionality Polymer Array. Lineage cocktail included: CD11b, CD11c, Gr-1,Nk1.1, B220, EpCAM, Ter119.

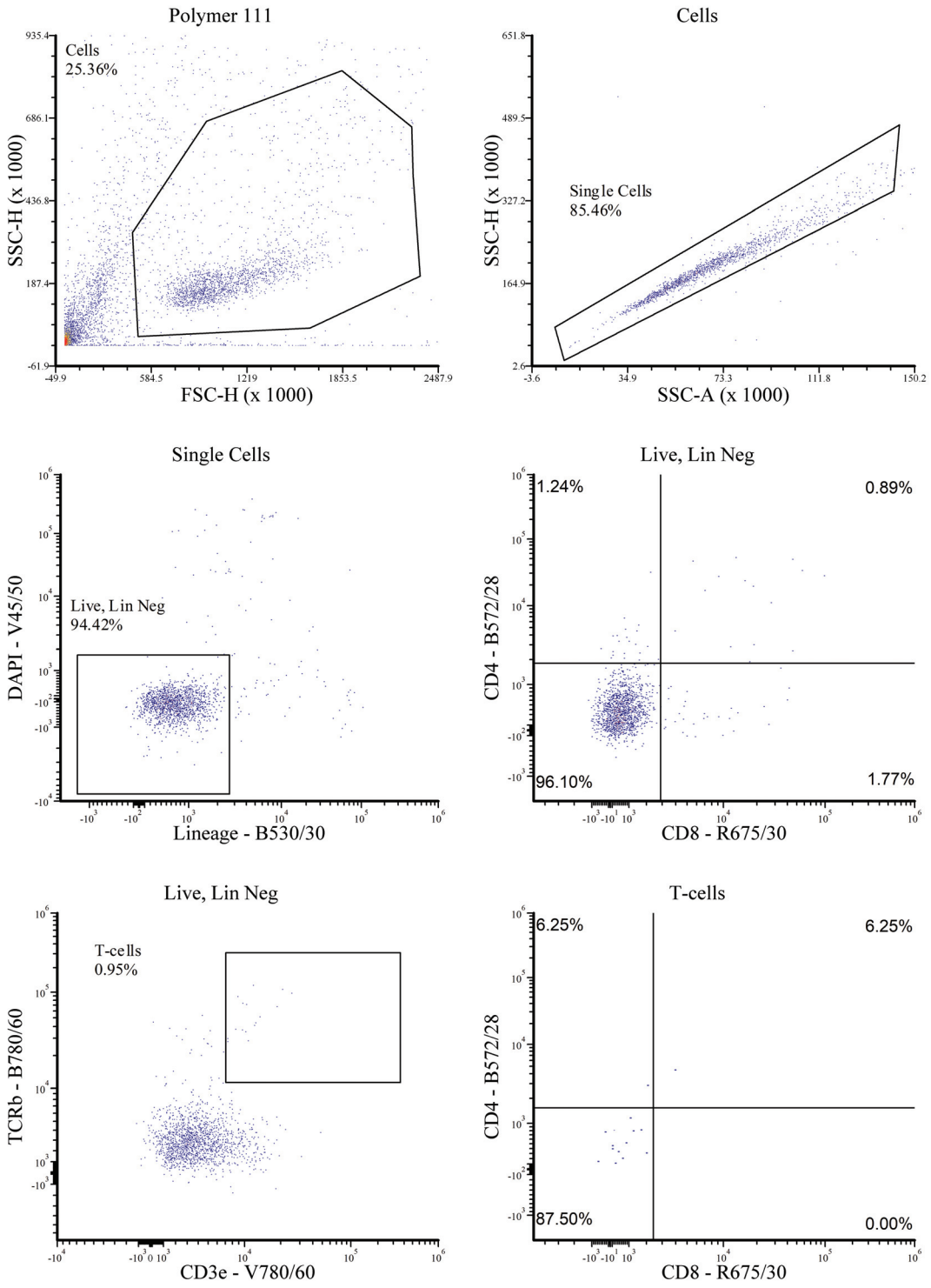

Figure C4.29: iTEC Functionality Polymer Array Representative Plots - Polymer 111

Flow cytometric profile of a representative replicate in the iTEC Functionality Polymer Array. Lineage cocktail included: CD11b, CD11c, Gr-1,Nk1.1, B220, EpCAM, Ter119.

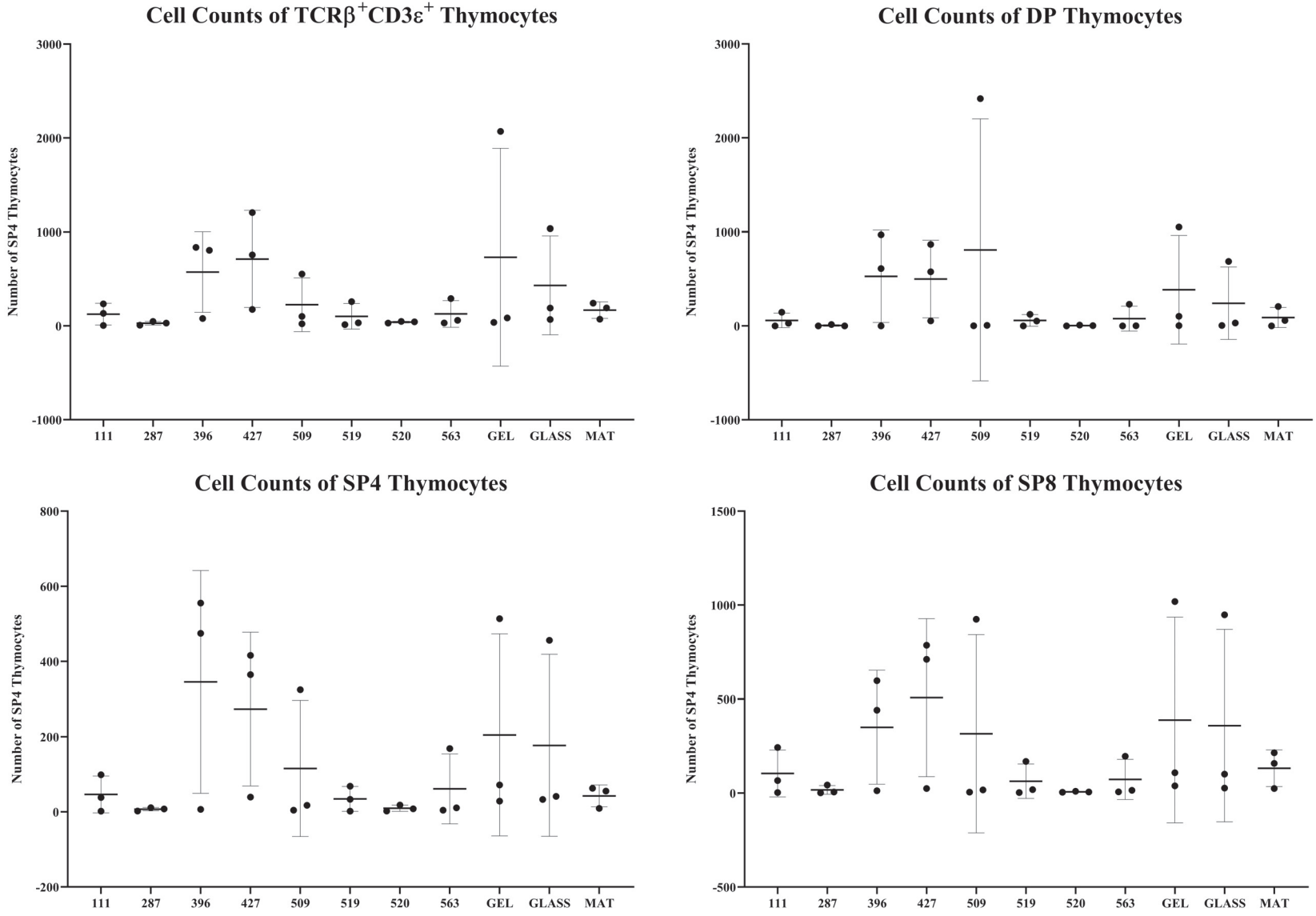

Figure C4.30: Candidate Polymers Did Not Significantly Affect iTEC Mediated T-cell Differentiation

Graphs depict the absolute cell numbers of the TCRβ^{+}CD3ε^{+} thymocyte subsets in the iTEC Functionality Polymer Array. Each data point is the mean of three technical replicates.

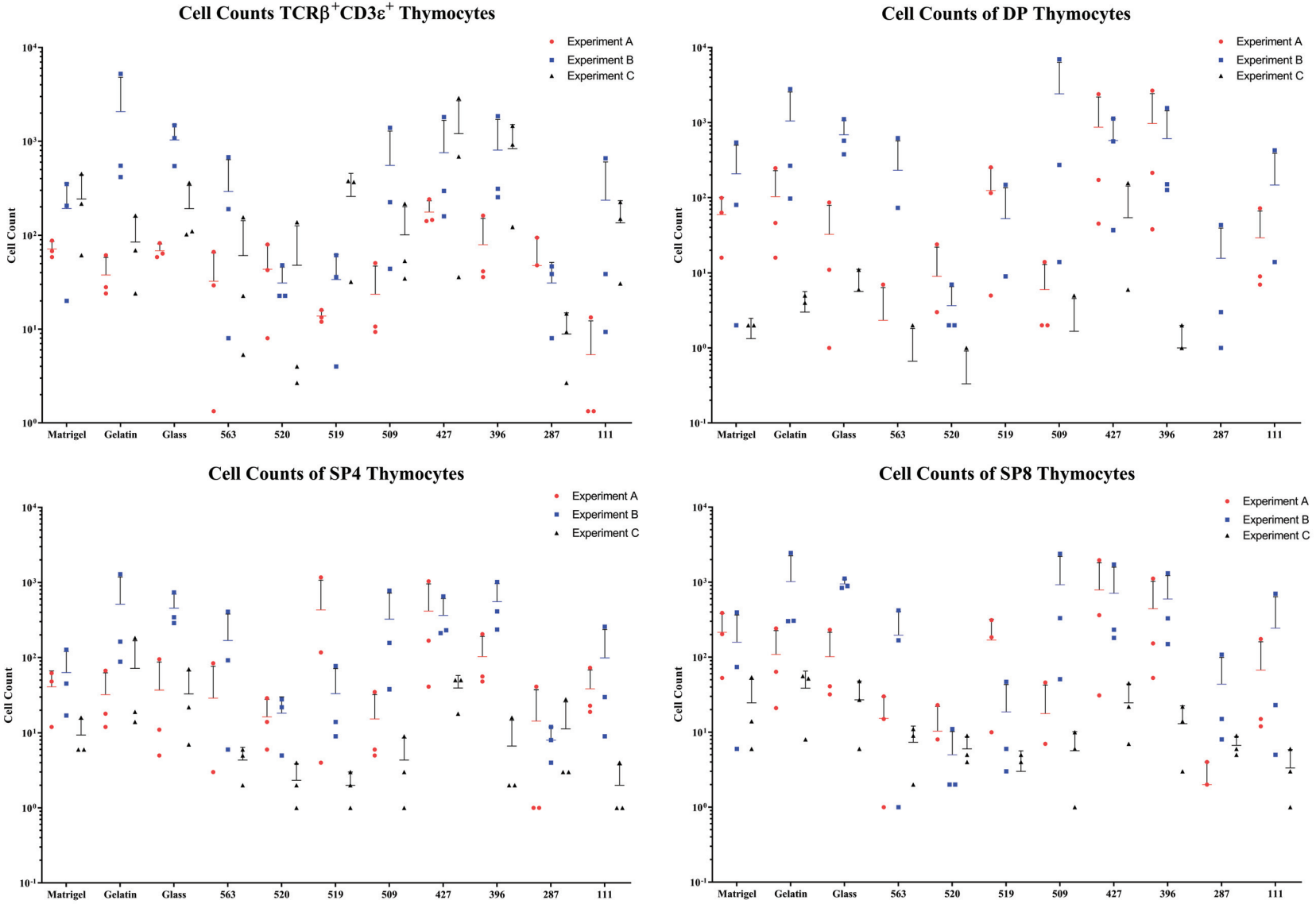

Figure C4.31: All Cell Counts in all Technical Replicates and Independent Experiments

Graphs depict the absolute cell numbers of the TCRβ^{+}CD3ε^{+} thymocyte subsets in every replicate of the iTEC Functionality Polymer Array. Note that this data was variable and necessitated using a logarithmic scale. Experiment A is represented as a red circle, B as a blue square and C as a black triangle.

Table C4.4: Mean Total Thymocyte Counts from iTEC Functionality Polymer Array.
Table shows the mean counts of each thymocyte subset found in each polymer condition.

Polymer	*T-cells*	*SP4*	*DP*	*SP8*	*DN*
Matrigel	168.7	42.56	89.56	132.7	4481
Glass	432	176.9	241.7	359.1	11109
0.1% gelatin	731.1	204.7	385.6	388.8	8306
563	128.3	61.22	78	73.11	5345
520	40.89	9.667	4.333	7.111	3800
519	102.1	34.56	58.89	63.67	4160
509	226.2	115.6	808.7	316	6783
427	712.9	273.3	499.9	507.6	15749
396	574.4	345.6	528	350.6	17107
287	29.19	7.222	5.222	17.44	1917
111	125.3	46.44	58.78	104.8	5114

Table C4.5: Thymocyte Counts from iTEC Functionality Polymer Array Experiment A. Table shows the mean counts of each thymocyte subset found in each polymer condition in Experiment A.

Polymer	*T-cells*	*SP4*	*DP*	*SP8*	*DN*
Matrigel	69	56	16	389	18404
Matrigel	202.6666666	62	99	203	3720
Matrigel	408	48	63	53	4648
0.1% gelatin	107	7	16	64	1061
0.1% gelatin	103	67	247	242	3770
0.1% gelatin	331	12	46	21	1435
Glass	88	18	1	41	5913
Glass	175	11	11	32	7187
Glass	25	95	86	232	8816
563	120	29	7	30	6452
563	5	0	0	1	4131
563	27	3	0	15	1791
520	5	5	3	8	911
520	27	14	24	23	24349
520	139	6	0	0	4477
519	32	84	253	313	8989
519	468	117	115	185	16763
519	408	4	5	10	6018
509	36	12	2	7	4232
509	167	35	14	46	15907
509	33	6	2	0	2453
427	36	41	45	31	5070
427	671	168	172	363	37508
427	3420	1039	2390	1966	46958
396	1527	1171	2661	1118	37261
396	120	48	38	53	13025
396	1019	205	214	153	18314
287	15	5	0	4	6279
287	3	1	0	2	2780
287	11	1	0	0	2255
111	31	73	72	175	19143
111	143	19	9	15	9276
111	200	23	7	12	3508

Table C4.6: Thymocyte Counts from iTEC Functionality Polymer Array Experiment B. Table shows the mean counts of each thymocyte subset found in each polymer condition in Experiment B.

Polymer	*T-cells*	*SP4*	*DP*	*SP8*	*DN*
Matrigel	104	45	80	74	4908
Matrigel	192	127	542	395	5320
Matrigel	11	17	2	6	2176
0.1% gelatin	503	345	377	887	34209
0.1% gelatin	757	736	1111	839	26096
0.1% gelatin	313	288	572	1120	15363
Glass	381	88	97	306	16179
Glass	2419	1290	2789	2447	37691
Glass	179	163	266	303	10284
563	32	92	73	168	10078
563	105	408	620	421	19869
563	379	6	0	1	4292
520	1	5	2	2	765
520	17	22	2	2	762
520	36	28	7	11	2326
519	15	9	0	6	646
519	1	77	148	47	3137
519	19	14	9	3	1466
509	9	157	273	332	10583
509	139	38	14	51	8563
509	32	779	6968	2391	17861
427	789	651	1131	1720	19420
427	1761	231	37	233	14869
427	163	212	562	181	12279
396	284	1018	1559	1313	39232
396	860	236	126	329	26739
396	135	412	151	150	17638
287	168	4	1	8	555
287	5	8	43	108	1186
287	43	12	3	15	1968
111	16	258	427	703	9997
111	493	30	14	23	1621
111	4	9	0	5	1526

Table C4.7: Thymocyte Counts from iTEC Functionality Polymer Array Experiment C. Table shows the mean counts of each thymocyte subset found in each polymer condition in Experiment C.

Polymer	*T-cells*	*SP4*	*DP*	*SP8*	*DN*
Matrigel	91	45	80	74	4908
Matrigel	78	127	542	395	5320
Matrigel	55	17	2	6	2176
0.1% gelatin	48	345	377	887	34209
0.1% gelatin	47	736	1111	839	26096
0.1% gelatin	81	288	572	1120	15363
Glass	28	88	97	306	16179
Glass	24	1290	2789	2447	37691
Glass	63	163	266	303	10284
563	53	92	73	168	10078
563	25	408	620	421	19869
563	8	6	0	1	4292
520	79	5	2	2	765
520	8	22	2	2	762
520	51	28	7	11	2326
519	12	9	0	6	646
519	13	77	148	47	3137
519	15	14	9	3	1466
509	9	157	273	332	10583
509	11	38	14	51	8563
509	35	779	6968	2391	17861
427	129	651	1131	1720	19420
427	141	231	37	233	14869
427	216	212	562	181	12279
396	39	1018	1559	1313	39232
396	35	236	126	329	26739
396	144	412	151	150	17638
287	13	4	1	8	555
287	72	8	43	108	1186
287	27	12	3	15	1968
111	13	258	427	703	9997
111	19	30	14	23	1621
111	0	9	0	5	1526

Table C4.8: Mean Thymocyte Proportions (%) Gated from Live, Lineage$^-$.
Table shows the mean proportion of CD4 and CD8 thymocyte subsets gated from the total T-cells population

Polymer	*SP4*	*DP*	*SP8*	*DN*
Matrigel	1.68	1.66	3.44	93.2
Glass	1.92	1.2	2.69	94.19
0.1% gelatin	2.12	2.20	3.28	92.38
563	0.7	0.49	1.31	97.46
520	1.066	0.16	1.51	97.25
519	1.25	0.92	1.36	96.46
509	0.89	3.1	1.80	94.12
427	2.13	4.09	2.57	91.2
396	1.37	1.51	2.10	95
287	0.88	0.39	2.11	96.61
111	0.89	0.58	1.47	97.06

Table C4.9: Coefficient of Variations (CoV) in the iTEC Functionality Array.
Table shows the CoV associated with each mean calculated between the three independent experiments of the iTEC functionally array

Polymer	*T-cells*	*SP4*	*DP*	*SP8 T-cells*	*Average*
Matrigel	52.09%	68.21%	119.00%	73.66%	*78.24%*
Glass	121.90%	136.80%	159.60%	142.60%	*140.23%*
0.1% gelatin	158.70%	131.20%	150.00%	140.60%	*145.13%*
563	110.80%	152.10%	169.90%	146.50%	*144.83%*
520	21.41%	83.62%	100.90%	39.87%	*61.45%*
519	133.20%	96.03%	106.00%	144.30%	*119.88%*
509	126.60%	156.80%	172.40%	166.80%	*155.65%*
427	72.45%	74.73%	82.60%	82.73%	*78.13%*
396	74.65%	85.73%	92.88%	86.31%	*84.89%*
287	66.49%	63.00%	173.20%	130.90%	*108.40%*
111	92.09%	105.50%	132.40%	118.80%	*112.20%*
Average	*93.67%*	*104.88%*	*132.63%*	*115.73%*	

4.5.C. Results of RT-qPCR on the iTEC Monolayers

4.5.C.I. Justification of Selection of Target Genes

I next set out to observe what effects, if any, resulted from culturing iTEC on selected polymers compared to on gelatin, by measuring changes in expression of key functional genes. Once thymocytes were removed from the underlying iTEC monolayer, two technical replicates were fixed for immunohistochemistry and one was lysed for mRNA preparation (Figure C4.32A). This approach allowed me to gain greater understanding of the iTEC cultured on the polymers, at the cost of increasing the probability that the variation in iTEC across all three technical replicates was not represented in the mRNA analysis. Furthermore, by relying upon a simple, physical method of separating the two cellular components, there was a risk that some remaining thymocytes would contaminate the iTEC mRNA.

To observe whether culturing iTEC on polymers affected gene expression, mRNA collected from each polymer condition was compared to mRNA isolated from 2×10^5 iTEC directly after purification of GFP^+ reprogrammed cells by FACS. This was termed time zero (t_0), since these iTEC were from the same pool as the iTEC seeded onto the polymers.

For a positive control, mRNA was isolated for 50 E13.5 *ex vivo* TEPC (Thymic Epithelial Progenitor Cells) defined as $EpCAM^+PLET1^+$. Note that given the scarcity of TEPC, a small cell population mRNA isolation and amplification method was used (CellsDirect Invitrogen). Whilst being a valid method of collecting mRNA, the increased amplification necessitated by this process is a confounding variable when comparing the gene expression of TEPC to the remaining conditions, which was isolated using methods suitable for larger populations (RNAEasy Invitrogen), so care was taken before making this comparison.

mRNA from Cre only MEFs was isolated as a negative control for the iFoxn1 transgene independently to the iTEC Functionality Polymer Array. Whilst it could be argued that this represents a weak control, the hypothesis that the iFoxn1 transgene reprograms MEFs into iTEC was rigorously tested in Chapter Three and this control is reinforced by previous conclusions. Additionally, one Cre Only MEF mRNA preparation failed, so this condition is only represented with two data points.

For this analysis, the gene panel analysed in Chapter Three was extended to 13 genes, plus housekeepers. The genes were chosen based upon cortical thymic function, with the exception of *Aire* which is an mTEC marker (Lopes *et al*., 2015): Endogenous *Foxn1*, Total *Foxn1*, *Dll4, Il-7* and *Psmb11* were included for the reasons justified in Chapter Three. The genes encoding the chemokines *Ccl25* and *Cxcl12* were included given their role in thymic trafficking and thymocyte immigration (Calderón and Boehm, 2011; Liu *et al*., 2006; Misslitz *et al*., 2004; Schwarz *et al*., 2007; Sultana *et al*., 2012; Zlotoff *et al*., 2010); The genes encoding the cytokines *Kitl* and *Flt3l* were also analysed given the role they play promoting thymocyte proliferation at various stages of thymopoiesis (Kenins *et al*., 2010; Rodewald *et al*., 1995); the Notch ligand *Dll1* was included given its ability to mediate *in vitro* T-cell commitment in the OP9-DLL1 and MS5-hDLL1 systems despite its redundancy in the native thymus (Koch *et al*., 2008; Schmitt and Zúñiga-Pflücker, 2002; Seet *et al*., 2017); Finally, *Ctsl1* and *MHC2Eβ2* (was taken as representative for the expression of the entire MHC2) were measured given their role in peptide processing and presentation for SP4 thymocytes (Takada *et al*., 2017). This analysis was conducted concurrently with the screen described above, which tested the capacity of iTEC to support T cell development when cultured on the polymers in serum-containing medium.

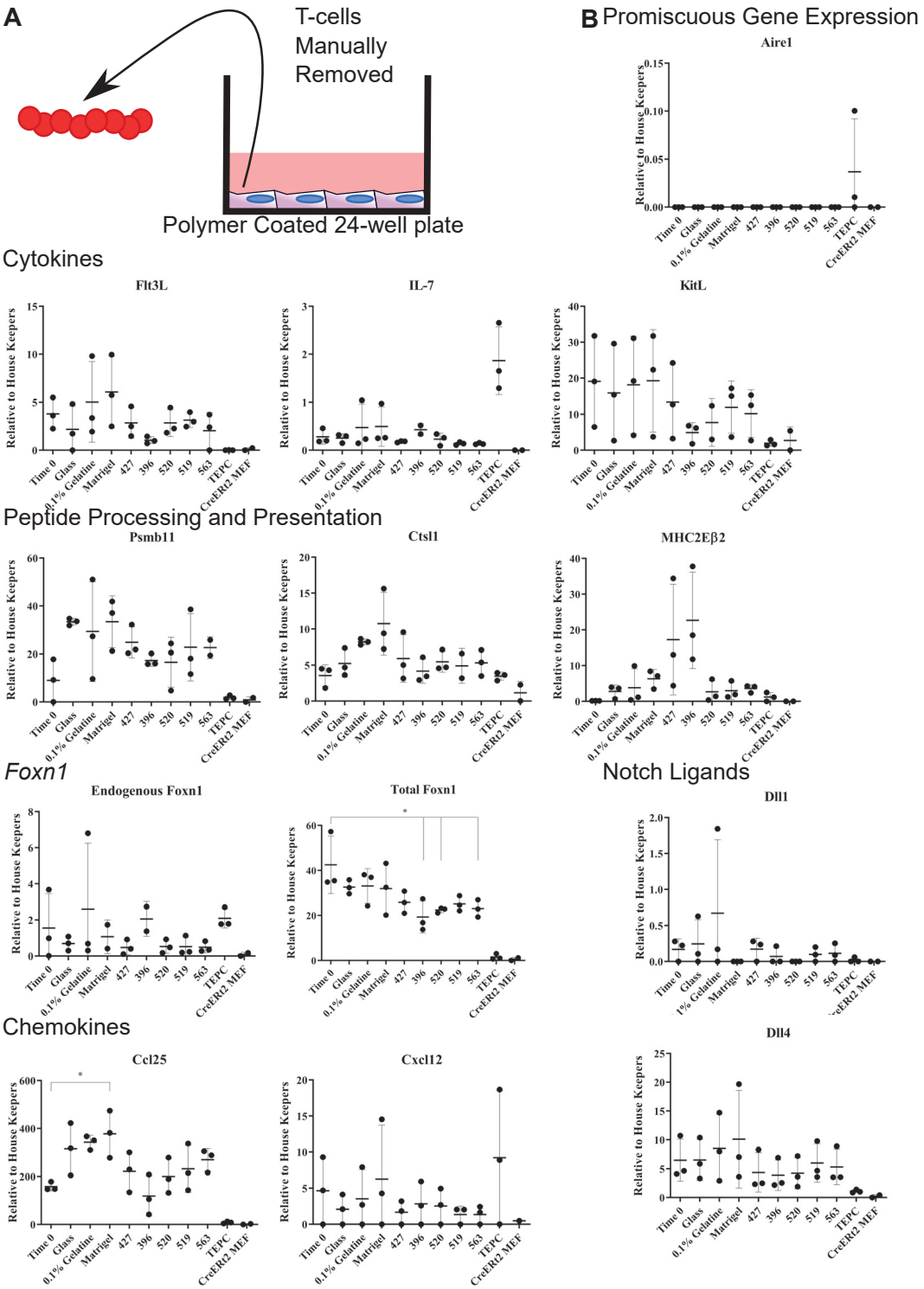

Figure C4.32: Gene Expression Profiles of iTEC Cultured on Polymers

A. Schematic of post-co-culture analysis. Haematopoietic cells were removed using tituration leaving the iTEC adhered to the well. In each biological replicate, one well was used for RT-qPCR and two were taken for immunohistochemistry. **B**. Gene expression profile of iTEC after 14 day co-culture. Ct values between 25 and 36 were accepted for iTEC mRNA while Ct values between 16 and 24 were observed for TEPC and MEF . Some conditions failed so Endogenous *Foxn1*: Matrigel and Polymer 396 have two data points and *Cxcl12*: CreERt2 MEF only has one. Each gene was analysed for significant difference between means. * denotes significance.

4.5.C.II. Results

The expression levels for each of the genes tested are shown in Figure C4.32B and were compared using one-way ANOVA. Normality was tested for using the Shapiro-Wilk test and all data sets were found to be normally distributed, except for *Dll4*, *Dll1*, Endogenous *Foxn1*, *Aire*, *Il7*, *MHC2Eβ2*. The Brown-Forsythe test found all data had homogeneous variances except for *Cxcl12* and these data were analysed using a Kruskal-Wallis test and Brown-Forsythe corrected ANOVAs, respectively.

In most conditions there was no significant difference between the gene expression profiles of iTEC cultured on the various polymers. The null hypothesis that polymers did not affect gene expression over time, which was tested by comparison with all post-co-culture conditions with t_0 iTEC, and across polymer groups was accepted. However, it is worth highlighting the exceptions. Firstly, comparison between t_0 and iTEC cultured on polymer 396, 520 and 563 showed a significant reduction in total *Foxn1* expression over time. Whether this is a biological effect and iTEC are epigenetically downregulating transgenic *Foxn1* or this is a result of incomplete separation of iTEC from thymocytes and dilution of iTEC mRNA is unclear. However, this is evidence that an initial assumption of this chapter, that culture conditions will not affect iTEC expression of *Foxn1* because it is genetically enforced, may be untrue.

Secondly, iTEC cultured on Matrigel had significantly greater expression of *Ccl25* than on polymer 396 and at t_0. Given the role of CCL25 in thymic homing, a redundant process in this system, the biological link between Matrigel, iTEC and CCL25 is not obvious. However, the fact that this was significant and others not, does highlight that other conditions and genes contain much greater variation and this lack of precision maybe responsible for insignificance.

MHC2Eβ2 was greatly upregulated in iTEC cultured on polymers 427 and 396 compared to other conditions. Although this effect did not reach statistical significance, as these data were variable and did not follow a normal distribution, the result warrants further investigation. Several conclusions can be drawn from the non-significant differences between data. All

polymers maintained a TEC-like profile retaining expression of most key genes through the co-culture, except for expression of *Il-7* that remained poorly expressed compared to E13.5 TEPC. There was no detectable *Aire* expression in any iTEC condition, providing substantial evidence against Objective C. However, this warranted further investigation in case *Aire* expressing iTEC were too uncommon to be identified using analysis of bulk mRNA.

4.5.D. Culture on the Selected Polymers Did Not Induce a Medullary Phenotype in iTEC

4.5.D.I. Results

The remaining two, fixed wells of iTEC stained for markers of mTEC. This was to test Objective C. iTEC were stained for expression of AIRE, the major regulator of promiscuous gene expression in mTEC; cytokeratin 14 (K14), which marks mTEC from early organogenesis onwards and ulex europaeus agglutinin I (UEA1), which binds glycoproteins and/or glycolipids on the surface of mTEC but not cTEC (Klug *et al*., 2002; Kyewski and Peterson, 2010). Each polymer condition had a pair of wells, one was used for the experimental stain and the other an isotype control (Figure C4.33A). Both were imaged and the true staining was calculated by subtracting the isotype control staining profile from the biological staining sample (Figure C4.33B). The staining pattern of AIRE is very specific, so a qualitative assay was used, since designing an automatic pipeline to segment such staining would be challenging and prone to error (Figure C4.33C).

Only a few iTEC displayed the K14 and UEA1 double staining pattern indicative of mTEC, and there was no evidence of AIRE expression, in agreement with previous mRNA analysis (Figures C4.32 and C4.33B). Despite the qualitative nature of the readout, it was concluded that polymers did not efficiently stimulate iTEC differentiation into mTEC.

Therefore, with respect to the aims of this chapter, there was evidence that iTEC downregulated transgenic *Foxn1* expression during culture on the polymers. This may be significant, given the clinical aim of iTEC to be used as a source of tissue for transplantation, if iTEC were to downregulate expression of key FOXN1 targets it would likely compromise the function of transplanted material after extended periods. We also cannot conclude that

polymers had a significant effect on the ability of iTEC to mediate T-cell differentiation but 427, 396 and 509 had promise and warrant further investigation in a more precise experimental design. However, it is not inconsequential to have identified synthetic, defined conditions that supports iTEC functionality and reduced variation (Table C4.9), particularly given the main objective to reduce variation in the system. Finally, there was no evidence that polymers stimulated iTEC to adopt a functional mTEC phenotype with evidence of promiscuous gene expression. I next wanted to design an experiment that would support the mRNA analysis suggesting that culture on polymers 427 and 396 either stimulated iTEC to upregulate *MHC2Eβ2* or selected cells with greater expression.

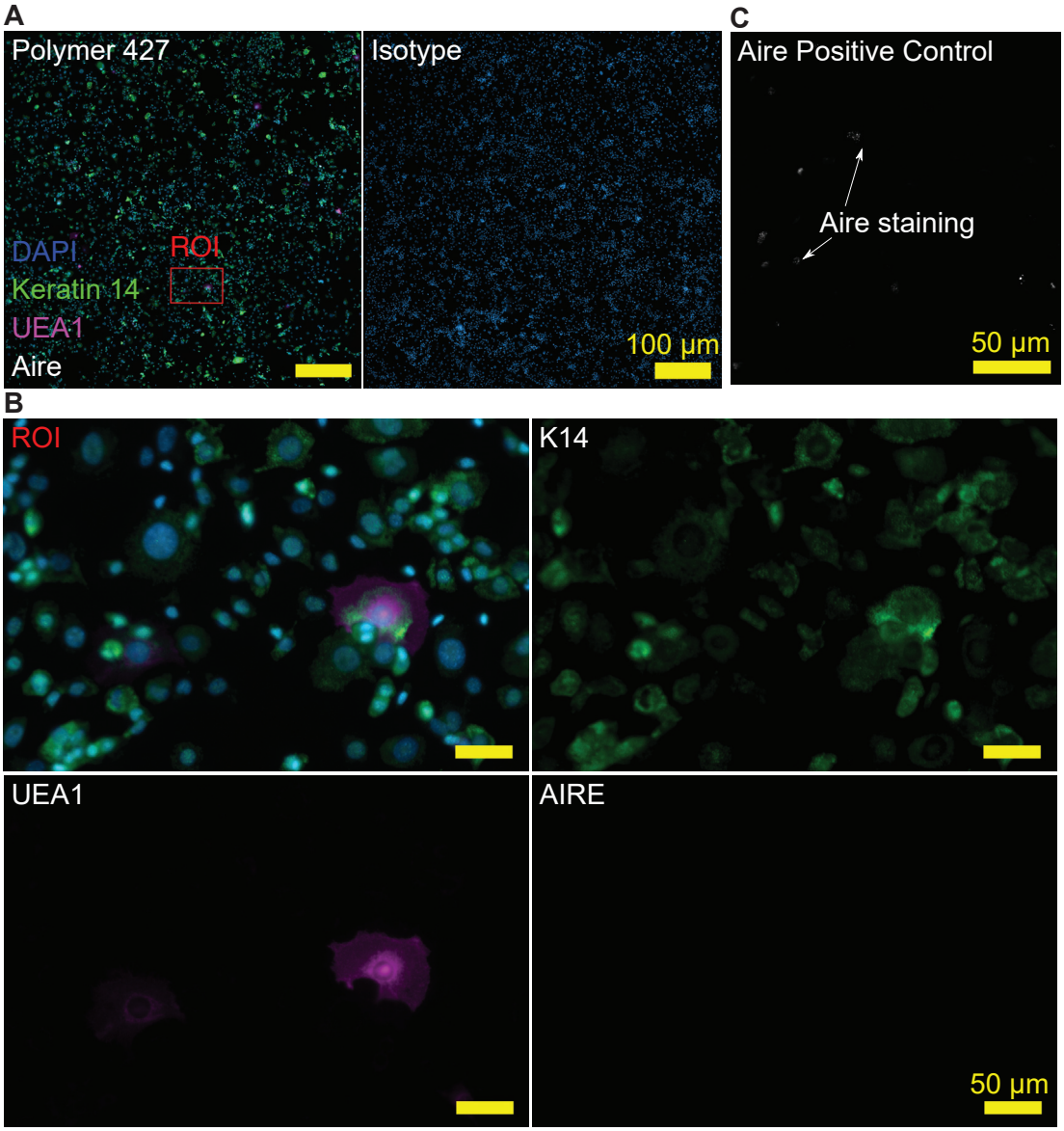

Figure C4.33: Polymers Did Not Promote iTEC Medullary Differentiation

A. After the co-culture hematopoietic cells were removed using tituration and iTEC were stained for key markers of medullary TEC: K14, UEA1 and Aire. In each independent experiment a control, isotype well *(right)* was performed concurrently to the experimental well *(left)*. The image of polymer 427 was representative of all conditions. **B**. ROI showing stained iTEC in greater detail. **C**. Positive control stains of Aire in four week postnatal thymus.

4.6. iTEC cultured on Polymer 427 Did not Upregulate MHC2

4.6.A. Method

To further investigate the result that iTEC showed greater expression of MHC2 when cultured on polymers 396 and 427 (Figure C4.32B) than on gelatin, albeit not at statistical significance, a 24-well plate was coated with polymer 427, 0.1% gelatin or Matrigel in triplicate. This was designed to be smaller in scale as using a more limited selection of conditions allowed more intensive analysis of each. Polymer 427 was selected over polymer 396 because both conditions produced the described upregulation of MHC2 but polymer 427 performed more robustly during the iTEC functionality polymer array. iTEC were seeded with adult ETPs, in the same co-culture procedure described in the iTEC Functionality Polymer Array. After 14-days the thymocytes were removed by trituration and the underlying iTEC monolayer fixed and stained for β5t, MHC2 and with cell mask blue (Molecular Probes) (Figure C4.34). Without β5t and MHC2, iTEC cannot process and present peptides for positive selection in a physiologically relevant fashion (Takada *et al*., 2017).

Given that there was no evidence that iTEC were able to differentiate into $K14^{+}UEA1^{+}AIRE^{+}$ mTEC-like cells, β5t was used in the segmentation strategy to focus on cTEC-like cells. Note that, as depicted in the segmentation strategy, the iTEC monolayer was contaminated with much smaller cells expressing MHC2. Many of these cells were removed by selecting on $\beta5t^{+}$ iTEC. However, this strategy was not completely effective. If polymers 427 and 396 were more conducive to the binding of these cells in the monolayer this effect probably contributed to the upregulation found by RT-qPCR. The nature of these cells was not defined and remains speculative, but they could represent either dendritic cells or iTEC that are differentiating into mTEC-like cells with the characteristic smaller morphology (Hirakawa *et al*., 2018).

Multiple micrographs, 70 per well, were images and segmented to establish the total number of cells, based on the assumption that each cell contained one nucleus. Cell mask blue, which binds brightly to the nucleus of cells and dimly to the cytoplasm, was employed to assist with the automated segmentation. This was found to be effective at segmenting most

cells but performed poorly on unusually large iTEC, which were incorrectly split into segments. This is because large nuclei contained a heterogenous spread of chromatin for the dye to bind too and consequently the varying brightness prevented correct segmentation. To count the number of iTEC from the number of cells, those that expressed β5t to a greater extent than the background were selected on and then the MFI of MHC2 within these cells was quantified.

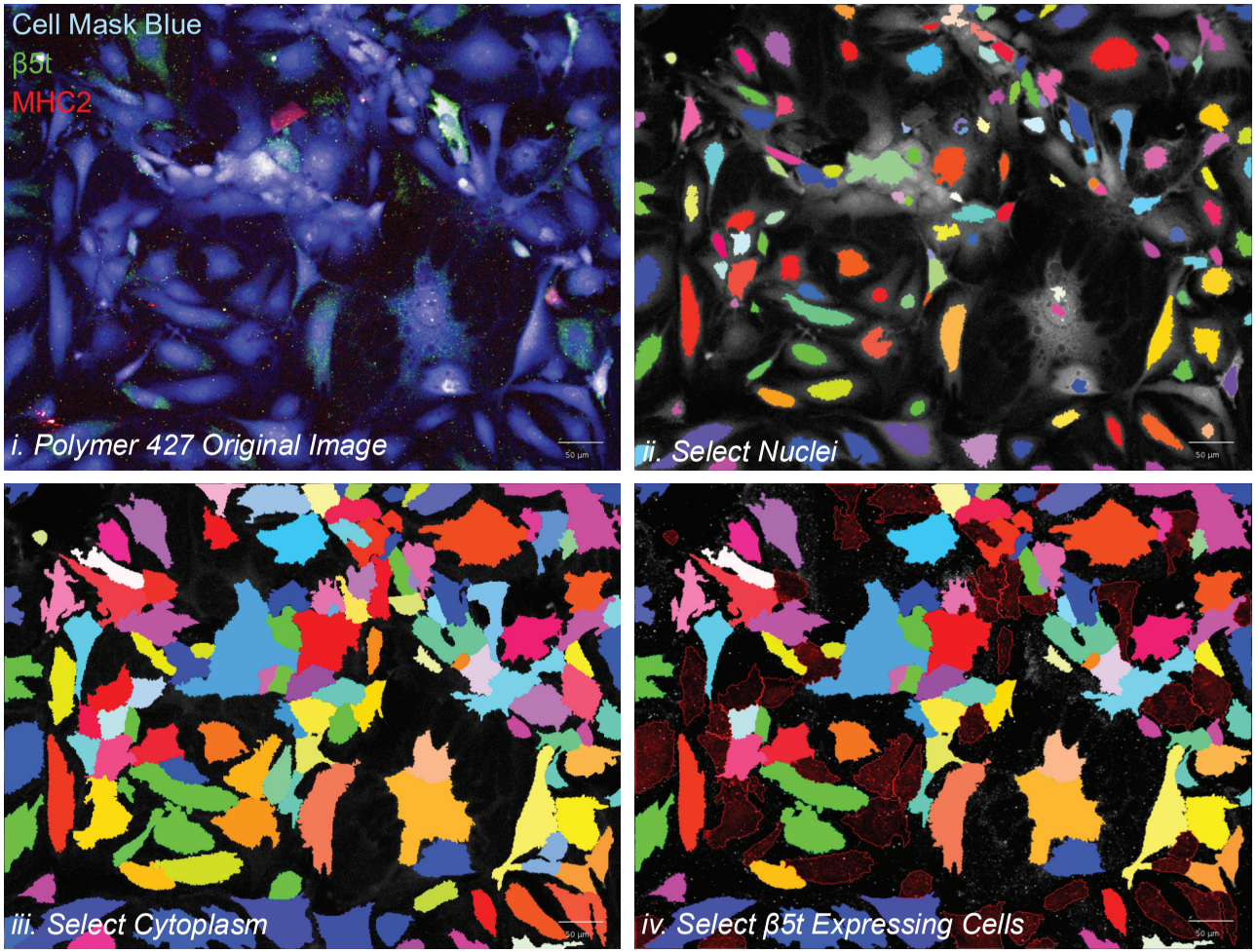

Figure C4.34: Pipeline to Count the Number cTEC-like iTEC and Quantify MHC2 MFI

Pipeline to count the number of iTEC that sucessfully reprogrammed into a β5t^{+}, cortical TEC-like cell and then to calculate the MFI of MHC2 expression. Individual segmented objects are represented in different colours.

4.6.B. Results

The data were analysed using a one-way ANOVA after normality and homogeneity of variance was confirmed. There was a large amount of variation found between biological replicates (Figures C4.35A and B). Following the same syllogism as previous experiments this was probably due to two factors. The first is the biologically differences between iTEC and the second is technical noise from inaccurate cell counting. Again, the latter was normalised by reporting the cell counts in proportion to a control. In this case, the Matrigel condition was used. It could be argued that given the heterogenous nature of Matrigel, this was a poor choice. However, the normalisation was satisfactory. Matrigel was associated with lower CoV than 0.1% gelatin. In the total cells data, Matrigel was associated with a CoV of 30.75% compared to 46.65% in 0.1% Gelatin (Figure C4.35C and D). The normalisation was performed as:

Equation C4.5:

$$Normalised\ Cell\ Count \frac{Cell\ Count}{Cell\ Count\ on\ Matrigel}.$$

Ultimately this reduced the total mean CoV in the total cell count from 44.38% to 15.91% and increased the R^2 associated with the statistical inferences quantifying total cell number from 0.1615 to 0.6045 and total iTEC number from 0.3498 to 0.8644. There was no significant difference in the total number of cells, the total number of iTEC, the percentage of cells that expressed β5t or the MFI of β5t or MHC2 between polymer 427 and 0.1% gelatin. The null hypothesis was accepted: iTEC co-cultured with adult ETPs on polymer 427 had similar levels of MHC2 as those on and 0.1% gelatin. The CoV in the percentage of β5t expressing cells was dramatically larger in the polymer 427 (30.9%) condition, than 0.1% gelatin (6.562%) and Matrigel (4.516%) but this difference was found to be statistically insignificant in the Brown-Forsythe test for equal variation between groups.

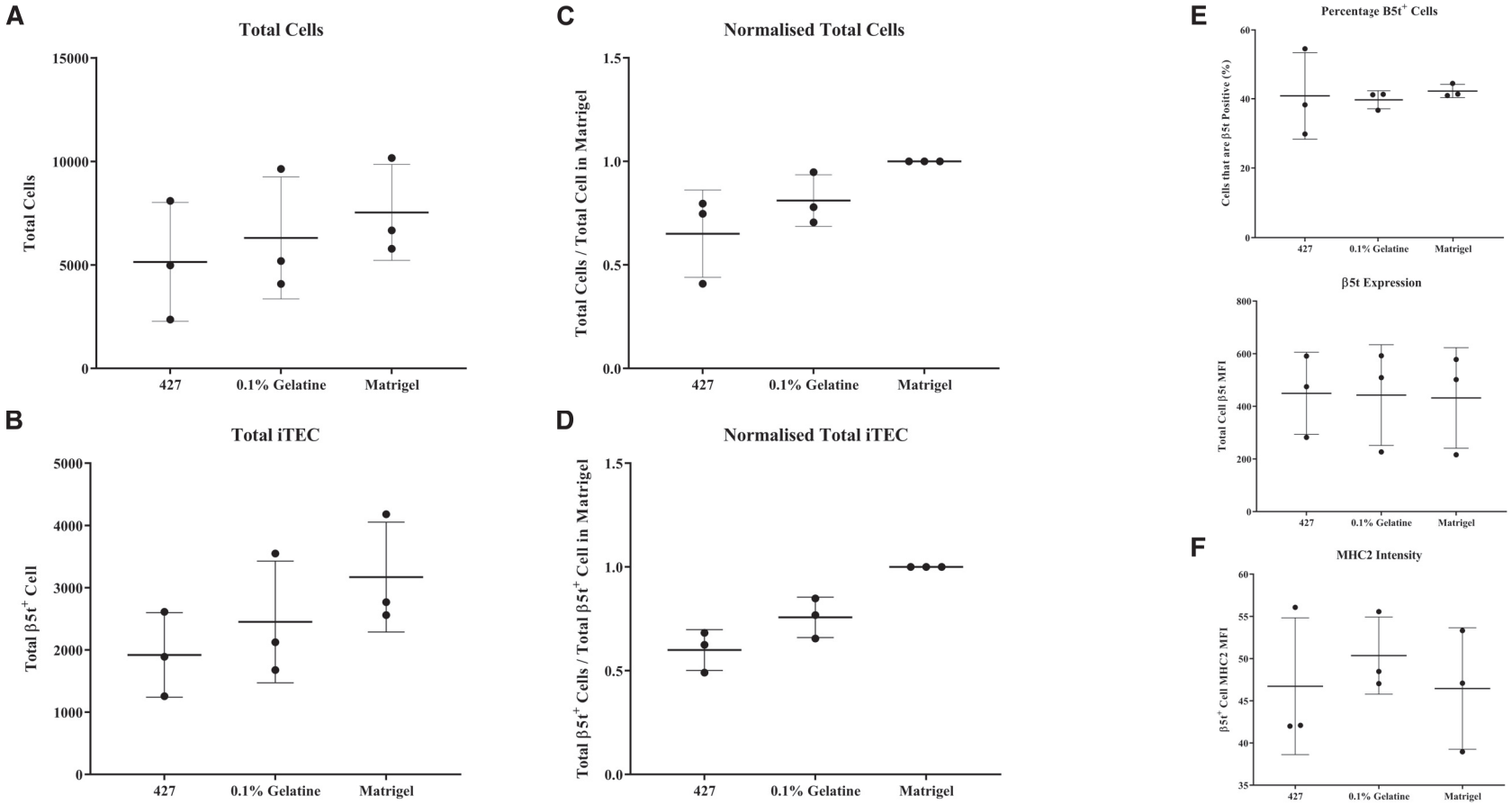

Figure C4.35: Culturing iTEC on Polymer 427 Did Not Affect MHC2 or β5t Expression

A. Total numbers of cells counted. **B**. Total number of cells that express β5t. **C**.Total number of cells normalised to the mean number of cell counted in wells coated with Matrigel. **D**. Total number of β5t expressing cells normalised to the mean number of cell counted in the Matrigel condition. **E**. The percentage and MFI of β5t within total cells. **F**. The MFI of MHC2 within β5t expressing cells. Data points are the mean of three technical replicates.

4.7. Discussion

4.7.A. Summary of Experimental Results

Strikingly, this chapter observed that iTEC and *ex vivo* TEC share a similar adhesion profile, which was shown by the similar preferences the cell types shared for the polymers. I then characterised the effect culturing both cell types on the polymers and showed that *ex vivo* TEC were unable to maintain *Foxn1* in this system, despite using a serum-free medium that was supplemented with relevant cytokines. When I examined how culturing iTEC on the polymers effected its ability to facilitate T-cell differentiation, I found that polymer 427 and 396 were strong candidates to reduce the variation of the co-cultures but also to improve the numbers of thymocytes produced by iTEC, although this did not produce significance. The reasons why this did not produce significance will frame an evaluation of the experimental design, before elucidating the likely mechanism of action the polymers effect and finally how to use this insight to design future experiments.

4.7.B. Variation in Monolayer Co-Culture Conditions

4.7.B.I. Potential Sources of Variation

There was a large amount of variation in the iTEC functionality array that arose from unmeasured independent variables. The ANOVA analysis that aimed to compare how the polymer affected the ability of iTEC to mediate thymopoiesis returned an R^2 of 0.338875, which is low and implies most of the variation did not originate from polymer condition. There are two main sources of variation that were not measured in this study. First, the biological variation within the input cell populations; and secondly, the variation in co-culture mechanics between wells.

4.7.B.II. Variable input populations

There were two cell types in the co-culture: iTEC and ETPs. iTEC must be considered a heterogeneous population. Evidence for this was presented in Chapter Three, iTEC-based Reaggregate Thymic Culture produced large variations in the number of thymocytes generated both inside and between batches of iTEC. If polymer condition only contributed a small difference in the ability of iTEC to mediate T-cell differentiation, it may be difficult to

detect. Furthermore, ETPs will also contain variation, although this was assumed to be much milder than the iTEC population, it is plausible that using 500 cells was insufficient to capture this total variance with a normal distribution. As a result, some wells may have had different starting thymocyte populations. The small initial starting population was justified by the relative rarity of the ETP population in the adult mouse, routinely only 3×10^5 ETPs were recoverable from a four-week old, female BL6/J mouse. It may be that the total variation in this study could be decreased by using a greater number of ETP and or a less mature cell population i.e. e.g. the Flk1$^+$ subpopulation of ETP, or haematopoietic stem cells.

4.7.B.III. Sampling Bias Across Time

In the native thymus, thymocytes interact with many TEC as they migrate through the thymus, this process thought to be an essential part of thymopoiesis (Petrie and Zúñiga-Pflücker, 2007). The density of cells is much greater in 3D structures, such a RTOC and the native thymus, than monolayers and this will reduce the number of thymocyte – iTEC interactions that can occur over time. Given the heterogeneity of the iTEC, it is likely that thymocytes in monolayers will not 'sample' the entire range of iTEC and as a result will behave differently. Comparison between the 3D culture methods used in Chapter Three and the monolayer co-culture employed here show a dramatically reduced efficiency of iTEC mediating the DN to DP transition, this could also be explained in the lower cell and Notch ligand density. It is notable to highlight here that the MS5-hDLL1 system was ineffective in a 2D system and necessitated the Artificial Thymic Organoid system (Seet *et al*., 2017). Therefore, it is likely that monolayers are inherently more variable than their 3D equivalents. Increasing the number of cell-to-cell interactions that occur within a co-culture would mitigate ETP sampling bias and could be achieved by implementing a 3D environment.

4.7.B.IV. Justification Not to Increase Power

The probability of statistical inference producing a type 2 error, i.e. failing to reject the null hypothesis when the hypothesis is false, is dictated by the power (β) of a study. It is scientific convention to use α=0.05 and β=0.8. G*Power was used to perform the power calculations (Faul *et al*., 2007). Focusing on the number of TCRβ$^+$CD3ε$^+$ thymocytes: the weighted

average of SD was 311.62 and the total effect size of the readout was 0.816. There were 11 groups with 33 total observations. The power of this experiment was 0.764, which was considered acceptable. A notable feature of this experiment was that most conditions had at least one technical replicate that produced no thymocytes. These were not excluded on technical grounds because the cells for all conditions were seeded from a shared pool. If at least one replicate was successful, then the experiment cannot be considered a technical failure. As a result, all conditions have at least one replicate with very low numbers of thymocytes causing the data to overlap. Further increasing β was likely to only find differences between very poorly performing polymers, such as polymer 520 and 287. Note, that completing one more biological replicate would increase the power to 0.93, which might be considered overpowered. Therefore, the inability to resolve differences was either due to the imprecision of the system or because polymers did not affect iTEC.

4.7.C. Polymer Structure

Each of the polymers was synthesised from two or three monomers, that each form a proportion of the total polymer (Table C4.3). Each monomer alters the physical and chemical properties of the polymer and affects its interaction with cells (Figure C4.11). Notable patterns emerged. Methoxyethyl methacrylate (MEMA) was the backbone in all polymers except for 394 and 396, which used EMA. All polymers had the presence of a monomer with an amine group, except for 509 that contained an amide. Interestingly, polymers with the same monomer but in different proportions scored differently. For example, polymer 394 (70% EMA, 30% DMAEMA) was a hit on the focused array while polymer 395 (50% EMA, 50% DMAEMA) was not successful on the initial microarray. Furthermore, a comparison between 394 and 396 (90% EMA, 10% DMEAEA) is interesting as the structure of the secondary monomers is similar yet 396 was successful across all tissues while 394 was specific to murine TEC. Whether this is due to human / mouse differences, inability of iTEC to recapitulate all elements of the TEC adhesion profile, differences in the relative embryonic maturity of the TEC, or a type 1 error is unanswerable. Ultimately, the properties required of a polymer to mediate cellular adhesion is a multifaceted process that required not only the presence of certain elements but also the presentation of these elements to the cell. An

interesting mechanism is that the charged polymers associate with specific proteins in the tissue culture medium, which acts as an intermediary between cells and the polymer. If this were proven correct, the synthetic polymers represent a unique method to establishing defined protein conditions for cell culture, this warrants further investigation.

4.7.D. Mechanisms of Action

There are two potential mechanisms that describe how polymers assert effects on cells. The first is that polymers selectively bind cells with a complementary adhesion profile. The second is that the polymers instruct the behaviours of bound cells (Duffy *et al*., 2014a, 2014b; Hay *et al*., 2011). It can be assumed that the iTEC population is composed of a heterogenous population of cells with a spread of biological variance between two extremes: a TEC-like phenotype and a MEF-like phenotype, although this excludes the possibility of the reprogramming strategy inducing the phenotype of another cell lineage that expresses *Foxn1*. If it is assumed that a cell's adhesion profile represents its phenotype, it can be postulated that culturing iTEC on polymers that bind the target TEC-like end of the range and, not the unwanted MEF-like end, will enrich the population towards more TEC-like iTEC. This is the selective binding mechanism. An alternative hypothesis is that synthetic polymers are instructive and can directly affect cellular behaviour. This notion is supported by previous research on synthetic polymers and is envisaged to work in a similar manner to ECM (Duffy *et al*., 2014a; Tourniaire *et al*., 2006). The *ex vivo* TEC bind to selected polymers because these recapitulated the signalling environment in the thymus. iTEC that bind to these polymers are receiving signals important to the behaviour of TEC, which will promote a TEC-like phenotype. This is an instructive mechanism.

4.7.D.I. Polymers Do Not Instruct TEC-Like Behaviour

The data collected in this thesis show that the polymers did not instruct TEC-like behaviours. One of the hallmarks of thymic organogenesis is initiation of *Foxn1*; without *Foxn1*, mice develop the nude phenotype and loss of *Foxn1* in TEC is a hallmark of thymic involution (O'Neill *et al*., 2016; Vaidya *et al*., 2016). Therefore, a potential minimum requirement of TEC-like behaviour is maintenance of *Foxn1* expression. There can be one of two outcomes

when *ex vivo* TEC are cultured on the polymers: either TEC maintain expression of *Foxn1* and, therefore, polymers instruct behaviour that promotes a native TEC phenotype; or TEC do not maintain expression of *Foxn1* and, therefore, polymers do not instruct such behaviour.

Culture on the polymers did not maintain *Foxn1* over time and therefore polymers did not instruct a TEC-like phenotype in the cells (Figure C4.13 and C4.15). There is also no evidence in the literature to suggest that ECM can maintain *Foxn1* in culture, the prevailing hypothesis is that using a 3D architecture is the most important factor to maintain native TEC behaviour *ex vivo.* However, the exact mechanism linking 3D structure to *Foxn1* is unclear but may reflect the presence of non-epithelial stromal cells, availability of growth factors or 3D environmental interactions (Mohtashami and Zuniga-Pflucker, 2006).

4.7.D.II. Polymers Selectively Bind iTEC with a TEC Adhesion Profile

4.7.D.II.a. The Three Assumptions

It was possible to test the selective binding mechanism because of the observation that iTEC interacted with the same synthetic polymers as *ex vivo* TEC (Table C4.2), and not with polymers successful for binding Cre only MEFs (Figure C4.2 and C4.3). A comparison between iTEC cultured on 0.1% gelatin and on polymers effectively equates to a comparison between the range of iTEC extremes, and iTEC selected to have a more TEC-like adhesion profile. The selective binding mechanism holds two assumptions:

A. Isolation GFP^+ MEFs does not completely remove all cells that have yet to adopt a TEC-like adhesion profile.

B. The adhesion profile of iTEC is representative of its function.

iTEC cultured on 0.1% gelatin and polymer 287 represent the conditions containing the full variation of iTEC, as these matrices bind both MEFs and iTEC (Figure C4.2 and C4.3). The remaining polymers were incapable to binding MEFs and may therefore selectively binding iTEC with a more TEC-like adhesion profile. iTEC cultured on polymers 111, 396, 427, 519 bound to both human and murine TEC; 520 bound to human TEC only and 563 bound to

murine TEC only (Table C4.2). Therefore, compared to gelatin most polymers will also prevent iTEC with a MEF-like adhesion profile from entering the co-culture. This is a variable and can have potential effects:

Ci. If fewer MEF-like iTEC in the co-culture positively impacts T-cell differentiation, then synthetic polymers will improve iTEC ability to mediate T-cell differentiation as an inhibitory factor, MEFs, is being removed.

Cii. If fewer MEF-like iTEC in the co-culture does not affect T-cell differentiation, then synthetic polymers will not affect iTEC ability to mediate T-cell differentiation as MEFs are to the co-culture.

Ciii. If fewer MEF-like iTEC in the co-culture negatively impacts T-cell differentiation, then synthetic polymers will reduce the ability of iTEC to mediate T-cell differentiation as MEFs contribute to the co-culture to a greater extent than iTEC.

4.7.D.II.b. Selective Binding Did Not Affect iTEC Function

Culturing iTEC upon polymers did not significantly affect ability to facilitate thymopoiesis (Figure C3.6). With respect to the prior assumptions we can now infer either:

A. GFP isolation removed all cells that still had a MEF-like adhesion profile and this rendered the selective binding of polymers obsolete

B. The adhesion profile of iTEC was not representative of its function so selectively binding those with a more TEC-like adhesion prolife did not affect the co-culture.

C. Having MEF-like iTEC in the co-culture does not affect T-cell differentiation, as these cells are irrelevant to the co-culture.

4.7.D.II.c. Is it Beneficial to Select Against MEFs?

If assumption C is true and assumptions A and B are false, given that the polymers screened here are known to select against iTEC with a MEF-like adhesion profile, it is important to understand the potential effects MEFs would have in the co-culture system. It is well-documented that MEFs are essential in RTOC experiments and using thymus-specific

mesenchyme provides further benefits (Anderson et al., 1998; Anderson and Jenkinson, 2007). The mechanism by which mesenchymal cells create this effect is undefined but hypothesised to be via secreted factors (Jenkinson *et al*., 2007). Therefore, a potential confounding variable in the iTEC functionality polymer array is that removing more MEF-like iTEC, removes beneficial secreted factors from the co-culture and this effect acts against the benefits of selecting for more TEC-like iTEC. Including MEFs in co-cultures but separating them from the iTEC and ETPs with a trans-well would help to investigate this confounding variable. There is evidence against this theory, polymer 287 was unique in that it was a hit polymer on the microarray for both iTEC and MEFs and like gelatin, bound all iTEC. However, it represents one of the worst performing polymers in the experiment, although this effect was not significant and so no firm conclusions were drawn.

4.7.D.II.d. Does Selective Binding Affect iTEC?

If assumption C was false, then the selective binding properties of polymers may be obsolete because isolating GFP$^+$ cells already removed all those cells with a more MEF-like adhesion profile or iTEC adhesion profile was irrelevant to function.

4.7.E. Future Experiments

4.7.E.I. Confirmation that Polymers Selectively Bind iTEC

Future experimentation will aim to resolve these differences. Unsorted iFoxn1 MEFs, 4-days after exposure to 4OHT, will be seeded onto polymers to create the three following groups: substrates that select the entire range of variation in iTEC (0.1% gelatin and polymer 287), polymers that bind more TEC-like cells (polymers, 396, 427, and 563) and polymer 509, which binds iTEC but not *ex vivo* TEC. FACS isolated GFP$^+$ iFoxn1 MEFs act as a positive control GFP$^+$ iFoxn1 MEFs and as a negative control Cre only MEFs will be seeded onto 0.1% gelatin.

To test assumption A, after several hours, unbound cells will be collected, and bound cells fixed. If there are no differences within the groups, assumption A is true: the GFP isolation has rendered the selective binding of polymers obsolete. To test assumption B, a co-culture assay could be performed on the above groups. If there are no differences within the groups,

assumption B is true: the adhesion profile of iTEC is not representative of its function. To test assumption C, the same experiment will be repeated with MEFs contributing secreted factors to the experiment but physical isolated in a trans-well. If there are no differences between the groups, MEFs are not a contributing cofounding variable in the assay.

If polymers are found to mediate selective binding, they can be an alternative to FACS, which is a costly and slow process that exposes cells to harsh conditions. Given that it is extremely probable that GFP^- iFoxn1 MEFs will present a more MEF-like adhesion profile, the polymers represent a novel sorting strategy. It is plausible and testable that polymers can sort in place of FACS: seeding iFoxn1 MEFs on polymers will remove unsuccessfully reprogrammed MEFs. This method would dramatically increase the scale-up potential of the iTEC system.

4.7.E.II. Observing Whether Polymers Affect *Ex Vivo* TEC Functionality

Unfortunately, the fact that polymers did not maintain *Foxn1* in *ex vivo* TEC made a direct comparison between TEC and iTEC impossible. TEC only maintain their phenotype in 3D techniques, such as RTOC, which is not compatible with the addition of the synthetic polymers tested herein (Anderson and Jenkinson, 2007). In order to make polymers compatible 3D techniques, they must be water-soluble. Designing shorter, hydrophilic polymers containing the monomer compositions observed to be preferable to TEC represents an interesting method to target cells. Whether the binding of water-soluble polymers will produce any functional changes in a TEC is challenging to predict, given the results of this chapter but represents a potentially novel pharmaceutical option targeting the cell – ECM interaction. Another alternative is to cross-link the polymers into a three-dimensional structure (Duffy *et al*., 2014b; Zhang *et al*., 2013). However, given that non-epithelial thymic stromal cells are beneficial for *ex vivo* thymic function, building such structures from polymers that actively select for TEC and potentially against the other stromal elements will share the disadvantages as highlighted by the exclusion of MEFs in iTEC Polymer Functionality Array. Note, that in the future the contribution of mesenchyme to these assays aims to be replaced, as previously discussed mesenchyme is hypothesised to

contribute to thymopiesis by secreting beneficial factors and once identified, these can be supplemented exogenously (Auerbach, 1960; Jenkinson et al., 2007).

4.8. Conclusion

In summary, this chapter identified 12 synthetic polymers that allowed the binding of TEC. These can be segmented into eight that allowed the binding of iTEC, eight for the binding of murine embryonic TEC and eight for human embryonic TEC. There was remarkable overlap in the polymers preferred by each cell type. These polymers were then tested against three objectives designed to parse thymic function into testable sections. Objective A investigated maintenance of *Foxn1* expression; Objective B measured the ability to mediate T-cell differentiation and Objective C looked for evidence of promiscuous gene expression. These objectives were designed to be sequential. i.e. promiscuous gene expression is irrelevant if a system cannot mediate T-cell differentiation, which in turn is unlikely if a system cannot maintain *Foxn1* expression.

The polymers identified to bind *ex vivo* murine embryonic TEC were unable to maintain *Foxn1*. Arguably this was an unlikely objective for the polymers to meet, given the emphasis the literature has on the importance of 3D cell culture and on growth factor inputs to *Foxn1* expression (Mohtashami and Zúñiga-Pflücker, 2006). Given that polymers are currently only compatible with monolayer culture, this was the technical extent to which the polymers could be tested using *ex vivo* TEC; it would have been a waste of resources to continue testing Objective B. However, the polymers will be beneficial for screens that seek to identify factors that are able to maintain Foxn1 given that they performed as well-as 0.1% gelatin but will contribute less variation.

The eight polymers selected by ability to bind iTEC were first tested for Objective B, because it was assumed that *Foxn1* expression would not be affected by the polymers given that it is genetically enforced in iTEC, and were found to be able to mediate T-cell differentiation albeit inefficiently compared to the 3D culture methods discussed in Chapter Three. Ultimately, this chapter identified defined culture substrates that replicate the behaviour of iTEC on undefined matrices such as 0.1% gelatin and Matrigel. Whilst these results did not

generate significance, polymers were at least as effective as undefined matrix such as Matrigel and 0.1 % gelatin but had the benefit of being associated with less variation. The results of this were difficult to resolve from technical noise and this chapter discussed short comings of using 2D culture techniques for these screening experiments, which ultimately contributed to the high variation found in the co-culture assays. Therefore, it opens an interesting technical niche of developing a 3D culture system that, unlike RTOC, can be performed in higher throughputs with lower variation.

5. Chapter Five: Designing a Miniaturised Reaggregate Thymic Organ Culture System

5.1. Introduction and Aims

The preferred technique for culturing thymic epithelial cells (TEC) is called reaggregate thymic organ culture (RTOC) (Auerbach, 1960; Jenkinson *et al*., 1992). The most common approach involves manual reaggregation of cells that are then cultured at the air-liquid interface upon a porous membrane, although many variations exist (Anderson *et al*., 1998; Anderson and Jenkinson, 2007; Jenkinson and Anderson, 1994; Sheridan *et al*., 2009). RTOC maintains *Foxn1* expression in *ex vivo* TEC, which allows them to recapitulate native functions (Mohtashami and Zúñiga-Pflücker, 2006). However, RTOC is not without limitations. The process of generating RTOC is technically difficult, leading to technical variation between experiments. Furthermore, creating a cell pellet that is large enough to be manually manipulated requires a substantial number of input cells. Given that the target tissue is embryonic murine thymus, this limits the number of conditions that can be compared concurrently in any RTOC experiment. It is also difficult to use RTOC when investigating rare tissues such as the human embryonic thymus. Finally, visualisation of live cells during the RTOC is impossible as light cannot pass through the porous membrane. As a result, the community has focused on end-point point read outs, typically flow cytometry or immunohistochemistry. These short comings prompted development of the leading *in vitro* T-cell generation systems, the OP9-DLL1, OP9-DLL4 and MS5-hDLL1 cell lines (Schmitt and Zúñiga-Pflücker, 2002; Seet *et al*., 2017). Whist overcoming the technical limitations associated with RTOC, these do not faithfully emulate positive selection or central tolerance, as the parental cells lines lack the TEC-specific functions required to mediate these processes. Furthermore, they are not patient-specific and thus have limited clinical value.

I set out to test whether use of the GRID3D system (SUN Biosciences; now commercially available), might allow scale-up and miniaturisation of the RTOC process. The GRID3D system is essentially a cellular mould, in which micro-wells of defined dimensions are printed into a hydrogel matrix specifically designed for insertion into wells of a 24- and 96-well plates (Figure C5.1). A single cell suspension is then applied to each well of for example the 96-well plate, and gravity pulls the cells into the micro-wells of the mould (Figure C5.1A). As the mould is created from polyethylene glycol (PEG), cells cannot bind to the mould itself and

instead bind to each other (Figure C5.1B). The cells autonomously reaggregate into a miniaturised organoid, which in the case of thymic cells, would be a miniaturised-reaggregate thymic organ culture (MTOC). MTOC, if they could be produced, would address the limitations of the current RTOC system: they would be compatible with low cellular inputs, would be technically unchallenging and would be scalable. As the GRID3D is compatible with live fluorescent live imaging, MTOC would allow interrogation of events with spatiotemporal resolution. The major drawback of the miniaturisation is that it is reductionist. Reducing the complexity of the culture system should provide the capacity for more precise observations, but such small clusters of cells are unlikely to recapitulate thymic function to the same extent as larger structured organoids or RTOC/FTOC. Nonetheless, lessons learnt from MTOC should provide valuable insights for generation of larger thymic organoids.

This chapter describes preliminary work in which I have optimised cellular inputs into the GRID3D system, created a pipeline to characterise the individual properties of reaggregates and evaluated the capacity of the system to support MTOC generation based on the key criteria proposed for the polymers in Chapter Four: determine whether MTOC can enforce maintenance of *Foxn1* in cultured *ex vivo* TEC and whether iTEC can mediate T-cell differentiation when cultured in MTOC.

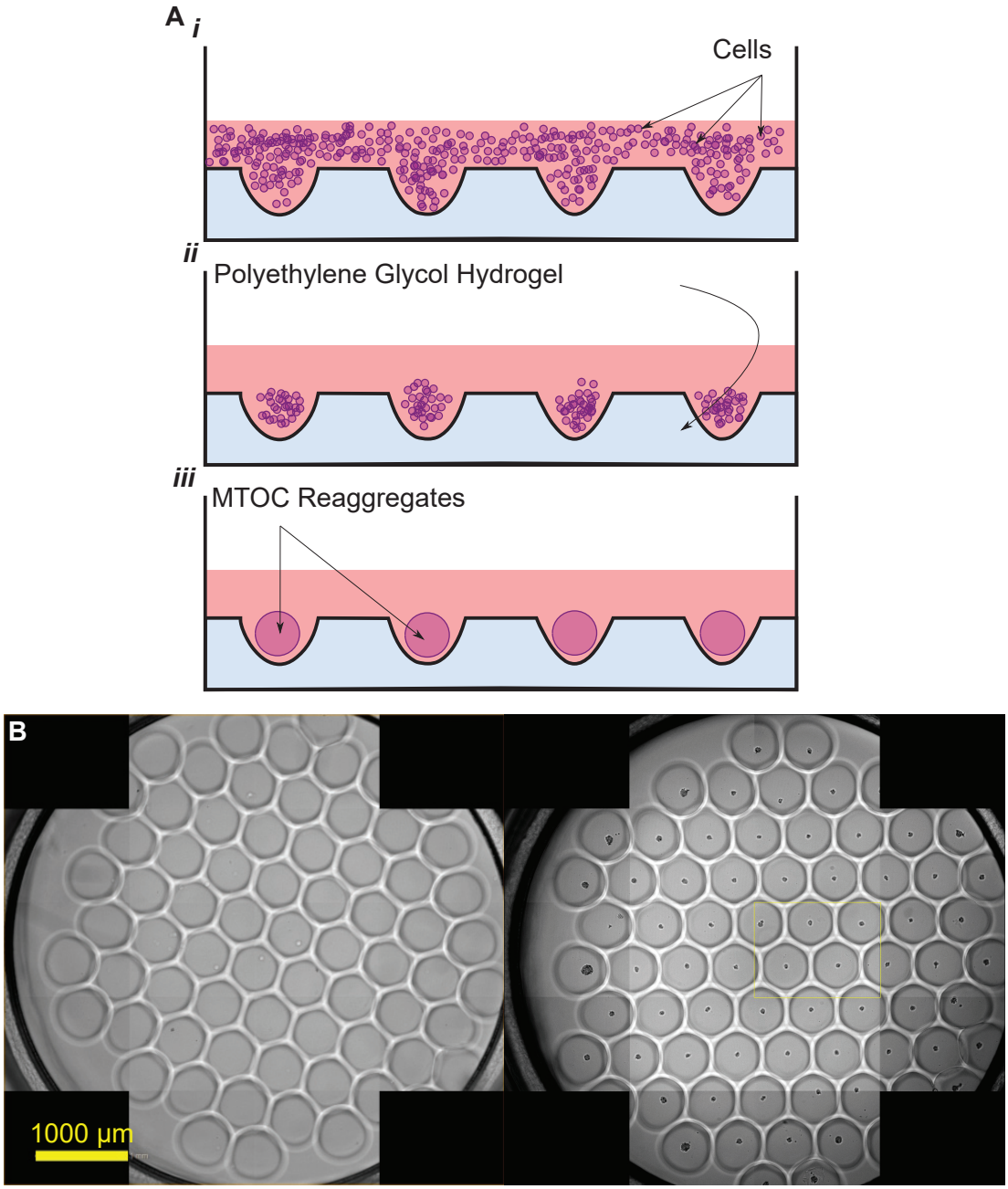

Figure C5.1: Description of the GRID3D Technology

A. Representation of MTOC system. Over time a single cell suspension coalesce, guided by the PEG hydrogel mould. **B**. The GRID3D system is completely flexible to experimental design. In this chapter, a mould was created that produced 70 micro-wells, with a diameter of 500 µm, in each well of a 96-well plate. The images shows a bright field image of this design without input cells *(left)* and 24-hours after seeding with 100 WT MEFs in each µwell *(right)*. Note that the yellow box on the right-hand image represents one field of view.

5.2. The GRID3D System Produced Many Independently Observable Reaggregates

5.2.A. Formatting the GRID3D System

To test whether the GRID3D system could support development of MTOC, I performed a series of pilot experiments in which I first aimed to see if the system could provide the readouts, discussed above, to address current limitations in culture technologies. Afterwards, I needed to observe evidence that dissociated thymus cells and iTEC could reaggregate themselves and whether this had a minimal cell input requirement. The GRID3D system is highly tuneable. The depth, number and diameter of the micro-wells can be altered depending on the application. For this thesis, shallow micro-wells were used, which should promote a more rapid reaggregation. The total tissue requirement is dependent on two factors, firstly the number of micro-wells and secondly the number of cells seeded per micro-well. The number of micro-wells printed into a well is dependent on the diameter of each micro-well. Initial observations found that using micro-wells with a diameter of both 200 μm and 500 μm was successful in creating reaggregates and both formats are exemplified in this chapter when relevant. However, most assays used the 500 μm format as this created fewer micro-wells and consequently the total tissue requirement was reduced. Printing micro-wells, with a diameter of 500 μm into an insert suitable for on well of a 96-well plate (called a 96well hereafter) produced 70 micro-wells (Figure C5.1B). To demonstrate that a small number of cells could reaggregate in this format, 7×10^4 wild type (WT) murine embryonic fibroblasts (MEFs) were seeded into one 96well. On average 100 MEFs were distributed randomly into each of the 70 micro-wells and over 24 hours the MEFs reaggregated (Figure C5.1B). Note that this produced an array of similar, but not identical, reaggregates.

5.2.B. Automatic Segmentation to Characterise Individual Reaggregates.

Given the large amount of technical noise reported in the iTEC polymer functionality array, I wished to test whether MTOC were able to provide more consistant readouts than other culture methods. There is no reason to assume that the miniaturised reaggregates created in MTOC are less variable than their larger scale counterparts in RTOC. In fact, it is more probable that there is less variation between RTOC as they contain many more cells, which

is more likely to encapsulate the total range of biological variance. In the MTOC system, it is improbable that each reaggregate will be created from the same number of similar cells and display identical behaviours as neighbouring reaggregates, given that each reaggregate comprises of such a small number of cells. Unless, each micro-well is seeded with a homogeneous stem cell population to derive clonally expanded organoids, which is not the case for this thesis and not be further discussed. However, the main advantage MTOC is that it produces many technical observations. It is more probable that the mean behaviour of 70 reaggregates within one well will be similar of the mean behaviour of 70 other reaggregates in another well subjected to the same experimental conditions. Given the small cell number input requirements of MTOC, the number of technical replicates can be dramatically increased compared to RTOC. Hypothetically, if we assume that each 96well of MTOC requires 20% of the tissue input for every individual RTOC for a given experiment, MTOC can produce 350 reaggregates for each RTOC. The mean behaviour of 350 reaggregates is more likely to reflect the true biological mean than a single RTOC.

To quantify properties of individual reaggregates in a high throughput imaging system, I created an automatic pipeline to segment each reaggregate into an independent object using the Columbus™ Image Storage and Analysis system (Perkin Elmer) (Figure C5.2A). This process employed a machine learning algorithm to differentiate between the texture of the PEG mould, noise and or artefacts, and the reaggregates. Notably, this negated the requirement of a counter stain to select on cells. The manufacturing process created small differences in the depth of each micro-well, which gave each reaggregate a different optimal, in focus, Z-plane, making automated image acquisition troublesome. To overcome this issue, each reaggregates was abstracted into its side, edges and ridges (SER) traits. These traits were observed to peak when each reaggregate was optimally in focus and SER Bright was used to identify the optimal Z-plane for each reaggregate (Figure C5.2B; I wish to thank Mr D. Rouse for kindly providing the script to organise and select reaggregates from the most in focus Z-plane). This GRID3D format and pipeline allows for automation characterisation of 6.72×10^3 reaggregates over one 96 well plate.

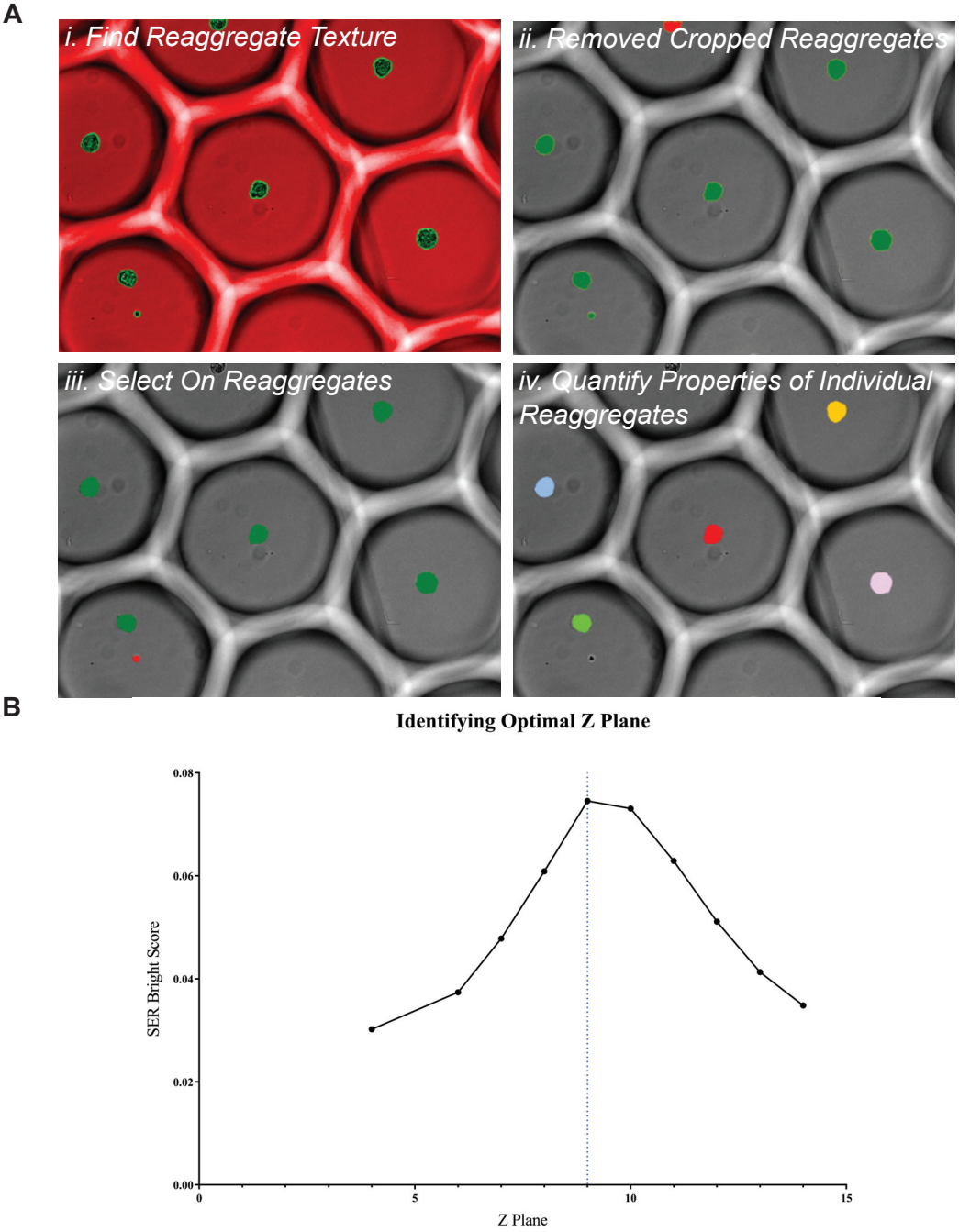

Figure C5.2: Creating a Pipeline to Segment Individual Reaggregates

A. WT MEFs were seeded into the GRID3D system to create an automatic pipeline to segment reaggregates into individual objects. ***i***. A texture analysis employed machine learning to isolate reaggregates from background in bright field images. ***ii***. Any cropped objects were removed to ensure data was collected only from whole reaggregates. ***iii***. The size and shape of reaggregates were quantified to select only clusters of cells that were target reaggregates. ***iv***. The properties of each reaggregate was quantified as individuals, which are represented in different colours. **B**. The reaggregates within each micro-well were on a different Z-plane due to variations in the PEG mould. The optimal Z-plane was identified by using the Z-plane in which reaggregates had the greatest SER Bright value. Blue line represents most in focus Z-plane by eye.

5.3. Identifying the Minimal Cellular Input of *Ex Vivo* Thymic Dissociate.

Tissue scarcity remains the largest factor with the potential to limit the size of MTOC experiments. Given that the strength of the system is dependent on creating large numbers of technical observations, it was pertinent to define the minimal input requirements to successfully reaggregate cells. For *ex vivo* tissue the decision was made to optimise the system in terms of thymic lobes rather than cell number. This was justifiable for many reasons. Firstly, Chapter Four provided evidence that seeding experiments in terms of thymic lobes was more accurate than using cell counts. Also, it was assumed that if the whole range of thymic stroma was present, cells would be more likely to recapitulate behaviours of the native tissue. Finally, the proportion of different cell types within the thymus changes dramatically during development. For example: the number of T-cells quickly dwarfs the number of TEC (Hirakawa *et al*., 2018). As a result, using 1000 cells per micro-well of E13.5 tissues and E17.5 tissues would not be a fair comparison as the thymic stromal cells must be assumed to be responsible for reaggregating into a structure.

Both E14.5 and E15.5 thymic lobes were used in this experiment. Thymi were dissociated into a single cell suspension and suspended in 25 µl of advanced DMEM/F12 supplemented with 2% fetal calf serum (2% medium) at the following concentrations: 100%, 50%, 25% and 10% of a thymic lobe. The 25 µl cellular suspension was applied to each 96well and incubated to allow the cell suspension to distribute between micro-wells. After thirty minutes, each 96well was topped up to 200 µl of medium and cultured for 14 days with a 50% medium change every two to three days. On day 14, the central thirty micro-wells of each condition were imaged, and the automatic pipeline quantified the number and area of the reaggregates (Figures C5.3A and C5.4A). The number of successful reaggregates was used to infer the minimal cellular input and this was reported as a percentage of potential possible reaggregates. The proportion of micro-wells in which a successful reaggregate formed decreased when less than 50% of- and 100% of- a whole thymic lobe was used for E15.5 and E14.5 tissue, respectively. For E15.5 tissues, using 25% of a thymic lobe resulted in 65.4% of micro-wells containing a successful reaggregate, while for E14.5 tissues, using

50% of a thymic lobe resulted in 29% of micro-wells producing successful reaggregates. The mean area of successful reaggregates was also calculated. Notably, using 50% of an E15.5 thymic lobe and one E14.5 generated reaggregates with a similar mean area (7332 μm^2 and 5500 μm^2, respectively), suggesting that this is the smallest size that yield successful reaggregates. These data are also consistent with the number of TEC doubling each day during thymic organogenesis (Hirakawa *et al*., 2018). It was decided that future experiments would be seeded with one E15.5 thymic lobe as this was sufficient to ensure formation of one reaggregate per micro-well.

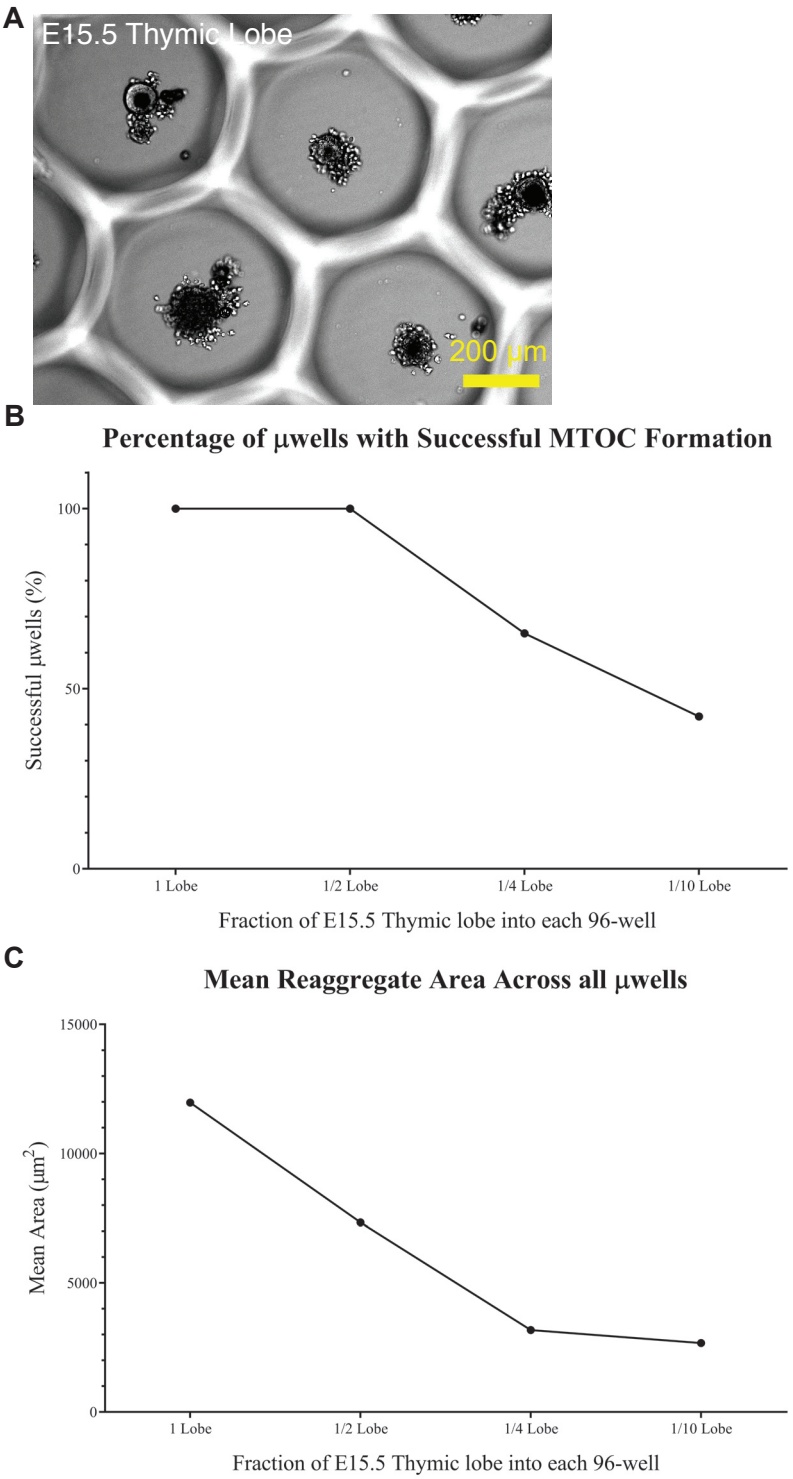

Figure C5.3: Optimising Input of E15.5 Thymic Dissociate into GRID3D System

A. Images show MTOC created by dissociating one E15.5 thymic lobe and seeding the suspension into a 96well, which contained 70 micro-wells. Therefore, each micro-well contained 1/70 of an E15.5 thymic lobe. MTOC were cultured for 14 days. **B**. Graph depicts that seeding less tissue, measured as a fraction of an E15.5 thymic lobe, into each 96-well reduced the amount of successful reaggregates. Thus, cell density is a limiting factor when creating MTOC. **C**. Reducing seeding tissue, measured as a fraction of an E15.5 thymic lobe, reduced mean reaggregate area. N=1.

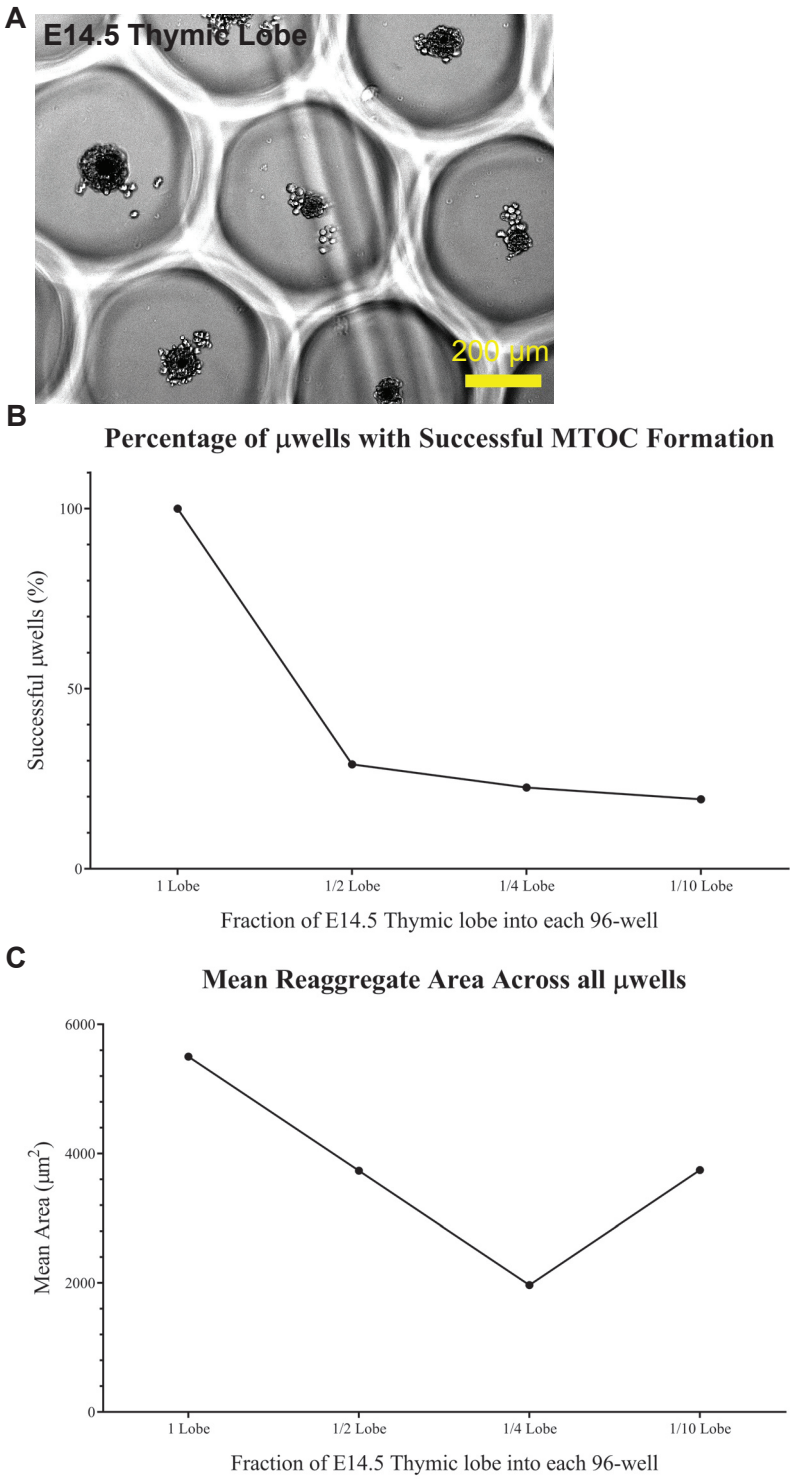

Figure C5.4: Optimising Input of E14.5 Thymic Dissociate into GRID3D System

A. Images show MTOC created by dissociating one E14.5 thymic lobe and seeding the cell suspension into a 96well which contained 70 micro-wells. Therefore, each microwell contains 1/70 of a E14.5 thymic lobe. MTOC were cultured for 14 days. **B**. Graph depicts that seeding less tissue, measured as a fraction of a thymic lobe, into each 96-well reduced the number of successful reagregates. Therefore, cell density is a limiting factor when creating MTOC. **C**. Reducing seeding tissue, measured as a fraction of an E14.5 thymic lobe, reduced mean reaggregate area. N=1.

5.4. *Foxn1* Expression in *Ex Vivo* TEC is Maintained in MTOC.

Chapter Four highlighted that current monolayer culture techniques are inadequate to maintain *Foxn1* expression in TEC. Given that downregulation of *Foxn1* has large effects on TEC behaviour, and this will confound any subsequent comparison between *ex vivo* and native TEC, MTOC were evaluated for the ability to maintain *Foxn1* in TEC (Vaidya *et al*., 2016). Mohtashami and Zúñiga-Pflücker (2006), provide reverse transcription-quantitative polymerase chain reaction (RT-qPCR) evidence that TEC maintain *Foxn1* in RTOC and fetal thymic organ culture (FTOC) for at least five days in culture. However, given the accessibility of MTOC to microscopy, the *Foxn1*^{G} transgene was employed to infer *Foxn1* expression from GFP mean fluorescence intensity (MFI) (Figure C4.12) (O'Neill *et al*., 2016). This was described, and justified, in Chapter Four. Briefly, *Foxn1*^{G} thymi were produced using a *Foxn1*^{G} x C57BL/6 cross as the transgene knocked a GFP into exon1 of the *Foxn1* locus, rendering it a null allele (Figure C4.12). A cell suspension, created from a mix of *Foxn1*$^{G/+}$ and WT thymic lobes, was created for each experiment so only 50% of all TEC will contain the *Foxn1*^{G} transgene but it was assumed that maintenance of *Foxn1* expression was uniform through all TEC within a reaggregate.

Four wells of a 96-well plate, which contained the GRID3D system were seeded at a concentration of one E15.5 thymic lobe per well, or 1/70 thymic lobes per micro-well. Every two to three days a 50% medium change of fresh 2% medium was performed. At 24 hours, seven and 14 days the central 30 micro-wells were imaged at a range of Z-planes to capture both the bright field and GFP channels (Figure C5.5A). The individual reaggregates were automatically segmented using the Columbus™ software (Perkin Elmer) in the bright field channel and the GFP MFI for each reaggregate was taken from the Z-plane with the highest SER bright value. The mean value was found at each time point in each 96well. A nonlinear regression analysis of these data was used to generate a quadratic curve and 95% confidence intervals for the data (Figure C5.5B). This line was significantly different from the line $\mathrm{Y} = 0x + 623$, which represents the null hypothesis that GFP MFI was not affected by time, and the null hypothesis was therefore rejected. Over the 14-day culture period, the GFP MFI of all the reaggregates increased significantly over time. Interestingly, variation

also increased over time, as described by the increasing coefficient of variation over time (Day1 = 3.551%, Day 7 = 10.75% and Day 14 = 17.89%). However, the quadratic equation was still associated with a reasonable R^2 value of 0.7417, indicating that time was the largest contributor of variation.

This variation is exemplified in the representative images of the experiment (Figure C5.5A). The central reaggregate in the image shown did not maintain high level *Foxn1* expression despite being exposed to the same external conditions as the neighbouring micro-wells. At day one there is nothing visually distinguishing this reaggregate from neighbouring reaggregates. By day seven, the reaggregate had expanded but the GFP was both lower and distributed thinly throughout the reaggregate. On day 14, this reaggregate had failed and both GFP expression and size of the reaggregate were reduced compared to day seven.

These data posed two interesting questions: Did the reaggregates increase GFP expression over time because TEC upregulated *Foxn1* or did the number of *Foxn1* expressing TEC increase in each reaggregate? And, why did only some reaggregates fail to maintain *Foxn1*? Did this represent a dichotomy or did some reaggregates confer a lower steady-stead level of *Foxn1* expression than others?

To test whether the increase in GFP MFI was a result of increased *Foxn1* in individual TEC or a collective increase of total TEC. The above experiment was repeated with the aim of collecting data at the single cell resolution. The ideal method to provide single cell resolution data using MTOC is confocal microscopy. This would be able to image live cells without substantial manipulation of the system. However, this process is still suboptimal, for reasons that will be discuss later in this chapter, and a flow cytometric readout was employed instead. This was not the ideal readout as MTOC as many cells are lost during processing for flow cytometry, which incorporates technical variation into assays (Hirakawa *et al*., 2018). These concerns are confounded when processing MTOC as the number of reaggregates is very small. Furthermore, by pooling together all reaggregates of a well, information on independent reaggregates is lost. Three different dissociation strategies were tested: mechanical force, enzymatic disassociation of extracellular matrix components and TrypLE

Express (Gibco), which targets cellular membrane-bound proteins. Only the latter, harsher dissociation provided enough cells for analysis, so the data presented is of only one 96well. Furthermore, the number of recoverable cells was low as indicated by the Z-axis of the histogram (Figure C5.6A). TEC were defined as $EpCAM^{+}$ cells.

Comparison with native E15.5 *Foxn1*^{G} thymic disassociate at time zero (t_0) indicated that some TEC in the MTOC were able to maintain the native steady-state level of *Foxn1* expression, with the GFP MFI remaining similar within the GFP^{high} TEC fractions. However, the proportion of TEC that maintained GFP expression at this level diminished markedly, from approximately 50% (actual value was 40.4% due to chance) to 12.05% in the recovered TEC. Focusing on the similarities, this provides evidence against the total GFP MFI increase in reaggregates, over time, being attributed to upregulation of *Foxn1* in TEC and supports that there are more TEC, contributing a similar amount of GFP over time (Figure C5.5B). The percentage reduction in GFP^{high} TEC is also informative. Unlike the t_0, E15.5 *Foxn1*^{G} thymic dissociate, the recovered cells have multiple GFP^{low} peaks. This can be interpreted in two ways. Firstly, that the peaks captured a temporal transition of TEC between the GFP^{high} and GFP^{low} groups. Alternatively, the peaks captured spatial information and each peak reflects a different environment within reaggregates that were conducive to a different steady-state level of *Foxn1* expression. Which mechanism is true is currently difficult to answer without being able to calculate gross properties of each reaggregate and then, using confocal analysis to calculating properties of individual TEC. However, the first part was calculated and shown in Figure C5.6B using the data displayed previously in Figure C5.5B. Technical replicate A stands out as not being able to produce reaggregates with very high GFP MFI and technical replicate D has a much greater deviation away from normal distribution with a shift over to producing reaggregates with lower GFP MFI. Whether this data spread reflects that some reaggregates maintain a lower steady state of *Foxn1* expression or this reflects that some reaggregates contain more TEC is impossible to distinguish. However, reaggregate size was not associated with GFP MFI (linear regression $R^2 = 0.2168$) Furthermore, given that this experiment was not designed to test this hypothesis, the

absence of a control group comprised of entirely WT TEC, which do not express GFP, prevents being able to distinguish which reaggregates are truly GFP negative.

Therefore, when cultured in MTOC, some TEC maintain *Foxn1* expression at a similar level to native tissue, while others downregulate *Foxn1* via a currently unknown mechanism. It is pertinent to draw comparison to the native thymus, in which TEC downregulate *Foxn1* at the onset of involution, although more data is required to contrast the mechanisms, involution highlights particular areas to explore (O'Neill *et al*., 2016). Of note, it seems unlikely that reaggregates failed because of the increased proliferative action of *Foxn1*$^{-}$ TEC, given the representative images in Figure C5.5A demonstrated a reduction in size as TEC downregulated *Foxn1*. Although these data must be repeated to confirm this finding, the high number of technical replicates performed give confidence in these data. Therefore, based on the criteria of maintenance of *Foxn1* expression, the MTOC system developed herein appeared superior to monolayer culture as an *in vitro* system that can mimic native thymus functions and was taken forward for further development

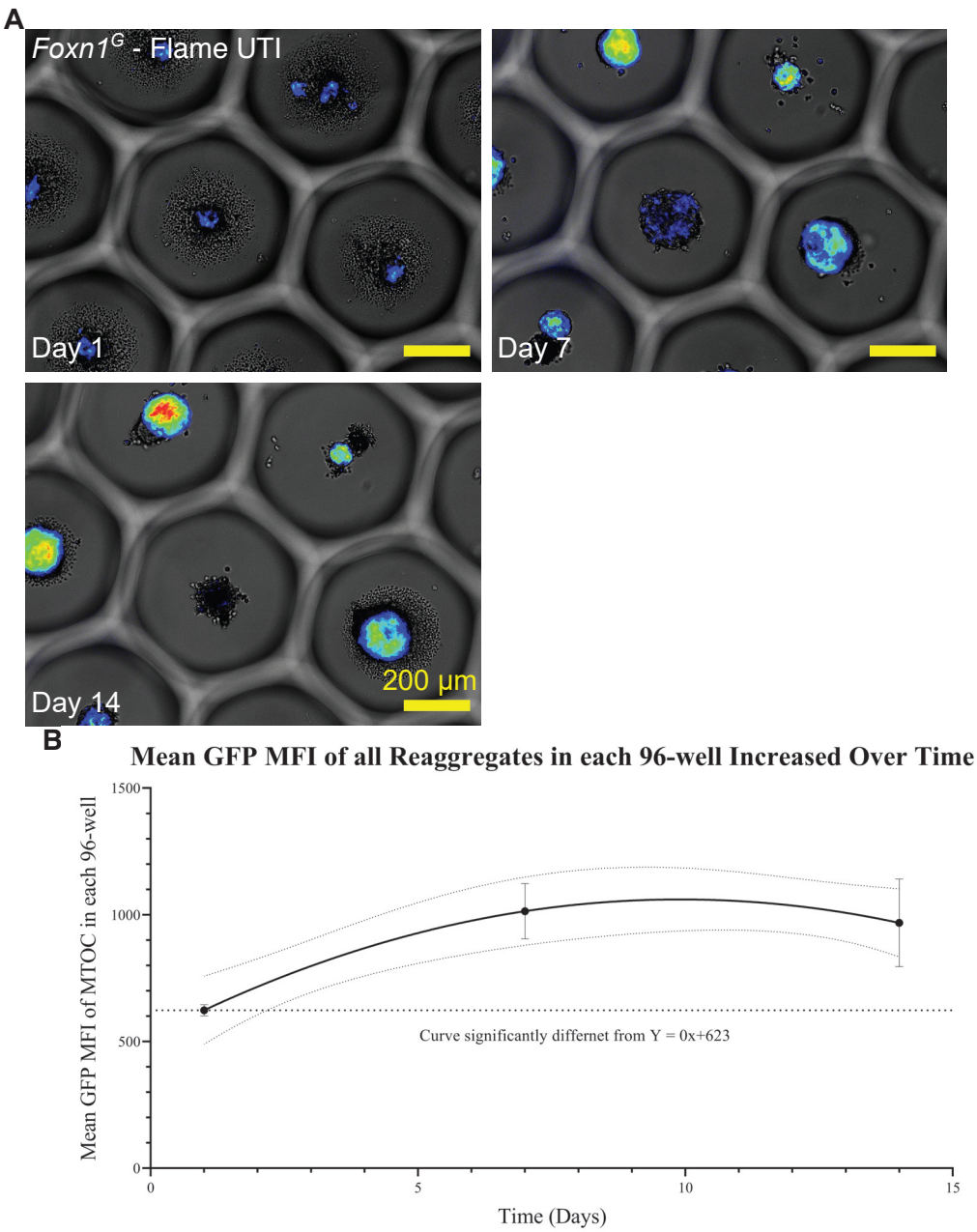

Figure C5.5: MTOC Created with Dissociate from One E15.5 Thymic Lobe Maintained *Foxn1* Over Time

A. Images show MTOC created using dissociate from one E15.5 thymic lobe, so each micro-well contained 1/70 of a thymic lobe. Embryos of *Foxn1*$^{G/+}$ x WT mating were used to produce a mix of thymic lobes, in which half of all TEC contain the *Foxn1*^{G} transgene. Note, the reaggregate in the central micro-well failed to maintain *Foxn1*^{G}. GFP is represented as a flame UTI. The histogram was consistent across time points so visual changes in GFP are biologically informative. **B**. The central 30 MTOC in each 96well, were automatically segmented into independent reaggregates at each time point and the MFI of each reaggregate in the GFP channel was quantified. The total mean of this value was calculated for four technical replicates. A quadratic regression analysis showed that the total mean MFI of GFP across all reaggregates in each 96-well increased over the 14 day culture period. N=1.

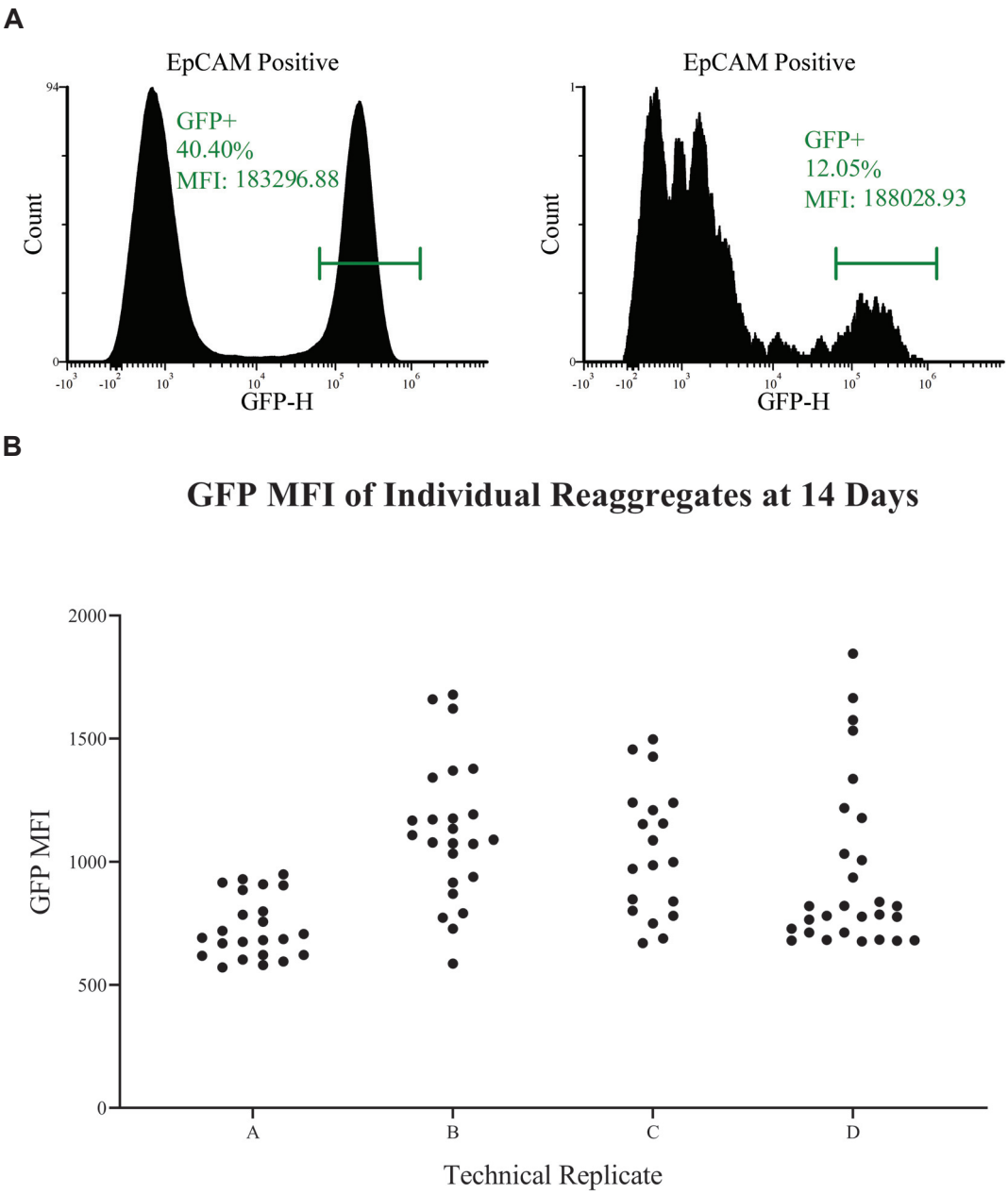

Figure C5.6: A Proportion of Reaggregates Failed to Maintain Foxn1 in TEC

A. Graphs show *Foxn1*^{G} TEC, which are defined as EpCAM^{+}, isolated from MTOC after 14 days in culture *(right)* compared to *Foxn1*^{G} TEC freshly isolated from a litter of E15.5 embryos *(left)*. MTOC were created using dissociate from one *Foxn1*^{G} E15.5 thymic lobe. Events represent one 96-well of MTOC that was enzymatically disassociated. Note, that the MFI of the GFP^{high} fraction remained consistent throughout culture. However, not all TEC maintained GFP expression and TEC lost GFP expression at different rates as indicated by the multiple peaks. **B**. Graph depicts the GFP MFI of all reaggregates in four technical replicates after 14 days in culture. Each replicate was seeded with dissociate from one *Foxn1*^{G} E15.5 thymic lobe. To calculate GFP MFI, each reaggregate was automatically segmented. Note, the GFP MFI was variable between reaggregates. N=1.

5.5. *Ex vivo* TEC Express Mitotic Marker Ki67 When Cultured in MTOC.

To further elucidate whether the observed GFP MFI increase over time in MTOC was a consequence of increasing numbers of TEC within each reaggregate, an experiment was performed to observe evidence of TEC proliferation. This experiment also provided the first opportunity to perform confocal analysis on MTOC. Given that PEG is a hydrogel, principally comprised of water, the refractive index of the GRID3D mould should be the same water. Therefore, live microscopic analysis through the PEG hydrogel should be like imaging through the same depth of water. However, in this initial attempt at imaging thymic material in such a manner, it was decided to use fixed tissue to mitigate some technical challenge. WT E15.5 thymic lobes were seeded into the GRID3D system at a concentration of one lobe per 96well or, 1/70 thymic lobes per micro-well. After seven days of culture using the above described process, the reaggregates were fixed within the GRID3D structure and stained for EpCAM and Ki67 and with 4′,6-diamidino-2-phenylindole (DAPI).

$EpCAM^{+}Ki67^{+}$ cells were observed at a low frequency within the MTOC (Figure C5.7). This was taken as further evidence supporting that the observed increase in GFP MFI over time was due to TEC proliferation within the reaggregates rather than increased *Foxn1* expression within individual TEC. However, the technical performance of this approach to imaging in the GRID3D system was poor. Note the dramatically lower light penetration between the reaggregate and the positive control. The positive control was an E13.5 thymic lobe, which was used over E15.5 because of its smaller total size, suspended in phosphate-buffered saline (PBS) in an imaging dish (IBDI). The major difference was the presence of the PEG hydrogel, which was concluded to reduce the penetration of light.

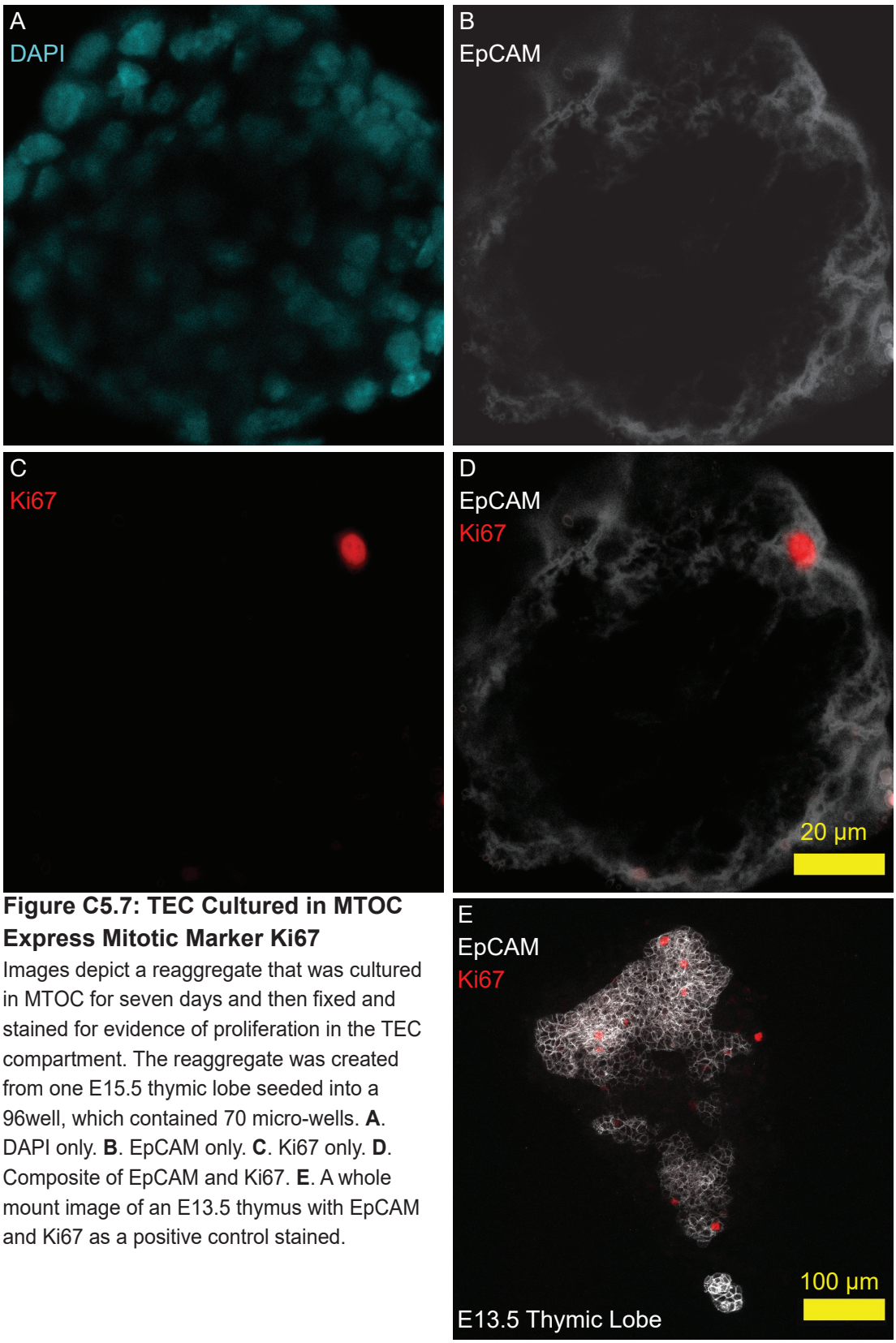

Figure C5.7: TEC Cultured in MTOC Express Mitotic Marker Ki67

Images depict a reaggregate that was cultured in MTOC for seven days and then fixed and stained for evidence of proliferation in the TEC compartment. The reaggregate was created from one E15.5 thymic lobe seeded into a 96well, which contained 70 micro-wells. **A**. DAPI only. **B**. EpCAM only. **C**. Ki67 only. **D**. Composite of EpCAM and Ki67. **E**. A whole mount image of an E13.5 thymus with EpCAM and Ki67 as a positive control stained.

5.6. *Ex vivo* TEC Cultured in MTOC for Seven Days Exhibit Regional Organisation.

Following the successful imaging of Ki67^{+} TEC within MTOC, reaggregates were stained for EpCAM and ulex europaeus agglutinin I (UEA1) and with DAPI. This was performed concurrently to the above described confocal analysis. Given that the input E15.5 thymic lobes contained both cTEC and mTEC, and that mTEC are traceable using the medullary TEC (mTEC) marker UEA1, it was interesting to see whether MTOC exhibited this patterning (Figure C5.8).

After seven days of culture in MTOC, reaggregates were fixed and stained. There were three possible outcomes. If there were no observable EpCAM^{+}UEA1^{+} cells, the input mTEC did not survive the seven-day culture period. If there were EpCAM^{+}UEA1^{+} cells but they were distributed randomly within reaggregates, mTEC were able to survive but not organise when cultured as MTOC. Finally, if EpCAM^{+}UEA1^{+} cells were present in distinct regions, mTEC were able to not only survive but also organise themselves when cultured as MTOC. EpCAM^{+}UEA1^{+} cells were found in clusters at the centre of reaggregates, providing evidence to support the final proposition (Figure C5.8). However, at this time there is insufficient data to concluded whether this pattern is the result of propagation of a single mTEC clone to form a medullary islet or spatial assembly of multiple input mTEC (Rodewald et al., 2001; Ulyanchenko et al., 2016). The positive control used for this was a sectioned E16.5 thymus. Arguably comparing sectioned to whole mounted samples produced a confounding variable. However, given that UEA1 patterning is only detectable after E15.5, the size of the sample would necessitate clearing, which was considered an equally large confounding variable.

Again, imaging through the GRID3D created technical challenges. Given the poor light penetration associated with imaging through the GRID3D mould, only the centre of the reaggregates were kept in frame. This prevented the outer areas from saturating the detectors, but it was impossible to image a whole reaggregate in one stack. Furthermore, staining the samples in the GRID3D system created small aggregates of antibody represented as the bright noise prominent in the EpCAM channel. Finally, in both Figure

C5.7 and C5.8 the DAPI stain did not show small nuclei, which are likely to represent thymocytes. There are two speculative answers to this. Firstly, this could be due to sampling bias. The poor light penetration meant that only the smaller reaggregates were imageable. It could be that the smaller reaggregates were small because of a failure to establish a thymocyte population. However, it could equally be a product of MTOC culture and, after seven days, the input thymocytes within reaggregates may have failed. Finding evidence that MTOC could maintain a thymocyte population became the top priority.

Overall, from these studies it was concluded that MTOC support TEC proliferation and mTEC viability and organisation. However, further work was required to establish whether the MTOC can maintain *ex vivo* thymocytes and whether *ex vivo* TEC, which are able to express *Foxn1*, can mediate thymopoiesis. Finally, further optimisation of the GRID3D system is required before confocal microscopy can probe live reaggregates at the single cell resolution. This is essential to understand whether downregulation of *Foxn1* in some TEC is explained by the temporal or spatial mechanisms outlined above.

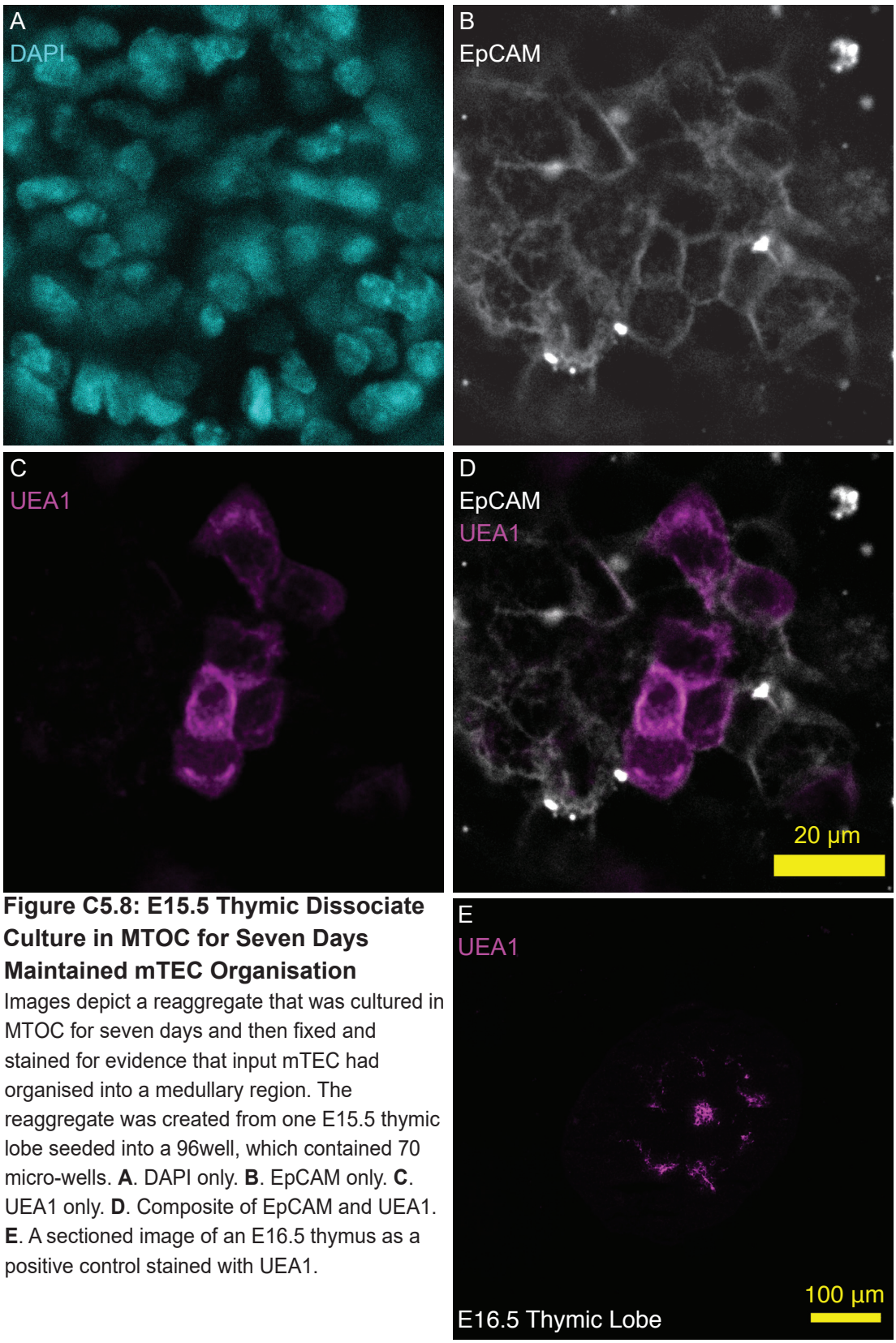

Figure C5.8: E15.5 Thymic Dissociate Culture in MTOC for Seven Days Maintained mTEC Organisation

Images depict a reaggregate that was cultured in MTOC for seven days and then fixed and stained for evidence that input mTEC had organised into a medullary region. The reaggregate was created from one E15.5 thymic lobe seeded into a 96well, which contained 70 micro-wells. **A**. DAPI only. **B**. EpCAM only. **C**. UEA1 only. **D**. Composite of EpCAM and UEA1. **E**. A sectioned image of an E16.5 thymus as a positive control stained with UEA1.

5.7. Identifying Minimal Cellular Input of iTEC

MTOC also has potential to be a useful tool to study iTEC. Given the inherent variability in cellular reprogramming, it is pertinent to evaluate iTEC using systems that are associated with low variability. Ultimately generating conclusions from the monolayer co-cultures in iTEC functionality polymer array (Chapter Four) was difficult due to the large contribution of stochastic variation to the results. The R^2 of the ANOVA was 0.338875, indicating most of the variation in the screen was not due to the dependant variable (polymer condition). Therefore, if polymers only contributed a small amount of variation it would be difficult to resolve from the noise of the technical variation. As discussed above, MTOC is more likely to fill this niche as it can provide a dramatic increase in the number of technical observations, while maintaining a 3D architecture.

The principal function of iTEC is to emulate TEC function, which is to mediate thymopoiesis. To what extend iTEC can do this was covered extensively in Chapter Three. For MTOC to be a useful culture method for iTEC, I needed to test two criteria. Firstly, whether iTEC could form reaggregates and secondly how to seed the haematopoietic component so it correctly interacted with the iTEC. There were two potential methods to introduce haemopoietic cells to the iTEC, allowing both to simultaneously reaggregate or testing whether the haematopoietic component could colonise pre-reaggregated iTEC. To answer these questions, the GRID3D system was set up in a 24-well plate. Each well contained 350 micro-wells with a diameter of 200 µm. iTEC were seeded into these wells at a concentration of 3.5×10^4 iTEC per 24well, or 100 iTEC per micro-well. The iTEC reaggregated over 24 hours at which time point, 7×10^4 haematopoietic stem cells ($Lin^-SCA\text{-}1^+c\text{-}KIT^+$) (LSKs) were added into the system (Figure C5.9 and C5.10A). Not all LSKs were able to infiltrate the iTEC-structure and these ‘excluded cells’ started to proliferate and adopted a cobble stone-like morphology (Figure C5.10B). By day, seven the LSKs had overgrown the micro-wells (Figure C5.10C). This failure prompted changes in the experimental design. Firstly, Adult ETPs were used in place of LSKs as it was assumed ETPs would have less proliferative capacity (Figure C4.17 outlines the ETP sorting strategy). ETPs were considered too scarce to be compatible with the 24-well plate format so this was changed to the 96-well plate

format, in which each 96well contained 70 micro-wells with a diameter of 500 μm. iTEC were seeded at 50, 100, 500 and 1000 iTEC plus 20 ETPS per micro-well, as 20 cells was indicated by SUN Bioscience to be the minimal number of cells necessary to ensure normal distribution of cells through all micro-wells. Bright field images were taken at 24 and 48 hours, seven and 14 days (Figure C5.11). All concentrations produced satisfactory reaggregates, which was a strikingly different result to that observed in the *ex vivo* thymic dissociate experiment. It maybe that purified TEC would also be able to reaggregate at any seeding density. The upper limit of 1000 iTEC per micro-well was justified by the total tissue requirement for a whole 96-well plate, which at this seeding density requires 6.72×10^6 cells and is the upper limit of what it is possible to produce using fluorescence activated cell sorting (FACS) over a period of two to three hours. For the next experiment, I wanted to test whether iTEC culture in MTOC were able to mediate T-cell differentiation. As discussed previously, low cell numbers limit the application of flow cytometric analysis to MTOC, so it was justified to make the aggregates as large as possible to mitigate this limitation in cell number.

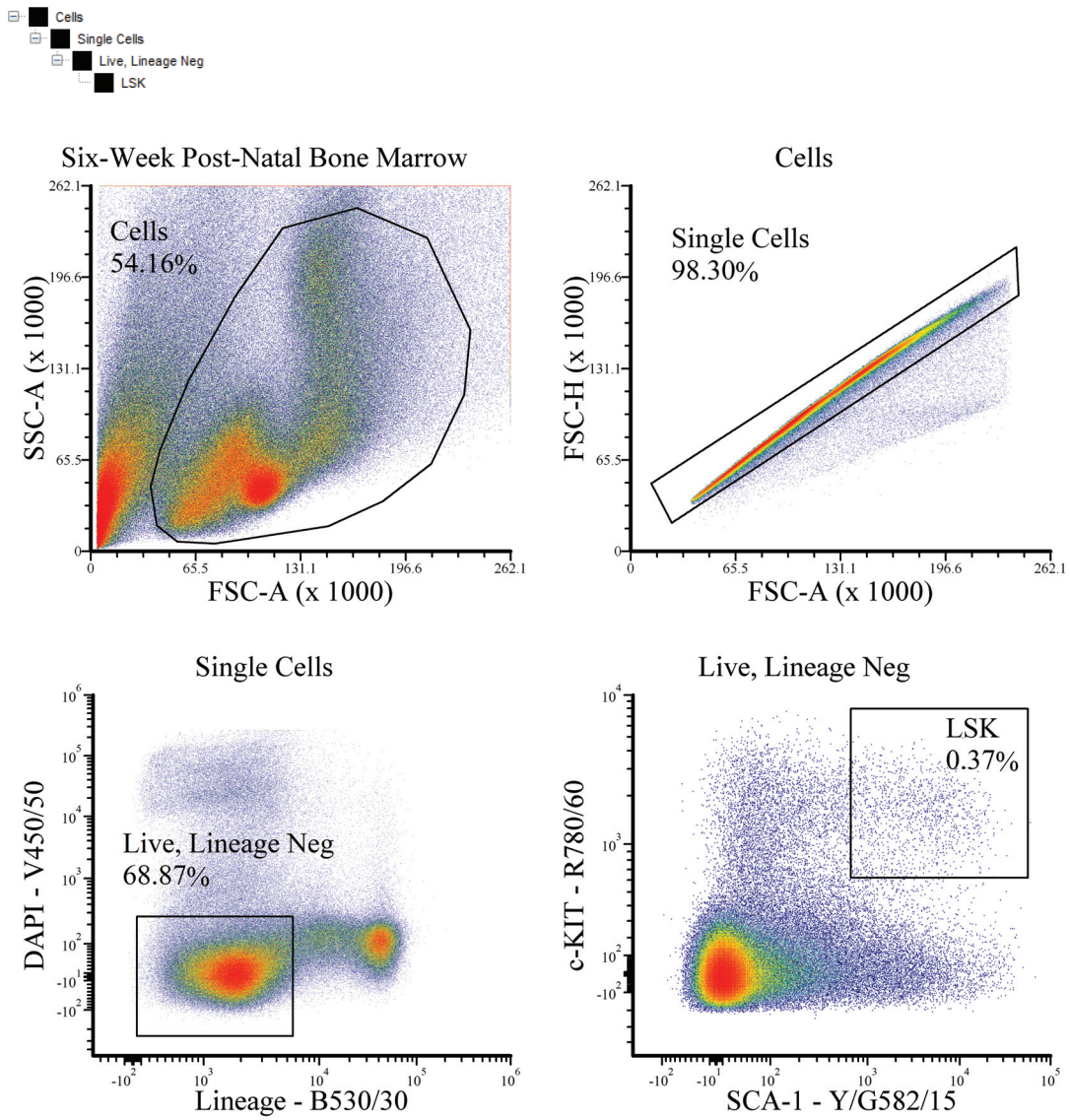

Figure C5.9: FACS Isolation Strategy for Post-Natal Murine Bone Marrow LSKs

The strategy use to FACS isolate LSKs from six-week post-natal murine bone marrow. LSKs were defined as Lineage$^-$SCA-1$^+$c-KIT$^+$ cells. The lineage cocktail included: CD3ϵ, CD4, CD5, CD11b, B220, Gr-1, TER-119.

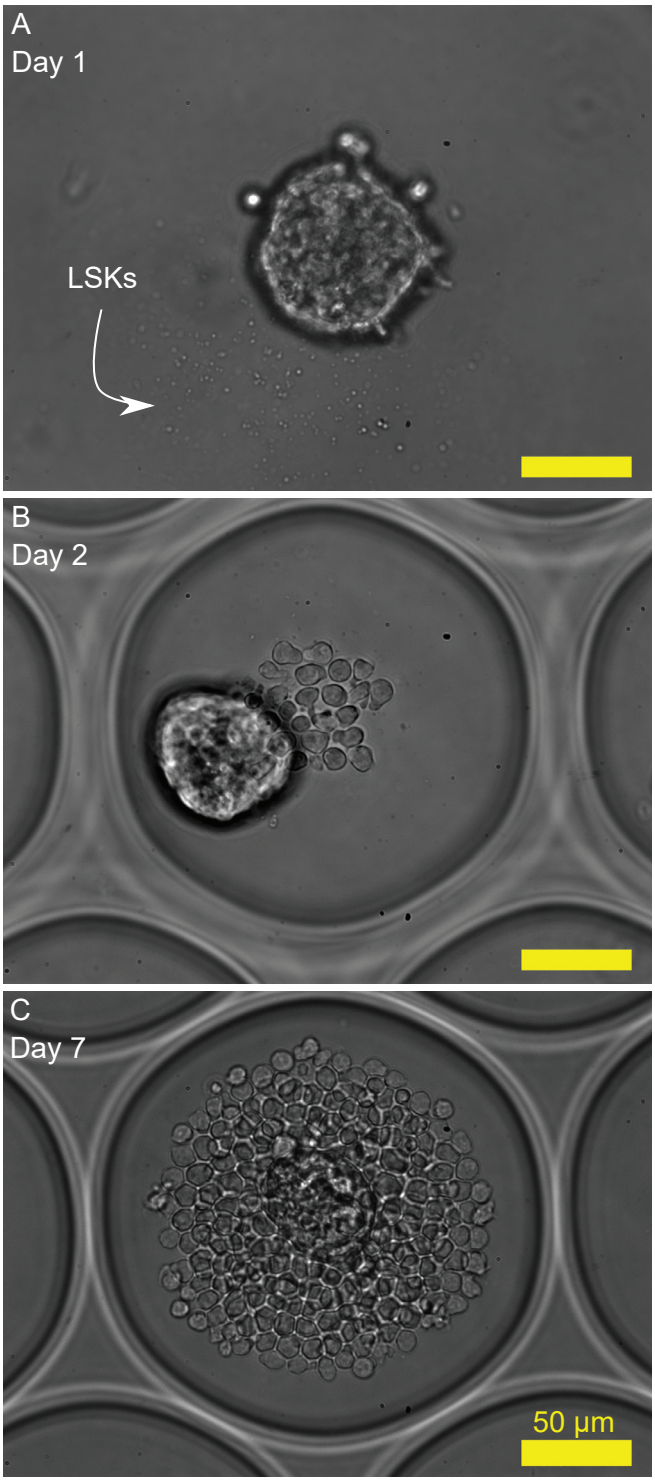

Figure C5.10: Seeding LSKs with iTEC Post-Reaggregation Failed to Control Proliferation

Images show iTEC seeded into the GRID3D system and allowed to reaggregate independently for 24 hours. This GRID3D mould used a diameter of 200 µm. **A**. LSKs were then seeded into the system to understand whether cells could infiltrate pre-aggregated structures. **B**. After a further 24 hours, LSKs that did not infiltrate the reaggregate adopted a cobble stone-like morphology. **C**. By day seven, LSKs proliferated uncontrollably and overgrew the micro-well.

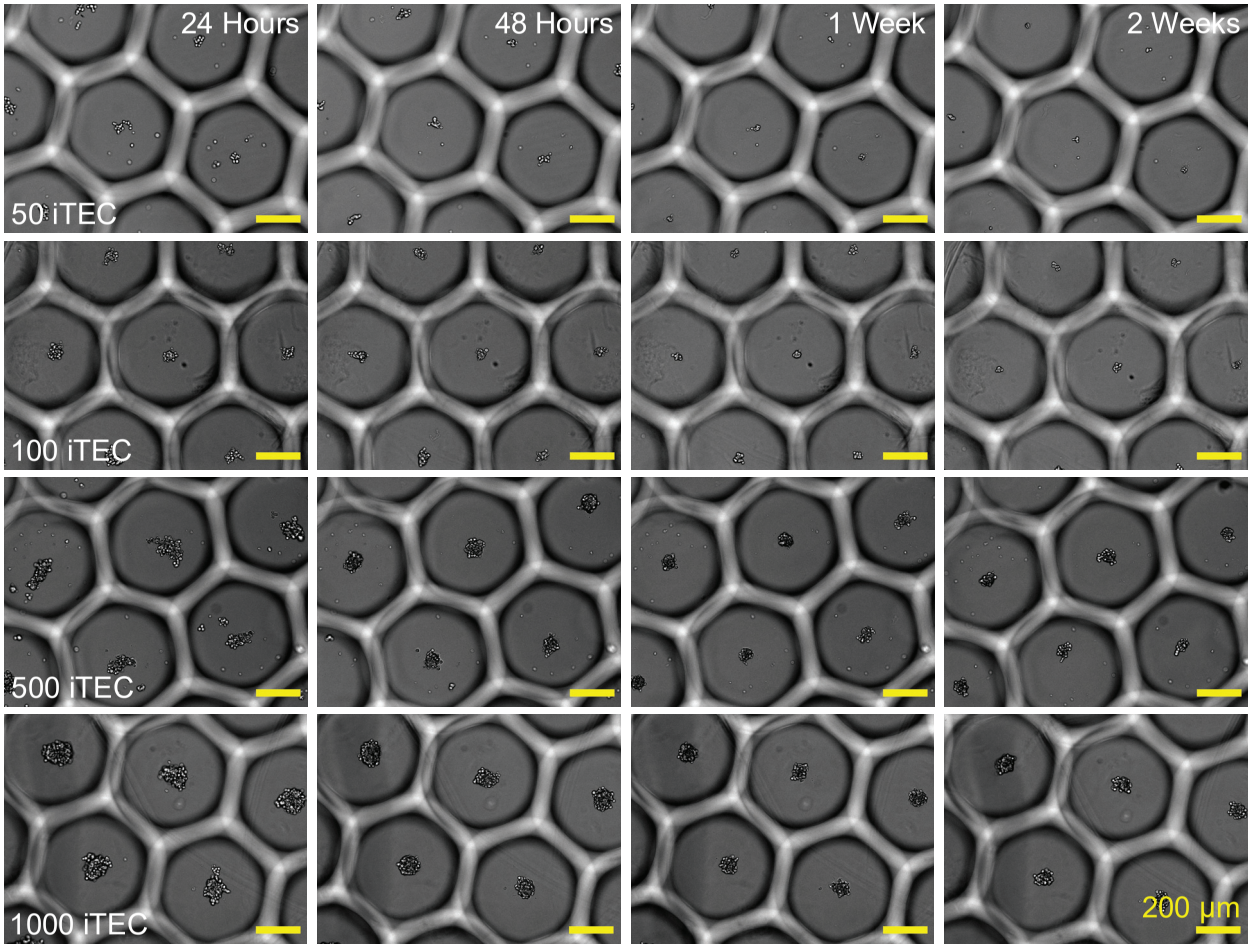

Figure C5.11: Optimising Seeding Density of iTEC Input into the GRID3D System

Images show reaggregates of iTEC and adult ETPs over 14 days cultured in MTOC. Each 96well contained 70 micro-wells with a diameter of 500 µm. Four seeding densities were tested: 50, 100, 500 and 1000 iTEC, each with 20 adult ETPs, per micro-well. Size of reaggregates was dependent on seeding density. All seeding densities, with the exception of 50 iTEC was considered capable of reaggregation.

5.8. iTEC Cultured in MTOC Mediate T-cell Differentiation More Consistently than Monolayers or RTOC

5.8.A. Enzymatic Digestion with TrypLE Express Affects Markers of Thymopoiesis

Flow cytometry was used to determine whether iTEC were able to mediate T-cell differentiation in MTOC. Given the success of TrypLE Express in disassociating reaggregates of *ex vivo* thymic tissue in MTOC, the same strategy was employed to prepare the iTEC-based reaggregates. Firstly, the action of TrypLE express on the markers of thymopoiesis was measured. WT thymocytes were isolated from a four-week postnatal thymus and separated into two groups. One was enzymatically digested with TrypLE express for five minutes at 37°C and agitated at 1400 rpm while one was incubated in FACS buffer. The cell suspensions were stained with the same panel outlined in Chapter Three to map thymopoiesis. CD25 and CD62L were undetectable in the treated group, while CD4, CD8, CD3ε and CD44 had decreased MFIs but were still effective as markers (Figure C5.1). Note that as in Chapter Three, the CD25 staining was not completely effective. TCRβ and CD69 were unperturbed in addition to the proportion of cells that were either 7-aminoactinomycin D (7AAD) or lineage positive. The lineage cocktail included: CD11b, CD11c, B220, Gr-1, Nk1.1, EpCAM, Ter119. Ultimately, it was decided that even with some perturbation of key markers, digestion with TrypLE express did not invalidate the flow cytometric readout.

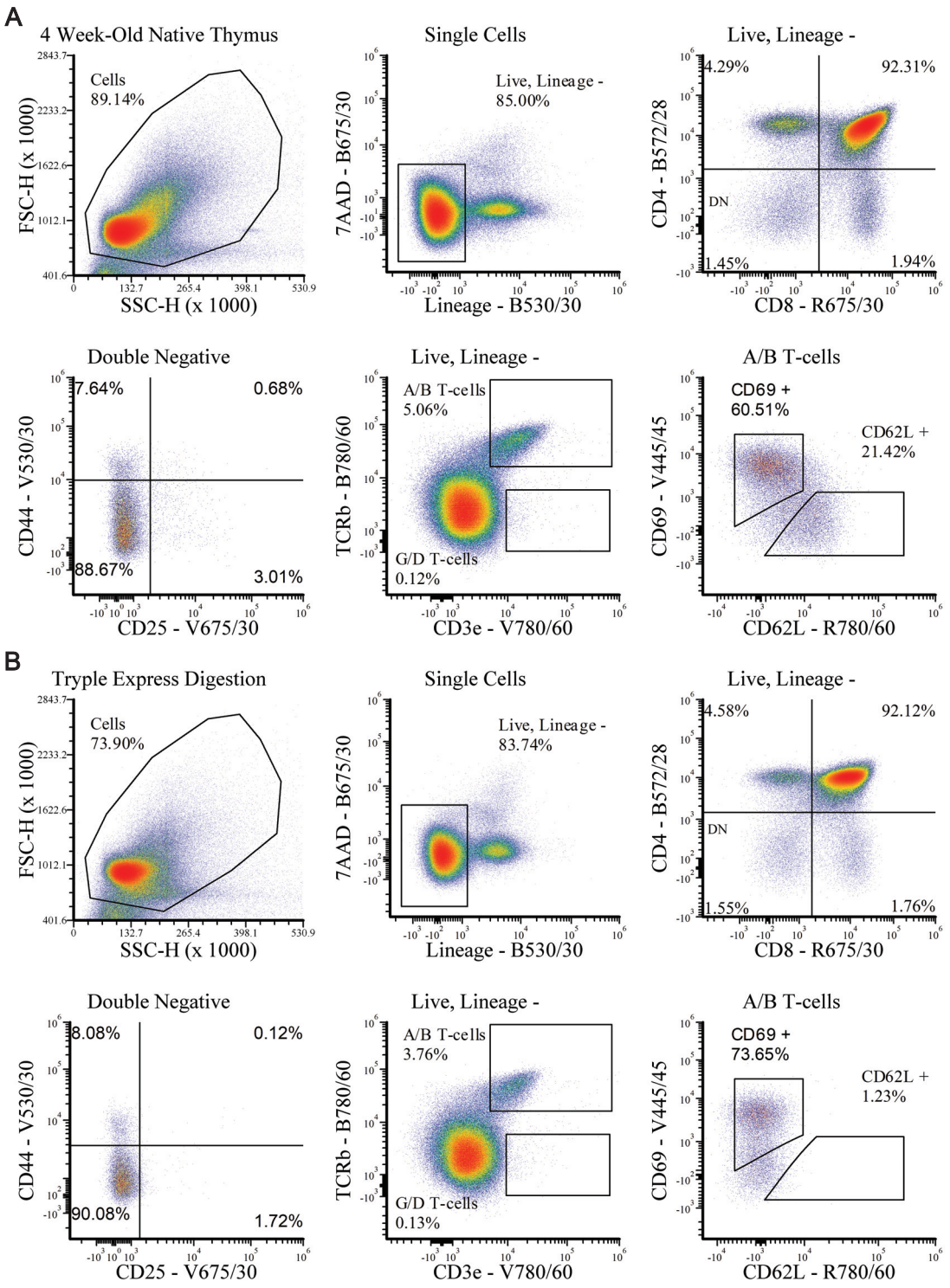

Figure C5.12: Characterising Enzymatic Action on Markers of Thymopoiesis

MTOC generates reaggregates with a small diameter, which are difficult to physically dissociate. An enymatic treatment protocol was optimised utilising TrypLE Express. Thymocytes were isolated from a four-week thymus and split into up groups. **A**. represented the untreated control. **B**. showed the effects of digestion. CD25 and CD62L were heavily effected while CD4, CD8 and CD44 showed a small decrease in MFI. Note the single cells plot was not biologically interesting and was omitted. CD11b, CD11c, B220, Gr-1, Nk1.1, EpCAM, Ter119.

5.8.B. iTEC Cultured in MTOC with Adult ETPs and WT MEFs Mediated T-cell Differentiation

An experiment was designed to find evidence that iTEC-based RTOC could mediate T-cell differentiation of adult ETPs. It was noted that mesenchyme is reported to be an essential RTOC component and MEFs are commonly used to supply mesenchymal cell function (Anderson *et al*., 1998, 1993; Anderson and Jenkinson, 2007; Suniara *et al*., 2000) Two conditions were tested as MTOC: One containing WT MEFs and one without. For the positive control, iTEC-based RTOC were generated using the compaction reaggregation method as described in Chapter Three (Sheridan *et al*., 2009). The numbers of input cells are listed in Table C5.1. The use of different input cell numbers between the MTOC and RTOC was unavoidable for technical reasons. Using the lower cell numbers for RTOC would not create a manually manipulatable cell pellet, while using higher numbers in the MTOC would saturate the moulds. After 14 days of culture in either method, reaggregates were enzymatically treated with TrypLE Express and then flow cytometrically analysed (Figures C5.13 – C5.20).

Firstly, it should be noted that there was a large difference in the performance of the iRTOC cultures, with one containing 198 DP thymocytes and the other 42,512 Figure C5.13 and C5.14. This was a larger difference than was observed in Chapter Three and it may reflect the use of a smaller number of adult ETPs rather than embryonic DN thymocytes. Focusing on the more successful replicate, 20% of the live lineage- gate was $CD4^{+}CD8^{+}$ double positive (DP) thymocytes, which was considered successful when compared to the iRTOC of Chapter Three, but there was a smaller than expected population of $CD4^{+}CD8^{-}$ single positive four (SP4) thymocytes. Furthermore, as seen previously in Chapter Three there was a large amount of $TCR\beta^{-}CD3\varepsilon^{+}$ cells in the live, $lineage^{-}$ gate, which were assumed to be γδ T-cells and these cells aberrantly contributed to the $CD4^{-}CD8^{+}$ single positive eight (SP8) subset. Both the bias away from SP4 thymocytes and bias toward γδ T-cells were reasoned to be associated with the batch of iTEC rather than the culture techniques.

Overall, the MTOC were considered capable of mediating T-cell differentiation however, the efficiency of this process was poor; much lower than in iRTOC as measured by the

proportion of DP thymocytes and TCRβ^{+}CD3ε^{+} αβ T-cells from the total live, lineage^{-} gate and there was an proportionate increase in the generation of TCRβ^{-}CD3ε^{+} γδ T-cells. Whether, this reflects that only a very smaller number of reaggregates were able to mediate this process or on average the ability of each reaggregates in MTOC was much poorer warrants further investigation and requires confocal microscopy to interrogate individual reaggregates. Interestingly, in accordance with the literature, the addition of WT MEFs was essential to observe any evidence of T-cell differentiation in the MTOC (Anderson *et al*., 1993).

The absolute cell counts of the CD4^{+}CD8^{+} (DP), CD4^{+}CD8^{-} (SP4), CD4^{-}CD8^{+} (SP8) and TCRβ^{+}CD3ε^{+} (αβ T-cells) were collected for each condition (Table C5.2). Note that monolayer data were taken from the iTEC Functionality Polymer Array, (Chapter Four) 0.1% gelatin, from independent experiment B. Although this was not collected concurrently and should not be directly compared to this experiment, it is representative of iTEC – ETP co-culture in monolayers and is useful for visualising the variance found in these experiments (Figure C5.21). It was decided that a comparison of means between iTEC-based RTOC and MTOC would be invalid. This is for two reasons. Firstly, the iRTOC was seeded with a 10-fold increase in ETPs compared to MTOC and the total thymocyte number is assumed to be dependent upon the availability of the niche, which must be greater in the larger RTOC structures. The format of the GRID3D system used in this experiment was a confounding variable. To compare RTOC with MTOC, the GRID3D system would need to contain just one micro-well, which would allow the same number of cells to be seeded into both culture methods. This would isolate the reaggregation process, which is likely to be slower in MTOC but free of the manual manipulation necessitated by RTOC. Secondly, the experiment was only performed once and comparing the means of just one technical replicate is unlikely to generate generalisable conclusions due to a lack of statistical power.

Given the ambition to develop MTOC as a methodology able to generate consistent outputs, the Coefficient of Variation (CoV) found between all technical replicates was compared (Table C5.3). Again, these data were collected from only one independent experiment, so no

statistics were performed. However, the variation was dramatically lower in the MTOC than the RTOC and monolayer groups.

Overall, these data indicate that iTEC cultured in RTOC outperform those cultured in MTOC, in terms of mediating T-cell differentiation. Whether the poor efficiency shown in MTOC was a product of only a few reaggregates being able to mediate T-cell differentiation or a lower ability on average across each 96well warrants further investigation. However, MTOC produced a much more consistant data set, and therefore would be a more suitable tool for screening experiments if the issues related to thymopoiesis could be overcome. iTEC within the experiment were unable to effectively support generation of SP4 thymocytes, reinforcing that this technology requires further optimisation. Finally, WT MEFs were found to be beneficial when included in MTOC and supported iTEC to mediate more efficient T-cell differentiation in MTOC.

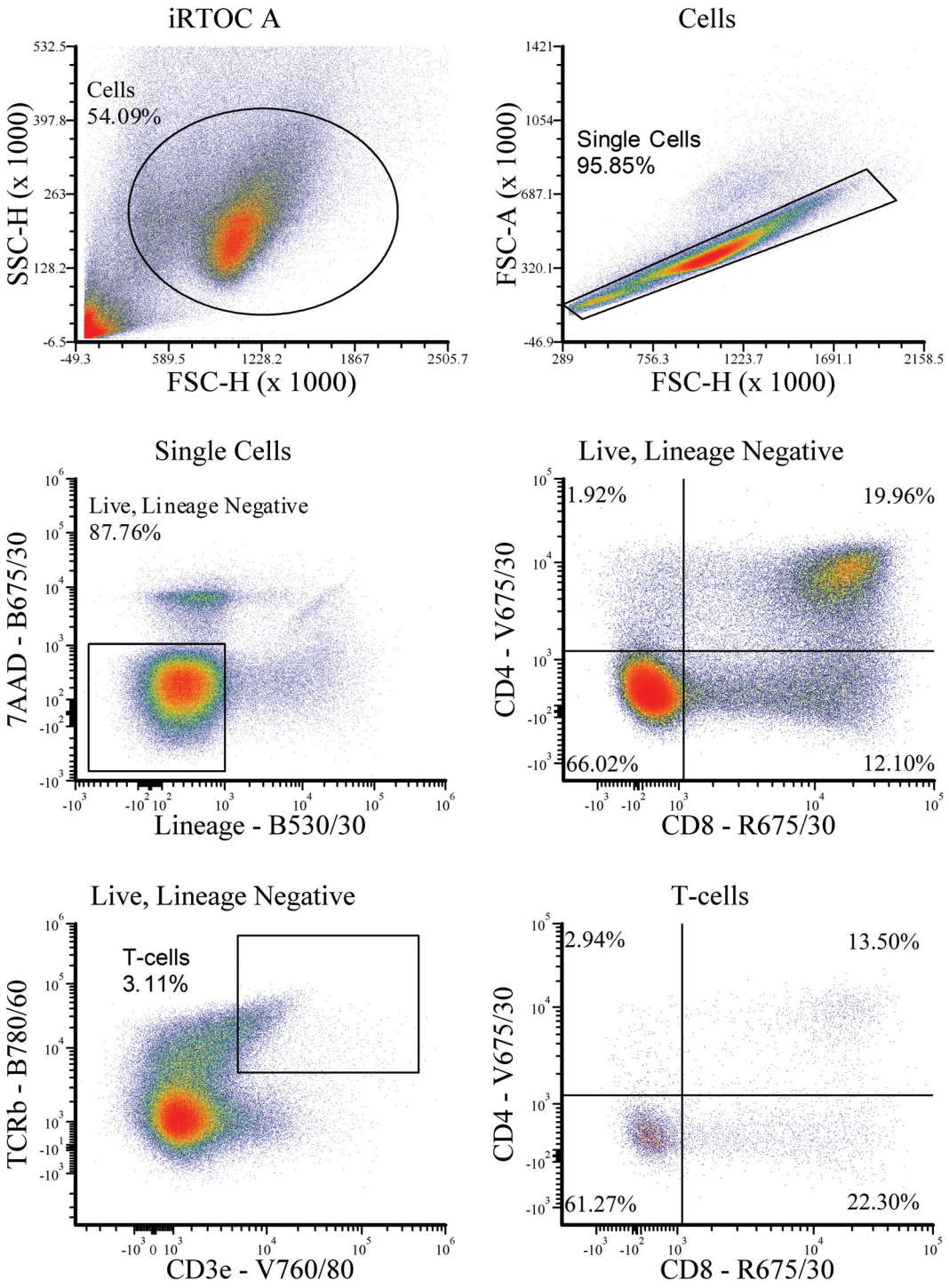

Figure C5.13: MTOC Mediated Thymopoiesis is Less Variable than Other Culture Methods - iRTOC A

iTEC, adult ETPS and WT MEFs were cultured using RTOC and MTOC. After 14 days of co-culture the structures were enzymatically disassociated. The plots show the thymocyte subset profile of iRTOC replicate A. Note that CD25, CD44 and CD62L were omitted from this thesis' routine panel due to the enzymatic digestion and the build up of TCRβ^{+}CD3ε^{+}CD4^{-}CD8^{-} thymocytes. Lineage cocktail includes: CD11b, CD11c, B220, Gr-1, Nk1.1, EpCAM, Ter119. N=1.

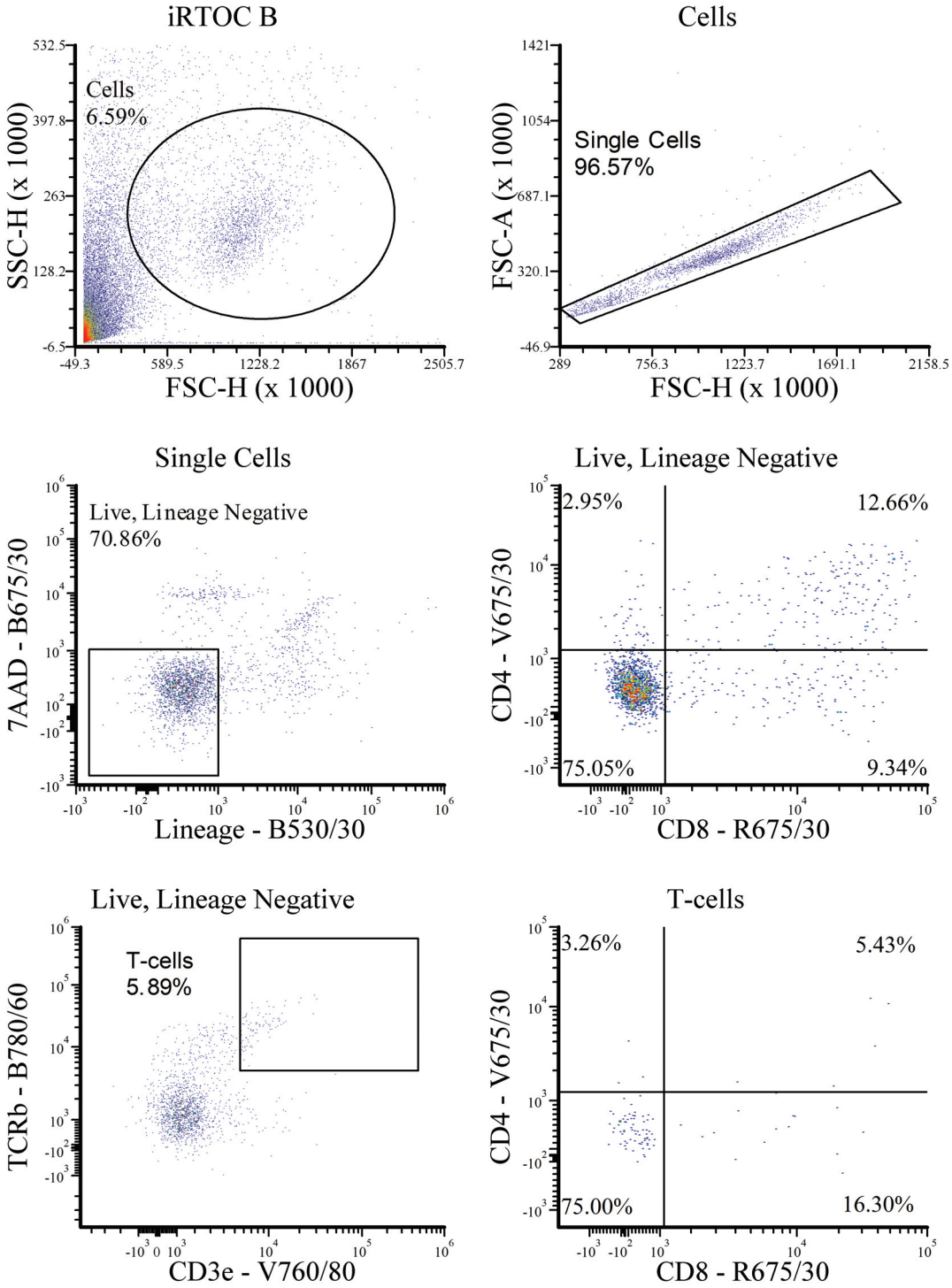

Figure C5.14: MTOC Mediated Thymopoiesis is Less Variable than Other Culture Methods - iRTOC B

iTEC, adult ETPS and WT MEFs were cultured using RTOC and MTOC. After 14 days of co-culture the structures were enzymatically disassociated. The plots show the thymocyte subset profile of iRTOC replicate B. Note that CD25, CD44 and CD62L were omitted from this thesis' routine panel due to the enzymatic digestion. Lineage cocktail includes: CD11b, CD11c, B220, Gr-1, Nk1.1, EpCAM, Ter119. N=1.

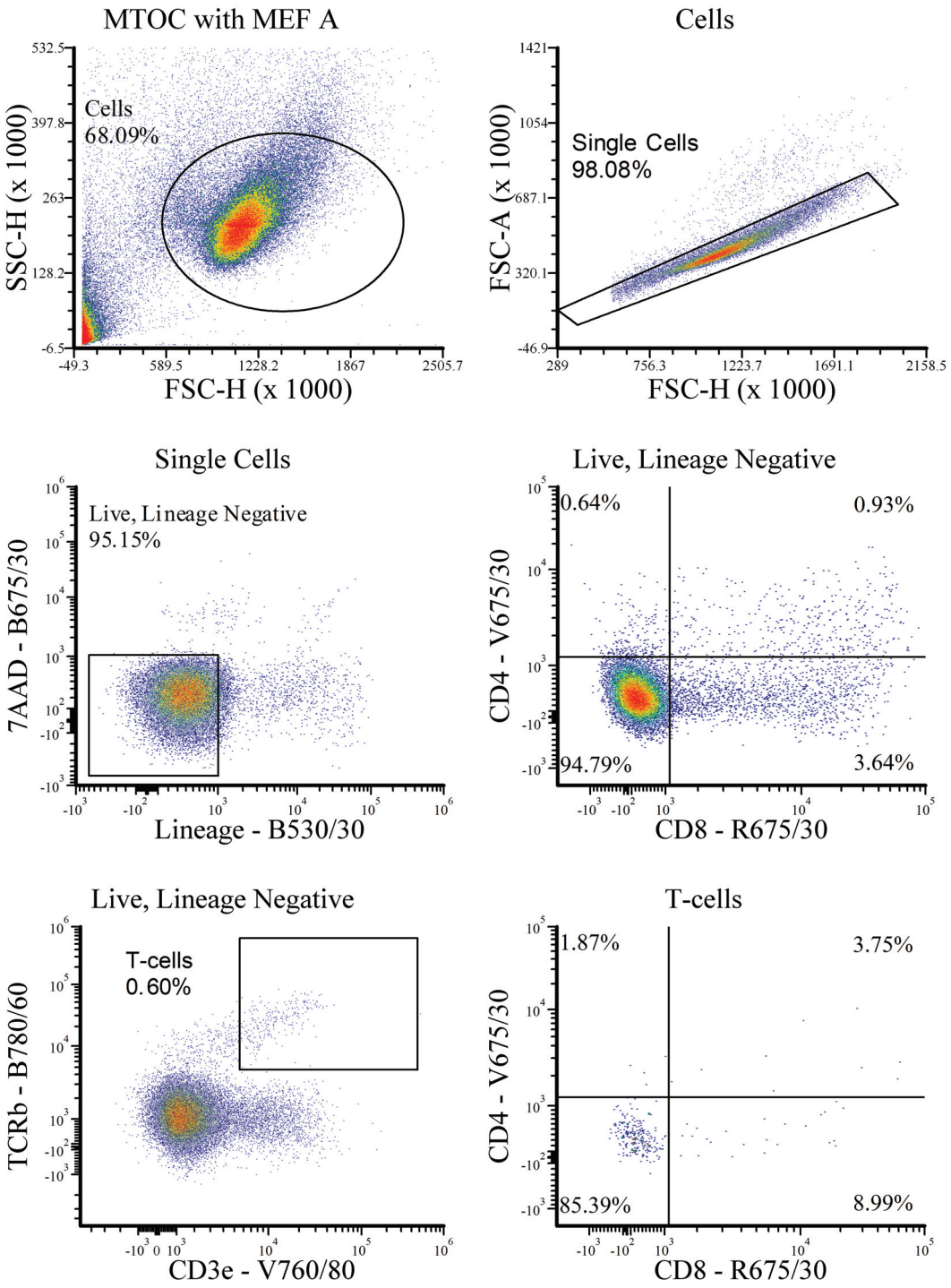

Figure C5.15: MTOC Mediated Thymopoiesis is Less Variable than Other Culture Methods - MTOC with MEFs A

iTEC, adult ETPS and WT MEFs were cultured in MTOC. After 14 days, all reaggreagtes were removed from the GRID3D system and enzymatically disassociated. The plots show the thymocyte subset profile of MTOC with MEFs replicate A. Note that CD25, CD44 and CD62L were omitted from this thesis' routine panel due to the enzymatic digestion. Lineage cocktail includes: CD11b, CD11c, B220, Gr-1, Nk1.1, EpCAM, Ter119. N=1.

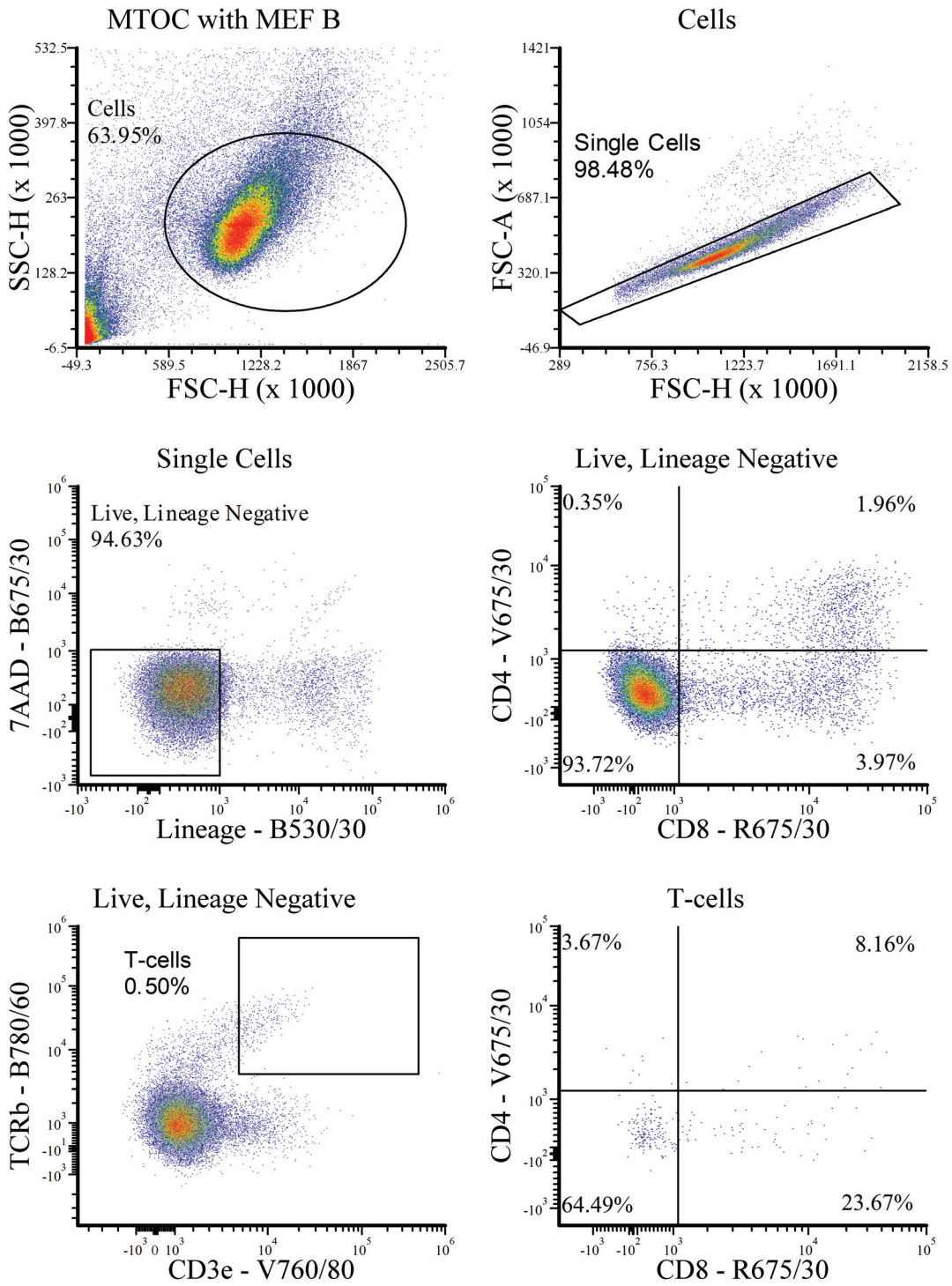

Figure C5.16: MTOC Mediated Thymopoiesis is Less Variable than Other Culture Methods - MTOC with MEFs B

iTEC, adult ETPS and WT MEFs were cultured using RTOC and MTOC. After 14 days of co-culture the reaggregates were enzymatically disassociated. The plots show the thymocyte subset profile of MTOC with MEFs replicate B. Note that CD25, CD44 and CD62L were omitted from this thesis' routine panel due to the enzymatic digestion. Lineage cocktail includes: CD11b, CD11c, B220, Gr-1, Nk1.1, EpCAM, Ter119. N=1.

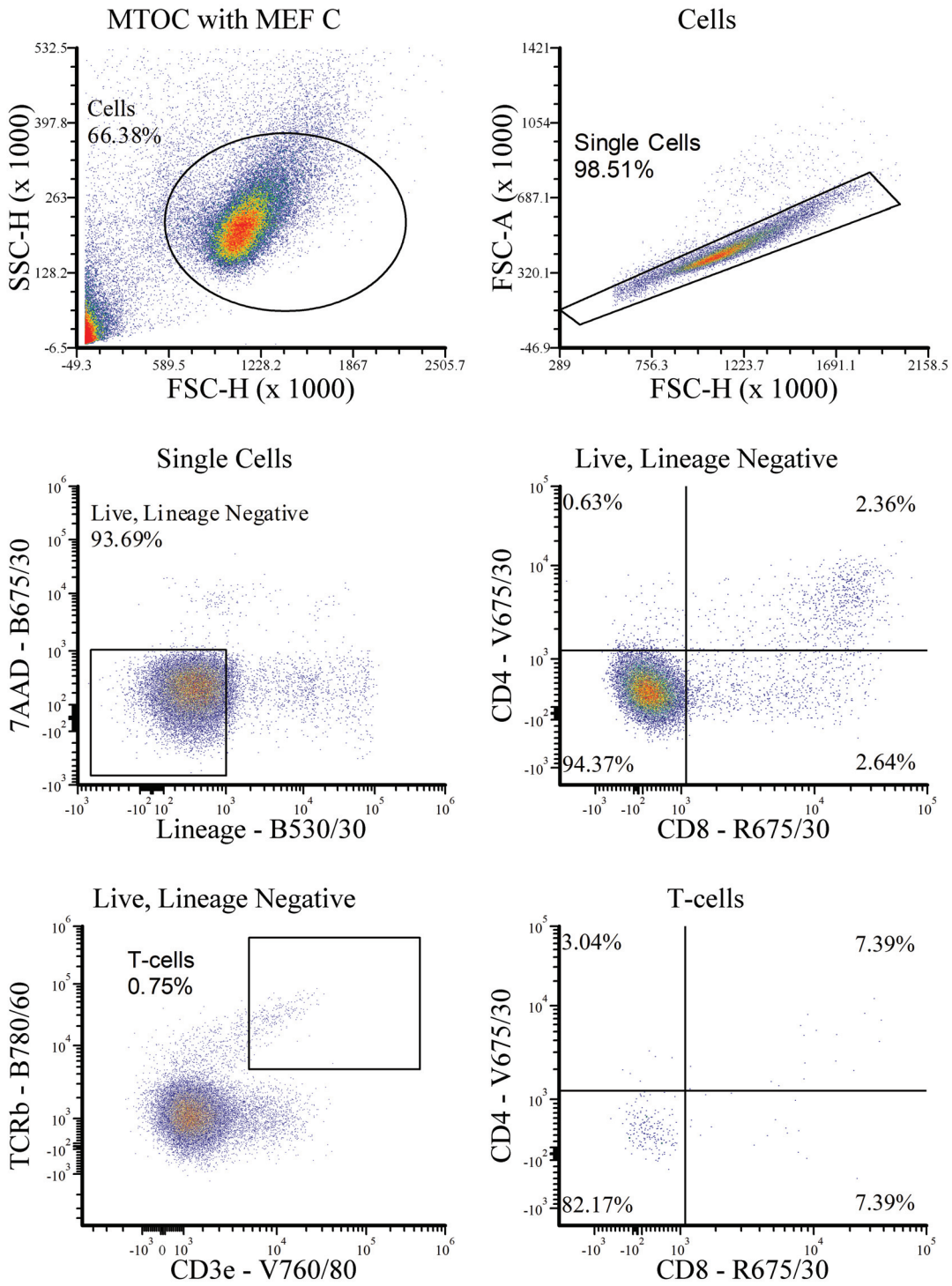

Figure C5.17: MTOC Mediated Thymopoiesis is Less Variable than Other Culture Methods - MTOC with MEFs C

iTEC and adult ETPS were cultured using MTOC. After 14 days of co-culture the reaggregates were enzymatically disassociated. The plots show the thymocyte subset profile of MTOC with MEFs replicate C. Note that CD25, CD44 and CD62L were omitted from this thesis' routine panel due to the enzymatic digestion. Lineage cocktail includes: CD11b, CD11c, B220, Gr-1, Nk1.1, EpCAM, Ter119. N=1.

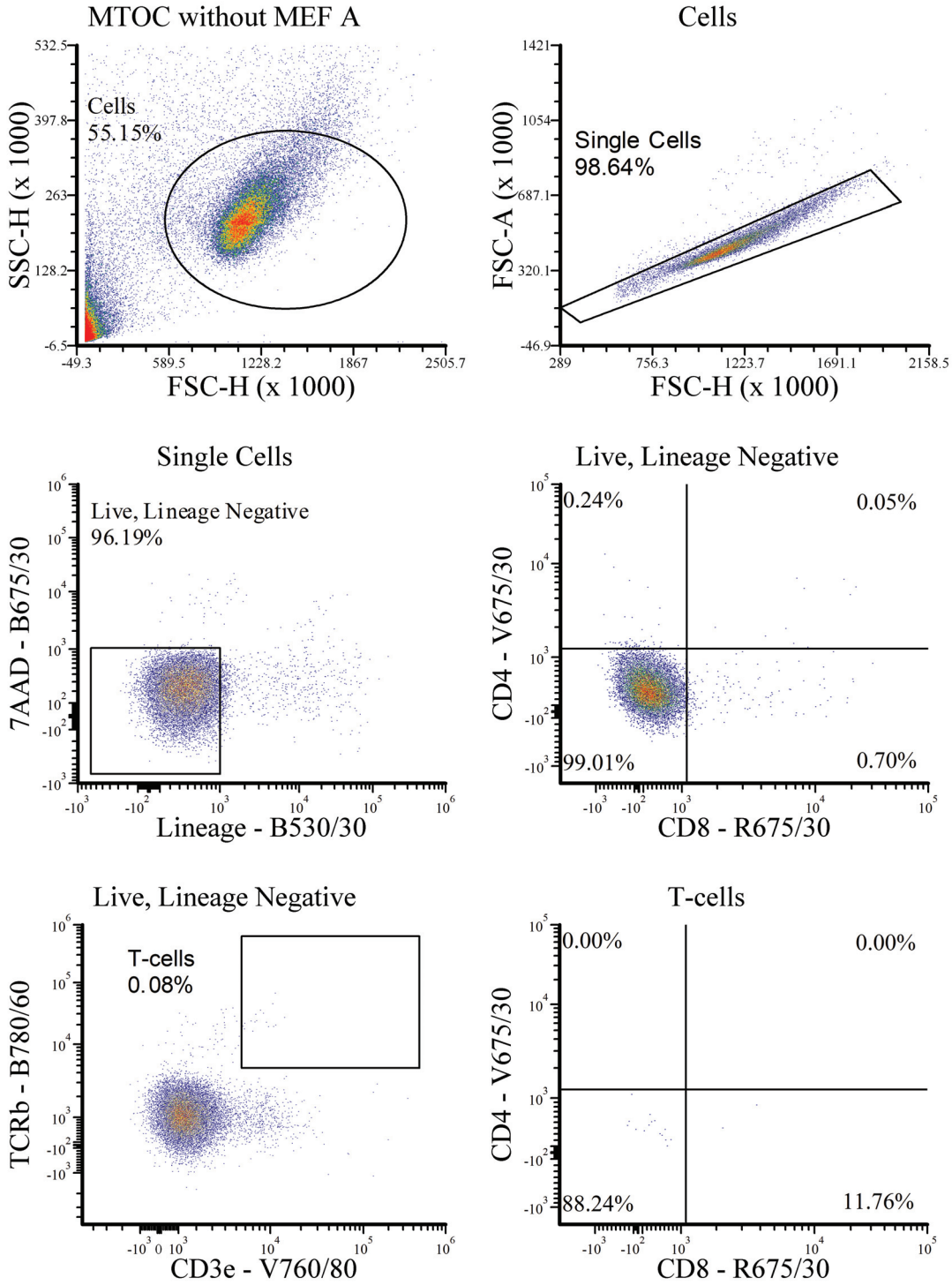

Figure C5.18: MTOC Mediated Thymopoiesis is Less Variable than Other Culture Methods - MTOC without MEFs A

iTEC and adult ETPS were cultured using MTOC. After 14 days of co-culture the reaggregates were enzymatically disassociated. The plots show the thymocyte subset profile of MTOC without MEFs replicate A. Note that CD25, CD44 and CD62L were omitted from this thesis' routine panel due to the enzymatic digestion. Lineage cocktail includes: CD11b, CD11c, B220, Gr-1, Nk1.1, EpCAM, Ter119. N=1.

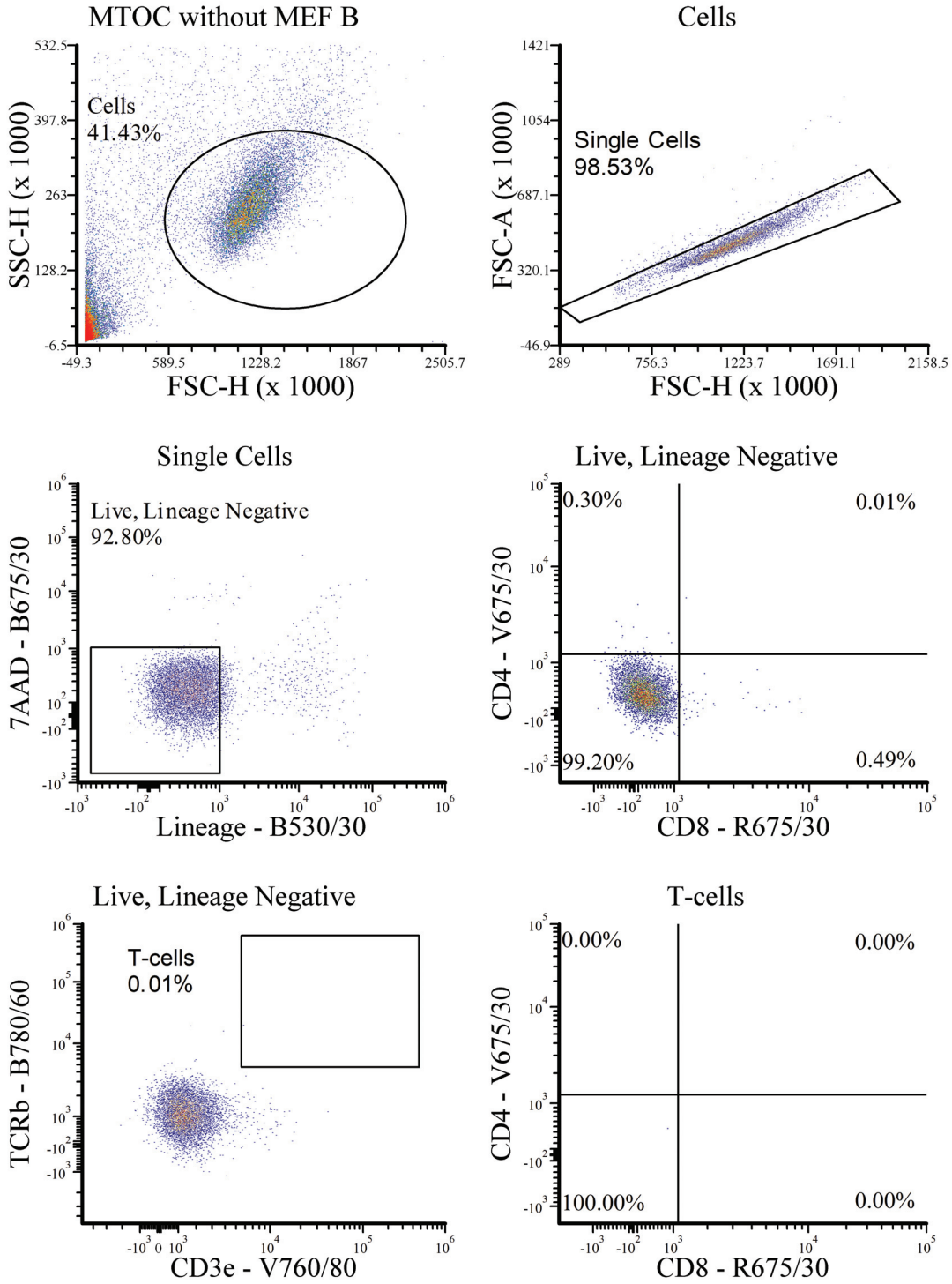

Figure C5.19: MTOC Mediated Thymopoiesis is Less Variable than Other Culture Methods - MTOC without MEFs B

iTEC and adult ETPS were cultured using MTOC. After 14 days of co-culture the reaggregates were enzymatically disassociated. The plots show the thymocyte subset profile of MTOC without MEFs replicate B. Note that CD25, CD44 and CD62L were omitted from this thesis' routine panel due to the enzymatic digestion. Lineage cocktail includes: CD11b, CD11c, B220, Gr-1, Nk1.1, EpCAM, Ter119. N=1.

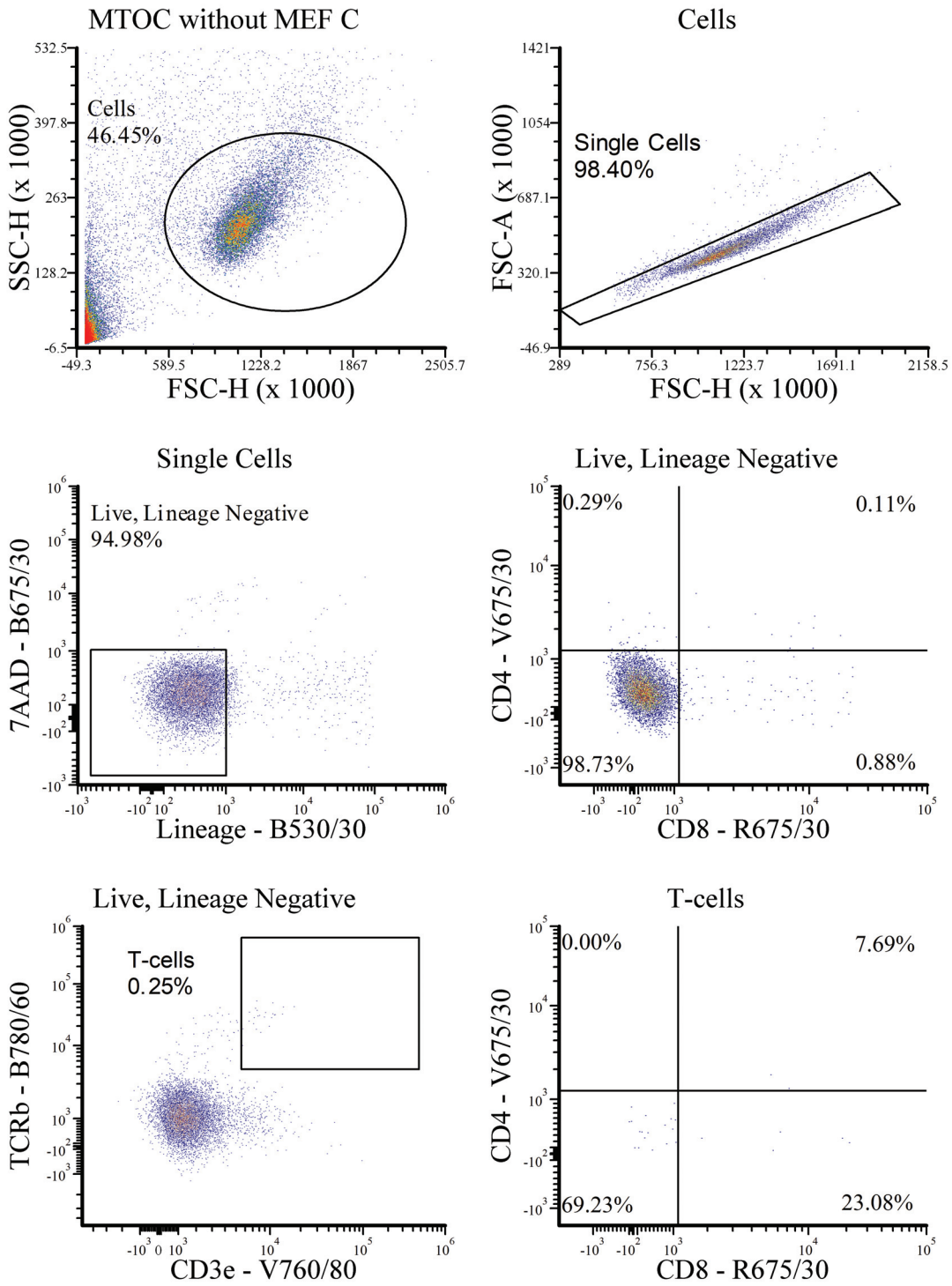

Figure C5.20: MTOC Mediated Thymopoiesis is Less Variable than Other Culture Methods - MTOC without MEFs C

iTEC and adult ETPS were cultured using MTOC. After 14 days of co-culture the reaggregates were enzymatically disassociated. The plots show the thymocyte subset profile of MTOC without MEFs replicate C. Note that CD25, CD44 and CD62L were omitted from this thesis' routine panel due to the enzymatic digestion. Lineage cocktail includes: CD11b, CD11c, B220, Gr-1, Nk1.1, EpCAM, Ter119. N=1.

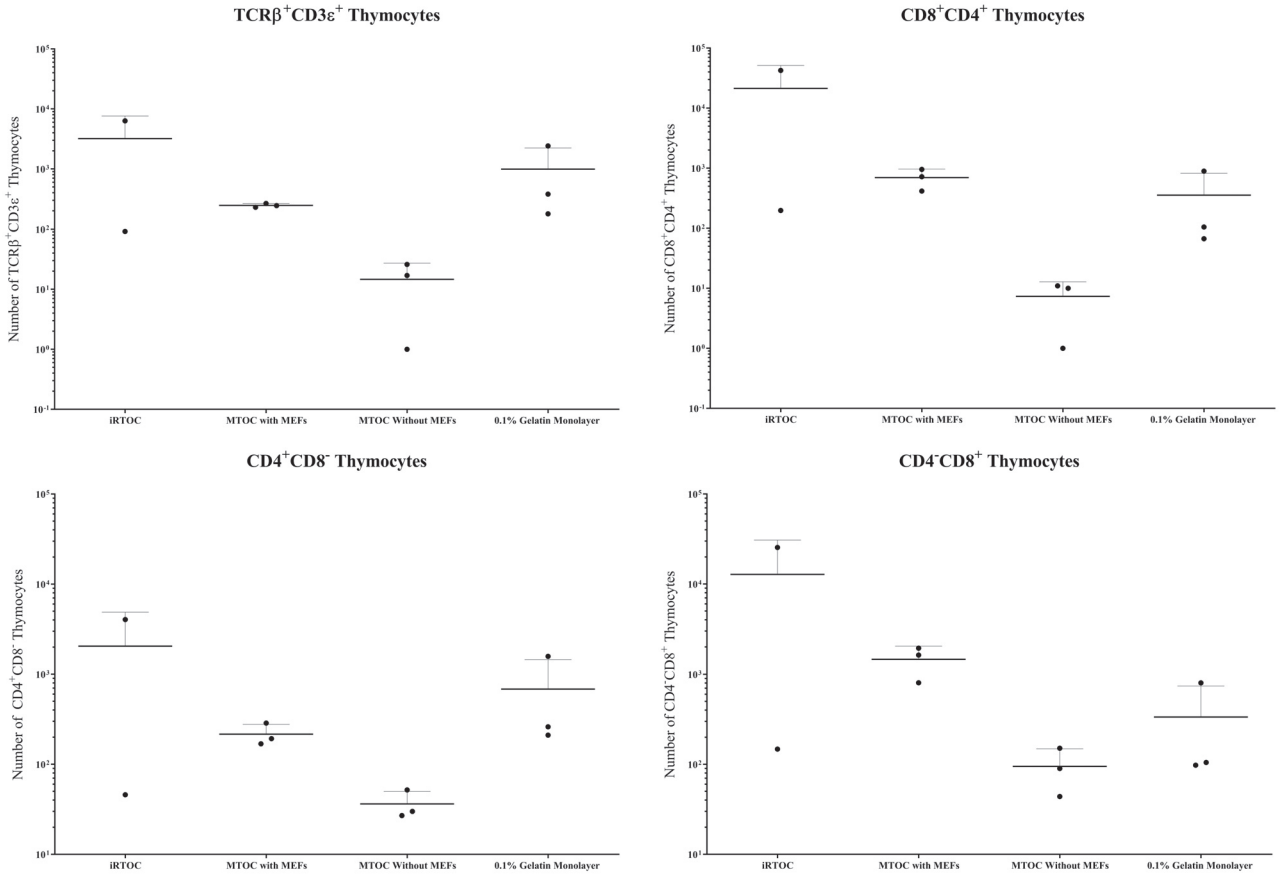

Figure C5.21 Absolute Thymocyte Counts of iTEC Co-cultured with ETPs using RTOC, MTOC and Monolayers After 14 Days

Graphs depicts the count of each thymocyte sub-population recovered after 14 days. iRTOC and MTOC with MEF conditions were co-cultures of iTEC, adult ETPs and WT MEFs, while Monolayer and MTOC without MEF groups contained only iTEC and ETPs. Each data point represents one iRTOC or one 96well of 70 MTOC reaggregates. N=1 for all conditions except the monolayer condition. This data was taken from biological replicate B of the 0.1% Gelatin condition from the iTEC polymer array and is representative of the data trends.

Table C5.1: Input Cell Numbers Used in the T-cell Differentiation Variation Test.
The table depicts the input cell numbers used in each condition

Cell Type	*RTOC per Reaggregate*	*MTOC with MEFS per well (i.e. per 70 micro-wells)*	*MTOC without MEFs per well (i.e. per 70 micro-wells)*	*Monolayer (per 24well)*
iTEC	7×10^5	7×10^4	7×10^4	2×10^4
ETP	7×10^3	7×10^2	7×10^2	5×10^2
MEF	1.2×10^5	1.2×10^4	-	-

Table C5.2: The Absolute Cell Count Collected from Each Culture Method in the T-cell Differentiation Variation Test.
The table shows the absolute cell counts of the thymocyte subsets found in each culture method per iRTOC or 96well of 70 reaggregates.

Culture Method and Replicate	*$CD4^+CD8^-$ Thymocytes*	*$CD4^-CD8^+$ Thymocytes*	*$CD4^+CD8^+$ Thymocytes*	*$TCR\beta^+CD3\varepsilon^+$ Thymocytes*
iRTOC A	4054	25507	42512	6333
iRTOC B	46	148	198	92
MTOC with MEF A	287	1627	417	267
MTOC with MEF B	169	1940	956	245
MTOC with MEF C	193	808	723	230
MTOC without MEF A	52	151	10	17
MTOC without MEF B	27	44	1	1
MTOC without MEF C	30	90	11	26

Table C5.3: CoVs in T-cell Differentiation Variation Test.
Table shows the CoV found between each replicate and compares this across culture method.

CoV of Thymocyte sub-population cell count	*RTOC*	*MTOC with MEFS*	*MTOC without MEFs*	*Representative 0.1% gelatin Monolayer*
$CD4^{+}CD8^{-}$	138.2%	28.8%	37.6%	113.5%
$CD4^{-}CD8^{+}$	139.8%	40.1%	56.5%	120.9%
$CD4^{+}CD8^{+}$	140.1%	38.7%	75.1%	131.5%
$TCR\beta^{+}CD3\varepsilon^{+}$	137.4%	7.5%	86.3%	124.8%

5.9. iTEC Differentiate into UEA1 Expressing mTEC-like Cells in MTOC

In the initial publication, it was reported that iTEC were able to differentiate into mTEC-like cells and form medullary regions when engrafted onto the kidney capsule of a syngeneic mouse (Bredenkamp *et al*., 2014). Thus, to test whether iTEC were able to differentiate into mTEC-like cells using the marker UEA1 in MTOC, 1000 iTEC were seeded into each micro-well of the 24well format, containing 350 micro-wells with a diameter of 200 μm, as previously described. After 14 days, the reaggregates were fixed and stained for cytokeratins and UEA1 and with DAPI. The confocal imaging was performed differently than in previous experiments, in that reaggregates were removed from the GRID3D system before imaging. This removed the factor limiting the penetration of light into reaggregates. Most reaggregates contained a central Cytokeratin^{+}UEA1^{+} cell, which was taken to be evidence of iTEC differentiating into a mTEC-like cell (Figure C5.22). Note, as explained in Chapter Four, UEA1 is not a functional marker of mTEC. However, these data represent an interesting first step in using iTEC as a tool to identify factors that promote medulla differentiation. Overall, this was taken as evidence that iTEC could differentiate into mTEC-like cells, but further investigation is warranted to observe whether such cells are genuinely mTEC, and were capable of promiscuous gene expression.

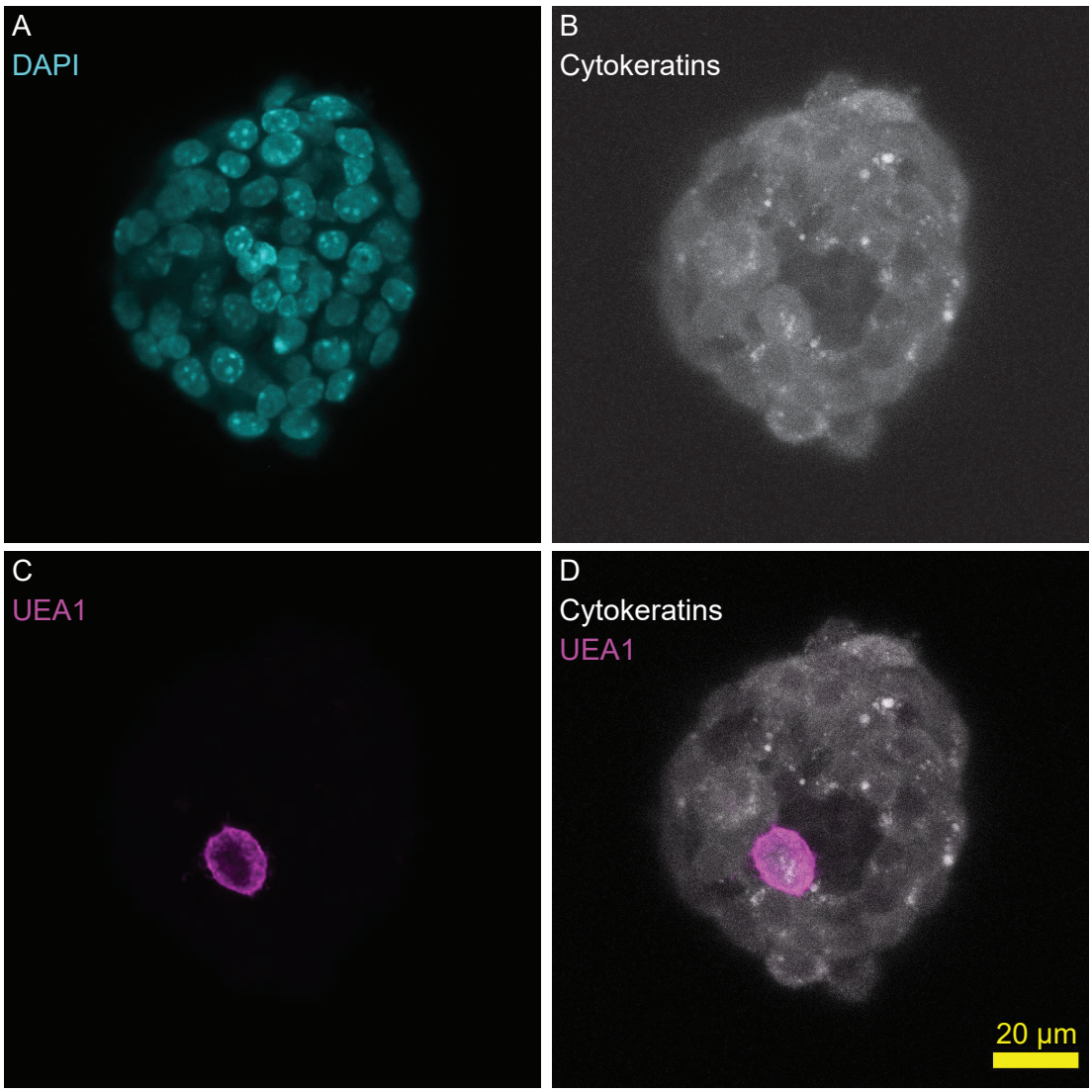

Figure C5.22: iTEC Differentiated into UEA1 Positive mTEC-like Cells when cultured in MTOC

Images show a reaggregate, created by seeding only iTEC into the GRID3D system and culturing for seven days as MTOC. At this point, all reaggregates were removed from the GRID3D system, fixed and stained for evidence of mTEC-like cells. Figure shows the representative, central UEA1^{+} iTEC found in reaggregates. **A**. DAPI only. **B**. Cytokeratins only. **C**. UEA1 only. **D**. Composite of cytokeratins and UEA1.

5.10. Concluding Remarks.

Chapters Three and Four employed RTOC and monolayer culture, respectively. These techniques ultimately comprise the entire traditional range of culture methods for thymus biology. However, this thesis identified that these methods are not optimal for screening experiments and there exists a technical niche to develop a tool for thymus biology that is able to deliver precision on specific readouts and in high throughput. While this chapter relies on some preliminary data (N=1), it argues that MTOC have the potential to fill that niche. Currently, MTOC requires further optimisation, this thesis has highlighted that areas in which the system should be improved, particularly to perform real time microscopy at the single cell resolution. However, MTOC proved to be able to meet the criteria of maintaining *Foxn1* expression in *ex vivo* TEC and for iTEC-based reaggregates to mediate T-cell differentiation. Further work is required to increase the number of replicates for these experiments, but confidence is conferred upon these conclusions as MTOC employs a large number of technical observations.

6. Chapter Six: Concluding Remarks

6.1. Summary of Experimental Results

This thesis investigated the manufacture of iTEC; whether novel polymer matrices could reduce the variation associated with iTEC culture in monolayers; and a new method of three-dimensional (3D) culture, which specifically aimed to deliver precision in a high throughput context.

In Chapter Three, I defined a process to maximise the number of iTEC produced from a single embryo, by increasing the number of passages that MEFs underwent before initiation of reprogramming and testing the possibility of including a cryopreservation step. I also optimised the medium conditions, concentration of (Z)-4-Hydroxytamoxifen (4OHT) and reprogramming length. To ensure the optimised method for manufacturing iTEC did not compromise on functionality, I compared the *in vitro* behaviour of iTEC to *ex vivo* TEC using reaggregate thymic organ culture (RTOC). From this I demonstrated that iTEC were able to efficiently mediate thymocyte transition from the $CD4^{-}CD8^{-}$ double negative (DN) stage to $CD4^{+}CD8^{+}$ double positive (DP) phase but there were differences between *ex vivo* TEC and iTEC in mediating positive selection and the transition between DP to $CD4^{+}CD8^{-}$ or $CD4^{+}CD8^{-}$ single positive (SP) phases, particularly in thymocyte expression of CD3ε, TCRβ, CD69. I also demonstrated that the outcomes of iTEC-mediated thymopoiesis remained highly variable both within a single batch, represented by differences between iTEC-based RTOC (iRTOC), and between batches.

In Chapter Four, I tested whether synthetic polymers that could specifically bind TEC rather than MEFs could be identified by screening a library of polymers; I was able to identify a panel of 12 polymers with this property. A major observation was that iTEC share a similar adhesion profile to *ex vivo* TEC, based on their compatibility with a similar set of synthetic polymers to native TEC. When I tested the effect of culturing iTEC upon the selected synthetic polymers, polymers 396 and 427 showed promise for both reducing the variablity shown by the iTEC system and improving the ability of iTEC to mediate T-cell differentiation, although this result did not produce significance. I also showed that culture on select polymers did not promote a functional medullary phenotype in iTEC. Furthermore, I showed

that culture of *ex vivo* TEC on the selected polymers was not sufficient to produce an environment conducive to the maintenance of *Foxn1* expression, either in the presence of serum or in serum-free medium supplemented with growth factors BMP4, FGF7 and EGF.

In Chapter Five, I employed the GRID3D system (SUN Bioscience), which uses the synthetic polymer polyethylene glycol, which does not allow cell adhesion, to create a miniaturised-reaggregate thymic organ culture (MTOC) system. I showed that MTOC was able to maintain *Foxn1* expression in *ex vivo* TEC when cultured as whole E14.5 and E15.5 thymic dissociates. However, it remains a striking observation that not all TEC were able to do this. Some reaggregates, within the same well and created from the same suspension of thymic dissociate, were unable to maintain *Foxn1* expression. Furthermore, I demonstrated that MTOC was able to mediate T-cell differentiation to produce more consistent results than in concurrent RTOC using the iTEC system.

6.2. Conclusions and Future Work

The overall hypothesis detailed in Chapter One was that iTEC in conjunction with synthetic matrices, could be used generate thymic organoids that recapitulate the fundamental processes via which TEC mediate T cell differentiation and repertoire selection. This overarching hypothesis was broken down into smaller hypotheses for each chapter and these will be discussed before returning to conclude the extent it was found to be true or false.

I tested the hypothesis in Chapter Three that the iTEC system could produce a large quantity of cells competent to recapitulate *ex vivo* TEC function *in vitro.* The first part was found to be true since increasing the passage number of MEFs increased the total yield of iTEC without comprising on functionally. Although expanding MEFs will not be able to generate the same number of cells as using cell lines such as the OP9-DLL1 and MS5-hDLL1, the number of iTEC that can be produced in a given timeframe is no longer limited by sourcing sufficient MEFs but in separating the GFP^+ from the GFP^- fractions.

With respect to how competent iTEC are in recapitulating the *ex vivo* behaviour of TEC in RTOC, it was concluded that iTEC were able to mediate T-cell differentiation, albeit at

reduced kinetics compared to *ex vivo* TEC, but may not able to mediate normal positive selection based on expression of CD3ε , TCRβ and CD69.

Therefore, I concluded that iTEC were able to be scaled up to provide a more abundant source of cells than the native thymus and iTEC were able to recapitulate some aspects of *ex vivo* TEC behaviour. However, whilst I made progress in progressing the iTEC system into a standardised tool, further optimisation is still required to reduce variation in the system, and to confer full TEC functionality as revealed by assays of fine details. Furthermore, given that iTEC express much of the machinery required to process and present peptides in a physiologically relevant manner, the differences between the ability of iTEC and *ex vivo* TEC to mediate positive selection warrants further investigation. Certainly, the reprogramming process can be further explored for instance by producing a serum-free strategy, which aims to both reduce variation and further phenocopy TEC (Parent *et al*., 2013; Sun *et al*., 2013), and by determining what elements of the TEC gene expression programme is missing from the current iTEC protocol. Furthermore, I begin to explore the idea that iTEC requires supplementation with non-epithelial thymic stroma and mTEC to completely recapitulate thymopoiesis.

Chapter Four tested the hypothesis that using defined culture substrates could create a more consistant iTEC phenotype, with respect to the essential functions of TEC. I concluded that, although culture on synthetic polymers did not enforce native TEC behaviour on *ex vivo TEC*, as demonstrated by a downregulation of *Foxn1*, or promote medullary differentiation in iTEC-progeny, there was potential for the selected polymers to decrease the variablity associated with the iTEC system and T-cell differentiation. Future work will focus on testing whether the polymers are capable of selectively binding iTEC that share a similar adhesion profile with native TEC. This mechanism will then be explored as a replacement for fluorescence activated cell sorting (FACS) to isolate MEFs that had successfully entered reprogramming based upon GFP expression, which will further increase the scale up capacity of the iTEC system but also may improve function and reduce variation. Throughout Chapter Four, I was critical of the monolayer co-culture system, which represents the most commonly used tool to perform *in vitro* T-cell specification when performed using OP9-DLL1.

I highlighted that monolayer culture could not produce effective positive controls as *ex vivo* TEC did not maintain *Foxn1* expression and that two-dimensional culture produced large amounts of technical variation, which may have been a result of the low cell density promoting thymocyte sampling biases.

In Chapter Five, given the technical limitations I observed in Chapter Four, I examined the hypothesis that: miniaturising the RTOC process could be conducive to creating a culture system for thymus biology that is amenable to high throughput screening applications but retained a 3D stature and a high cell density. I found evidence for this and concluded that MTOC has the potential to be a useful tool in thymus biology by providing a method for producing large numbers of micro-physiological thymi for testing specific hypotheses. I concluded that not all reaggregates within a well were able to maintain *Foxn1* expression in *ex vivo* TEC, despite being in the same culture conditions and being generated from the same input pool of cells. I also concluded that MTOC could mediate much more consistent T-cell differentiation processes than RTOC, albeit with a much lower efficiency. Further effort is required to clarify if this was a product of the reductionist nature of MTOC and that the small reaggregates were on average much less efficient that the concurrent iRTOC, or whether only a few, of the 70 in total, reaggregates were successful and that the failed reaggregates diluted the result. Therefore, MTOC has the potential to be a variant of RTOC that inhabits a 3D, high content screening niche. Future work will focus on increasing the number of biological replicates to satisfactory levels and overcoming highlighted technical limitations such a poor light penetration through the GRID3D system.

Therefore, with respect to the overarching hypothesis: this thesis presents evidence that iTEC, like the OP9-DLL1 and MS5-Dll1 can be used to overcome tissue limitation in thymus biology, but unlike the aforementioned systems, without comprising the extent that the fundamental processes associated with TEC are recapitulated. However, iTEC in its current state are not able to completely emulate *in vitro* positive or negative selection.

7. References

Abramson, Anderson, 2017. Thymic Epithelial Cells. Annual Review of Immunology 35, 85–118. https://doi.org/10.1146/annurev-immunol-051116-052320

Akiyama et al., 2016. Identification of embryonic precursor cells that differentiate into thymic epithelial cells expressing autoimmune regulator. The Journal of Experimental Medicine. https://doi.org/10.1084/jem.20151780

Akiyama et al., 2008. The Tumor Necrosis Factor Family Receptors RANK and CD40 Cooperatively Establish the Thymic Medullary Microenvironment and Self-Tolerance. Immunity. https://doi.org/10.1016/j.immuni.2008.06.015

Alfonso et al., 2006. CD69 down-modulation and inhibition of thymic egress by short- and long-term selective chemical agonism of sphingosine 1-phosphate receptors. European Journal of Immunology. https://doi.org/10.1002/eji.200535127

Allende et al., 2004. Expression of the Sphingosine 1-Phosphate Receptor, S1P1, on T-cells Controls Thymic Emigration. Journal of Biological Chemistry. https://doi.org/10.1074/jbc.M314291200

Allman et al., 2003. Thymopoiesis independent of common lymphoid progenitors. Nature Immunology. https://doi.org/10.1038/ni878

Amand et al., 2016. A comparison of strategies for immortalizing mouse embryonic fibroblasts. Journal of Biological Methods. https://doi.org/10.14440/jbm.2016.110

Anderson et al., 2004. Nanoliter-scale synthesis of arrayed biomaterials and application to human embryonic stem cells. Nature Biotechnology. https://doi.org/10.1038/nbt981

Anderson et al., 2002. Projection of an immunological self shadow within the thymus by the aire protein. Science. https://doi.org/10.1126/science.1075958

Anderson et al., 1998. Studies on thymic epithelial cells in vitro. Developmental and Comparative Immunology. https://doi.org/10.1016/S0145-305X(98)00011-1

Anderson et al., 1993. MHC class II-positive epithelium and mesenchyme cells are both required for T-cell development in the thymus. Nature. https://doi.org/10.1038/362070a0

Anderson, Jenkinson, 2007. Fetal thymus organ culture. CSH Protoc. https://doi.org/10.1101/pdb.prot4808

Auerbach, 1960. Morphogenetic interactions in the development of the mouse thymus gland. Developmental Biology. https://doi.org/10.1016/0012-1606(60)90009-9

Bai et al., 2007. Kruppel-Like Factor 2 Controls T Cell Trafficking by Activating L-Selectin (CD62L) and Sphingosine-1-Phosphate Receptor 1 Transcription. The Journal of Immunology. https://doi.org/10.4049/jimmunol.178.12.7632

Baik et al., 2016. Relb acts downstream of medullary thymic epithelial stem cells and is essential for the emergence of RANK+ medullary epithelial progenitors. European Journal of Immunology. https://doi.org/10.1002/eji.201546253

Bain et al., 2016. Tissue-specific roles for sonic hedgehog signaling in establishing thymus and parathyroid organ fate. Development (Cambridge). https://doi.org/10.1242/dev.141903

Balciunaite et al., 2002. Wnt glycoproteins regulate the expression of FoxNI, the genes defective in nude mice. Nature Immunology. https://doi.org/10.1038/ni850

Bankovich et al., 2010. CD69 suppresses sphingosine 1-phosophate receptor-1 (S1P1)

function through interaction with membrane helix 4. Journal of Biological Chemistry. https://doi.org/10.1074/jbc.M110.123299

Bell, Bhandoola, 2008. The earliest thymic progenitors for T cells possess myeloid lineage potential. Nature. https://doi.org/10.1038/nature06840

Bennett et al., 2002. Identification and characterization of thymic epithelial progenitor cells. Immunity 16, 803–814. https://doi.org/10.1016/S1074-7613(02)00321-7

Benz et al., 2004. Homing of immature thymocytes to the subcapsular microenvironment within the thymus is not an absolute requirement for T cell development. European Journal of Immunology 34, 3652–3663. https://doi.org/10.1002/eji.200425248

Bhandoola et al., 2007. Commitment and Developmental Potential of Extrathymic and Intrathymic T Cell Precursors: Plenty to Choose from. Immunity 26, 678–689. https://doi.org/10.1016/j.immuni.2007.05.009

Blackburn et al., 1996. The nu gene acts cell-autonomously and is required for differentiation of thymic epithelial progenitors. Proceedings of the National Academy of Sciences. https://doi.org/10.1073/pnas.93.12.5742

Bleul et al., 2006. Formation of a functional thymus initiated by a postnatal epithelial progenitor cell. Nature 441, 992–996. https://doi.org/10.1038/nature04850

Bleul, Boehm, 2005. BMP Signaling Is Required for Normal Thymus Development. The Journal of Immunology. https://doi.org/10.4049/jimmunol.175.8.5213

Bonfanti et al., 2010. Microenvironmental reprogramming of thymic epithelial cells to skin multipotent stem cells. Nature. https://doi.org/10.1038/nature09269

Brauer et al., 2016. T Cell Genesis: In Vitro Veritas Est? Trends in Immunology. https://doi.org/10.1016/j.it.2016.09.008

Bredenkamp, Nicholas et al., 2014. An organized and functional thymus generated from FOXN1-reprogrammed fibroblasts. Nature Cell Biology 16, 1–7. https://doi.org/10.1038/ncb3023

Bredenkamp, N. et al., 2014. Regeneration of the aged thymus by a single transcription factor. Development. https://doi.org/10.1242/dev.103614

Brisson et al., 2015. The thymus-specific serine protease TSSP/PRSS16 is crucial for the antitumoral role of $CD4^+$ T cells. Cell Reports. https://doi.org/10.1016/j.celrep.2014.12.009

Brugnera et al., 2000. Coreceptor reversal in the thymus: signaled CD4+8+ thymocytes initially terminate CD8 transcription even when differentiating into CD8+ T cells. Immunity 13, 59–71. https://doi.org/S1074-7613(00)00008-X [pii]

Buono et al., 2016. A dynamic niche provides Kit ligand in a stage-specific manner to the earliest thymocyte progenitors. Nature Cell Biology 18, 157–167. https://doi.org/10.1038/ncb3299

Calderón, Boehm, 2011. Three chemokine receptors cooperatively regulate homing of hematopoietic progenitors to the embryonic mouse thymus. Proceedings of the National Academy of Sciences of the United States of America 108, 7517–7522. https://doi.org/10.1073/pnas.1016428108

Carlyle et al., 1997. Identification of a novel developmental stage marking lineage commitment of progenitor thymocytes. Journal of Experimental Medicine. https://doi.org/10.1084/jem.186.2.173

Chen et al., 2009. Foxn1 is required to maintain the postnatal thymic microenvironment in a dosage-sensitive manner. Blood. https://doi.org/10.1182/blood-2008-05-156265

Chung et al., 2014. Engineering the human thymic microenvironment to support thymopoiesis in vivo. Stem cells (Dayton, Ohio) 32, 2386–96. https://doi.org/10.1002/stem.1731

Ciofani, Zúñiga-Pflücker, 2005. Notch promotes survival of pre–T cells at the β-selection checkpoint by regulating cellular metabolism. Nature Immunology 6, 881–888. https://doi.org/10.1038/ni1234

Clark et al., 2005. Human skin cells support thymus-independent T cell development. Journal of Clinical Investigation. https://doi.org/10.1172/JCI24731

Cosway et al., 2017. Redefining thymus medulla specialization for central tolerance. Journal of Experimental Medicine. https://doi.org/10.1084/jem.20171000

Cowan et al., 2014. Differential requirement for CCR4 and CCR7 during the development of innate and adaptive alpha beta T cells in the adult thymus. Journal of Immunology 193, 1204–1212. https://doi.org/10.4049/jimmunol.1400993.Differential

De Obaldia et al., 2013. Early T-cell progenitors are the major granulocyte precursors in the adult mouse thymus. Blood. https://doi.org/10.1182/blood-2012-08-451773

Depreter et al., 2008. Identification of Plet-1 as a specific marker of early thymic epithelial progenitor cells. Proceedings of the National Academy of Sciences. https://doi.org/10.1073/pnas.0711170105

Duffy et al., 2014a. A high-throughput polymer microarray approach for identifying defined substrates for mesenchymal stem cells. Biomaterials Science 2, 1683–1692. https://doi.org/10.1039/c4bm00112e

Duffy et al., 2014b. Long term mesenchymal stem cell culture on a defined synthetic substrate with enzyme free passaging. Biomaterials. https://doi.org/10.1016/j.biomaterials.2014.04.013

Dyall, Nikolic-Zugić, 1999. The final maturation of at least some single-positive CD4(hi) thymocytes does not require T cell receptor-major histocompatibility complex contact. The Journal of experimental medicine 190, 757–64. https://doi.org/10.1084/jem.190.6.757

Dzhagalov, Phee, 2012. How to find your way through the thymus: A practical guide for aspiring T cells. Cellular and Molecular Life Sciences. https://doi.org/10.1007/s00018-011-0791-6

Fabre et al., 2008. FOXO1 Regulates L-Selectin and a Network of Human T Cell Homing Molecules Downstream of Phosphatidylinositol 3-Kinase. The Journal of Immunology. https://doi.org/10.4049/jimmunol.181.5.2980

Falk, Eichmann, 2002. Heterogeneity of the DN4 (CD44-CD25-) subset of CD4-CD8- double negative thymocytes; dependence on CD3 signaling, in: Immunology Letters. https://doi.org/10.1016/S0165-2478(02)00027-5

Fan et al., 2015. Bioengineering thymus organoids to restore thymic function and induce donor-specific immune tolerance to allografts. Molecular therapy : the journal of the American Society of Gene Therapy 23, 1262–77. https://doi.org/10.1038/mt.2015.77

Farley et al., 2013. Dynamics of thymus organogenesis and colonization in early human development. Development 140, 2015–2026. https://doi.org/10.1242/dev.087320

Farley, 2010. Characterisation of epithelial progenitor cells for human and mouse thymus. University of Edinburgh.

Faul et al., 2007. G*Power 3: A flexible statistical power analysis program for the social, behavioral, and biomedical sciences, in: Behavior Research Methods. https://doi.org/10.3758/BF03193146

Fiorini et al., 2009. Dynamic regulation of notch 1 and notch 2 surface expression during T cell development and activation revealed by novel monoclonal antibodies. Journal of immunology (Baltimore, Md. : 1950) 183, 7212–7222. https://doi.org/10.4049/jimmunol.0902432

Fisher et al., 1990. Human thymocyte development in mouse organ cultures. International Immunology. https://doi.org/10.1093/intimm/2.6.571

Foster et al., 2008. Contribution of Neural Crest-Derived Cells in the Embryonic and Adult Thymus. The Journal of Immunology. https://doi.org/10.4049/jimmunol.180.5.3183

Galandrini et al., 1997. Different functions of the GTpase Rho in prothymocytes and late pre-T cells. Immunity 7, 163–174. https://doi.org/10.1016/S1074-7613(00)80519-1

Gehre et al., 2015. A stromal cell free culture system generates mouse pro-T cells that can reconstitute T-cell compartments in vivo. European Journal of Immunology. https://doi.org/10.1002/eji.201444681

Germain, 2002. T-cell development and the CD4-CD8 lineage decision. Nature reviews. Immunology 2, 309–322. https://doi.org/10.1038/nri798

Germeraad et al., 2003. Development of thymic microenvironments in vitro is oxygen-dependent and requires permanent presence of T-cell progenitors. Journal of Histochemistry and Cytochemistry. https://doi.org/10.1177/002215540305100913

Gill et al., 2002. Generation of a complete thymic microenvironment by MTS24+thymic epithelial cells. Nature Immunology. https://doi.org/10.1038/ni812

Gjorevski et al., 2014. Bioengineering approaches to guide stem cell-based organogenesis. Development (Cambridge, England) 141, 1794–804. https://doi.org/10.1242/dev.101048

Godfrey et al., 1993. A developmental pathway involving four phenotypically and functionally distinct subsets of CD3-CD4-CD8- triple-negative adult mouse thymocytes defined by CD44 and CD25 expression. Journal of immunology (Baltimore, Md. : 1950). https://doi.org/10.4049/jimmunol.0903296

Gogoi, Chiplunkar, 2013. Targeting gamma delta T cells for cancer immunotherapy: bench to bedside. The Indian journal of medical research 138, 755–61.

Gommeaux et al., 2009. Thymus-specific serine protease regulates positive selection of a subset of CD4+ thymocytes. European Journal of Immunology. https://doi.org/10.1002/eji.200839175

Gordon et al., 2010. Evidence for an early role for BMP4 signaling in thymus and parathyroid morphogenesis. Developmental Biology. https://doi.org/10.1016/j.ydbio.2009.12.026

Gordon et al., 2004. Functional evidence for a single endodermal origin for the thymic epithelium. Nature immunology 5, 546–553. https://doi.org/10.1038/ni1064

Gordon et al., 2001. Gcm2 and Foxn1 mark early parathyroid- and thymus-specific domains in the developing third pharyngeal pouch. Mechanisms of Development 103, 141–143. https://doi.org/10.1016/S0925-4773(01)00333-1

Griffith et al., 2009. Increased thymus- and decreased parathyroid-fated organ domains in Splotch mutant embryos. Developmental biology 327, 216–27. https://doi.org/10.1016/j.ydbio.2008.12.019

Groll et al., 1997. Structure of 20S proteasome from yeast at 2.4 Å resolution. Nature. https://doi.org/10.1038/386463a0

Hameyer et al., 2007. Toxicity of ligand-dependent Cre recombinases and generation of a conditional Cre deleter mouse allowing mosaic recombination in peripheral tissues.

Physiological Genomics. https://doi.org/10.1152/physiolgenomics.00019.2007

Hay et al., 2011. Unbiased screening of polymer libraries to define novel substrates for functional hepatocytes with inducible drug metabolism. Stem Cell Research. https://doi.org/10.1016/j.scr.2010.12.002

Hayflick, 1965. The limited in vitro lifetime of human diploid cell strains. Experimental Cell Research. https://doi.org/10.1016/0014-4827(65)90211-9

Hirakawa et al., 2018. Fundamental parameters of the developing thymic epithelium in the mouse. Scientific Reports. https://doi.org/10.1038/s41598-018-29460-0

Hogquist et al., 2005. Central tolerance: learning self-control in the thymus. Nature reviews. Immunology 5, 772–782. https://doi.org/10.1038/nri1707

Hogquist et al., 1994. T cell receptor antagonist peptides induce positive selection. Cell. https://doi.org/10.1016/0092-8674(94)90169-4

Honey et al., 2002. Cathepsin L Regulates CD4+ T Cell Selection Independently of Its Effect on Invariant Chain: A Role in the Generation of Positively Selection Peptide Ligands. J Exp Med. https://doi.org/10.1084/jem.20011904

Hozumi et al., 2008. Delta-like 4 is indispensable in thymic environment specific for T cell development. The Journal of Experimental Medicine. https://doi.org/10.1084/jem.20080134

Hsieh et al., 2002. A Role for Cathepsin L and Cathepsin S in Peptide Generation for MHC Class II Presentation. The Journal of Immunology.

Huang et al., 2001. Cutting edge: histone acetylation and recombination at the TCR γ locus follows IL-7 induction. Journal of immunology 167, 6073–6077. https://doi.org/10.4049/jimmunol.167.11.6073

Hun et al., 2017. Native thymic extracellular matrix improves in vivo thymic organoid T cell output, and drives in vitro thymic epithelial cell differentiation. Biomaterials. https://doi.org/10.1016/j.biomaterials.2016.11.054

Itoi et al., 2007. Mesenchymal cells are required for functional development of thymic epithelial cells. International Immunology. https://doi.org/10.1093/intimm/dxm060

Itoi et al., 2001. Two distinct steps of immigration of hematopoietic progenitors into the early thymus anlage. International Immunology. https://doi.org/10.1093/intimm/13.9.1203

James et al., 2018. T-cell egress from the thymus: Should I stay or should I go? Journal of Leukocyte Biology. https://doi.org/10.1002/JLB.1MR1217-496R

Janas, Turner, 2010. Stromal cell-derived factor 1α and CXCR4: Newly defined requirements for efficient thymic β-selection. Trends in Immunology. https://doi.org/10.1016/j.it.2010.07.002

Jenkinson et al., 2007. PDGFRα-expressing mesenchyme regulates thymus growth and the availability of intrathymic niches. Blood. https://doi.org/10.1182/blood-2006-05-023143

Jenkinson et al., 1992. Studies on T cell maturation on defined thymic stromal cell populations in vitro. The Journal of experimental medicine. https://doi.org/10.1084/JEM.176.3.845

Jenkinson et al., 1982. Effect of deoxyguanosine on lymphopoiesis in the developing thymus rudiment in vitro: Application in the production of chimeric thymus rudiments. European Journal of Immunology 12, 583–587. https://doi.org/10.1002/eji.1830120710

Jenkinson, Anderson, 1994. Fetal thymic organ cultures. Current Opinion in Immunology. https://doi.org/10.1016/0952-7915(94)90104-X

Jenkinson, Owen, 1990. T-cell differentiation in thymus organ cultures. Seminars in Immunology.

Kapur et al., 1985. A new method for gray-level picture thresholding using the entropy of the histogram. Computer Vision, Graphics, & Image Processing. https://doi.org/10.1016/0734-189X(85)90125-2

Kenins et al., 2010. Flt3 ligand-receptor interaction is important for maintenance of early thymic progenitor numbers in steady-state thymopoiesis. European Journal of Immunology 40, 81–90. https://doi.org/10.1002/eji.200839213

Kim et al., 2000. Epithelial cell-specific laminin 5 is required for survival of early thymocytes. Journal of immunology (Baltimore, Md. : 1950) 165, 192–201. https://doi.org/10.4049/jimmunol.165.1.192

Kincaid et al., 2016. Specialized proteasome subunits have an essential role in the thymic selection of CD8+ T cells. Nature Immunology. https://doi.org/10.1038/ni.3480

Kishimoto et al., 1996. Differing roles for B7 and intercellular adhesion molecule-1 in negative selection of thymocytes. The Journal of experimental medicine 184, 531–7.

Klein et al., 2014. Positive and negative selection of the T cell repertoire: What thymocytes see (and don't see). Nature Reviews Immunology. https://doi.org/10.1038/nri3667

Klein et al., 2009. Antigen presentation in the thymus for positive selection and central tolerance induction. Nature reviews. Immunology 9, 833–844. https://doi.org/10.1038/nri2669

Klug et al., 2002. Cutting Edge: Thymocyte-Independent and Thymocyte-Dependent Phases of Epithelial Patterning in the Fetal Thymus. The Journal of Immunology. https://doi.org/10.4049/jimmunol.169.6.2842

Klug et al., 1998. Interdependence of cortical thymic epithelial cell differentiation and T-lineage commitment. Proceedings of the National Academy of Sciences of the United States of America. https://doi.org/10.1073/pnas.95.20.11822

Koch et al., 2008. Delta-like 4 is the essential, nonredundant ligand for Notchl during thymic T cell lineage commitment. Journal of Experimental Medicine. https://doi.org/10.1084/jem.20080829

Koch, Radtke, 2011. Mechanisms of T cell development and transformation. Annual review of cell and developmental biology 27, 539–562. https://doi.org/10.1146/annurev-cellbio-092910-154008

Kurobe et al., 2006. CCR7-dependent cortex-to-medulla migration of positively selected thymocytes is essential for establishing central tolerance. Immunity 24, 165–177. https://doi.org/10.1016/j.immuni.2005.12.011

Kyewski, Peterson, 2010. Aire, Master of Many Trades. Cell 140, 24–26. https://doi.org/10.1016/j.cell.2009.12.036

Lai et al., 2011. Mouse embryonic stem cell-derived thymic epithelial cell progenitors enhance T-cell reconstitution after allogeneic bone marrow transplantation. Blood. https://doi.org/10.1182/blood-2011-03-340794

Lai, Jin, 2009. Generation of thymic epithelial cell progenitors by mouse embryonic stem cells. Stem Cells. https://doi.org/10.1002/stem.238

Lam et al., 2019. Tissue-specific extracellular matrix accelerates the formation of neural networks and communities in a neuron-glia co-culture on a multi-electrode array. Scientific Reports. https://doi.org/10.1038/s41598-019-40128-1

Lauritsen et al., 2009. Marked Induction of the Helix-Loop-Helix Protein Id3 Promotes the γδ

T Cell Fate and Renders Their Functional Maturation Notch Independent. Immunity 31, 565–575. https://doi.org/10.1016/j.immuni.2009.07.010

Le Douarin, Jotereau, 1975. Tracing of cells of the avian thymus through embryonic life in interspecific chimeras. Journal of Experimental Medicine. https://doi.org/10.1084/jem.142.1.17

Levéen et al., 1994. Mice deficient for PDGF B show renal, cardiovascular, and hematological abnormalities. Genes and Development. https://doi.org/10.1101/gad.8.16.1875

Li et al., 2017. Induced pluripotent stem cells, form in vitro tissue engineering to in vivo allogeneic transplantation. Journal of Thoracic Disease. https://doi.org/10.21037/jtd.2017.02.77

Li et al., 2007. Developmental pathway of CD4+CD8- medullary thymocytes during mouse ontogeny and its defect in Aire-/- mice. Proceedings of the National Academy of Sciences of the United States of America 104, 18175–18180. https://doi.org/10.1073/pnas.0708884104

Lieberam, Förster, 1999. The murine beta-chemokine TARC is expressed by subsets of dendritic cells and attracts primed CD4+ T cells. European journal of immunology 29, 2684–94. https://doi.org/10.1002/(SICI)1521-4141(199909)29:09<2684::AID-IMMU2684>3.0.CO;2-Y [pii]

Littman, 2016. How Thymocytes Achieve Their Fate. The Journal of Immunology 196, 1983–1984. https://doi.org/10.4049/jimmunol.1600032

Liu et al., 2006. Coordination between CCR7- and CCR9-mediated chemokine signals in prevascular fetal thymus colonization. Blood 108, 2531–2539. https://doi.org/10.1182/blood-2006-05-024190

Livák et al., 1999. Characterization of TCR Gene Rearrangements during Adult Murine T Cell Development. Journal of Immunology 162, 2575–2580.

Lopes et al., 2015. Thymic crosstalk coordinates medulla organization and T-cell tolerance induction. Frontiers in Immunology. https://doi.org/10.3389/fimmu.2015.00365

Lu et al., 2005. The Earliest Thymic Progenitors in Adults Are Restricted to T, NK, and Dendritic Cell Lineage and Have a Potential to Form More Diverse TCR Chains than Fetal Progenitors. The Journal of Immunology 175, 5848–5856. https://doi.org/10.4049/jimmunol.175.9.5848

Luc et al., 2012. The earliest thymic T cell progenitors sustain B cell and myeloid lineage potential. Nature immunology 13, 412–9. https://doi.org/10.1038/ni.2255

Luis et al., 2016. Initial seeding of the embryonic thymus by immune-restricted lympho-myeloid progenitors. Nature Immunology. https://doi.org/10.1038/ni.3576

Lundberg et al., 1995. Intermediate steps in positive selection: differentiation of CD4+8int TCRint thymocytes into CD4-8+TCRhi thymocytes. The Journal of experimental medicine 181, 1643–51. https://doi.org/10.1084/jem.181.5.1643

Maillard et al., 2006. The requirement for Notch signaling at the beta-selection checkpoint in vivo is absolute and independent of the pre-T cell receptor. The Journal of experimental medicine 203, 2239–45. https://doi.org/10.1084/jem.20061020

Manley, Condie, 2010. Transcriptional regulation of thymus organogenesis and thymic epithelial cell differentiation. Progress in Molecular Biology and Translational Science 92, 103–120. https://doi.org/10.1016/S1877-1173(10)92005-X

Marshall et al., 2003. T Cell Generation Including Positive and Negative Selection Ex Vivo in a Three-Dimensional Matrix. Journal of Hematotherapy & Stem Cell Research.

https://doi.org/10.1089/152581603322448277

Martins et al., 2012. Thymus-autonomous T cell development in the absence of progenitor import. The Journal of Experimental Medicine 209, 1409–1417. https://doi.org/10.1084/jem.20120846

Matloubian et al., 2004. Lymphocyte egress from thymus and peripheral lymphoid organs is dependent on S1P receptor 1. Nature 427, 355–60. https://doi.org/10.1038/nature02284

Mayer et al., 2016. Dynamic spatio-temporal contribution of single β5t+ cortical epithelial precursors to the thymus medulla. European Journal of Immunology. https://doi.org/10.1002/eji.201545995

McCune et al., 1988. The SCID-hu mouse: Murine model for the analysis of human hematolymphoid differentiation and function. Science. https://doi.org/10.1126/science.2971269

McKee, Komarova, 2017. Is it time to reinvent basic cell culture medium? American Journal of Physiology-Cell Physiology. https://doi.org/10.1152/ajpcell.00336.2016

McQualter et al., 2010. Evidence of an epithelial stem/progenitor cell hierarchy in the adult mouse lung. Proceedings of the National Academy of Sciences. https://doi.org/10.1073/pnas.0909207107

Meek et al., 2011. T cells fail to develop in the human skin-cell explants system; an inconvenient truth. BMC Immunology. https://doi.org/10.1186/1471-2172-12-17

Mei et al., 2010a. Combinatorial development of biomaterials for clonal growth of human pluripotent stem cells. Nature Materials. https://doi.org/10.1038/nmat2812

Mei et al., 2010b. A high throughput micro-array system of polymer surfaces for the manipulation of primary pancreatic islet cells. Biomaterials. https://doi.org/10.1016/j.biomaterials.2010.08.029

Melkoumian et al., 2010. Synthetic peptide-acrylate surfaces for long-term self-renewal and cardiomyocyte differentiation of human embryonic stem cells. Nature Biotechnology. https://doi.org/10.1038/nbt.1629

Michie, Zúñiga-Pflücker, 2002. Regulation of thymocyte differentiation: Pre-TCR signals and Beta-selection. Seminars in Immunology. https://doi.org/10.1016/S1044-5323(02)00064-7

Misslitz et al., 2004. Thymic T cell development and progenitor localization depend on CCR7. The Journal of experimental medicine 200, 481–91. https://doi.org/10.1084/jem.20040383

Mohtashami et al., 2010. Direct comparison of Dll1- and Dll4-mediated Notch activation levels shows differential lymphomyeloid lineage commitment outcomes. Journal of immunology (Baltimore, Md. : 1950) 185, 867–876. https://doi.org/10.4049/jimmunol.1000782

Mohtashami, Zuniga-Pflucker, 2006. Cutting Edge: Three-Dimensional Architecture of the Thymus Is Required to Maintain Delta-Like Expression Necessary for Inducing T Cell Development. The Journal of Immunology. https://doi.org/10.4049/jimmunol.176.2.730

Montel-Hagen et al., 2019. Organoid-Induced Differentiation of Conventional T Cells from Human Pluripotent Stem Cells. Cell Stem Cell. https://doi.org/10.1016/j.stem.2018.12.011

Moore-Scott, Manley, 2005. Differential expression of Sonic hedgehog along the anterior-posterior axis regulates patterning of pharyngeal pouch endoderm and pharyngeal endoderm-derived organs. Developmental Biology.

https://doi.org/10.1016/j.ydbio.2004.10.027

Müller et al., 2008. Neural Crest Origin of Perivascular Mesenchyme in the Adult Thymus. The Journal of Immunology. https://doi.org/10.4049/jimmunol.180.8.5344

Müller et al., 1997. Involvement of E-cadherin in thymus organogenesis and thymocyte maturation. Immunity 6, 257–264. https://doi.org/10.1016/S1074-7613(00)80328-3

Mulroy et al., 2002. Wnt-1 and Wnt-4 regulate thymic cellularity. European Journal of Immunology. https://doi.org/10.1002/1521-4141(200204)32:4<967::AID-IMMU967>3.0.CO;2-6

Murata et al., 2007. Regulation of CD8+ T cell development by thymus-specific proteasomes. Science. https://doi.org/10.1126/science.1141915

Nakagawa et al., 1998. Cathepsin L: Critical role in Ii degradation and CD4 T cell selection in the thymus. Science. https://doi.org/10.1126/science.280.5362.450

Nehls et al., 1994. New member of the winged-helix protein family disrupted in mouse and rat nude mutations. Nature. https://doi.org/10.1038/372103a0

Nitta et al., 2010. Thymoproteasome Shapes Immunocompetent Repertoire of CD8+ T Cells. Immunity. https://doi.org/10.1016/j.immuni.2009.10.009

Notarangelo et al., 2001. Recombinase activating gene enzymes of lymphocytes. Current opinion in hematology 8, 41–46. https://doi.org/10.1097/00062752-200101000-00008

Nowell et al., 2011. Foxn1 regulates lineage progression in cortical and medullary thymic epithelial cells but is dispensable for medullary sublineage divergence. PLoS Genetics. https://doi.org/10.1371/journal.pgen.1002348

O'Neill et al., 2016. Foxn1 is dynamically regulated in thymic epithelial cells during embryogenesis and at the onset of thymic involution. PLoS ONE. https://doi.org/10.1371/journal.pone.0151666

Ohigashi et al., 2013. Aire-expressing thymic medullary epithelial cells originate from B5t-expressing progenitor cells. Proceedings of the National Academy of Sciences. https://doi.org/10.1073/pnas.1301799110

Ortman et al., 2002. Molecular characterization of the mouse involuted thymus: Aberrations in expression of transcription regulators in thymocyte and epithelial compartments. International Immunology. https://doi.org/10.1093/intimm/dxf042

Parent et al., 2013. Generation of functional thymic epithelium from human embryonic stem cells that supports host T cell development. Cell Stem Cell 13. https://doi.org/10.1016/j.stem.2013.04.004

Patel et al., 2006. Bmp4 and Noggin expression during early thymus and parathyroid organogenesis. Gene Expression Patterns. https://doi.org/10.1016/j.modgep.2006.01.011

Penit, 1988. Localization and Phenotype of Cycling and Post-Cycling Murine Thymocytes Studied by Simultaneous Detection of Bromodeoxyuridine and Surface Antigens. The Journal of Histochemistry and Cytochemistry 36, 473–478. https://doi.org/10.1177/36.5.2895787

Pernagallo et al., 2009. A cooperative polymer-DNA microarray approach to biomaterial investigation. Lab on a Chip. https://doi.org/10.1039/b808363k

Petrie et al., 2000. Precursor thymocyte proliferation and differentiation are controlled by signals unrelated to the pre-TCR. Journal of immunology (Baltimore, Md. : 1950) 165, 3094–8.

Petrie et al., 1995. T cell receptor gene recombination patterns and mechanisms: cell death, rescue, and T cell production. The Journal of experimental medicine 182, 121–7.

Petrie et al., 1990. Development of immature thymocytes: initiation of CD3, CD4, and CD8 acquisition parallels down-regulation of the interleukin 2 receptor alpha chain. Eur.J.Immunol. 20, 2813–2815. https://doi.org/10.1002/eji.1830201243

Petrie, Zúñiga-Pflücker, 2007. Zoned out: functional mapping of stromal signaling microenvironments in the thymus. Annual review of immunology 25, 649–679. https://doi.org/10.1146/annurev.immunol.23.021704.115715

Pinto et al., 2013. An Organotypic Coculture Model Supporting Proliferation and Differentiation of Medullary Thymic Epithelial Cells and Promiscuous Gene Expression. The Journal of Immunology. https://doi.org/10.4049/jimmunol.1201843

Plotkin et al., 2003. Critical role for CXCR4 signaling in progenitor localization and T cell differentiation in the postnatal thymus. Journal of immunology (Baltimore, Md. : 1950) 171, 4521–4527. https://doi.org/10.4049/jimmunol.171.9.4521

Poznansky et al., 2000. Efficient generation of human T cells from a tissue-engineered thymic organoid. Nature Biotechnology 18, 729–734. https://doi.org/10.1038/77288

Prockop et al., 2002. Stromal cells provide the matrix for migration of early lymphoid progenitors through the thymic cortex. Journal of immunology (Baltimore, Md. : 1950) 169, 4354–61. https://doi.org/10.4049/jimmunol.169.8.4354

Prockop, Petrie, 2004. Regulation of thymus size by competition for stromal niches among early T cell progenitors. Journal of immunology (Baltimore, Md. : 1950) 173, 1604–1611. https://doi.org/10.4049/jimmunol.173.3.1604

Radtke et al., 1999. Deficient T cell fate specification in mice with an induced inactivation of Notch1. Immunity. https://doi.org/10.1016/S1074-7613(00)80054-0

Ramsey, 2002. Aire deficient mice develop multiple features of APECED phenotype and show altered immune response. Human Molecular Genetics. https://doi.org/10.1093/hmg/11.4.397

Ranga et al., 2014. 3D niche microarrays for systems-level analyses of cell fate. Nature communications 5, 4324. https://doi.org/10.1038/ncomms5324

Renier et al., 2016. Mapping of Brain Activity by Automated Volume Analysis of Immediate Early Genes. Cell. https://doi.org/10.1016/j.cell.2016.05.007

Revest et al., 2001. Development of the Thymus Requires Signaling Through the Fibroblast Growth Factor Receptor R2-IIIb. The Journal of Immunology. https://doi.org/10.4049/jimmunol.167.4.1954

Ripen et al., 2011. Ontogeny of thymic cortical epithelial cells expressing the thymoproteasome subunit β5t. European Journal of Immunology. https://doi.org/10.1002/eji.201041375

Roberts et al., 2012. Rank Signaling Links the Development of Invariant γδ T Cell Progenitors and Aire + Medullary Epithelium. Immunity. https://doi.org/10.1016/j.immuni.2012.01.016

Rodewald, 2008. Thymus Organogenesis. Annu. Rev. Immunol 26, 355–88. https://doi.org/10.1146/annurev.immunol.26.021607.090408

Rodewald et al., 2001. Thymus medulla consisting of epithelial islets each derived from a single progenitor. Nature. https://doi.org/10.1038/414763a

Rodewald et al., 1995. Intrathymically expressed c-kit ligand (stem cell factor) is a major factor driving expansion of very immature thymocytes in vivo. Immunity 3, 313–319.

https://doi.org/10.1016/1074-7613(95)90116-7

Rossi et al., 2007. Redefining epithelial progenitor potential in the developing thymus. European journal of immunology 37, 2411–8. https://doi.org/10.1002/eji.200737275

Rossi et al., 2006. Clonal analysis reveals a common progenitor for thymic cortical and medullary epithelium. Nature 441, 988–991. https://doi.org/10.1038/nature04813

Sakiyama-Elbert, Hubbell, 2002. Functional Biomaterials: Design of Novel Biomaterials. Annual Review of Materials Research. https://doi.org/10.1146/annurev.matsci.31.1.183

Saldaña et al., 2016. Sonic Hedgehog regulates thymic epithelial cell differentiation. Journal of Autoimmunity. https://doi.org/10.1016/j.jaut.2015.12.004

Schmitt et al., 2004. Maintenance of T cell specification and differentiation requires recurrent notch receptor-ligand interactions. The Journal of experimental medicine 200, 469–479. https://doi.org/10.1084/jem.20040394

Schmitt, Zúñiga-Pflücker, 2002. Induction of T cell development from hematopoietic progenitor cells by delta-like-1 in vitro. Immunity 17, 749–756. https://doi.org/10.1016/S1074-7613(02)00474-0

Schwarz et al., 2007. Selective thymus settling regulated by cytokine and chemokine receptors. Journal of immunology (Baltimore, Md. : 1950) 178, 2008–2017. https://doi.org/10.4049/jimmunol.178.4.2008

Seet et al., 2017. Generation of mature T cells from human hematopoietic stem and progenitor cells in artificial thymic organoids. Nature Methods. https://doi.org/10.1038/nmeth.4237

Sekai et al., 2014. Medullary thymic epithelial stem cells maintain a functional thymus to ensure lifelong central T cell tolerance. Immunity. https://doi.org/10.1016/j.immuni.2014.10.011

Serre et al., 2015. Central tolerance spares the private high-avidity $CD4^+$ T-cell repertoire specific for an islet antigen in NOD mice. European Journal of Immunology. https://doi.org/10.1002/eji.201445290

Sheridan et al., 2017. Thymospheres Are Formed by Mesenchymal Cells with the Potential to Generate Adipocytes, but Not Epithelial Cells. Cell Reports. https://doi.org/10.1016/j.celrep.2017.09.090

Sheridan et al., 2009. A novel method for the generation of reaggregated organotypic cultures that permits juxtaposition of defined cell populations. Genesis. https://doi.org/10.1002/dvg.20505

Sheridan, 2007. Generation of a compartmentalised thymus organoid in vitro using fetal thymic epithelial progenitor cells. The University of Edinburgh.

Shi et al., 1999. Cathepsin S required for normal MHC class II peptide loading and germinal center development. Immunity.

Shores et al., 1991. Disorganization and restoration of thymic medullary epithelial cells in T cell receptor-negative scid mice: Evidence that receptor-bearing lymphocytes influence maturation of the thymic microenvironment. European Journal of Immunology. https://doi.org/10.1002/eji.1830210711

Shortman et al., 1990. The generation and fate of thymocytes. Semin.Immunol. 2, 3–12.

Shortman, Naik, 2007. Steady-state and inflammatory dendritic-cell development. Nature reviews. Immunology 7, 19–30. https://doi.org/10.1038/nri1996

Shukla et al., 2017. Progenitor T-cell differentiation from hematopoietic stem cells using

Delta-like-4 and VCAM-1. Nature Methods. https://doi.org/10.1038/nmeth.4258

Simons et al., 2018. Generation of adult human T-cell progenitors for immunotherapeutic applications. Journal of Allergy and Clinical Immunology. https://doi.org/10.1016/j.jaci.2017.10.034

Singh, Zúñiga-Pflücker, 2018. Producing proT cells to promote immunotherapies. International immunology. https://doi.org/10.1093/intimm/dxy051

Smith et al., 2015. In vitro T-cell generation from adult, embryonic, and induced pluripotent stem cells: Many roads to one destination. Stem Cells. https://doi.org/10.1002/stem.2115

Soh et al., 2014. FOXN1GFP/w reporter hESCs enable identification of integrin-β4, HLA-DR, and EpCAM as markers of human PSC-derived FOXN1+thymic epithelial progenitors. Stem Cell Reports. https://doi.org/10.1016/j.stemcr.2014.04.009

Solanki et al., 2018. Gli3 in fetal thymic epithelial cells promotes thymocyte positive selection and differentiation by repression of *Shh*. Development. https://doi.org/10.1242/dev.146910

Soriano, 1994. Abnormal kidney development and hematological disorders in PDGF β-receptor mutant mice. Genes and Development. https://doi.org/10.1101/gad.8.16.1888

Soza-Ried et al., 2008. Maintenance of thymic epithelial phenotype requires extrinsic signals in mouse and zebrafish. Journal of immunology (Baltimore, Md. : 1950) 181, 5272–5277. https://doi.org/10.4049/jimmunol.181.8.5272

Spangrude et al., 1988. Purification and characterization of mouse hematopoietic stem cells. Science (New York, NY) 241, 58–62. https://doi.org/10.1016/0952-7915(91)90046-4

Su et al., 2015. Efficient in vitro generation of functional thymic epithelial progenitors from human embryonic stem cells. Scientific Reports. https://doi.org/10.1038/srep09882

Sultana et al., 2012. Expression of Functional P-Selectin Glycoprotein Ligand 1 on Hematopoietic Progenitors Is Developmentally Regulated. The Journal of Immunology 188, 4385–4393. https://doi.org/10.4049/jimmunol.1101116

Sun et al., 2013. Directed differentiation of human embryonic stem cells into thymic epithelial progenitor-like cells reconstitutes the thymic microenvironment in vivo. Cell Stem Cell. https://doi.org/10.1016/j.stem.2013.06.014

Suniara et al., 2000. An essential role for thymic mesenchyme in early T cell development. Journal of Experimental Medicine. https://doi.org/10.1084/jem.191.6.1051

Suzuki et al., 1995. Asymmetric signaling requirements for thymocyte commitment to the CD4+ versus CD8+ T cell lineages: A new perspective on thymic commitment and selection. Immunity 2, 413–425. https://doi.org/10.1016/1074-7613(95)90149-3

Swann et al., 2017a. Cooperative interaction of BMP signalling and Foxn1 gene dosage determines the size of the functionally active thymic epithelial compartment. Scientific Reports. https://doi.org/10.1038/s41598-017-09213-1

Swann et al., 2017b. Elevated levels of Wnt signaling disrupt thymus morphogenesis and function. Scientific Reports. https://doi.org/10.1038/s41598-017-00842-0

Taghon et al., 2006. Developmental and molecular characterization of emerging β- and γδ-selected pre-T cells in the adult mouse thymus. Immunity. https://doi.org/10.1016/j.immuni.2005.11.012

Takaba et al., 2015. Fezf2 Orchestrates a Thymic Program of Self-Antigen Expression for Immune Tolerance. Cell. https://doi.org/10.1016/j.cell.2015.10.013

Takada et al., 2017. Generation of Peptides That Promote Positive Selection in the Thymus. The Journal of Immunology. https://doi.org/10.4049/jimmunol.1601862

Takada et al., 2015. TCR affinity for thymoproteasome-dependent positively selecting peptides conditions antigen responsiveness in CD8+ T cells. Nature Immunology. https://doi.org/10.1038/ni.3237

Takahama, 2006. Journey through the thymus: stromal guides for T-cell development and selection. Nature reviews. Immunology 6, 127–35. https://doi.org/10.1038/nri1781

Tang et al., 2016. Thymic DCs derived IL-27 regulates the final maturation of CD4+ SP thymocytes. Scientific Reports 6, 30448. https://doi.org/10.1038/srep30448

Tani-ichi et al., 2013. Interleukin-7 receptor controls development and maturation of late stages of thymocyte subpopulations. Proceedings of the National Academy of Sciences of the United States of America 110, 612–7. https://doi.org/10.1073/pnas.1219242110

Tanigaki et al., 2004. Regulation of alphabeta/gammadelta T cell lineage commitment and peripheral T cell responses by Notch/RBP-J signaling. Immunity 20, 611–622. https://doi.org/10.1016/S1074-7613(04)00109-8

Taniuchi, 2018. CD4 Helper and CD8 Cytotoxic T Cell Differentiation. Annual Review of Immunology. https://doi.org/10.1146/annurev-immunol-042617-053411

Tare et al., 2009. A microarray approach to the identification of polyurethanes for the isolation of human skeletal progenitor cells and augmentation of skeletal cell growth. Biomaterials. https://doi.org/10.1016/j.biomaterials.2008.10.038

Tourniaire et al., 2006. Polymer microarrays for cellular adhesion. Chemical Communications. https://doi.org/10.1039/b602009g

Trampont et al., 2010. CXCR4 acts as a costimulator during thymic beta-selection. Nat Immunol 11, 162–170. https://doi.org/10.1038/ni.1830

Tsai et al., 2003. BMP4 acts upstream of FGF in modulating thymic stroma and regulating thymopoiesis. Blood 102, 3947–3953. https://doi.org/10.1182/blood-2003-05-1657

Ucar et al., 2014. Adult thymus contains foxN1- epithelial stem cells that are bipotent for medullary and cortical thymic epithelial lineages. Immunity. https://doi.org/10.1016/j.immuni.2014.07.005

Ueno et al., 2005. Development of T-lymphocytes in mouse fetal thymus organ culture. Methods Mol Biol. https://doi.org/10.1385/1-59259-838-2:117

Ulyanchenko et al., 2016. Identification of a Bipotent Epithelial Progenitor Population in the Adult Thymus. Cell Reports. https://doi.org/10.1016/j.celrep.2016.02.080

Unno et al., 2002. The structure of the mammalian 20S proteasome at 2.75 Å resolution. Structure. https://doi.org/10.1016/S0969-2126(02)00748-7

Vaidya et al., 2016. FOXN1 in thymus organogenesis and development. European Journal of Immunology. https://doi.org/10.1002/eji.201545814

Van Coppernolle et al., 2009. Functionally Mature CD4 and CD8 TCR Cells Are Generated in OP9-DL1 Cultures from Human CD34+ Hematopoietic Cells. The Journal of Immunology. https://doi.org/10.4049/jimmunol.0900714

Van De Walle et al., 2011. Jagged2 acts as a Delta-like Notch ligand during early hematopoietic cell fate decisions. Blood 117, 4449–4459. https://doi.org/10.1182/blood-2010-06-290049

Vestweber, 2015. How leukocytes cross the vascular endothelium. Nature Reviews Immunology 15, 692–704. https://doi.org/10.1038/nri3908

Vielkind et al., 2005. Integrin regulation by RhoA in thymocytes. Journal of immunology (Baltimore, Md. : 1950) 175, 350–357. https://doi.org/10.4049/jimmunol.175.1.350

Viret et al., 2015. The T Cell Repertoire–Diversifying Enzyme TSSP Contributes to Thymic Selection of Diabetogenic CD4 T Cell Specificities Reactive to ChgA and IAPP Autoantigens. The Journal of Immunology. https://doi.org/10.4049/jimmunol.1401683

von Boehmer, 2005. Unique features of the pre-T-cell receptor alpha-chain: not just a surrogate. Nature reviews. Immunology 5, 571–7. https://doi.org/10.1038/nri1636

Wada et al., 2008. Adult T-cell progenitors retain myeloid potential. Nature. https://doi.org/10.1038/nature06839

Wang et al., 1999. T lymphocyte development in the absence of CD3ε or CD3γδεζ. Journal of Immunology.

Wasserstein et al., 2019. Moving to a World Beyond “p < 0.05.” American Statistician 73, 1–19. https://doi.org/10.1080/00031305.2019.1583913

Wei, Condie, 2011. A focused in situ hybridization screen identifies candidate transcriptional regulators of thymic epithelial cell development and function. PLoS ONE 6. https://doi.org/10.1371/journal.pone.0026795

Wilson et al., 1994. Two waves of recombinase gene expression in developing thymocytes. The Journal of experimental medicine 179, 1355–60. https://doi.org/10.1084/jem.179.4.1355

Witt et al., 2005. Directed migration of positively selected thymocytes visualized in real time. PLoS Biology 3, 1062–1069. https://doi.org/10.1371/journal.pbio.0030160

Wong et al., 2014. Multilineage potential and self-renewal define an epithelial progenitor cell population in the adult thymus. Cell reports 8, 1198–209. https://doi.org/10.1016/j.celrep.2014.07.029

Xing et al., 2016. Late stages of T cell maturation in the thymus involve NF-κB and tonic type i interferon signaling. Nature Immunology. https://doi.org/10.1038/ni.3419

Xu et al., 2002. Eya1 is required for the morphogenesis of mammalian thymus, parathyroid and thyroid. Development.

Ye et al., 2001. The IL-7 receptor controls the accessibility of the TCR?? locus by Stat5 and histone acetylation. Immunity 15, 813–823. https://doi.org/10.1016/S1074-7613(01)00230-8

Yu et al., 2006. Cytokine signal transduction is suppressed in preselection double-positive thymocytes and restored by positive selection. The Journal of Experimental Medicine 203, 165–175. https://doi.org/10.1084/jem.20051836

Yu et al., 2004. IL-7 Receptor Signals Inhibit Expression of Transcription Factors TCF-1, LEF-1, and RORγt. The Journal of Experimental Medicine 200, 797–803. https://doi.org/10.1186/1754-6834-5-63

Zamisch et al., 2005. Ontogeny and regulation of IL-7-expressing thymic epithelial cells. The Journal of Immunology 174, 60–7. https://doi.org/10.4049/jimmunol.174.1.60

Zhang et al., 2013. A thermoresponsive and chemically defined hydrogel for long-term culture of human embryonic stem cells. Nature Communications. https://doi.org/10.1038/ncomms2341

Zinkernagel, Althage, 1999. On the role of thymic epithelium vs. bone marrow-derived cells in repertoire selection of T cells. Proceedings of the National Academy of Sciences of the United States of America. https://doi.org/10.1073/pnas.96.14.8092

Zlotoff et al., 2010. CCR7 and CCR9 together recruit hematopoietic progenitors to the adult thymus. Blood 115, 1897–1905. https://doi.org/10.1182/blood-2009-08-237784

Zook et al., 2011. Overexpression of Foxn1 attenuates age-associated thymic involution and prevents the expansion of peripheral CD4 memory T cells. Blood. https://doi.org/10.1182/blood-2011-03-342097

Žuklys et al., 2016. Foxn1 regulates key target genes essential for T cell development in postnatal thymic epithelial cells. Nature Immunology. https://doi.org/10.1038/ni.3537